SEDIMENT TRANSPORT DUE TO IRREGULAR WAVES

Koen TROUW

Supervisor:
Prof. J. Berlamont

Members of the Examination Committee:
Prof. A. Bultheel, chairman
Prof. J. Monbaliu, secretary
Prof. G. De Roeck
Prof. E. Van den Bulck
dr. J. van de Graaff (Delft University)
Prof. J. Williams (ABPmer)

Dissertation presented in partial fulfillment of the requirements for the degree of Doctor in Engineering Science

September 2013

ISBN 978-94-6018-717-9
D/2013/7515/103

Acknowledgments

I wish to express my thanks to Prof. Berlamont who gave me the opportunity to join his team of researchers. He built a strong team and although working on diverse themes, we worked closely together inspired by him. Many thanks also for your to the point comments and your pragmatic approaches.

Prof. Monbaliu guided me in the new world of science. Thank you for the many discussions and advice. But, you also made me suffer on the hills around Leuven when I joined the KULeuven cycling team…

I am also grateful to prof. Smets (+) for sharing his enthusiasm for coastal research and the many talks we had. He also gave me the opportunity to have my first experience with physical modeling in the wave flume of Flanders Hydraulics.

dr. Van de Graaff gave me the opportunity to work for half a year at Delft University. This was a fruitful period and up to now I still benefit from contacts with famous coastal engineers in Delft. You also learned me that an extensive formulation of the question already gives 80% of the answer.

Doing physical experiments with the team of prof. Williams in the Deltaflume learned me a lot, not only scientifically. Also later meetings and discussions learned me a lot about in situ measuring techniques.

Thanks to the members of my jury for reading and commenting my thesis. I received many thoughtful comments. Special thanks to Prof. De Roeck and Prof. Van den Bulck for reading and commenting my thesis although it is partly outside their main interests.

I enjoyed working with the colleagues at the Hydraulics Laboratory in Leuven and Delft University. Working in the office of prof. Toorman was enriching.

My other colleagues and clients helped me enjoying solving other coastal engineering problems.

I am also grateful to dr. Dohmen-Janssen who introduced me in the Dutch coastal engineering world.

At Flanders Hydraulics I would like to thank especially Jef Engels and Karel Van den Broeck, who were really motivated to assist me with the wave flume experiments.

I am also grateful to IWT (the Flemish agency for Innovation by Science and Technology) who offered me a Ph.D. grant. I also benefited from the opportunity given by the EU – LIP program to carry out experiments in big physical research facilities. I could participate in two programs: ”Evaluation of the performance of field equipment used in studies of near bed

hydrodynamics and sediment dynamics" and "Vertical sediment mechanisms in oscillatory flow conditions".

Although propositions are not common in Ph.D. thesis's at the KULeuven, I would like to give one for new researchers. Don't think you will easily finish you Ph.D. research after starting a new job. In the years after leaving Leuven, I met many people who thought the same as me. Some finished soon, others late and some didn't finish at all. And for most of us, it was our own responsibility.

Last but not least, I would like to thank my family to live together with me in the world outside coastal engineering and supporting me when needed.

I especially want to thank my parents, who gave me all opportunities. Their support was and is always important for me.
My late mother gave me, from my birth on, the love for the beach and the sea. Mama, for me you are still present and I continuously feel your support.

Samenvatting

Sediment transport door onregelmatige golven is een treffende illustratie van de problemen die ontstaan wanneer kleine verschillen van grote getallen bepaald moeten worden. Het is zelfs moeilijk te voorspellen in welke richting het transport netto beweegt. Zowel bij transport over ribbels als het transport over een uitgevlakt bed kan het transport (op het eerste zicht verrassend) tegengesteld zijn aan een aanwezige kleine stroming of bij asymmetrische golven tegengesteld zijn aan de golfrichting.
In deze thesis werd getracht door middel van numerieke en fysische modellering een bijdrage te leveren aan het onderzoek naar sediment transport door golven.
Voor de fysische modellering is het belangrijk de schaaleffecten te kennen. Daarnaast is het ook belangrijk dat de golven in een golfgoot correct worden gemodelleerd. Fouten bij de fysische modellering kunnen leiden tot verkeerde conclusies, zelfs wat betreft de transportrichting. Dit werd geïllustreerd met het opgebouwde numerieke model, dat door middel van de hieronder beschreven fysische experimenten werd gevalideerd. De beste schaling gebeurt door het zogenaamde "Sand Model", waarbij de valsnelheid van het zand geschaald wordt met de schaal van de orbitaalsnelheid. Voor fijn zand in prototype leidt dit echter tot korrelgroottes die voor zand te klein zijn (wordt cohesief materiaal). Ook bleek dat de verticale as van het concentratieprofiel geschaald dient te worden met de ribbelhoogte. Voor de ribbelhoogte in prototype omstandigheden dient dan een schatting gemaakt te worden op basis van empirische formules.
In de Deltagoot van Deltares werd een meetframe van Proudman Oceanographic Laboratory (UK) dat normaal op de zeebodem wordt uitgezet, getest onder gecontroleerde omstandigheden. Het meetframe bevatte sensoren om de snelheid en sedimentconcentraties op verschillende dieptes te meten en ook om de evolutie van de bedvormen onder het frame akoestisch te registreren. Ook langs de wanden van de Deltagoot werden sensoren geplaatst. Uit de vergelijking bleek dat de overeenkomst tussen de metingen die door het frame mogelijk beïnvloed werden en de ongestoorde metingen goed was, behalve voor de turbulentie-karakteristieken relatief hoog boven de bodem. De proeven lieten ook toe de formules om ribbeldimensies te berekenen te valideren. Voor regelmatige golven geven de formules van Nielsen (1992) goede resultaten. Voor onregelmatige golven geven de formules van Van Rijn (1993) betere resultaten, mogelijks omdat deze vooral op gelijkaardige experimenten zijn gebaseerd. De verticale sedimentconcentratie profielen werden onderling vergeleken om de invloed van korrelgrootte, golfhoogte en golfperiode te kennen. Ook werd de invloed van de relatieve positie van de meetsonde t.o.v. de ribbeltop bekeken. Tevens werd onderzocht in welke mate turbulentiekarakteristieken uit de metingen afgeleid konden worden.

In de golftunnel van Deltares werden metingen uitgevoerd met snelheids- en concentratiemeters die ook in het mobiel grensvlak tussen water en sedimentbed kunnen meten. Tevens werden door de universiteit van Edinburgh PIV-metingen uitgevoerd, waarbij de snelheid van sedimentclusters bepaald werd. Uit de metingen bleek dat als de orbitaalsnelheid verhoogd werd, de sedimentconcentratiepieken bij het keren van de stromingsrichting hoger maar ook scherper werden. Ook bleek dat de tijdsverschuiving tussen het keren van de stroming en het ontstaan van een concentratiepiek groter werd, naarmate er verder van de bodem gemeten werd. De tijdsverschuiving verkleinde indien de orbitaalsnelheid verhoogd werd. Door gebruik te maken van 2 concentratiemeters op korte afstand van elkaar, kon ook de snelheid in het water – sedimentbed grensvlak gemeten worden. Hieruit bleek duidelijk dat net boven het bed de sedimentconcentraties zeer sterk stijgen bij het keren van de stroming, terwijl de concentratie onder het oorspronkelijk bedniveau sterk daalde. Dit wees erop dat het sedimentbed omhoog gelift wordt. Doordat dit instrument toeliet om zowel concentraties en snelheden in de bedlaag te meten, was het ook mogelijk om het sedimenttransport in deze laag te bepalen. De PIV-metingen waren tijdens de uitvoering van de metingen nog in een experimentele fase. De resultaten bleken echter goed overeen te komen met klassieke puntsnelheidsmetingen. De verticale snelheid werd wel beïnvloed door de valsnelheid van het zand in suspensie. Ook werd aangetoond dat de ADV gebruikt kan worden om de belangrijkste turbulentie-karakteristieken te bepalen.

Tot slot werd in de CFD (Computation Flow Dynamics) software Phoenics een module geschreven om ook de sedimentconcentraties boven ribbels te berekenen. Het model werd gevalideerd aan de hand van de uitgevoerde fysische proeven. Uit de toepassingen van het model bleek dat de gemiddelde sedimentconcentratie dicht bij de bodem weinig afhankelijk is van het aantal golven in een golfgroep, maar verder van de bodem steeg de concentratie wel met het aantal golven in een golfgroep. Ook het ogenblikkelijke concentratieprofiel werd sterk door het aantal golven in de groep beïnvloed. De modellering bevestigde ook de sterke afhankelijkheid van de sedimentconcentratie met de horizontale afstand tot de ribbeltop. Het is daarom belangrijk om tijdens metingen ervoor te zorgen dat over de volledige ribbellengte metingen beschikbaar zijn (bijvoorbeeld door lang genoeg te meten, waardoor een volledige ribbel onder de sensor door kan lopen). De modellering bevestigde ook dat de sedimentconcentratie het hoogst is bij de passage van de hoogste golven. Door de aanwezigheid van lange golven, zal hierdoor een netto sediment transport in de tegengestelde richting van de golven kunnen ontstaan.

Summary

Sediment transport due to irregular waves is an illustration of the problems that occur when small differences of two big numbers have to be determined. It is even difficult to estimate the direction of the net sediment transport. Both for ripples and sheet flow conditions, the transport can be opposite to a small mean current or, for asymmetrical waves, opposite to the mean wave direction.

This thesis aimed to give a contribution for the knowledge of sediment transport due to waves, using both physical and numerical models.

For physical modelling, it is important to know the scaling effects. It is also important that the waves in the wave flume are correctly generated. Errors may lead to wrong conclusions, even about the direction of the net sediment transport. This was illustrated by the constructed numerical model, that was validated by the physical models described below. The best scaling is obtained using the so called "Sand Model", in which the settling velocity of the sand is scaled with the scale of the orbital velocity. However, for fine sand, this leads to grain sizes which are too small (resulting in cohesive material). If the Sand Model is used, the vertical axis of the concentration profile has to be scaled with the ripple height. To do this, the ripple height at prototype scale should be derived from empirical formulations to estimate the ripple height.

In the Delta flume of Deltares, the measuring frame of Proudman Oceanographic Laboratory (UK), that was normally used at the sea bottom, was tested under controlled circumstances. The frame contained sensors to measure at different heights above the bottom the velocity and the sediment concentration and also to record the evolution of the ripples beneath the frame. Also at the walls of the flume, sensors were installed for comparison. The comparison indicated that the measurements of the frame compared well with the undisturbed wall measurements, except for the turbulence characteristics relative far from the bed. The experiments also allowed to validate the existing formulations to calculate ripple dimensions. For regular waves, the formulae of Nielsen (1992) gave good results. For irregular waves, the correspondence was worse, better results were obtained with Van Rijn (1993). This might be explained by the use of comparable experiments by Van Rijn to derive his formulations. The vertical sediment concentration profiles were compared to learn about the influence of the grain size, the wave height and the wave period. Also the relative horizontal distance between sensor and ripple crest was analysed. Also it was examined which turbulence characteristics could be derived from the available instrumentation.

In the wave tunnel of Deltares, measurements were carried out with instruments that allowed to measure velocities and concentrations in the sheet flow layer. Also PIV measurements (measurement of the velocity of a cluster/pattern of sediment particles) were organized by the University of Edinburgh. The measurements indicated that the effect of increasing the orbital

velocity was to greatly enhance the magnitude and sharpness of the concentration peaks generated at backward flow reversal and to increase the magnitude of the peaks which appeared to be associated with flow maxima. The suspension events near backward flow reversals exhibited a lag with increasing elevation above the bed. This lag decreased with increasing peak orbital velocities. A pair of concentration sensors made it possible to obtain velocities and concentrations inside the sheet flow layer. The lifting up of the bed is clearly visible near flow reversals, with an important increase of the concentrations above the original bed level, and a decrease of concentrations below this level. The combination of velocities and concentrations makes it possible to predict sediment transport in the sheet flow layer. The PIV measurements were able to derive a velocity field on a reliable way, when comparing with traditional point measurements. However, the vertical velocities seem contain the settling velocity of the sand particles in the water. It was also proven that the ADV could be used to derive turbulence characteristics.

Finally, in the CFD (Computation Flow Dynamics) software a script was written to calculate the time varying sediment concentration above ripples. The model was validated with the results of the physical experiments. Applying the model, learned that the number of waves in a wave group mainly influences the averaged concentration at relative high levels above the bed and the instantaneous concentration profile. The modeling also confirmed that one must be careful with the interpretation of measurements in one vertical, since they are not representative for the whole ripple length. Averaging the near bed concentration at the time interval of the highest waves gives an important difference with averaging them over the time interval of the lowest waves. This is important since wave groups induce bound long waves, with on offshore flux for the highest waves and an onshore flux for the lowest waves. The net transport can become onshore directed.

Contents

Symbols

A	: amplitude of a wave (=H/2)	(m)
$\hat{A}$	: amplitude of orbital wave motion	(m)
a_g	: amplification factor of electronic amplifier of OpCon (factor 1 or 10)	(-)
a_c	: electronic conversion factor for the log-amplifier of the OpCon	(-)
c	: wave celerity	(m/s)
c	: concentration	(m^3/m^3)
d	: grain size	(m)
D_*	: dimensionless grain size	(-)
f	: friction coefficient	(-)
F	: force	(kg m/s^2)
F_*	: densimetric Froude-number	(-)
g	: acceleration of gravity	(m/s^2)
h	: water depth	(m)
H	: wave height	(m)
H_s	: significant wave height	(m)
H_{rms}	: root mean square wave height	(m)
k	: wave number	(m^{-1})
k_s	: grain roughness	(m)
K_1	: actual calibration factor OpCon	(kg/m^3/Volts)
L	: wavelength	(m)
l_s	: relative length	(-)
m	: ratio wave height – displacement wave paddle	(-)
N	: scale ratio	(-)
p	: pressure	($kg/m/s^2$)
q_s	: sediment transport rate per unit width	(m^2/s)
Re	: Reynolds number	(-)
R_*	: grain size-Reynoldsnumber	(-)
s	: relative density	(-)
S_0	: displacement wave paddle	(m)
t	: time	(s)
T	: (wave-)period	(s)
u	: horizontal velocity	(m/s)
$\hat{U}$	: amplitude of orbital velocity	(m/s)
u_*	: shear velocity	(m/s)
V	: vertical velocity	(m/s)
V_{ws}	: relative settling velocity	(-)
w	: vertical velocity	(m/s)
w_s	: settling velocity	(m/s)
X	: position of wave paddle	(m)
z	: vertical coordinate, distance to the bottom	(m)

Greek symbols

β	: slope	(-)
γ	: specific weight	(-)
δ	: thickness of boundary layer	(m)
Δ	: ripple height	(m)
η	: water level	(m)
Θ	: Shields parameter	(-)
κ	: reflection coefficient	(-)
λ	: (ripple) length	(m)
ν	: viscosity	(m^2/s)
ξ	: water level	(m)
ρ	: density	(kg/m^3)
τ	: shear stress	($kg/m/s^2$)
φ	: wave potential – phase	(-)
ψ	: mobility parameter	(-)
ω	: phase velocity	(s^{-1})

subscripts

0	: deep-water
cr	: critical value
d_i	: i% van the volume of grains is finer then d_i
i	: i-the component of a wave spectrum
I	: incoming wave component
R	: reflected wave component
rms	: root mean square
δ	: just outside the boundary layer
ε	: phase difference between incoming and reflected wave
s	: sediment
w	: wave related

superscript

(1) (2)	: first – second order

1 Introduction

The estimation of the sediment transport is a key element in the solution of many coastal engineering problems. Infrastructural works in the coastal environment can modify the water and sediment movement and nature is confronted with this new situation resulting in adaptations. For example a dredged navigation channel will generate sedimentation in the channel; the construction of groynes can cause sedimentation (upstream) and erosion (downstream); the mining of sand on sand banks can, if not compensated by extra natural transport and sedimentation at the mining location result in higher waves reaching the beaches. A good estimation of the impact of human interventions makes it possible to include all expected extra economical and ecological costs during the design.

Mathematical models are evolving from a set of empirical expressions to models describing the physics of all processes. These models make it possible to estimate the sedimentation in e.g. navigation channels or the effect of groynes. In this chapter a small overview will be given of the various aspects of these models. Three components of modelling are important: hydrodynamics, sediment transport and morphology. These three components influence each other strongly in a non-linear way and make models more complicated and long time predictions very uncertain. For example, small errors in predicted morphological changes (which may be due to the wrong modelling of the hydrodynamics or the sediment transport) can grow rapidly. Often the boundary conditions are unknown and even if all processes can be modelled well, errors can be introduced and grow rapidly.

Waves and currents cause a non-uniform motion of the water. The waves and currents will interact. The interaction can be observed in the hydrodynamics of the boundary layer and farther from the bottom where currents will change wave characteristics and waves will cause additional currents. The interaction of the water with the bottom causes shear stresses and turbulence. The water does not move uniformly and a velocity profile is developed depending on the magnitude of the water movement and the roughness of the bottom. The shear stress also acts on the material of the bottom. When the shear stress exceeds the critical shear stress of the sediments, the sediments will start moving. The turbulence in the water stirs up the sediments. If the hydrodynamic conditions do not change rapidly, an equilibrium concentration profile will build up with high concentrations at the bottom and lower concentrations higher in the water column (with upward transport due to the turbulence (diffusion) and downward transport due to the settling of the sediments). However, for time varying hydrodynamical conditions very important time lags can occur between the instantaneous conditions and the equilibrium concentration profile.
Once the concentration profile is calculated, it has to be multiplied with the velocity profile in order to estimate the total sediment flux. This is calculated at appropriate time steps and

locations in order to estimate the sediment transport. This is then used to assess net erosion and accretion. The resulting change in bathymetry in turn will change the waves and currents and in turn modify relationships between waves/currents and the near bed hydrodynamic conditions.

Although a lot of research has been undertaken, predictions of sediment transport and associated morphological changes remain uncertain. During the last decades sediment transport mechanisms have been examined starting from the fundamentals of sediment transport. This has been advanced through the use of novel instrumentation quantifying sediment transport. The more research is done, the more it becomes clear that it is hard to make correct predictions. The difficulties can be demonstrated with two examples: a) the direction of net transport is in some cases sensitive to ripple dimensions, grain size, current velocity or wave period; b) high waves in an irregular wave train are grouped and time lags makes the sediment concentration sensitive to the number of waves in a group, making sediment transport a process with an important 'memory'.

Content

This thesis explores the relationship between hydrodynamics and sediment transport.

In Chapter 2 a summary is given of the hydrodynamical theory which is important for morphological models: theory of regular and irregular waves, wave groups, wave induced currents and wave set up and set down mechanisms due to irregular waves which can cause extra transport.

Chapter 3 describes the scale effects introduced when using a (small) wave flume: to which exend can results obtained in a flume be used to describe prototype scale processes ? Also the necessary preparatory work and spurious effects in a wave flume are described.

In Chapter 4 and 5 physical experiments in the Deltaflume and in a wave tunnel with 'near reality but manageable' conditions are described.
In the Deltaflume the bed was mainly rippled. A tripod was used to measure in detail the bed morphology, concentration profiles, velocities and turbulence characteristics. It will become clear that results from measurements can differ a lot from test to test, from location to location and from time to time, even when the hydrodynamic boundary conditions are the same. This complicates interpretation and emphasises once more the complexity of sand transport and the use of experimental data to obtain generally applicable transport formulae.
In the wave tunnel the currents and oscillating motion were strong enough to wash out ripples resulting in sand transport which was dominated by sheet flow. Because of the relative small size of the tunnel, it was very well manageable: after each test the bed could be restored.

Hydrodynamic conditions were horizontally uniform. The experiments described were part of a long series of experiments in the wave tunnel to examine sheet flow conditions. Attention was paid to indications of high shear stresses close to the bottom at flow reversal and to the influence of oscillating period and magnitude to the intrawave concentrations.

In Chapter 6 a numerical model is described and validated to model velocities and sediment concentrations over a rippled bed. This model was used to quantify scale effects, to examine and interpret the results of measurements and to look at the effect of wave groups.

It will be illustrated that numerical and physical modelling can support each other's interpretation and both are necessary to understand the physical processes and to apply formulae to calculate sediment transport (which is not a goal of this thesis).

Chapter 7 summarises this thesis and gives recommendations for further research.

In Chapter 8 some further developments are presented that are published between the research for this thesis and its publication.

2 Wave hydrodynamics

The movement of water over sediment particles generates friction and can lift up these sediments. Friction also generates turbulence, which can bring and keep the sediments in suspension. If no currents are present and the waves are regular and symmetric, sediments will be in suspension without any net transport.

A study of the motion of the water particles makes clear that waves induce net currents and also higher order frequency waves are generated. Due to these phenomena real waves displace sediments. Waves only resuspend sediment and currents transport it. However the wave induced net transport can influence the magnitude and more importantly, it can move sediments in other directions (e.g. cross shore sediment transport).
In this chapter the basic concepts of the hydrodynamics of waves and currents are presented. The important parameters responsible for resuspension (shear stress and turbulence) will be discussed at the end of the chapter.

2.1 Description of waves

2.1.1 Regular waves

The waves that are object of this study are wind waves: waves generated by wind with periods typically between 1 and 20 seconds. They are classified as gravity waves.

The simplest wave is the regular wave, characterised by the wave height (vertical distance between wave crest and trough) and wave period. Although this wave seldom occurs in nature, it is often theoretically examined.

If the fluid is non-viscous and irrotational, the hydrodynamics can be described with a potential (ø), which makes it easier to describe the wave mathematically.

2.1.1.1 Potential wave theory

The solution of the Laplace equations becomes (assuming that the maximal surface elevation is small relative to the wavelength) (Dean and Dalrymple,1991):

$$\eta = \frac{H}{2}\cos(\omega t - kx) \tag{2-1}$$

$$u = \frac{\pi H}{T}\frac{\cosh(kz)}{\sinh(kh)}\cos(\omega t - kx) \tag{2-2}$$

$$w = -\frac{\pi H}{T}\frac{\sinh(kz)}{\sinh(kh)}\sin(\omega t - kx) \tag{2-3}$$

where u and w are the horizontal and vertical orbital velocity respectively, η the surface elevation, H the wave height, T the wave period, k (=2π/L) the wave number, ω (=2π/T) the cyclic frequency and h the mean water depth and z is the height above the bed. The wave number (k) is defined using the dispersion relation:

$$\omega^2 = gk\tanh(kh) \tag{2-4}$$

It is obvious from these formulae that the stream lines are ellipses and that the orbital velocity is increasing with distance above the bed.

Parameters often used in the field of sediment transport are the orbital velocity $\hat{U}_\delta$ =πH/Tsinh(kh) and orbital radius $\hat{A}_\delta$ = H/2sinh(kh) near the bed (just outside the wave boundary layer). These parameters determine the shear stress on the bed and thus the resuspension of sediments. If second order terms are included (finite surface elevation) the second order Stokes wave is obtained (see Dean and Dalrymple, 1991).

2.1.1.2 Net wave induced currents for ideal fluids

After one wave cycle it can be observed that a water particle has made a net movement in the direction of the wave propagation. When a particle moves forward (first half wave cycle) its vertical position is higher than when moving backward. Because of its higher position it also moves faster during the first half wave cycle as compared to the second half wave cycle. The net movement can be calculated by integrating Eq.2.2, with adaptation of the co-ordinates of the particle (Longuet-Higgins, 1953):

$$\overline{U} = \frac{1}{2c}\left(\frac{\pi H}{T}\right)^2\left(\frac{\cosh\ (2kz)}{\sinh^2(kh)}\right) \tag{2-5}$$

with $\bar{U}$ the wave period averaged velocity and c the wave celerity (=L/T). Near the bottom the wave induced net velocity of a particle is $(\hat{U}_\delta)^2$ /2c. Although the averaged Eulerian velocity is zero in each point (except between wave crest and wave trough, see below) the Langrangian velocity is positive.

The net movement of water can also be demonstrated with the Eulerian velocities. Points at elevations between wave trough and wave crest are dry during part of the wave cycle, which implies that negative (Eulerian) velocities are reduced, resulting in a net positive movement.

The net movement of water can be obtained by integrating Eq.2.5 over the depth or by integrating the Eulerian velocities between wave trough and crest over a wave period. This results in a net discharge q_{drift}:

$$q_{drift} = \frac{gTH^2}{8L} \tag{2-6}$$

2.1.1.3 Viscosity effects

If the fluid is viscous, the phase shift between the horizontal and vertical velocity differs from 90°; the flow is rotational. This induces an extra stress term, analogous to the Reynolds stress, calculated by Longuet-Higgins (1953):

$$\overline{uv} = \frac{\omega^2 H^2 \pi \delta_s}{8L\sinh^2 kh}(1 - e^{-\xi}(2\cos\xi - e^{-\xi} + 2\xi\sin\xi)) \tag{2-7}$$

with δ_s the Stokes length ($=\sqrt{2\nu/\omega}$, ν the laminar viscosity) and $\xi=(h-z)/\delta_s$. Inserting Eq.2.7 in the time-averaged Navier-Stokes equations:

$$\nu\frac{d^2\overline{U}_{el}}{dz^2} = \frac{d}{dz}(\overline{uv}) + \frac{1}{\rho}\frac{\overline{dp}}{dx} \tag{2-8}$$

gives the (Eulerian) net velocity, which is positive in the direction of wave propagation:

$$\overline{U}_{el} = \frac{\omega H^2 \pi}{2L\sinh^2 kh}\left(3 - 2(\xi+2)e^{-\xi}\cos\xi - 2(\xi-1)e^{-\xi}\sin\xi + e^{-2\xi}\right) \tag{2-9}$$

$\bar{U}_{el}$ is the wave averaged Eulerian velocity due to viscosity effects with a laminar boundary layer. The same expression can be used for turbulent flow by replacing the laminar viscosity by the turbulent viscosity. Outside the boundary layer the terms depending on the laminar viscosity are almost zero.

The previous expressions are valid if no pressure gradient occurs. The influence of this assumption is of minor importance for unbounded domains (Craik, 1982). This is no longer possible for bounded channels (e.g. wave flumes). From the condition that the net flux has to be zero, the pressure gradient can be determined. Inserting the pressure gradient in Eq.2.9 gives the total mass transport velocity (including the Langrangian component) (Craik, 1982):

$$\overline{U_t} = \frac{\omega H^2 \cot gh(kh)}{h^2} z\left(\frac{3}{4}(\frac{z}{h}-2)+\frac{1}{2}k^2h^2(3\frac{z}{h}-2)\right)+\frac{\omega H^2 k}{8\sinh^2 kh}\left(\frac{9}{4}(\frac{z}{h}-1)^2-\frac{3}{4}+\cosh(2kh)\right) \tag{2-10}$$

2.1.2 Asymmetric waves

Waves are often asymmetric, which can cause net sediment transport. Two components can be distinguished. Equations 2.1 to 2.3 are only valid if the elevation of the water surface is small. If one incorporates second order effects, a bound second harmonic has to be added to the solution, making the wave asymmetric (and yielding the Stokes second order (bounded) wave):

$$\eta = A_1 \cos(\omega t - kx) + A_2 \cos(2(\omega t - kx)) \tag{2-11}$$

with A_1 =H/2 and A_2=3kH^2/16(kh)^3 (the wave number of the second harmonic wave is 'bounded' with the wave number of the first harmonic). Free waves are another cause of wave asymmetry, with a frequency of twice the main wave. The wave number k for the second harmonic can be calculated with the dispersion relation (Eq. 2.4).

2.1.3 Radiation stress

The radiation stress, the excess flow of momentum, is formed by a pressure component and a component due to wave-induced velocities. The pressure varies during the wave period. At the wave crest an increased (dynamic) stress exists on a larger area (vertical) than the area under the wave trough with a reduced (dynamic) stress. The averaged pressure is higher than the pressure for still water.

The second component is due to velocity fluctuations. The integration of these fluctuations over time are larger than zero.

The radiation stress (S) is defined as the wave induced component of the horizontal momentum flux and can be calculated as:

$$S = \overline{\int_0^{h+\eta} (p+\rho u^2)dz} - \int_0^h p_0 dz \tag{2-12}$$

A gradient in radiation stress causes a net force on the water body. This gradient (e.g. due to a gradient of the wave height) causes a gradient in water level or currents (e.g. longshore current due to waves travelling oblique to the shoreline). The currents will generate a compensational bed shear stress. More details can be found in literature (e.g. Longuet-Higgins and Stewart, 1964).

2.1.4 Irregular waves

The waves one can see at sea are generated by wind. Since the wind has a very turbulent character, the waves are irregular. The instantaneous water level becomes a stochastic parameter. In order to study the effects of irregular waves, a statistical analysis is necessary. A useful approach is to describe the wave as the sum of regular waves with random phases. Measurements at sea and numerical models make it possible to describe the amplitudes as function of the frequency either relatively or absolutely (if wind data are available). The high frequent changes in water level induce also long (low frequent) waves, which are important for the transport of sediments, as will be demonstrated in Chapter 6.

2.1.4.1 Mathematical description

The water level at a point (x,y) at time t is often described as the sum of the water levels from different regular waves coming from different directions with random phases.

$$\eta(x,y,t) = \sum_{m=1}^{\infty} \sum_{n=1}^{\infty} a_{mn} \cos\left(k_m x \cos\alpha_n + k_m y \sin\alpha_n - 2\pi f_m t + \varepsilon_{mn}\right) \quad (2\text{-}13)$$

a_{mn} en ε_{mn} are the amplitude and phase of component mn, k_m is the wave number corresponding with frequency f_m and α_n is the direction of the wave component. The amplitude is also a stochastic parameter!

The amplitudes are represented by wave spectra. Often an energy density spectrum (S) is used:

$$S(f_m,\alpha_n)\Delta f\Delta\alpha = \frac{< a_{mn}^2 >}{2} \quad (2\text{-}14)$$

<.> is used for the mean value of a stochastic parameter. S is the expected wave energy.
Eq.2.15 gives the relation between the measured water elevation during n time steps, the standard deviation (root mean square) of the water level (σ), the first order moment m_0 of the spectrum, the energy per unit area (E), the amplitudes of the wave spectrum, the amplitudes

in the energy density spectrum (S), the root mean square of the wave amplitudes (a_{rms}) and the root mean square wave height (H_{rms}).

$$\frac{\sum_i \eta_i^2}{n} = \sigma^2 = m_0 = \frac{E}{\rho g} = \sum_{mn} S_{mn} \Delta f \Delta \alpha = \frac{\sum_{mn} < a_{mn}^2 >}{2} = \frac{a_{rms}^2}{2} = \frac{H_{rms}^2}{8} \qquad (2\text{-}15)$$

It is important to note that the root mean square wave amplitude is not equal to the standard deviation of the water level. Some authors use a_{rms} for the standard deviation of the water level.

Transfer functions make it possible to translate the energy spectrum in e.g. a velocity spectrum. Since the spectrum does not contain any information on the phases, it is not possible to get the time evolution of the velocity but with the aid of the spectrum it is possible to derive statistics for the velocity.
Example: The spectrum of the velocities U(ω) can be calculated by applying the transfer function $T_u(\omega)$ on the spectrum of the water levels H(ω):

$$U(\omega) = T_u(\omega).H(\omega) \qquad (2\text{-}16)$$

T_u can be calculated with Eq.2.1 and Eq.2.2:

$$T_u(\omega) = \omega \frac{\cosh(kz)}{\sinh(kh)} \qquad (2\text{-}17)$$

The spectra are also useful to derive some statistics. The probability that a certain water level η is exceeded can be calculated with the probability density function:

$$P(\eta) = \frac{1}{\sqrt{2\pi m_0}} e^{-\frac{\eta^2}{2m_0}} \qquad (2\text{-}18)$$

m_0 is defined in Eq.2.15.
If the wave height for irregular waves is defined as the difference between crest and trough only wave heights are accounted for which the crest and trough are respectively above and below mean water level. If the spectrum contains only one peak, it is observed that the wave heights have a Rayleigh distribution. In that case 1) the probability density function p(H) can be calculated as:

$$p(H) = \frac{H}{4m_0} e^{-\frac{H^2}{8m_0}} \qquad (2\text{-}19)$$

and 2) the root mean square wave height H_{rms} ($= \sqrt{\overline{H^2}}$) is related to the more frequently used significant wave height H_s (mean wave height of the 33% highest waves) $H_s = 1.416 H_{rms}$.

2.1.4.2 Shape of a wave spectrum

Wave spectra can be represented in 2 dimensions (frequency and amplitude) or 3 dimensions (frequency, direction and amplitude). If the observed waves have one clear cause (e.g. a storm) all waves will come from the same direction and a 2 dimensional graph will give all information (except phase). These spectra contain one peak at the peak period T_p. If waves from a previous storm or another wave field further away are present, there will be more peaks in the spectrum.

The evolution of wind waves is described by Hasselmann et al. (1973) and can be defined using a wave spectrum called the JONSWAP spectrum:

$$S_J(f) = S_{PM}(f)\,\nu^{\beta} \tag{2-20}$$

$$S_{PM}(f) = \alpha\, g^2 (2\pi)^{-4} f^{-5} \exp\left(\frac{-5}{4}\left(\frac{f}{f_p}\right)^{-4}\right) \tag{2-21}$$

$$\beta = \exp\left(\frac{-(f - f_p)^2}{2\sigma^2 f_p^2}\right) \tag{2-22}$$

with:

S_{PM}: Pierson-Moskowitz spectrum

f_p: peak frequency

α: Phillips' constant (=0.0081)

ν: peak factor $1 \leq \nu \leq 7$

σ: width of the peak (=0.07 for $f \leq f_p$, =0.09 for $f > f_p$)

A higher peak factor results in a narrower spectrum and thus a more regular wave pattern. Waves that are still influenced by a wind field have broader spectra. If the wind waves are fully developed (adapted to the wind field), ν is equal to one and the JONSWAP spectrum becomes equal to the Pierson-Moskowitz spectrum.

More information about the development of wave spectra can be found in Monbaliu (1992) and Luo (1995).

2.1.4.3 Wave groupiness and currents due to irregular waves

In a train of waves observed at sea, it can be seen that high waves are grouped.
Since the radiation stress depends on the wave height, the 'mean' water level will be lower under a group of high waves, and higher under the small waves (in order to compensate the energy flux, Longuet-Higgins and Stewart, 1964). This movement of the water level can be considered as a bound long wave, travelling with the wave group speed (wave celerity). This

also causes currents, which are directed offshore under the high waves and onshore under the low waves. Since the suspended sediment concentration is higher under the high waves, this will cause a sediment transport component in the offshore direction. Effects of these groups on sediment concentration and wave groupiness parameters are discussed in Chapter 6.

2.2 Hydrodynamics of waves and currents in the bottom boundary layer

2.2.1 Boundary layer theory

The bottom boundary layer is defined as the layer where the flow is influenced significantly by the bottom. The flow over the bed and the velocity gradient causes small unorganised eddies. This random motion of the water particles is called turbulence. The random motion of the water particles exchanges fast moving water to slower parts and vice versa (turbulent or eddy viscosity). This reduces the velocity gradient.

Very close to the bed the velocity fluctuations are damped and laminar (molecular) viscosity of the water is much more important than the turbulent viscosity. This layer is called the viscous sublayer. If the roughness elements of the bed are smaller than the viscous sublayer the flow is called smooth. The size of the roughness elements does not influence the velocity outside the boundary layer. If the roughness elements are higher, they will influence the velocity: the flow is called rough. Between these two conditions the flow is called transitional.

The general flow equations are the Navier-Stokes equations (in two dimensions with x the direction of the flow and z perpendicular to this flow):

$$\rho \frac{du}{dt} = \rho\left(\frac{\partial u}{\partial t} + u\frac{\partial u}{\partial x} + w\frac{\partial u}{\partial z}\right) = -\frac{\partial p}{\partial x} + \frac{\partial \tau}{\partial z} \tag{2-23}$$

$$\frac{\partial p}{\partial z} = 0 \tag{2-24}$$

The shear stress is defined as $\tau = \rho\nu\frac{\partial u}{\partial z} - \rho\langle u'w'\rangle$, where $\langle\rangle$ is the time-averaged value and u' and w' are respectively the instantaneous horizontal and vertical direction velocity fluctuations. The terms describe respectively the laminar and the turbulent part of the shear stress. The turbulent term can be described in a manner similar to the laminar term by defining the eddy viscosity $\nu_t = -\langle u'w'\rangle / (du/dz)$.

The roughness height is given by k_s. It is the diameter of identical spherical particles that give the same roughness as the bed material considered. This value is typically a function of the size of the material on the bottom and the dimensions of the bottom structure (e.g. ripples).

The shear velocity u_* ($=\sqrt{\tau_b / \rho}$) is often used because it has the same dimensions as the velocity (with τ_b the shear stress at the bottom).

2.2.2 Currents

The flow type is based on experimental results:
Hydraulically smooth flow for:

$$\frac{u_* k_s}{\nu} \leq 5 \tag{2-25}$$

Hydraulically rough flow for:

$$\frac{u_* k_s}{\nu} \geq 70 \tag{2-26}$$

Hydraulically transitional flow for:

$$5 < \frac{u_* k_s}{\nu} < 70 \tag{2-27}$$

The current-only boundary layer can be divided in different layers (see Figure 2-1):

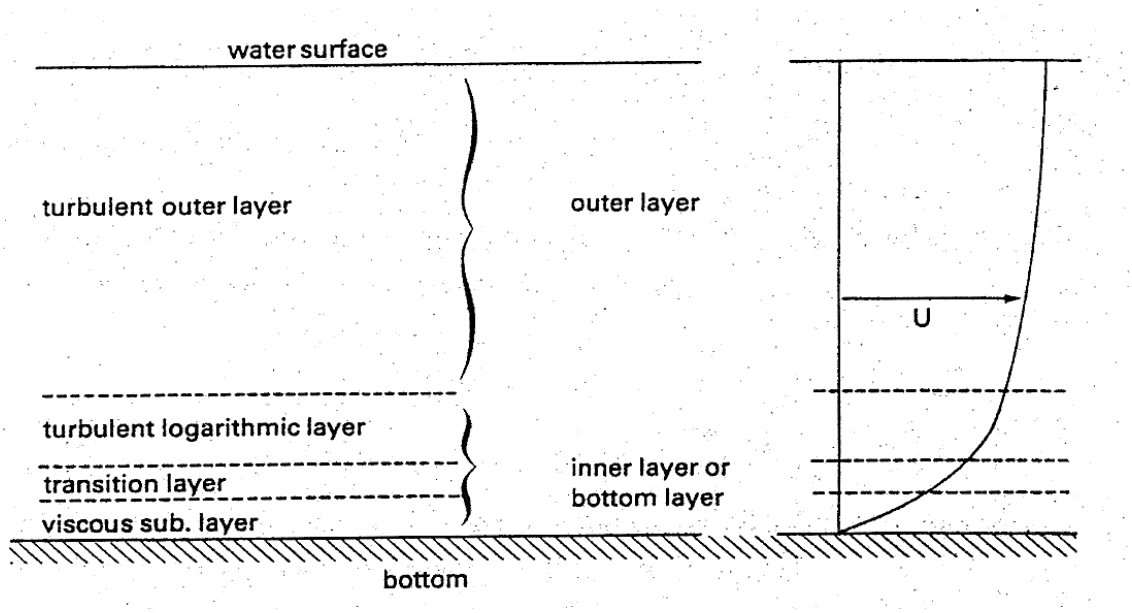

Figure 2-1 Schematic representation of the current boundary layer

In the viscous sublayer the shear stress is constant:

$$\tau(z) = \tau_b = \rho\nu\frac{\partial u}{\partial z} \tag{2-28}$$

and after integration a linear velocity profile is obtained:

$$u(z) = \frac{u_*^2}{\nu} z \tag{2-29}$$

In the turbulent logarithmic layer the viscous shear stress can be neglected:

$$\tau(z) = \tau_b = -\rho\overline{u'w'} = \nu_t \rho\frac{du}{dz} \tag{2-30}$$

Different methods exist to estimate ν_t or $-\rho\overline{u'w'}$. With the turbulence model of Prandtl a logarithmic velocity profile is obtained:

$$\frac{u(z)}{u_*} = \frac{1}{\kappa}\ln(\frac{z}{z_0}) \tag{2-31}$$

with:

- for hydraulically smooth flow:

$$z_0 = 0.11\frac{\nu}{u_*} \tag{2-32}$$

- for hydraulically rough flow:

$$z_0 = \frac{k_s}{30} \tag{2-33}$$

- for hydraulically transitional flow:

$$z_0 = 0.11\frac{\nu}{u_*} + \frac{k_s}{30} \tag{2-34}$$

In the outer zone ($z>0.2h$) the turbulent shear stress decreases:

$$\tau(z) = \tau_b(1-\frac{z}{h}) \tag{2-35}$$

and the evolution of the turbulent viscosity is parabolic:

$$\nu_t(z) = \kappa(1-\frac{z}{h})u_* \tag{2-36}$$

2.2.3 Waves

The boundary layer for "waves only" conditions is much thinner than for currents. When the velocity increases, the boundary layer is growing, but since the velocities reverse after half a wave period, the boundary layer does not get time enough to build up. The thickness of the boundary layer varies during the oscillating cycle.

The equation of motion in the boundary layer can be written as (Fredsøe et al., 1992):

$$\rho \frac{\partial}{\partial t}(U_\delta - U) = -\frac{\partial \tau}{\partial z} \tag{2-37}$$

where U_δ is the horizontal velocity at the edge of the boundary layer.

For waves, not only the turbulence part is important in the shear stress, but also non-zero covariances between horizontal and vertical velocities:

$$\bar{\tau} = -\rho\overline{u'w'} - \rho\overline{\tilde{u}\tilde{w}} + \nu\frac{\partial \bar{u}}{\partial z} \tag{2-38}$$

where the second term defines the correlation between the oscillatory terms. This term can become important for e.g. asymmetric waves, over ripples (due to induced vorticity).

For waves the traditional Reynolds stresses (first term in Eq. 2.38) are much smaller than the bottom shear. More information can be found in Nielsen (1992), Rose (1997), Rivero and Arcilla (1995).

Eq. 2.37 can be solved for laminar flow, which gives (Nielsen, 1992)

$$\frac{\tau_b}{\rho} = \frac{\sqrt{2}\nu\hat{U}_\delta}{\delta_w}\sin(\omega t + \frac{\pi}{4}) \tag{2-39}$$

with $\delta_w = \sqrt{2\nu/\omega}$, the maximal thickness of the wave boundary layer and $\hat{U}_\delta$ the amplitude of the orbital velocity. In this solution the shear stress is 45° ahead of the orbital velocity.

For turbulent flow, only a differential equation can be derived, without an analytical solution. The shear stress is written as function of the orbital peak velocity by introducing the empirical parameter f_w (wave friction coefficient):

$$\tau_{\max} = \frac{1}{2}\rho f_w \hat{U}_\delta^2 \qquad \tau(t) = \frac{1}{2}\rho f_w \hat{U}_\delta^2 \cos^2(\omega t) \tag{2-40}$$

for a rough bottom the friction coefficient can be written as:

$$f_w = 0.04(\frac{\hat{A}_\delta}{k_s})^{-1/4} \qquad \frac{\hat{A}_\delta}{k_s} > 50 \tag{2-41}$$

and for a smooth bottom:

$$f_w = 0.035\,\mathrm{Re}^{-0.16} \tag{2-42}$$

with k_s the roughness height, $\hat{A}_\delta$ the orbital radius and Re the Reynolds number

($\mathrm{Re} = \hat{U}_\delta \hat{A}_\delta / \nu$). Other expressions for f_w can be found in Van Rijn (1993).

While for laminar flow, the shear stress is 45° ahead the flow, this phase difference is reduced for turbulent flow due to eddies which cause strong mixing.

The variation of the friction coefficient and the maximal thickness of the boundary layer is given in Figure 2-2 and Figure 2-3.

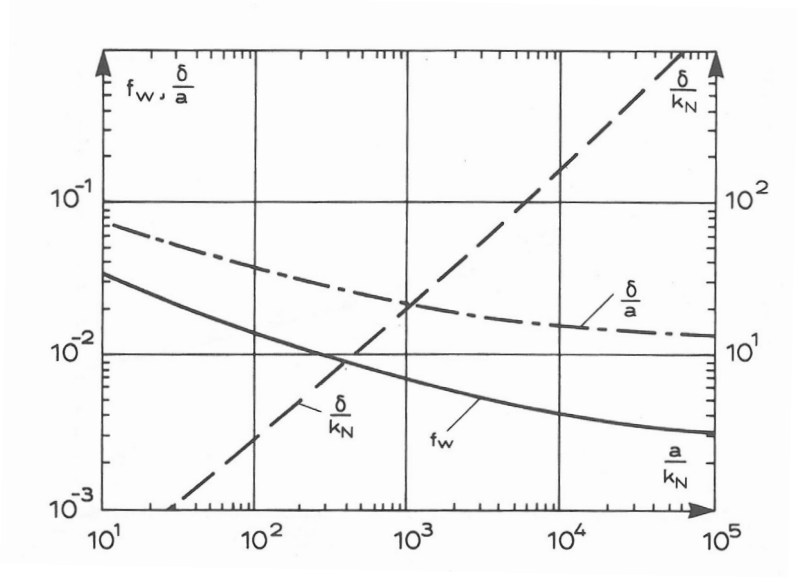

Figure 2-2Variation of the friction coefficient and the thickness of the wave boundary layer (Fredsøe and Deigaard, 1992)(a in the figure = $\hat{A}_\delta$, k_N=k_s)

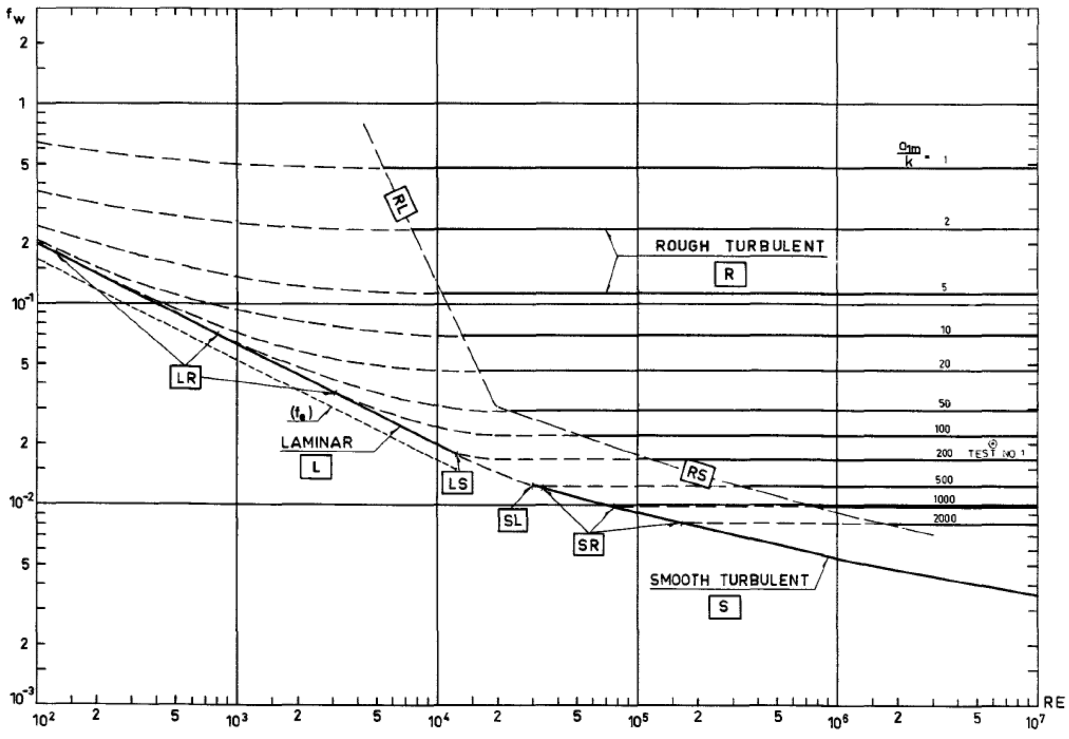

Figure 2-3 Variation of the friction coefficient (Jonsson, 1966)

The roughness height is a function of the grain size and the ripple dimensions (e.g. Fredsøe and Deigaard (1992), Van Rijn(1993)). The roughness height due to the ripples is experienced by the main oscillating flow, locally (along the ripple surface) the grain roughness height is felt.
For irregular waves an expression for the grain related shear stress (flat bed) has been derived by Nielsen (1992):

$$\tau(t) = \frac{1}{2} f_w \rho A_{rms} (\cos\varphi_\tau \omega_p U_\delta(t) + \sin\omega_p \frac{dU_\delta}{dt}) \qquad (2\text{-}43)$$

with A_{rms} the wave orbital radius based on the peak frequency (ω_p) and the rms of $U_\delta(t)$ and with φ_τ the phase lag between shear stress and flow. It is now possible to construct a transformation function to relate the velocity spectrum to the shear stress spectrum.

The hydraulic regimes for wave conditions is given in Figure 2-4

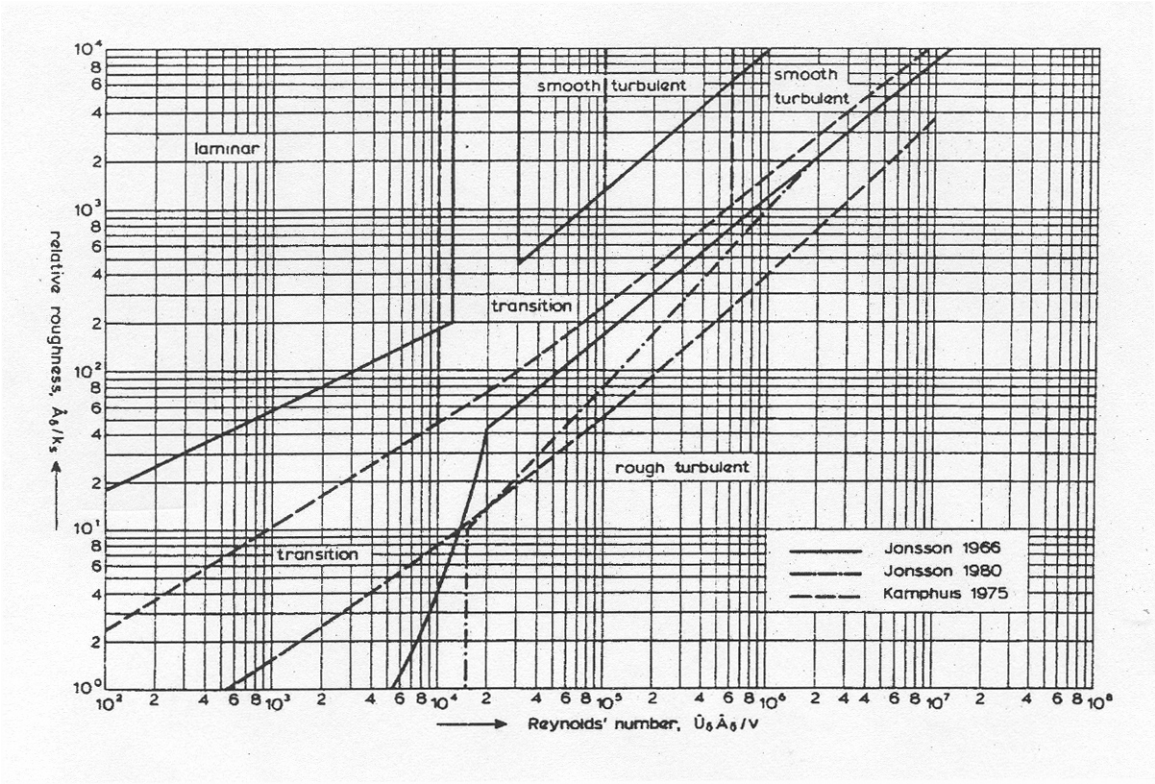

Figure 2-4 Hydraulic regimes for wave motion (Van Rijn, 1993)

The eddy viscosity varies during the wave cycle since the velocity gradient and the shear stress are not in phase. A detailed description can be found in Nielsen (1992).

Streaming

The water motion of waves is different from a purely oscillating motion: the flow is not horizontally uniform cf. $U_\delta = \hat{U}_\delta \sin(\omega t - kx)$. For waves, the boundary layer thickness varies in the wave direction, which is not the case for a purely oscillating motion.
The displacement thickness is defined as (Fredsøe and Deigaard, 1992):

$$U_\delta \delta^* = \int_0^\delta (U_\delta - U) dz \tag{2-44}$$

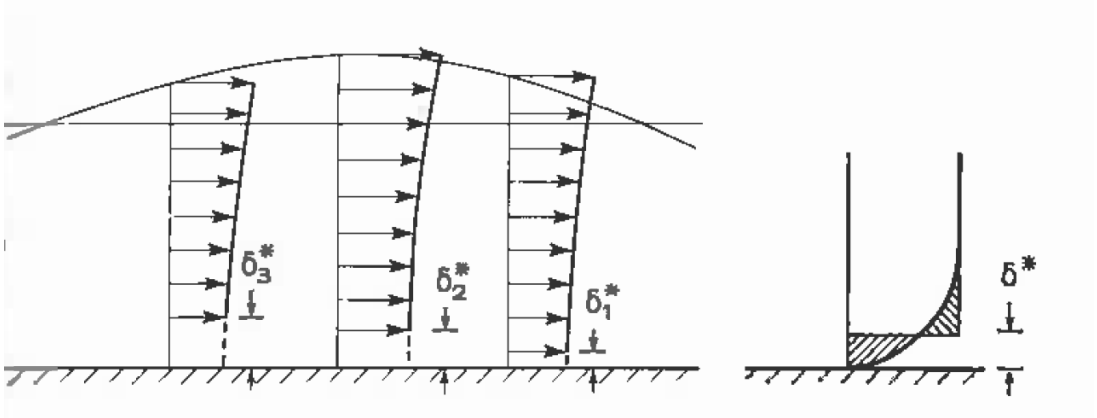

Figure 2-5 Variation of the displacement thickness and its definition

The continuity condition requires that a vertical velocity exists and can be calculated as:

$$W_\delta = \frac{\partial}{\partial x}(U_\delta \delta^*) \tag{2-45}$$

or:

$$W_\delta = -\frac{\partial}{\partial x}(\int_0^\delta (U - U_\delta) dz) = \frac{1}{c}\int_0^\delta \frac{\partial}{\partial t}(U - U_\delta) dz = \frac{-(\tau_b - \tau_\delta)}{\rho c} \tag{2-46}$$

The vertical velocity at the top of the boundary layer (W_δ) is downward when the flow is positive (same direction as the direction of the wave propagation) and upward when the flow is negative. This induces a positive shear (flow).
Fredsøe and Deigaard (1992) used this expression to derive the time-averaged shear stress at the bed due to streaming (for a laminar boundary layer):

$$\overline{\tau}_b = \rho \frac{\pi}{2} \frac{\delta_w}{L} \hat{U}_\delta^2 \tag{2-47}$$

For turbulent streaming the shear stress is about 50% smaller (Brøker, 1985). A mean Eulerian flow will be experienced near the bottom. This was first shown by Longuet-Higgins (1953), who derived the Eulerian net current at the edge of the boundary layer:

$$U_{s,\delta} = \frac{3}{4} \frac{\hat{U}_\delta^2}{c} \tag{2-48}$$

with c the wave celerity (=L/T).
Davies & Villaret (1998) compared experiments and concluded that the mean Eulerian flow is reduced for rough turbulent flow. When waves are asymmetric, also the turbulence intensity is asymmetric, which gives a residual current. This current is in offshore (against wave propagation) direction for plane bed flow (transition zone). For a rippled bed the shedding of eddies over the ripple crests reduces the streaming. They concluded that Eq.2.48 overestimates the drift for rough and rippled beds in the rough turbulent regime (especially for asymmetric waves) and underestimates the drift for wave conditions in the transitional flow. Since this drift results in net sediment transport, also the sediment transport is over- or underestimated.

2.2.4 Wave-current interactions

Waves will cause an augmentation of the roughness felt by the current, described with an apparent bed roughness $k_a=\alpha k_s$ ($\alpha>1$). This is offset by wave action at the bed which reduces the current related shear stress. Also the shape of the velocity profile changes: the near bed velocities are lower both for a following as for an opposing wave; for following waves the near surface currents decrease, while they increase for opposing waves (Nieuwjaar & van der Kaaij, 1987). Klopman (1994) carried out detailed experiments for different kind of waves.

2.2.5 Shields parameter and mobility parameter

Two important parameters in this thesis are the Shields parameter (θ) and the mobility parameter (ψ). The Shields parameter is the ratio of the shear force on a sediment particle to the force on the particle due to its (submerged) weight:

$$\theta = \frac{\tau}{(\rho_s - \rho)gd} \tag{2-49}$$

with ρ_s and ρ the density of the sediment and water respectively and d the diameter of a particle.
Since this requires knowledge of the shear stress acting on the bed, also the mobility parameter is often used, which does not require shear information:

$$\psi = \frac{\hat{U}_\delta^2}{(s-1)gd} \tag{2-50}$$

with $s = \rho_s / \rho$

Sediment will start moving if the critical Shields stress is exceeded (θ_{cr}). Ripples will be formed. This occurs for Shields parameters up to 0.8 – 1, or for a mobility parameter up to ~250. If the flow velocity increases further the sediment transport mechanism will be sheet flow (without ripples).

3 Physical experiments: scaling effects and wave flume set up

When you can measure what you are speaking about and express it in numbers, you know something about it; but when you cannot express it in numbers, your knowledge is of meagre and unsatisfactory kind; it may be the beginning of knowledge, but you have scarcely in your thoughts advanced to the state of science, whatever the matter may be.
LORD KELVIN

3.1 Introduction

Many experiments have been done in the past in situ, in wave flumes and in wave tunnels. These experiments have given insight in the processes of shear stress, turbulence and sediment entrainment. Numerical models were improved with this new knowledge. Most collected data are the result of a combination of processes (e.g. net sediment transport rates are a result of a velocity profile and a concentration profile, the concentration profile is due to shear near the bottom, turbulence). When models do not predict the sediment transport rate correctly, it is often difficult to identify the reason and to improve the model. Recent developments in instrumentation now make it possible to measure the driving processes (such as turbulence in turbid water, instantaneous concentration profiles, velocities in the sheet flow layer) with greater precision. New scientific experiments should focus on these basic processes.

The experimental facilities in laboratories allow control of the boundary conditions (wave action, net discharge and type of sediments) and instruments can be positioned relatively simply. In situ, the circumstances at the bed are difficult to control. However, most facilities cannot reproduce in situ conditions owing to their limited size (wave flumes) or because they only reproduce a uniform horizontal movement of the water (water tunnels).

The experimental work in laboratories can be divided into two categories: the study of an in situ problem and experiments to resolve scientific questions. When studying in situ problems (e.g. harbour-design, beach problems, coastal structures) all processes have to be simulated together and depend on each other (currents, waves, sediment transport, changing boundary conditions). There are also some important disadvantages: scale effects, huge cost and inflexible. A combination of a physical model with a numerical model may solve some of these problems. The physical model can be used to improve the equations in a numerical model or to calibrate it. The numerical model can then be used to model different cases (e.g. different layouts of the harbour).
For the scientific study of physical processes usually only one parameter is varied in each experiment. The influence of parameters is examined by variation of the parameters. Scale effects occur due to size limitations in laboratory facilities. Since there is still a big lack in

the understanding of the scale effects and the necessary interpretation of the results, scale effects will be examined first.

3.2 Laboratory scaling of wave induced sediment transport

However, engineers do not appear to care that specialists in sediment transport have declared that the movable-bed scale models are wrong; so, just like the bumblebee who goes on flying even though it has been declared aerodynamical impossible for him to do so, engineers keep using the movable-bed scale model, and most of the time with great success.
LeMéhauté, 1976

Some questions need to be answered when using physical models:

- Can measured data in wave flumes, in which the flow conditions are usually laminar or rough turbulent (because of the presence of steep ripples) be related to the field situation where the bottom is smooth because the ripples are washed out ?
- What are the effects of wrong scaling of the main transport mechanism (shear stress, turbulence, vorticity) ?
- Are there any relations to account for the scale effects when relating the experimental results to field situations?

Some questions will be answered using the basic scale relations (literature) and a developed numerical model (described in Chapter 6). Calculations are done for the prototype (nature) and the physical model of this situation. A comparison of these results gives information about the scale effects.

Two types of physical models can be distinguished: fixed-bed models and movable-bed models. Fixed-bed models are also called hydrodynamic models, although in both the hydrodynamic aspects are important. Only movable-bed models will be considered in this thesis.

3.2.1 Hydrodynamic aspects of physical modelling

From the Navier-Stokes equations for short waves (h/L>1/20) some scaling laws can be derived (Hughes, 1993):

- short wave models cannot be distorted geometrically (horizontal scale factor should be equal to the vertical scale factor),
- the Froude number ($V/\sqrt{gh}$) should be the same in model and prototype (from the gravity term),
- the Strouhal number (L/VT) should be the same in model and prototype (from the acceleration term),

- the Reynolds number (VL/ν) should be the same in model and prototype (from the viscosity term),
- the Euler number ($p/\rho V^2$) should be the same in model and prototype (from the pressure term).

If the Froude condition is fulfilled, all other conditions are fulfilled automatically except the Reynolds condition. With the Strouhal condition, the time scale can be calculated ($N_V = \sqrt{N_L}$ *or* $N_T = \sqrt{N_L}$). N is the ratio of the prototype scale and the model scale. Now, all parameters are modelled correctly, except the viscosity. If the Reynolds condition should be fulfilled, one is obliged to work on a large scale (near prototype). However, the Reynolds condition is less important than the Froude condition since the viscosity is mostly relatively small (for turbulent conditions). In a water tunnel, it is possible to work on a large scale, but other disadvantages have to be considered (see chapter 5).

A turbulent rough boundary layer will be modelled correctly if the roughness scale is the same as the geometrical length scale ($N_{ks}=N_L$) (Hughes,1993):

With $\hat{\tau}_0 = \frac{1}{2}\rho f_w \hat{U}_\delta^2$ and $f_w = 0.47(\frac{k_s}{\hat{A}_\delta})^{\frac{3}{4}}$ the scale of the shear stress can be calculated: $(N_{\tau_0})_{wave} = (N_L)^{\frac{1}{4}}(N_{k_s})^{\frac{3}{4}}$. But the Froude conditions give $(N_{\tau_0})_{wave} = \frac{N_F}{N_L^2} = N_L$. This is only posible is $N_{ks}=N_L$. (i.e. the size of the roughness elements (ripples, sand grains) has to be scaled with the length scale (e.g; wavelength or water depth)

3.2.2 Basic scale relations and models for sediment transport

From a dimensional analysis of the sediment transport problem five dimensionless constants can be derived which have to be the same in the physical model and in nature (Kamphuis, 1985):

- grain size Reynolds number: $\mathrm{Re}_* = \frac{u_* d}{\nu}$

- Shields parameter: $\theta = \frac{\rho u_*^2}{\gamma d}$

- Dimensionless density: $S_s = \frac{\rho_s}{\rho}$

- Relative length: $l_s = \frac{\lambda}{d}$

- Relative settling velocity: $V_{w_s} = \frac{w_s}{u_*}$

(with u_* :the shear velocity, d: the grain size, ν: the viscosity, ρ: the density, γ (=$g(\rho_s-\rho)$): submerged unit weight of sediment, λ: a typical length and w_s the settling velocity)
Because it is impossible to fulfil all of these conditions, some parameters have to be relaxed. Four different models can be considered (Kamphuis, 1985):

Model	Re_*	θ	S_s	l_s	V_{ws}
Best Model		x	x	X	
Lightweight model	x	x	x_1		
Densimetric Froude Model		x	x_1		
Sand Model			x		

x: satisfied

x_1: not satisfied but:$1.05<\rho_s/\rho<2.65$

Table 3-1 Types of scale models

In the *Best Model*, the grain size is scaled with the length scale, which results (except for coarse sediments) in particles with cohesive behaviour. The model can only be considered for relatively large grain sizes. The settling velocity will be scaled too strongly compared to the water velocity. Because the grain size Reynolds number is relaxed, viscous forces on sediment particles are scaled wrongly. This scale effect can become important if the flow is rather laminar (viscous).

The using of *lightweight materials* is usually avoided because of the wrong scaling of accelerations (Hughes, 1993):

$$N_{dV/dt} = N_{\gamma_s} N^{-1}_{\rho_s/\rho} > 1 \qquad (3\text{-}1)$$

(instead of 1, according to the Froude scaling).
The transport velocities are underestimated and the amount of sand that goes into suspension is overestimated. Because the length scale is scaled wrongly the bed forms are also modelled wrongly.
Kamphuis (1985) concluded: “The seriousness of these limitations of a lightweight coastal movable-bed model is now understood by most laboratories, and it has become unusual to see a coastal movable-bed model using lightweight material, unless the motion of the material is used to give only qualitative answers away from the surf zone.”
This makes coastal modelling with unsteady behaviour much more difficult than river modelling with quasi-steady behaviour.

The *Densimetric Froude Model* combines the disadvantages of the Lightweight model with the problems of the viscous forces in the Best Model.

It is more realistic to choose the particle size in such a way that a good resemblance between the relative movement of the particles in the field and in the wave flume is obtained. In the *Sand Model* the only requirement is that the material used in the model has the same relative density as in the prototype. The size of the grains can be chosen freely. If the settling velocity is Froude scaled ($N_{w_s} = \sqrt{N_L}$) the same relative movement of the sediment and water particles is obtained. Dean (1985) stated that this also scales the initiation of movement well. However the Shields parameter will be scaled too strongly:

$$N_\theta \overset{(1)}{=} \frac{N_\tau}{N_\gamma N_d} \overset{(2)}{\approx} \frac{(N_L)^{1/4}(N_d)^{3/4}}{N_d} = \left(\frac{N_L}{N_d}\right)^{1/4} \qquad (3\text{-}2)$$

Eq. (1) in 3.2 follows from the definition of the Shields parameter, (2) is calculated with $\tau=0.5\rho f_w(U_\delta)^2$, assuming that the friction coefficient $f_w \sim(k_s/A_\delta)^{3/4}$ (e.g.Kamphuis,1985), the roughness height $k_s \sim d$ and $N\gamma=N\rho=1$.
This can have important consequences for the bed concentration. Also the time of no erosion during a wave cycle will be exaggerated.
Since the length scale is larger than the grain scale, the Densimetric Froude condition is not fulfilled; the relative force on the grains is scaled too strongly. This causes a larger time during a wave period for which the Shields parameter is smaller than the critical Shield parameter and the transport for small velocities is underestimated.
Dean (1995) argues that actually the Densimetric Froude condition is fulfilled when the ratio between settling velocity and shear velocity is scaled correctly.

Hughes (1993) concludes that the Sand Model is useful for the modelling of sediment transport, but the evaluation of scale effects should be done, preferably by the use of scale series or by comparison with in situ measurements. If the prototype is scaled with a series of different scales, conclusions can be made about the effect of the scale, and these conclusions can be extrapolated to the prototype scale.

The distortion of the grain size scale also causes a wrong scaling of the mobility parameter ($\psi = U_\delta^2/(s-1)gd$) and thus also a wrong scaling of the ripple dimensions. If the bedforms in the model differ too much from the expected bedforms in the prototype, the "Best Model" has to be reconsidered (see example below).

The Reynolds parameters are also scaled wrongly, causing a different type of flow. Drift currents due to waves (see Chapter 2) will be scaled wrongly (e.g. Davies and Villaret, 1998). This indicates already that in fact only rough turbulent bottoms can be considered when one wishes to scale appropriately, because then the viscosity can be ignored and the type of flow

does not change too much. Sheet flow conditions can only be studied in large scale facilities or in oscillating wave tunnels (also because ripples will be formed in the small scale model, see example).

It can be concluded that the type of flow can change completely after scaling (smooth turbulent becomes rough turbulent or laminar). Because the type of flow and the bed forms are important for the transport of sediment (even for its direction!), this has to be avoided. Literature makes clear that there are no realistic alternatives. One has to take care of all these effects when bringing together experimental results for finding trends and relations.

Example (using the Sand Model)

Consider a wave with a significant wave height of 2m, a period of 7s, a mean water depth of 8m and a bed covered with sand with a diameter of 300μm. To simulate these conditions in a typical wave flume, the length scale (N_L) has to be at least 10. This results (with $N_L \approx 13$) in a wave with a significant wave height of 15cm, a period of 2s, a mean water level of 60cm and a bed covered with sand with a diameter of 125μm (Froude scaling of the settling velocity). Using the generally accepted formulae to calculate sediment transport parameters (Van Rijn(1993), Fredsøe et al.(1992)) Table 3.2 can be obtained:

	field	model	scale ratio
wave height H (m)	2	0.15	13
wave period T (s)	7	1.91	3.6
water depth h (m)	8	0.6	13
orbital radius A_δ(m)	0.97	0.07	13
orbital velocity U_δ (m/s)	0.87	0.23	3.6
Reynolds number Re (-)	840000	16800	50
grain size d_{50}(μm)	300	125	2.4
settling velocity w_S (m/s)	0.044	0.012	3.6
Shields parameter θ(-)	0.75	0.23	3
ripple height Δ(cm)	0.2	1	0.2
ripple length λ(cm)	8.4	8	1
grain size Reynolds number Re_*(-)	18.4	2.7	7
type of flow	transition/ smooth	transition/ rough	

Table 3-2 Scaling of a near sheet flow problem

This leads to a totally different situation in the model. In the physical model the presence of ripples will cause vortices in which the sediments are caught. When the flow reverses, the sediment cloud travels over the ripple crest. If the waves are asymmetric or a small current in the direction of the waves is present (e.g. tidal current or drift currents), a bigger cloud will be formed when the velocity is forward (and thus relatively higher), being transported by the backward velocity. The net sediment transport will be backward. In the field situation the bed is almost plane, resulting in a totally different kind of transport (sheet flow), with possibly forward transport.

3.2.3 Numerical investigation of different scale models

With a numerical model, both the prototype ("Nature"-model) and the scale model can modelled. The numerical model is typically a CFD-model (Computational fluid dynamics-model). This model resolves the basic flow equations. Calibration of these models with measurements is necessary. In Chapter 6 such a model is constructed and validated, using the results of experiments in the Delta Flume (Chapter 4). Since this model was validated with measurements described after the discussion about scale effects, this model is used already for this chapter. Even if the model would be badly calibrated, it can be used to identify qualitatively scale effects.

Simulations are done with this numerical model both for natural situations and for the physical models of the corresponding case. With the result of these calculations the validity of the different physical models can be checked. Because it is generally accepted that the Lightweight and the Densimetric Froude model gives, bad results, only the Best Model and the Sand Model are compared.

If sheet flow occurs in the field, the scaling will result in a rippled bed in the flume. So this kind of cases should not be examined: scaling is impossible. Thus only rippled beds are considered. Because the numerical model is not able to calculate the shape of the ripple, some assumptions have to be made. Different expressions exist to relate the ripple length (λ) and ripple height (Δ) to e.g. the wave orbital radius, the mobility parameter: $\psi = U_\delta^2 /(s-1)gd$, or the Shields parameter. If the shear stress is not too big the maximum slope of the ripple can be equal to the angle of repose, but for high values of the Shields parameter (θ>0.8) or the mobility parameter (ψ>250), the ripples will start to wash out.

The following expressions (Nielsen, 1992) will be used because they are validated with a lot of measurements:
For waves in a flume:

$$\frac{\lambda}{A_\delta} = 2.2 - 0.345\psi^{0.34} \tag{3-3}$$

$$\frac{\Delta}{A_\delta} = 0.275 - 0.022\psi^{0.5} \tag{3-4}$$

For waves in nature:

$$\frac{\lambda}{A_\delta} = \exp\left(\frac{693 - 0.37\ln^8\psi}{1000 + 0.75\ln^7\psi}\right) \tag{3-5}$$

$$\frac{\Delta}{A_\delta} = 21\psi - 1.85 \tag{3-6}$$

The geometry used is a parabola:

$$y = \frac{4\Delta}{\lambda^2}x^2 - \frac{4\Delta}{\lambda}x + \Delta \tag{3-7}$$

(in which x and y are respectively the horizontal and vertical co-ordinates)

Since it is not possible to use the Best Model for fine sediments (as also the example will show), a distinction will be made between fine and coarse sediments. With the simulations for the fine sediments the Sand Model can be examined. The Best Model is examined with the simulations for coarse sediments.

Fine sediments

In Table 3-3 a realistic situation is scaled with the Sand Model (with the grain size scaled in order to have a Froude scaled settling velocity) and the Best Model. It is clear that sand particles with a grain size of 35μm do not exist and thus the Best Model cannot be used. For the Sand Model the length scale is 6, the ripple height is only scaled with a factor 3, and the ripple length with a factor 4.

	Prototype	Sand Model	Best Model
water depth(h)[m]	8	1.3	1.3
wave height(H)[m]	1.1	0.2	0.2
wave period[s]	5	2	2
orbital velocity($\hat{U}_\delta$)[m/s]	0.355	0.145	0.145
grain size (d)[mm]	0.210	0.115	0.035
settling velocity (w_s) [m/s]	0.025	0.01	-
mobility parameter(ψ)	37	11	-
ripple length (λ) [m]	0.256*	0.066	-
ripple height (Δ) [m]	0.03*	0.01	-

Table 3-3 Scaling of a nature situation with fine sediments (geometrical scale factor = 6)

(*: measured values during the wave tunnel experiments, calculated values are resp 0.28m and 0.035m)

The "nature" situation is chosen to be comparable with an experiment in the wave tunnel of Delft Hydraulics (Ribberink et al., 1989). In Chapter 6 the obtained (numerical) results are compared with the measurements.

In Figure 3-1 the movement of the sediment cloud in "Nature" and in a scaled situation, with scaling using the Sand Model-rules can be compared during half a wave cycle ($U_\delta = \hat{U}_\delta \sin(\varphi)$, $\varphi=\omega t$) together with velocity vectors. Since the mobility parameter ψ is scaled with $(N_U)^2/N_d = N_L/N_d > 1$, and $\lambda / \hat{A}_\delta$ increases if ψ decreases, $\lambda / \hat{A}_\delta$ will be too big in the Sand Model (1.4 instead of 0.9). So the sediment cloud reaches the next ripple crest earlier in Nature than in the (Sand) Model. Also the shape of the travelling cloud is somewhat different, because the sediment cloud needs more time to be swept over the first crest (at flow reverse) in the Sand Model (probably because the ripple is somewhat steeper). At $\varphi=0°$ and 30°, the travelling cloud of the previous half cycle is still distinguishable in the Sand Model, which is not anymore the case in Nature, where it merge with the new cloud that starts travelling. The new cloud starts travelling later in the Sand Model. At $\varphi=90°$ the travelling cloud already passed the next ripple crest in Nature, but not yet in the Sand Model. But in Nature the travelling cloud is caught by the new vortex behind the ripple crest when passing the next ripple crest between $\varphi=120°$ and 150°, while in the Sand Model the travelling cloud is swept over the vortex and continues travelling.

In Nature the old cloud is caught by the new-formed vortex, while in the Sand Model the cloud is swept over the vortex, because of the strong positive velocities above the vortex.

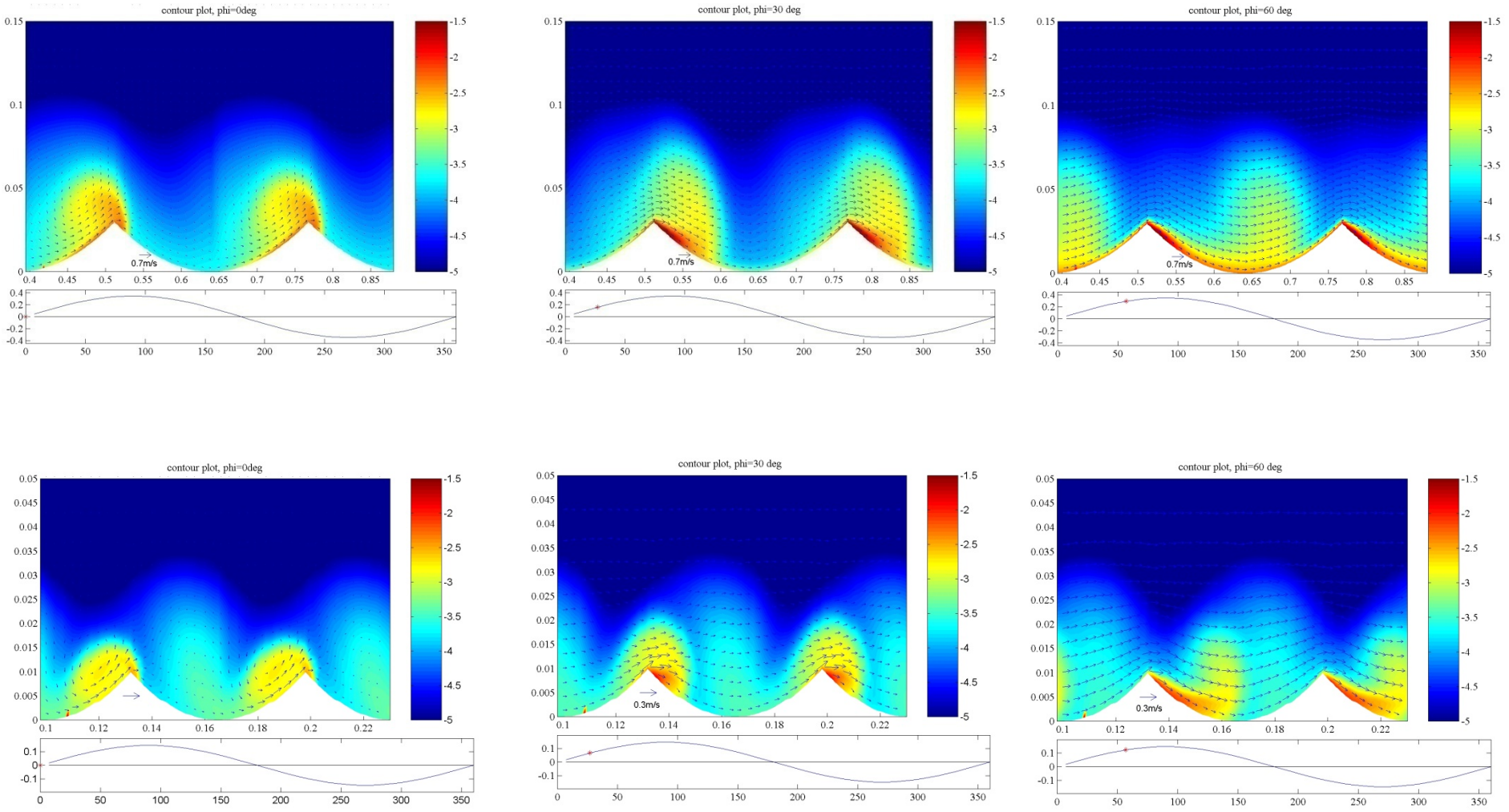

Figure 3-1a Concentrations (m^3/m^3, log-scale) for Nature (top) and Sand Model (bed) (0º;30º;60º)

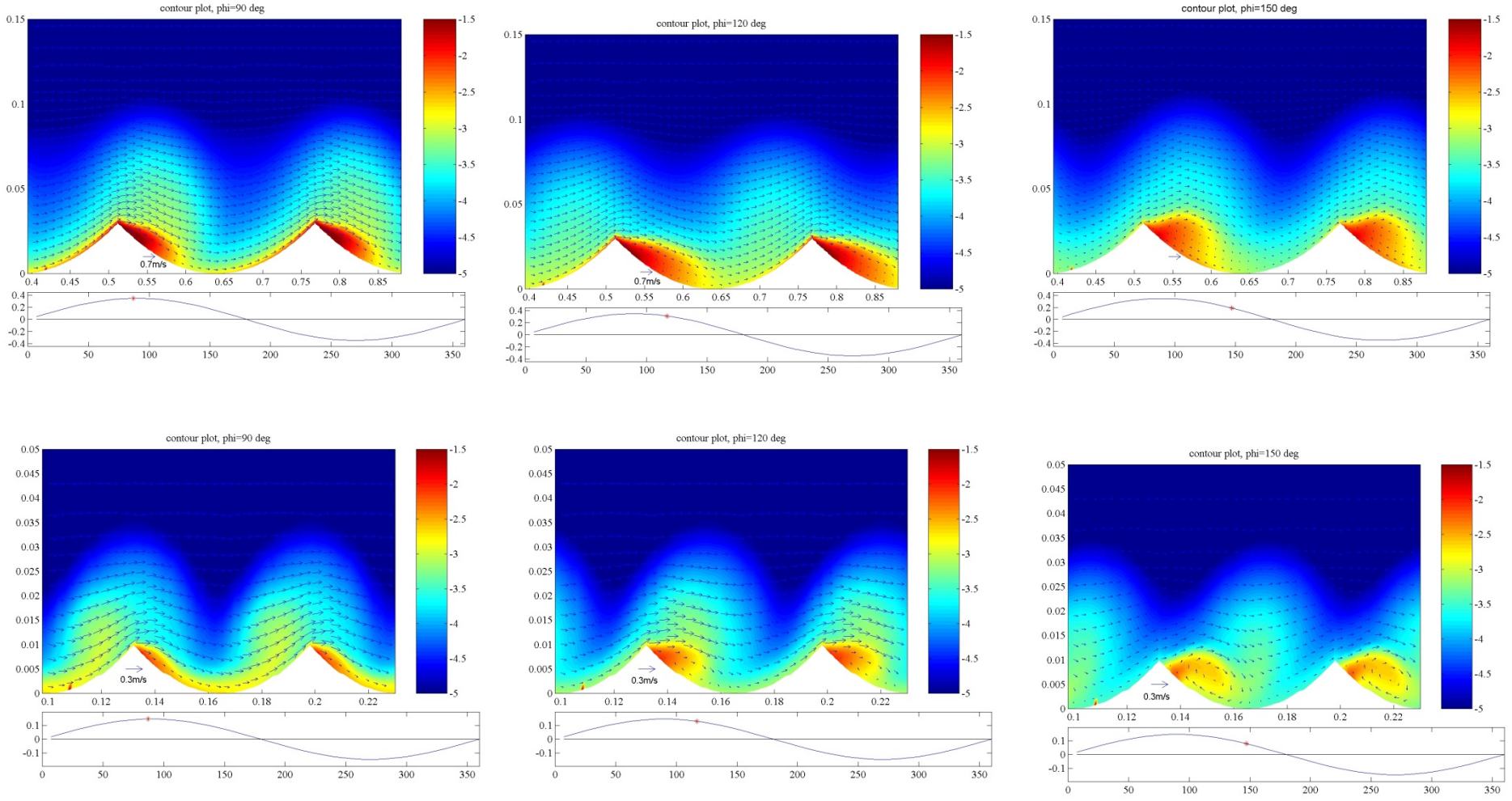

Figure 3-1b Concentrations (m^3/m^3, log-scale) for Nature (top) and Sand Model (bed) (90º;120º;150º)

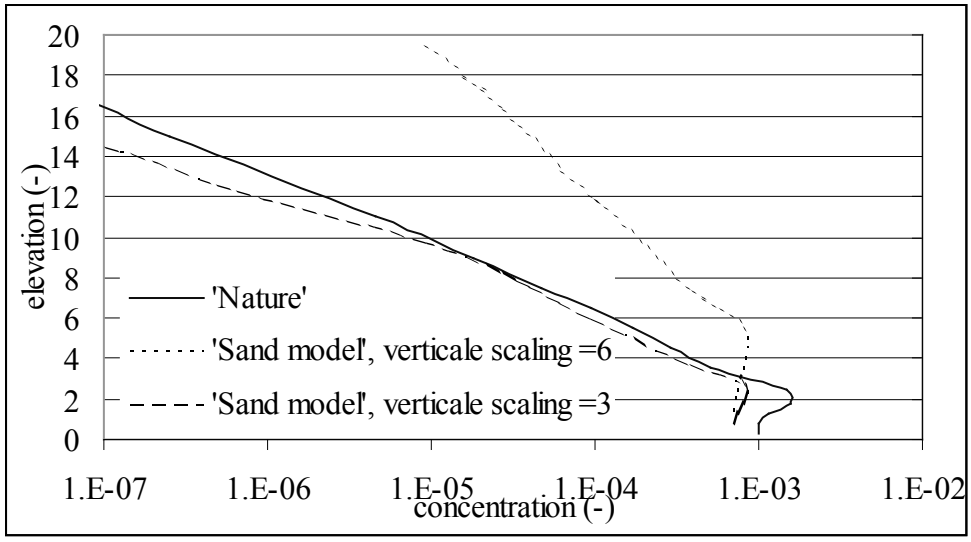

Figure 3-2 Comparison of the mean concentration in nature and Sand Model

In Figure 3-2 the time averaged and horizontally averaged concentration profiles are visible. The elevation of the Sand Model is scaled resp. with a factor 6 (expected length scale, Table 3-3) and with a factor 3 (ratio of the ripple heights). Scaling with the length scales of the ripple heights gives much better results.

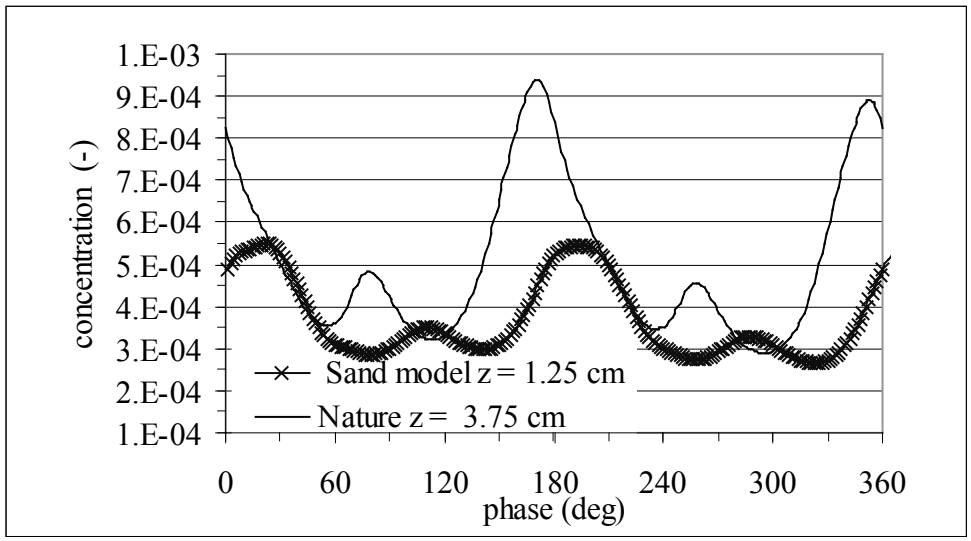

Figure 3-3 Comparison between the horizontal averaged intra wave concentrations at the same (scaled) height between 'Nature' and Sand Model: just above crest level

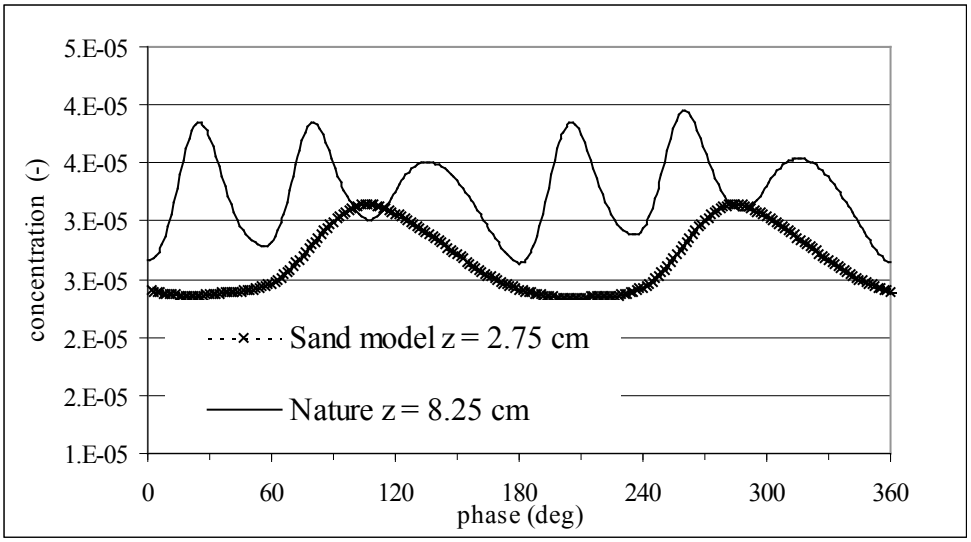

Figure 3-4 Comparison between the horizontal averaged intra wave concentrations at the same (scaled) height between 'Nature' and Sand Model: at a level of 2 times the ripple height above the crest

From Figure 3-3 it can be seen again that in the Sand Model the sediment cloud is swept over the crest later than in 'Nature', giving a phase lag in concentration at the level just above the crest. Also the second smaller peak (from the new sediment cloud being formed) is later.
Figure 3-4 shows that at higher levels, in 'Nature' more variation due to the passing of the sediment clouds is visible. The elevation of the sediment cloud is thus scaled too strongly.
The near bed velocity is more ahead of the free stream velocity in the Sand Model (zero at 155˚ and 335˚) than in nature (zero at 165˚ and 345˚), which may be due to a smaller Reynolds number (e.g. the phase shift of 45° for laminar flows, which decreases with increasing turbulence).

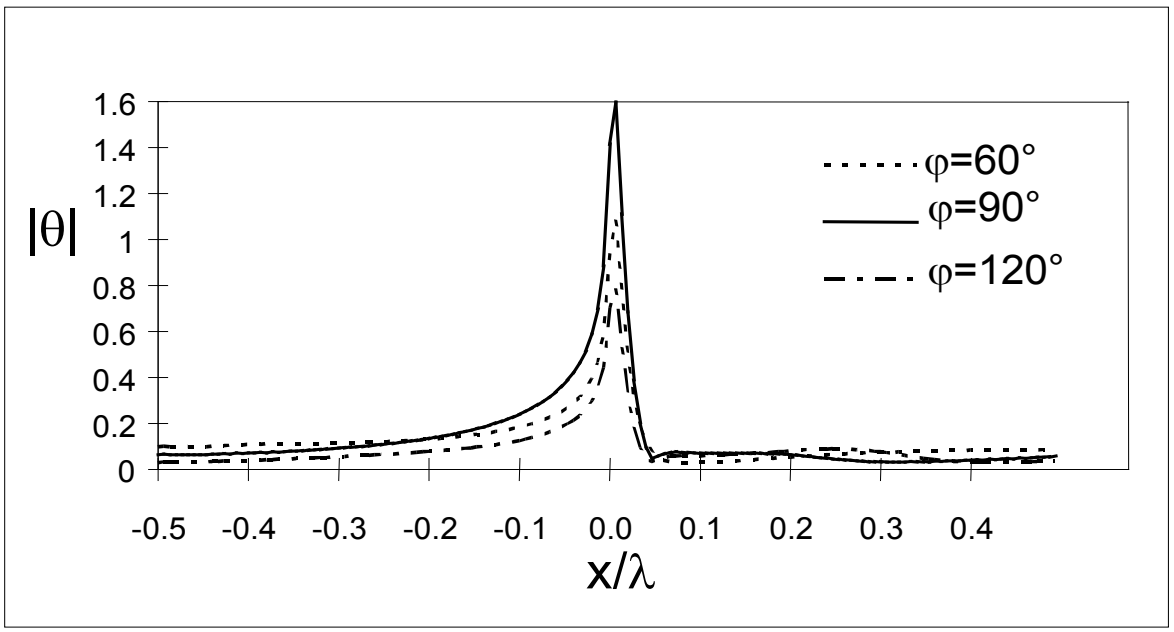

Figure 3-5 Shields parameter for different time steps over the ripple (nature)(φ: phase, x horizontal distance from the ripple crest)

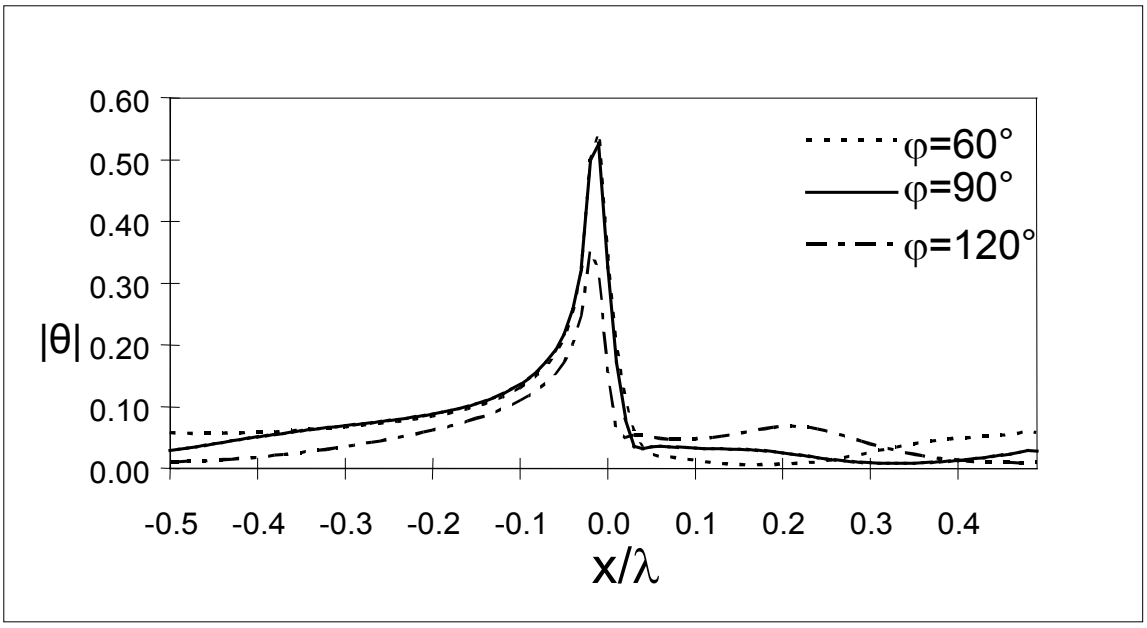

Figure 3-6 Shields parameter for different time steps over the ripple (Sand Model)

From Figure 3-5 and Figure 3-6 the reason for the smaller concentration near the bed in the Sand Model can be seen. The Shields parameter is underestimated by a factor 1.6/0.6 (comparison of Shields parameter in Figure 3-5 and Figure 3-6 for φ=90°). The direction of the shear stress changes behind the ripple crest (because of the negative velocities near the bed in the vortex), which can be seen by the sudden change in the gradient of the Shields

parameter (where the sign of the shear stress changes). In the Sand Model the vortex is formed earlier and is somewhat stronger.

Best Model (for coarse sediments)

To be able to examine the Best Model, tests are done with coarse sediments.

	Nature	Sand Model	Best Model
water depth(h)[m]	6.5	1.3	1.3
wave height(H)[m]	0.8	0.14	0.14
wave period[s]	4.5	2	2
orbital velocity(U)[m/s]	0.32	0.145	0.145
grain size (d)[mm]	0.6	0.230	0.115
settling velocity (w_s) [m/s]	0.07	0.03	0.01
mobility parameter(ψ)	12	6	12
ripple length (λ) [m]	0.33	0.072	0.066
ripple height (Δ) [m]	0.05	0.01	0.01

Table 3-4 Scaling of a prototype situation 'nature' with coarse sediments (geometrical scale factor = 5)

In the Best Model the parameters are equal to the parameters of the previous discussed Sand Model for fine sediments, so the formation and movement of the sediment cloud for the Best Model can be seen in Figure 3-1.
From calculations for "Nature" and the Sand Model (not shown, since almost no sediments are in suspension), it can be seen that both in the Sand Model and in Nature, the sediment cloud doesn't move over the ripple crest due to the high settling velocity. However in the Best Model the sediment cloud travels over the crest because the settling velocity is scaled too strongly compared with the water velocity.
As expected, the Shields parameter is scaled well with the Best Model (Figure 3-7).

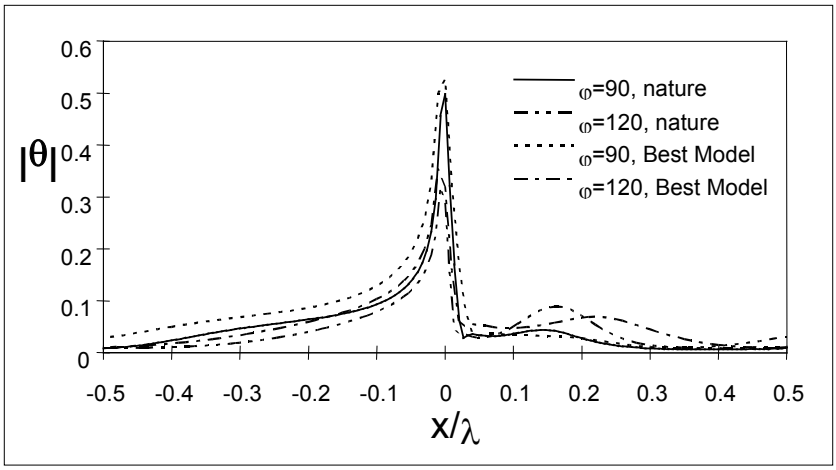

Figure 3-7 Comparison of the Shields parameter for nature and Best Model

It can be concluded that the Best Model gives worse results than the Sand Model due to the wrong scaling of the settling velocity.

3.2.4 Conclusions

If large waves (in situ) are modelled in a wave flume the characteristics of sediment transport (e.g. shear stresses) change completely. For this reason, the resulting sediment transport in the wave flume is not representative for the sediment transport in situ (no scaling can be done).

From calculations of the velocity and the sediment concentration above ripple crests, it may be concluded that the Sand Model gives better results than the Best Model. Better results are obtained if the elevation is scaled relative to the ripple heights in stead of the actual length scale. The excursion of the sediment cloud is different in the model because of the wrong scaling of the ripple length. It seems that physical models cannot be used to give quantitative results. However, physical experiments remain most interesting to examine some sub-processes in more detail and to know something about the physics behind these processes.

The more we know of the law of sediment transport (and we still have a lot to learn), the more the scientists of the profession become convinced that similitude is impossible.

3.3 Wave flumes

A wave flume is a (relatively narrow) channel with a moving paddle to move the water and with at the end a structure to control reflection or to simulate a beach. Since the flume has no roof (or at least the water should not touch the roof) waves are progressive, with crests and troughs (and thus with vertical velocities). These vertical velocities don not occur in the wave tunnel, which can be a problem to simulate sediment transport correctly.

The mechanism to generate waves and to avoid reflection is never able to simulate sea conditions perfectly. Large waves, secondary motions, decreasing water level and other

problems will occur and should be examined carefully. For this study, experiments are done in the wave flume of Flanders Hydraulics Research Division and the Deltaflume of Delft Hydraulics. The flume of Flanders Hydraulics Research Division gave the possibility to study in more detail problems that can occur when generating waves in a flume and master students used afterwards the flume to study the initiation of motion of sand particles. Because the intended tests are used for the study of waves on a horizontal bed, it was important to minimise reflection end undesired second harmonics.

The method for the generation of regular waves is described in literature but measurements show that this is not enough to get the desired result. The wave amplitude will change with location of measuring, the spectrum shows important higher harmonics. These anomalies are not acceptable for the study of sediment transport because they can cause considerable net transport of sands and different concentration profiles. In the next paragraph some of the problems are discussed.

3.3.1 Construction of the wave flume of Flanders Hydraulics Research Division

The flume is 35m long, 0.7m wide and 0.85m high. Waves can be generated with a piston-type wave board. A following current flows through an inlet in the bed of the flume, just in front of the wave board. Special attention was paid to damp oscillations at the downstream end of the flume. The desired water level can be controlled at the end of the flume with a gate.

3.3.2 Wave paddle

The wave paddle is of the piston type (translation movement), driven by an electrical engine, steered by a central computer. The movement is positional steered with a maximal horizontal displacement of 52cm.

The ratio of the excursion of the wave paddle and the wave height can be obtained by integrating the Laplace equation, with the necessary boundary conditions. The first order solution is (Dean & Dalrymple, 1991)

$$m = \frac{H}{S_0} = \frac{4\sinh^2 kh}{\sinh 2kh + 2kh} \tag{3-8}$$

where H (m) is the wave height, S_0 (m) the excursion of the wave paddle, h (m) the water depth and k(m^{-1}) the wave number.

If the water is relatively shallow, the equation can be simplified as $H/S_0=kh$ (e.g. a wave period of 2s, with a water depth of 0.5m gives a ratio of 0.8).
The movement of the wave paddle induces second order movements, which make the wave asymmetric (see §3.3.6.2).
Local disturbances at the wave paddle occur because the wave paddle does not follow exactly the water motion. A term should be added in the wave potential from which the wave height and velocity can be calculated:

$$\phi(x,z,t) = A\cosh(kz)\sin(kx - \omega t) + \cos(\omega t)\sum_{n=1}^{\infty} C_n e^{-k_n x}\cos(k_n z) \qquad (3\text{-}9)$$

($\omega_n^2=-gk_n\tan(k_nh)$, n=1,2,...)
The last term represents a standing wave, which is damped out with distance from the wave paddle.

3.3.3 Generation of regular waves

Moving the wave paddle with a frequency equal to the desired wave frequency and an excursion calculated with Eq. 3.8 generates regular waves. To avoid long waves, the paddle excursion and frequency should be increased slowly until the desired values are reached.

3.3.4 Generation of irregular waves

When generating irregular waves, it is important that all necessary frequencies occur with the exact amplitude (given by the spectrum, e.g. JONSWAP). The phases between the wave components should be random. Principally, the signal should not repeat itself during an experiment.

The basic idea (Monbaliu, 1986) is to calculate a spectrum (of the position of the piston) and to generate corresponding random phases. The achieved signal is generated in the flume and the obtained wave height is measured. The measured spectrum is compared with the original scaled spectrum. The original (scaled) spectrum is then for each frequency separately, corrected using the difference between spectra multiplied by a feed back parameter (smaller than 1, in order to avoid oscillations). The method is implemented on the steering computer of the wave flume of Flanders Hydraulics Research Division.

In Figure 3-8 the spectra measured after the first iteration step and the seventh iteration step are compared with the desired spectrum (H_{rms}=5cm, T_p=2s, h=0,6m).

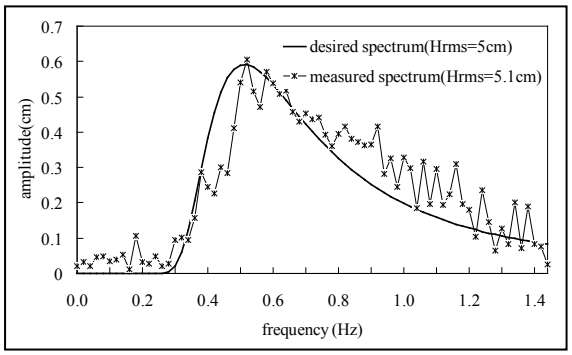

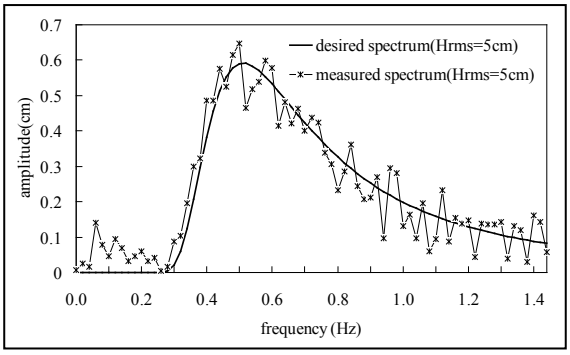

Figure 3-8 a) Wave spectrum after one run *b) Wave spectrum after 7 runs*

The first spectrum shows that at the first trial, too much energy is localised in the higher frequencies. After 7 iterations the energy is well distributed. The long waves are visible in the spectra (frequencies between 0 and 0.2 Hz).

3.3.5 Reflection

3.3.5.1 Definition and measurements

When a wave reaches a boundary it will be partly absorbed but also partly reflected. If the incoming wave can be described as:

$$\eta_I = \frac{H_I}{2}\sin(k_I x - \omega t) \tag{3-10}$$

then the reflected wave can be described as

$$\eta_R = \frac{H_R}{2}\sin(k_I x + \omega t + \varepsilon) \tag{3-11}$$

A summation of both components gives the water level as function of time and location:

$$\eta_t = \eta_I + \eta_R = (\frac{H_I}{2}\cos(kx) + \frac{H_R}{2}\cos(kx + \varepsilon))\cos(\omega t) + (\frac{H_I}{2}\sin(kx) - \frac{H_R}{2}\sin(kx + \varepsilon))\sin(\omega t) \tag{3-12}$$

If the wave is reflected completely, a standing wave can occur:

$$\eta = H\cos(kx)\cos(\omega t) \tag{3-13}$$

Some characteristics for standing waves can be derived:
Wave potential:

$$\phi = H\frac{g}{\omega}\frac{\cosh(kz)}{\cosh(kh)}\cos(kx)\sin(\omega t) \tag{3-14}$$

horizontal velocity:

$$u = H\frac{gk}{\omega}\frac{\cosh(kz)}{\cosh(kh)}\sin(kx)\sin(\omega t) \tag{3-15}$$

vertical velocity:

$$w = -H\frac{gk}{\omega}\frac{\sinh(kz)}{\cosh(kh)}\cos(kx)\sin(\omega t) \tag{3-16}$$

Locations with maximal wave height (2H) are called “antinodes”, locations with minimal wave height (0) are called “nodes”, between the two the movement of the water evolves from completely vertical to completely horizontal. The water particles do not follow anymore elliptic paths.

The conditions to get standing waves are obtained by comparing these equations with the boundary conditions (length of the flume).

A partly reflected wave can now be described as the sum of two standing waves (compare Eq.3.12 and Eq.3.13). The waves are called ‘partly standing waves’ and can be written as:

$$\eta_t = I(x)\cos(\omega t) + F(x)\sin(\omega t) \tag{3-17}$$

The envelope of this wave is obtained after time derivation:

$$[\eta_t(x)]_{\max} = \pm\sqrt{(\frac{H_I}{2})^2 + (\frac{H_R}{2})^2 + \frac{H_I H_R}{2}\cos(2kx + \varepsilon)} \tag{3-18}$$

The maximal amplitude is given as (with cos(2kx+ε)=1):

$$\eta_{t,\max} = \frac{H_I + H_R}{2} \tag{3-19}$$

The minimal amplitude is given as (with cos(2kx+ε)=-1):

$$\eta_{t,\min} = \frac{H_I - H_R}{2} \tag{3-20}$$

The horizontal distance between a point with maximal amplitude and a point with minimal amplitude is L/4.
The velocity can be calculated after derivation of the wave potential (Dean,1991):

$$u = -\frac{\partial\phi}{\partial x} = \frac{H_I}{2}\frac{gk}{\omega}\frac{\cosh(kz)}{\cosh(kh)}\cos(kx - \omega t) + \frac{H_R}{2}\frac{gk}{\omega}\frac{\cosh(kz)}{\cosh(kh)}\cos(kx + \omega t + \varepsilon) \tag{3-21}$$

These equations deliver methods to calculate the reflection coefficient. The reflection coefficient is defined as the ratio of the reflected wave height and the incoming wave height. This coefficient can be calculated if the minimal and maximal wave elevations are determined (measurements of water levels over a length L/4). Combining Eq.3.19 and Eq. 3.20 gives:

$$\kappa = \frac{H_R}{H_I} = \frac{\eta_{t,\max} - \eta_{t,\min}}{\eta_{t,\max} + \eta_{t,\min}} \tag{3-22}$$

where κ is the reflection coefficient (=H_R/H_I)
Another method uses 2 or 3 wave height measurements at fixed locations. Both amplitude and phase are measured (Hughes, 1993).

With Eq.3.21 it is possible to calculate the maximal orbital velocity in the flume:

$$u_{\max,part} = u_{\max,prog}(1+\kappa) \tag{3-23}$$

with:

$u_{max,prog}$: maximal orbital velocity for a progressive wave without reflection

$u_{max,part}$: maximal orbital velocity for a partly standing wave

The maximal orbital velocity increases due to reflection, causing higher sediment concentrations.

The water level for irregular waves can be written as:

$$\eta_t = \sum_{i=1}^{\infty} [a_{I_i} \cos(\Phi_{I_i} - \omega_i t) + a_{R_i} \cos(\Phi_{R_i} + \omega_i t)] \tag{3-24}$$

where $\Phi_{Ii}=k_ix+\varepsilon_{Ii}$ and $\Phi_{ri}=k_ix+\varepsilon_{Ri}$

The reflection coefficient can be determined for each component of the spectrum (assuming that there are no important bound higher harmonics). Many methods exist to calculate the reflection coefficient. The method of Goda and Suzuki (1976) is used by the author in the wave flume of Flanders Hydraulics Research Division.
If two wave probes at a distance of Δl measure the water levels, the first one will e.g. measure the water level described by Eq.3.24, the second one will registrate:

$$\eta_2 = \sum_{i=1}^{\infty} [a_{I_i} \cos(\Phi_{I_i} - \omega_i t + k_i \Delta l) + a_{R_i} \cos(\Phi_{R_i} + \omega_i t + k_i \Delta l) \tag{3-25}$$

or:

$$\eta_1 = \sum_{i=1}^{\infty} [\, A_{1_i} \cos \omega_i t + B_{1_i} \sin \omega_i t]$$
$$\eta_2 = \sum_{i=1}^{\infty} [\, A_{2_i} \cos \omega_i t + B_{2_i} \sin \omega_i t \tag{3-26}$$

with:

$$\begin{aligned} A_{1_i} &= a_{I_i} \cos \Phi_{I_i} + a_{R_i} \cos \Phi_{R_i} \\ B_{1_i} &= a_{I_i} \sin \Phi_{I_i} - a_{R_i} \sin \Phi_{R_i} \\ A_{2_i} &= a_{I_i} \cos(k_i \Delta l + \Phi_{I_i}) + a_{R_i} \cos(k_i \Delta l + \Phi_{R_i}) \\ B_{2_i} &= a_{I_i} \sin(k_i \Delta l + \Phi_{I_i}) - a_{R_i} \sin(k_i \Delta l + \Phi_{R_i} \end{aligned} \tag{3-27}$$

These are 4 equations and 4 unknowns for each component (a_{Ii},a_{Ri},Φ_{Ii},Φ_{Ri}). The solution of these equations results in:

$$a_{I_i} = \frac{1}{2 |\sin k_i \Delta l|} [(A_{2_i} - A_{1_i} \cos(k_i \Delta l) - B_{1_i} \sin(k_i \Delta l))^2 + (B_{2_i} - B_{1_i} \cos(k_i \Delta l) + A_{1_i} \sin(k_i \Delta l))^2]^{1/2}$$
$$a_{R_i} = \frac{1}{2 |\sin k_i \Delta l|} [(A_{2_i} - A_{1_i} \cos(k_i \Delta l) + B_{1_i} \sin(k_i \Delta l))^2 + (B_{2_i} - B_{1_i} \cos(k_i \Delta l) - A_{1_i} \sin(k_i \Delta l))^2]^{1/2}$$
$$\Phi_{I_i} = a \tan[\frac{-(A_{2_i} - A_{1_i} \cos(k_i \Delta l) - B_{1_i} \sin(k_i \Delta l))}{(B_{2_i} - B_{1_i} \cos(k_i \Delta l) + A_{1_i} \sin(k_i \Delta l))}]$$
$$\Phi_{R_i} = a \tan[\frac{(A_{2_i} - A_{1_i} \cos(k_i \Delta l) + B_{1_i} \sin(k_i \Delta l))}{(B_{2_i} - B_{1_i} \cos(k_i \Delta l) - A_{1_i} \sin(k_i \Delta l))}] \tag{3-28}$$

in which k_i the wavelength of component i, A_i and B_i are obtained from a Fourier analysis of the measured water levels. The equations contain a singularity for $\sin(k_i \Delta l)=0$ or $\Delta l/L_i=n/2$. Goda en Suzuki(1976) suggested following limitation to avoid (numerical) inaccuracy:

$$0.05 < \frac{\Delta l}{L} < 0.45 \tag{3-29}$$

They also suggest to measure not closer than one wavelength from the reflecting structure. A low energy content of a component will result in large errors because of the large noise to signal ratio.

Miche (1951) derived a theory to estimate the reflection coefficient of a plane soft coast with slope β. First the critical wave steepness is defined as:

$$(\frac{H}{L})_{crit} = (\frac{2\beta}{\pi})^{1/2} \frac{\sin^2 \beta}{\pi} \tag{3-30}$$

For wave steepnesses smaller than the critical steepness the reflection coefficient is equal to one, for steeper waves the reflection coefficient is given by:

$$\kappa = \frac{(\frac{H}{L})_{crit}}{\frac{H_0}{L_0}} \tag{3-31}$$

H_0 and L_0 are deep water values. It is clear that long waves are strongly reflected and that a steeper coast gives more reflection.

3.3.5.2 Wave absorbers (Hughes, 1993)

a) Passive wave absorbers

Generally it is accepted that the reflection coefficient in a wave flume should be smaller than 10%. The best results are obtained with gentle sloping coasts (e.g. with a slope of 1:10), made from porous material. For most flumes this would occupy too much of the length of the flume. The coast can be built with a wide range of materials like stones, screens of wire mesh, crushed rock. The ideal slope of a coast is parabolic: the incoming high waves feel a gentle slope, the wave height is reduced and the slope becomes slowly steeper the further the waves approach (and thus the smaller the wave height)
If it is not possible to use these kind of coasts (limitations in length, flexibility,…) also damping packages can be used. The length should be at least one wavelength, which makes it difficult to damp the longest waves. The packages give better results if they are put on a slope and if the absorption capacity is increased progressively (for the same reason as the benefits of a parabolic coast). Steep waves require material with high porosity, mild waves require a low porosity.

b) Active wave absorbers

In some flumes an active wave absorption is installed. This system can be used at the downstream site (requires two paddles) and/or at the wave generation site (only one paddle required). A pressure sensor is put in front of the paddle and the wave paddle compensates for the measured reflected wave (or anticipates the incoming wave at the downstream end of the flume). An active wave absorber on the wave-generating paddle can be useful if the coast cannot absorb the long waves. If the wave generating paddle reflects these long waves completely, a long standing wave will develop in the flume.

c) Results for the Flanders Hydraulics Research Division flume

Originally the wave damper consists of a wooden board with 25% gaps, covered with a thick cloth of horsehair, which was immersed in pitch. In front of the wave damper a rubber package was placed with a length of 1.4m. Regular waves were produced. The water depth was 45cm, no net currents were generated. It should be noted that the experiments are well reproducible. The reflection coefficient was calculated for the amplitude of the first harmonic. The following reflection coefficients were obtained:

	T=1s	T=2s	T=3s
H=5cm	2%	23%	23%
H=10cm	7.5%	28%	21%

Table 3.3 Reflection coefficients before improving the coast

The large reflection coefficient for T=2 can be explained by resonance at the end of the flume (in the basement). The oscillations in the basement with a period of 2s generate waves back in the flume. This is discussed in more detail in §3.3.6.1.

Because the damping packages are not sufficient, it was decided to construct a "beach" with a gentle slope (1:11), constructed with the same material.

The tests are redone for some cases. The reflection was reduced significantly and the reflection coefficient was small enough (less than 10%) for the target waves.

	T=1s	T=2s
H=10cm	2.5%	7.5%

Table 3.4 Reflection coefficients after improving the wave damper

For irregular waves the reflection coefficients are calculated for the improved wave damper per frequency (Figure 3-9). The reflection coefficients appear to be generally less than 10%, except for the long waves. The long waves are difficult to absorb but the reflection coefficient is also often exaggerated due to the large noise to signal ratio (since the "signal" is weak for the small wave components).

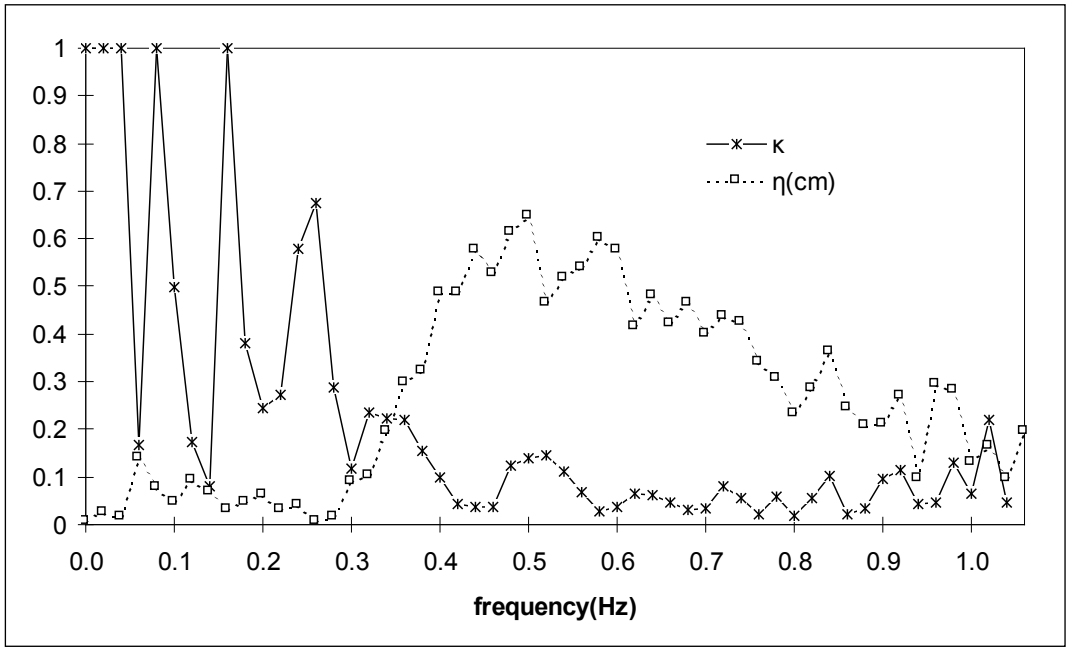

Figure 3-9 Reflection coefficient (κ) and amplitude (η) for the components of an irregular wave (H_s = 5cm, T=2s, h=60cm)

3.3.6 Higher and sub harmonics

The wave spectrum of a regular wave contains more peaks than the one expected peak at the generated wave frequency (e.g. Figure 3-10) Also the low and high frequencies contain energy. The energy at the low frequencies can be explained partly by a small continuous decrease of the water level during the tests (see §3.3.7.1), but most of the energy is explained by long waves travelling in the flume. Some of these long waves occur in nature and should be generated correctly if the sediment balance is important (long wave induced net sediment transport) other long wave components are spurious and should be reduced.

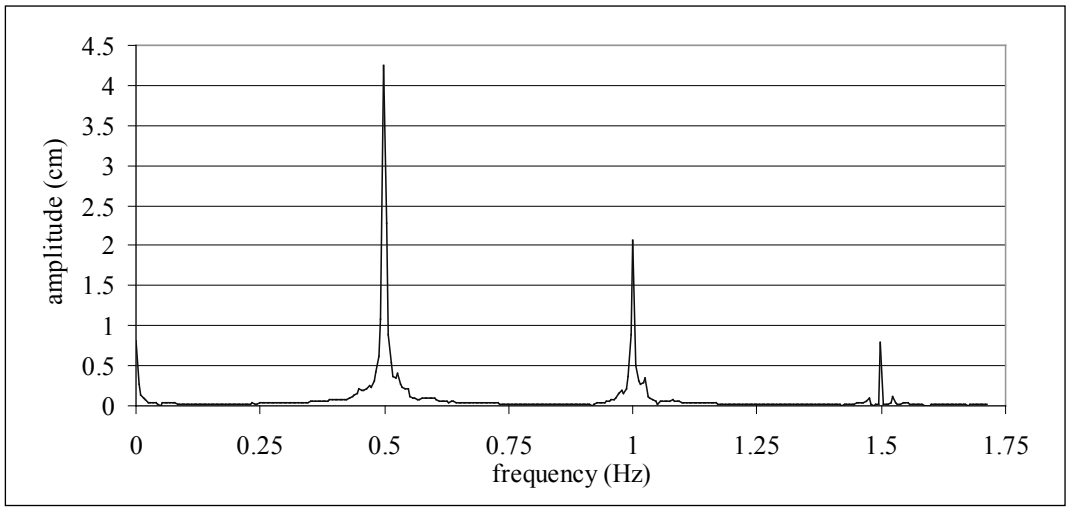

Figure 3-10 Wave spectrum for a regular wave with higher and sub harmonics (H=10cm, T=2s, h=45cm)

3.3.6.1 Long waves (sub harmonics)

The long waves can be divided in bound long waves and spurious long waves. The bound long waves do not obey the dispersion relation (L=f(T) or c=f(k)), but they follow the wave groups. A huge problem for long waves is their almost complete reflection. It is experimentally and theoretically demonstrated that when the long waves obey the resonance conditions, long standing waves are generated (Flick et al., 1980). Dally (1991) compared experiments with irregular waves generated during respectively 30 and 5 minutes. It was observed that the bed profile was flatter for the experiments of 30 minutes, indicating that the long standing waves flattened the ripples.

a) Bound long waves

When looking to an irregular wave field, it can be observed that the highest waves are grouped ("wave groupiness"). Because the energy is larger under the highest waves and because the flux of momentum should be constant, the augmentation of wave energy has to

be compensated by a lowering of the water level (wave set-down). This wave set-down (and wave set-up due to the smaller waves) is called a bound long wave, because it does not obey the dispersion relation. Since its influence on sediment transport, a bound long wave should be reproduced correctly, especially if the sediment transport rate and direction are important.

b) Free long waves

The wave paddle is steered with the first order solution of the Laplace equation. The negligence of the other terms introduces spurious waves. None of these waves occur in nature and should be eliminated. Three kinds of long free waves can be distinguished (Hughes, 1993).

Parasitic long waves are generated because the boundary conditions at the wave paddle do not correspond with the necessary conditions for the existing bound long wave.

Displacement long waves are generated because of the finite movements of the wave paddle, where the boundary conditions at the wave paddle are considered at x =0 and thus not at the actual position of the paddle.

Local disturbance long waves are due to the exponential declining of the summation terms in the first order wave generating theory. The waves are generally small compared to the other free long waves and would be zero if the wave paddle could follow exactly the calculated water movements.

c) Adaptations to the wave paddle motion

To get the desired long bound waves and to eliminate the spurious free long waves, it is necessary to give the wave paddle the necessary anticipating movement. The derivation of the bound and free long waves can be obtained with the second order solution of the Laplace equation. The bound long waves can also be studied using the radiation stress principle. The second order solution of the Laplace equation has to be superposed on the first order position of the wave paddle.

Sand(1982) gives the method to move the paddle in order to eliminate the spurious long waves and to get the desired bound long waves. The long wave can be described as the summation of the contribution of each pair of two components n and m:

$$\xi(t) = \sum_{n-m=1}^{\infty} \sum_{m=m^*}^{\infty} \xi_{nm}(t) \; ; \; m^* = \frac{f^*}{\Delta f} \qquad (3\text{-}32)$$

with f^* the lowest frequency of the spectrum and Δf the frequency interval in the Fourier-spectrum. It is now sufficient to find an expression for ξ_{nm}. With a_i en b_i the Fourier-amplitudes of component i, Sand gets:

$$\frac{\xi_{nm}(t)}{h} = G_{nm}\, h[(\frac{a_n a_m + b_n b_m}{h^2})\cos(\Delta\omega_{nm} t - \Delta k_{nm} x) + (\frac{a_m b_n - a_n b_m}{h^2})\sin(\Delta\omega_{nm} t - \Delta k_{nm} x)] \tag{3-33}$$

G_{nm} is a transfer function, which can be calculated analytically, but which is also presented graphically (Sand,1982).

To get the desired long waves in the flume, the wave paddle has to make an additional second order movement, based on Eq.3.34 :

$$X^{(2)}(t) = \sum_{n-m=1}^{\infty} \sum_{m=m^*}^{\infty} X_{nm}^{(2)}(t)\,; m^* = \frac{f^*}{\Delta f} \tag{3-34}$$

with:

$$\begin{aligned} \frac{X_{nm}^{(2)}}{h} &= [(\frac{a_n b_m - a_m b_n}{h^2}) F_1 h + (\frac{a_n a_m + b_n b_m}{h^2}) F_{23} h] \cos(\Delta\omega_{nm} t) \\ &+ [(\frac{a_n a_m + b_n b_m}{h^2}) F_1 h + (\frac{a_m b_n - a_n b_m}{h^2}) F_{23} h] \sin(\Delta\omega_{nm} t) \end{aligned} \tag{3-35}$$

$F_1h=F_{11}h+F_{12}h$

Also $F_{11}h$,$F_{12}h$ and $F_{23}h$ can be calculated analytically or obtained from graphs. The terms with $F_{11}h$ give the bound long wave and eliminates the parasitic long wave ($F_{11}h$ is function of $G_{nm}h$). $F_{12}h$ eliminates the free long displacement waves. $F_{23}h$ eliminates the free long local disturbance waves.

At deep water the compensation for the spurious long waves will dominate, at shallow water the movement for the bound long wave will dominate.

Because the generation of long waves require a large wave paddle motion, it is not always possible to generate these long waves correctly. This is also the problem in the wave flume of Flanders Hydraulics Research Division.

3.3.6.2 Higher harmonics

Higher harmonics make the wave asymmetric, with a higher maximum positive water elevation and a smaller negative water elevation. The shape of the waves changes with position along the flume because the first and second free harmonic move with a different speed. An example obtained during the experiments is shown in Figure 3-11.

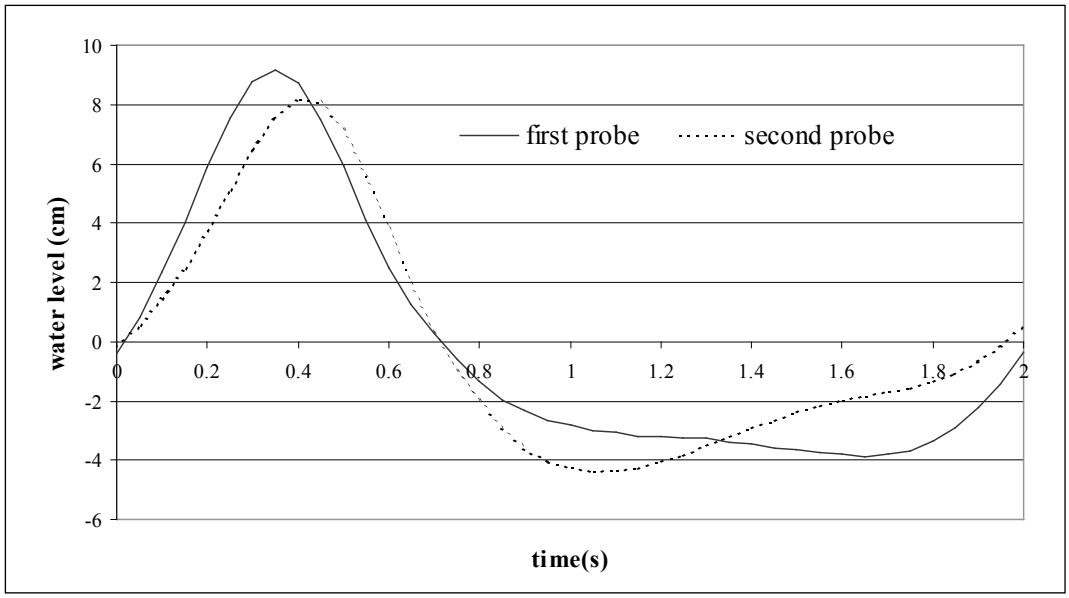

Figure 3-11 Water levels measured by two probes at distance of 0.85m

The amplitude of the second harmonic can be as high as 40% of the amplitude of the first harmonic.

Svendsen(1985) gives a qualitative explanation for the second order effect. The movement of the wave paddle is described as $X(z,t)=X_0e^{i\omega t}$. At x=X, the water particle velocity differs from the velocity at x=0 of order of magnitude X^2 (second term in the Taylor development). If the wave paddle moves perfectly sinusoidal, the error on the desired water velocity will be proportional to $e^{2i\omega t}$, resulting in an "error" movement of the water proportional to sin 2ωt. To this free second harmonic a bound second harmonic has to be added (Stokes second order wave), resulting in a wave which can be described as:

$$\eta = a_{1S}\cos(\omega t - k_1 x) + a_{2S}\cos 2(\omega t - k_1 x) + a_{2F}\cos(2\omega t - k_{2F} x + \alpha) \qquad (3\text{-}36)$$

with:

$$\omega^2 - g k_1 \tanh k_1 h = 0 \qquad (3\text{-}37)$$

and:

$$(2\omega)^2 - g\, k_{2F} \tanh k_{2F} h = 0 \qquad (3\text{-}38)$$

where a_{1S} the amplitude of the first harmonic, a_{2F} the amplitude of the free second harmonic and a_{2S} the amplitude of the bounded second harmonic wave.

An analytical solution can be found in Hughes(1993). He solved the Laplace equation for the second order term. The solution is split in a part close to the wave paddle and a part important for the whole wave flume.

The solution in the flume:

$$\phi_{21}(x,z,t) = \frac{3\omega H^2}{32}\frac{\cosh(2k(z+h))}{\sinh^4 kh}\sin 2(kx - \omega t) \tag{3-39}$$

This is a bound wave (known as the Stokes second order component) not caused due to the wave generation. For tests that aim to simulate natural conditions, this term does not have to be removed, since it also occurs in nature and obeys the scale laws.

The solution at the wave paddle is given as:

$$\frac{\partial \phi_{22}}{\partial x} = \frac{d X_{02}}{dt} + \frac{\omega H^2}{16h}\left(\frac{2}{m} - \frac{3\cosh kh}{\sinh^3 kh}\right)\cos(2\omega t) \tag{3-40}$$

If this wave has to be eliminated, $\partial\phi_{22}/\partial x$ has to be zero. The second order position of wave paddle becomes:

$$X_{02}(t) = \frac{H^2}{32h}\left(\frac{3\cosh(kh)}{\sinh^3 kh} - \frac{2}{m}\right)\sin(2\omega t) \tag{3-41}$$

Madsen(1971) stated that this can only be used if:

$$\frac{HL^2}{h^3} < \frac{8\pi^2}{3} \tag{3-42}$$

Svendsen(1985) gives some indication for practical applications:

- the free second harmonic wave can be reduced to 5 à 10 % of the Stokes second order wave, by generating the compensating wave (Eq.3.41)
- the theoretical compensating wave is too high, experimental fitting is necessary
- leakage at the wave paddle can influence the wave generating process considerably, which can be compensated.

It can be interesting to know which part of the second harmonic is free and which part is bounded (eg. when the free harmonic component has to be compensated).
The difference of two signals measured at an interval of half a wavelength can be calculated:

$$\begin{aligned}\Delta\eta_2 &= a_{2F}\sin(2\omega t - k_2 x + \alpha) + a_{2S}\sin(2\omega t - 2kx + \beta) + a_{2F}\sin\left(2\omega t - k_2\left(x + \frac{L}{2}\right) + \alpha\right) + \\ &\quad a_{2S}\sin\left(2\omega t - 2k\left(x + \frac{L}{2}\right) + \beta\right) \\ &= 2a_{2F}\cos\left(2\omega t - k_2 x + \alpha - \frac{k_2 L}{4}\right)\sin\left(\frac{k_2 L}{4}\right) + 2a_{2S}\cos\left(2\omega t - 2kx + \beta - \frac{kL}{2}\right)\sin\left(\frac{kL}{2}\right) \\ &= 2a_{2F}\cos\left(2\omega t - k_2 x + \alpha - \frac{k_2 L}{4}\right)\sin\left(\frac{k_2 L}{4}\right) + 2a_{2S}\cos(...).0\end{aligned} \tag{3-43}$$

from which a_{2F}, the amplitude of the free second harmonic, can be calculated. Because $(a_2)^2 \neq (a_{2F})^2 + (a_{2S})^2$ ($(a_2)^2$ depends on the phase between the bound and free component and thus depends on the horizontal position in the flume), the bound second harmonic has to be calculated by using another distance between the measurements (eg. with $\sin(k_2 \Delta x/4)=0$) or after determining a_2 (using measurements at different locations).

3.3.7 Initial surge

When the first waves are generated important long waves were visible during the preparation experiments (Figure 3-12). These waves are damped out, but are again visible after the wave generation is stopped.

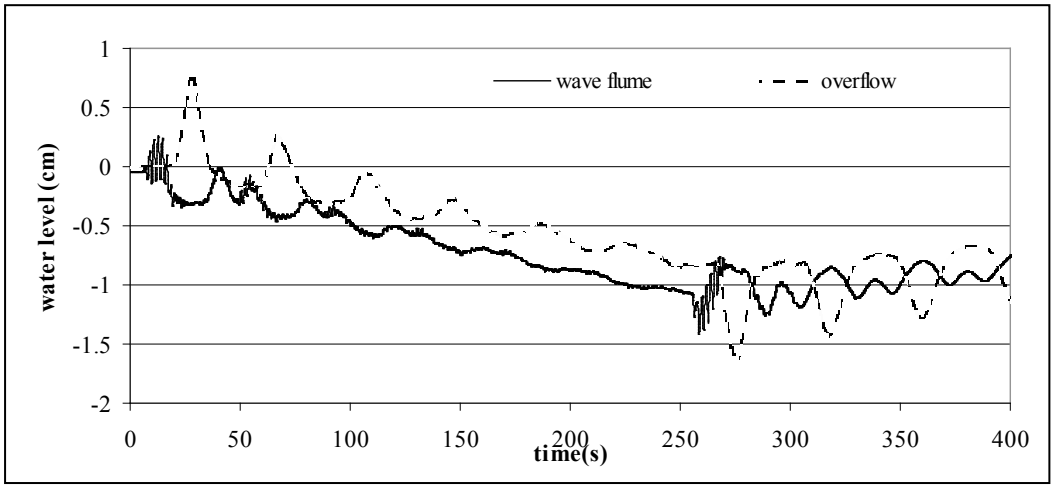

Figure 3-12 Mean water level (H=10cm, T=2s, h=50cm) at the beginning (0 – 100s), during (100-250s) and after wave generation(250-400s) at 2 locations (in the wave flume and at the overflow (the basement, cf. Figure 3-13)

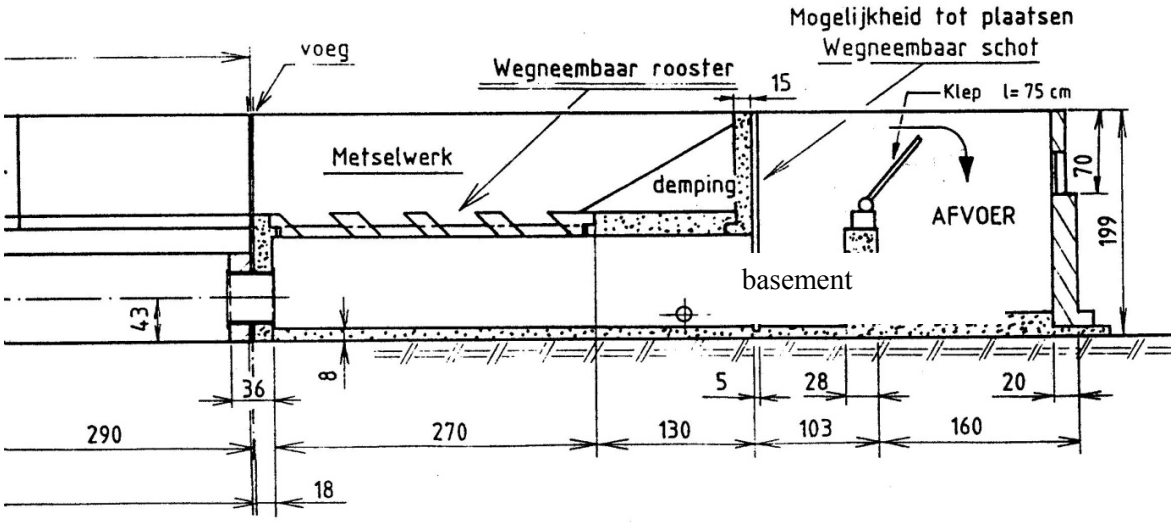

Figure 3-13 Detail of the wave flume : the basement

Svendsen(1985) describes the phenomena of initial surge. The sudden change of radiation stress due to the first waves causes an acceleration of the water particles (in addition to that corresponding to the oscillatory wave motion). The water level lowers and a long wave is generated which damps out only slowly. The opposite occurs when the generation of waves is stopped. The downward trend is caused by the loss of water at the overflow, the upward trend at the end is because the filling of the flume. The long waves are also clearly visible behind the wave damper, in the basement. Although it seems interesting to start the measuring program as early as possible after the start of the wave generation to avoid reflected waves in the signal, the initial surge might be too strong at that moment.

3.3.7.1 Loss of water at the overflow

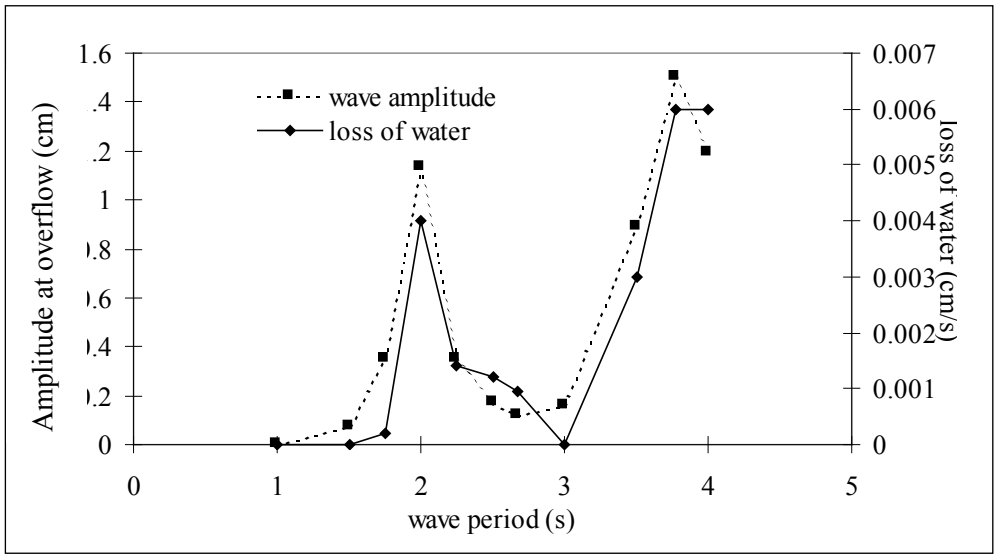

Figure 3-14 Relation between wave period and loss of water/ wave amplitude at overflow

For some wave periods the loss of water at the overflow is considerable, causing a decreasing water level (see Figure 3-14). One wave gauge was placed in the flume, the other one after the beach at the overflow.

It is clear that the loss of water is due to the propagation of the generated wave through the wave damper (which is permeable) and in the overflow. Long waves (T>4s) are not absorbed in the wave damper, part of the wave is reflected, the other part travels towards the overflow.

For T=2s a clear peak can be observed. It is likely that this wave period corresponds with the resonance frequency of the system. The reflection coefficient for this wave is 7%, which means that 93% is absorbed or transmitted by the beach structure. The basement was filled with damping packages in order to solve the problem.

3.4 Summary

In the first part the author used a literature study and his developed numerical model to study the scale effects in wave flumes.
With the numerical model for the development of concentration profiles over rippled beds (presented in Chapter 6), the effects due to scaling on the concentration profile and on the development of sediment clouds were examined. It could be concluded that the development and travelling of the sediment cloud over the ripples is not the same in prototype and model if the Sand Model is used. Is is advised to scale the vertical axis of the concentration profile with the ratio of ripple height in prototype and model. If the Best Model can be used (i.e. if the sediment is not too fine (cohesive), the obtained development and movement of the sediment cloud in the model is exaggerated in comparison with the prototype since the settling velocity is scaled too strongly. It can be concluded that the Sand Model is better than the Best Model.

The second part describes the work that is done by the author to prepare the wave flume of Flanders Hydraulics Research Division. It consisted of a literature study and the implementation of the methods during the testing of the wave flume (occurrence of bound and free higher and lower harmonics, reflection and initial surge). Some adaptations are done in the flume: construction of an optimal wave damper at the end, generation of irregular waves with a desired energy spectrum and elimination of oscillations in the basement). After the preparation of the flume a Laser-Doppler Anemometer (LDA) was used to measure turbulence above a movable bed (Trouw, 1996). Two students were guided in their research on erosion due to waves and currents (Flokman & Goemaere, 1996).
The obtained knowledge was also used during and after the experiments in the Deltaflume of Delft Hydraulics (Chapter 4).

4 Physical experiments in the Delta (wave) Flume

4.1 Introduction

As described in Chapter 3 scale effects can be important in the evaluation of sediment transport rates. Small wave flumes can help to understand the sediment transport mechanisms, but cannot be used to test the whole hydrodynamic scale of conditions. Measurement campaigns in the field on the other hand struggle with some drawbacks like an unknown influence of the instrument on the results and the many unknown parameters involved (e.g. grain characteristics of the sand being eroded further away from the instrument).

This chapter describes research undertaken in the large Deltaflume facility (Figure 4-1) of Delft Hydraulics during a six-week period in July and August 1997. Since instruments (can) influence the results, it was important to evaluate the performance of STABLE (Sediment Transport And Boundary Layer Equipment, Humphery and Moores, 1994) (Figure 4-2). The second aim of the experiments was to measure in detail bed sediment response to forcing by waves. STABLE consists of a large, heavy deployment frame equipped with a comprehensive suite of instruments and onboard data logging facilities. STABLE was deployed in the Deltaflume on test beds of medium and fine sand. In situ measurements of wave characteristics, flow turbulence, bedforms and vertical suspended sediment concentration profiles were obtained for regular and irregular waves. Hydrodynamic conditions below, close to and exceeding the threshold for resuspension of the bed material were examined. Independent measurements of wave-induced flow and vertical suspended sediment concentration profiles were obtained from locations close to the sidewall of the Deltaflume.
The limited availability of velocity measurements close to the bottom makes it difficult to determine sediment transport.

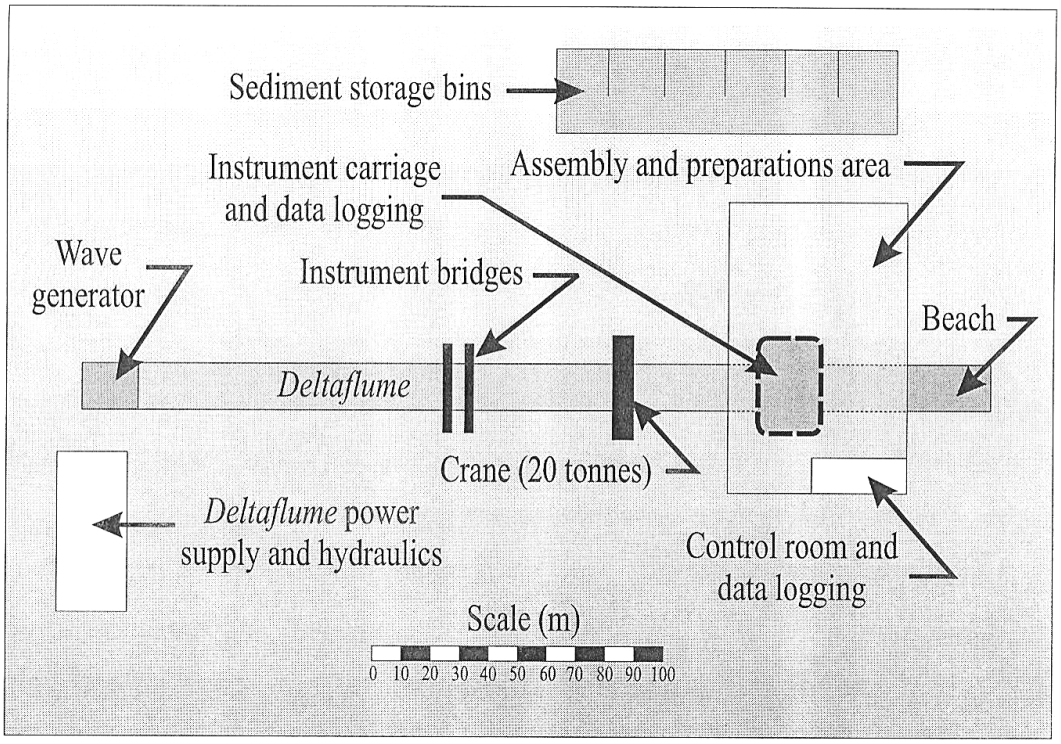

Figure 4-1 Schematic plan view of the Deltaflume research facility (Delft Hydraulics)

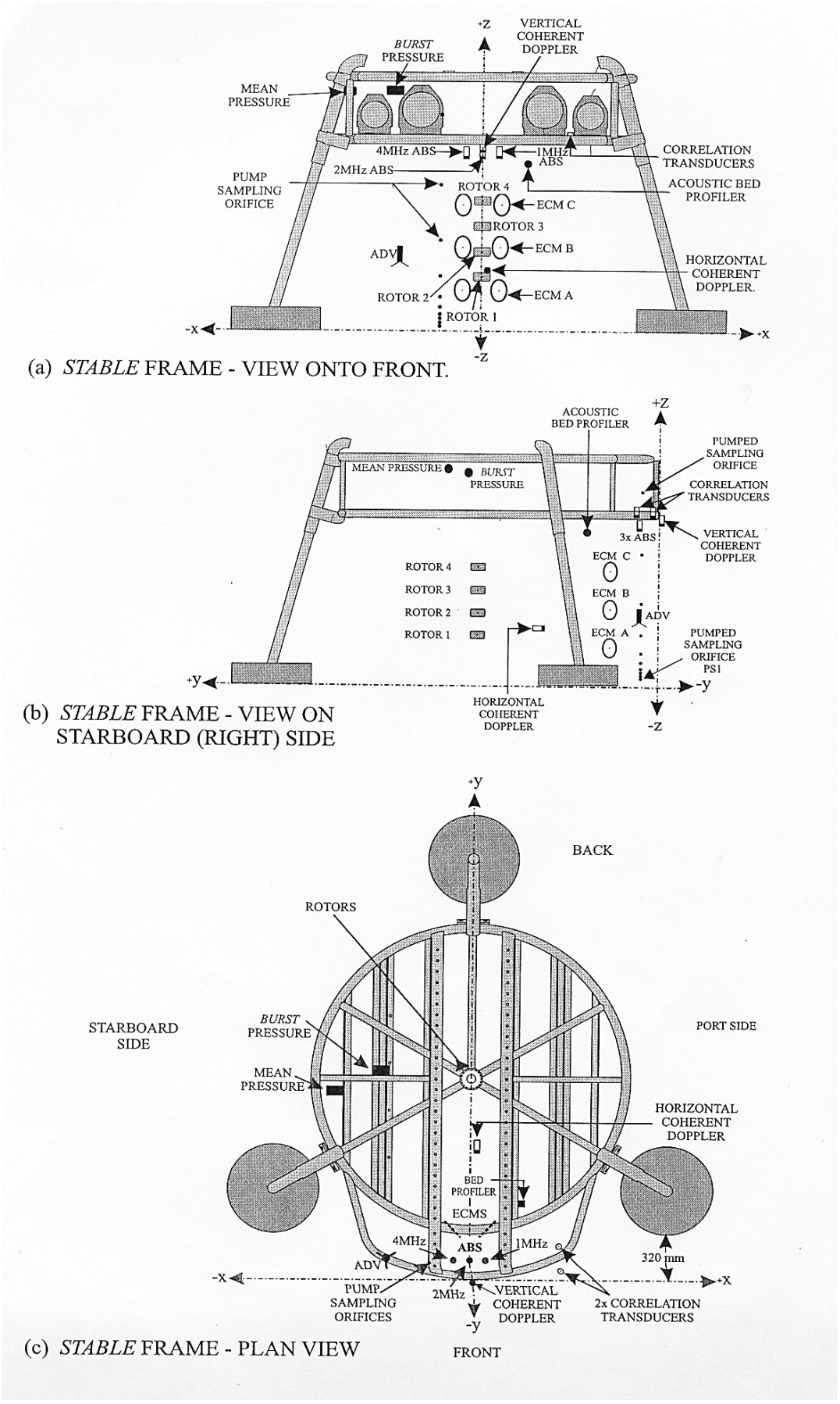

Figure 4-2 STABLE (a) front elevation; (b) side elevation; and (c) plan

4.2 Background

The autonomous boundary layer rig STABLE has been deployed in a number of funded field experiments (MAST 2: CSTAB and OMEX (Hannay et al., 1994, O'Connor et al., 1994, Williams et al., 1996, Huthnance, 1994). Whilst in all cases useful data pertaining to wave-current sediment interaction has been obtained during these deployments, there has always been uncertainty regarding the nature of and changes in the morphology of the sea bed during a given experiment. Further, it has not been possible to obtain in situ samples of sediment in suspension. In some cases this has lead to ambiguity in the interpretation of certain experimental results. The EU TMR Programme 'Access to large-scale facilities' provided an opportunity to use field-scale laboratory facilities to test the instruments and to examine the movement of sediment for a full range of hydrodynamic conditions.
Also the extent to which the frame interferes with the physical processes was studied.
The project was a co-operation of Proudman Oceanographic Laboratory, K.U.Leuven, University of Birmingham and the University College of North Wales. Part of the analysis of the data is published in a paper (Williams et al., 1998), a report (Williams et al., 1998) and a master thesis at the K.U.Leuven (Aerts,G., Kinget,G., 1998). Metje(2000) continued analysing the data for her Ph.D. thesis.

4.3 Experimental facilities and procedure

4.3.1 The Deltaflume

The Deltaflume is located in the De Voorst and owned by Delft Hydraulics Laboratory, and operational since 1980, the Deltaflume is a large scale facility allowing full-scale simulation of waves in controlled laboratory conditions. The Delft Hydraulics Laboratory Deltaflume is 230 m long, 5 m wide and 7 m deep (Figure 4-1). Regular and irregular waves with a height up to 2 m (or a significant wave height of 1.75 for irregular waves) and a wave period between 2 and 10 s, can be generated according to a required time history. The wave flume is at both ends closed and no currents can be generated. The 'beach' at the end of the flume has a slope of 1:6. The wave paddle is steered (interactively) in order to prevent reflection of waves from the wave board and eliminates low frequency resonant waves.
Frequently the Deltaflume is used for the testing and calibration of field equipment, for the development of remote sensing techniques for the measurement of waves, for assessing the performance of wave energy devices and floating wave energy absorbers, for the study of dune and dike stability under storm conditions, for the training and testing of underwater construction procedures and for the testing of underwater vehicles.

Before starting any work, the Deltaflume was thoroughly cleaned to remove sediments used in previous test programmes.

The sand bed used in the first series of tests (code A) was composed of medium sand (median grain size, d_{50} = 329μm). In the second series of tests (code F) fine sand was used (d_{50} = 162μm). The bed was approximately 30m long, 5 m wide and 0.5 m deep, and was placed approximately 105 m from the wave generator. Both ends of the test bed have a gentle slope towards the flume bed to reduce erosion and drainage was laid beneath the sediment bed to allow the free passage of water during filling of the flume. The sand bed composed of medium sand just is shown in Figure 4-4 (photo before filling of the Deltaflume with water).
Prior to any experimental work, regular waves with a height H of 1m and period T of 5s were generated for a period of approximately 3 hours. These waves were large enough to mobilise the bed sediments and generate regular bedforms. In addition, the waves also forced entrapped air out of the bed. The latter effect was especially significant, as any airbubbles present in the water during tests would seriously be harmful to the accuracy of the acoustic measurements of suspended sediment concentration. Small quantities of fine material present in the bed sediments were released into the water during this bed preparation phase of the work and resulted in a marked deterioration in visibility in the water. Consequently, tests using an underwater video camera to record entrainment mechanisms were abandoned. Large waves in the flume during tests A12A are shown in Figure 4-3.

Figure 4-3 Large waves in the Deltaflume

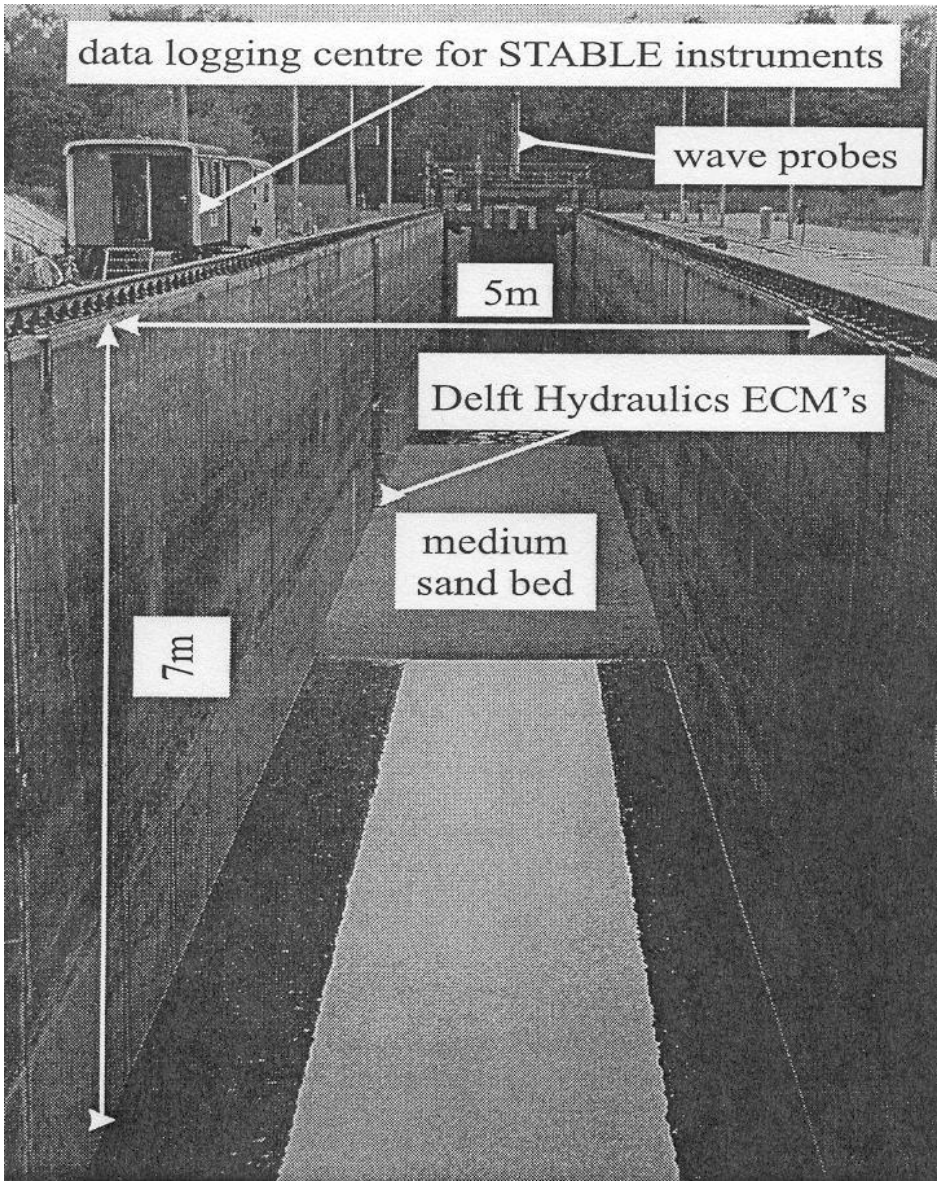

Figure 4-4 The medium sand bed before filling the Deltaflume

Measurement of velocities and wave heights

During the present tests, 4 cm discus-shaped electromagnetic current meters (E-40) were fitted to the side-wall of the flume at heights z = 25 cm, 50 cm, 100 cm, 150 cm and 250 cm above the bed at a distance y = 120.9 m from the wave generator (positions are shown in Figure 4-7) and 1m from the wall. The measuring volume has a cylindrical shape with approximately a thickness of 10 mm and 60 mm diameter, situated just below the electrodes.

Two resistive wave measurement probes positioned at 117.9 m and at 120.9 from the wave paddle (Figure 4-1 and Figure 4-7) were used to measure the instantaneous water level, from which wave characteristics can be derived. These instruments are mechanically driven up and down to maintain contact with the water surface. The distance between the two instruments is chosen in order to be able to analyse the reflection of the most important wave

components (see Chapter 3). Data from these instruments were logged at 25 Hz. Delft software was used to calculate a number of wave parameters including wave periods, wave heights and reflection coefficients.

Measurements of bed morphology

After the filling of the flume and the generation of waves during 3 hours, the bathymetry of the test beds of sand was measured using a mechanical ripple-profiling device. This consists of a lightweight wheel mounted on the end of a vertical support (Figure 4-5). When driven forward, the pressure applied to the wheel was held constant by moving the vertical support up or down in response to changes in bed elevation thereby permitting the measurement of bed morphology. The horizontal position of the instrument was referenced to accurate datum marks. The vertical position of the instrument was calibrated from a zero datum on the beach of the flume.

Figure 4-5Mechanical ripple-profiling device

Measurements of suspended sediment concentration by pump sampling

Samples of suspended sediment were obtained at 10 heights above the sand bed using pump sampling equipment deployed using vertical guide rails at 121.5 m from the wave paddle. This consisted of an array of 10 intake nozzles (diameter 4 mm) orientated at 90° to the wave orbital motion. Each nozzle in the array was connected to a plastic pipe through which the

mixture of water and sediment was drawn to the surface by means of a peristaltic pump. The resulting water/sand mixture from each sampling position in a given array was collected in 10 litre buckets (Figure 4-6). Once full, the sediment was allowed to settle to the bed of the buckets and excess water was then poured away. The remaining water/sand mixture was then poured carefully into a calibration tube and the volume of sand was measured. A pre-determined calibration was then applied to convert the volume of sediment into a concentration value (Bosman et al., 1987). This relation accounts for (in)efficiency (order of magnitude is 70%) of the suction and nozzle orientation. All samples were sealed in plastic bags for subsequent grain size and settling velocity analyses and for accurate measurement of the suspended sediment concentration (by weighing the samples).

Sometimes the nozzles got stucked due to large grains (which could be removed by turning the pump direction for a while) or due to sinking of the nozzle-device in the sand bed (for the one mounted on STABLE). The latter gave a useful reference of the height of the other nozzles above the bed.

Figure 4-6 Collection of water/sand mixture in buckets with peristaltic pumps

4.3.2 STABLE

STABLE, is an autonomous instrument platform, which is used to measure near-bed hydrodynamic conditions and sediment transport in wave-current flows. STABLE is a robust multi-sensor rig designed to be deployed on the sea bed and withstand the hydrodynamic forces generated by waves and tidal currents in shelf sea bottom boundary layers. The structure and instruments were further designed to be a minimum obstruction to the flow. The galvanised steel tripod has lead ballast feet and supports the circular instrument platform at 1.2 m above the bed.

Instrumentation on STABLE measured waves, flow turbulence and suspended sediment concentrations (see Figure 4-2 and Figure 4-7).

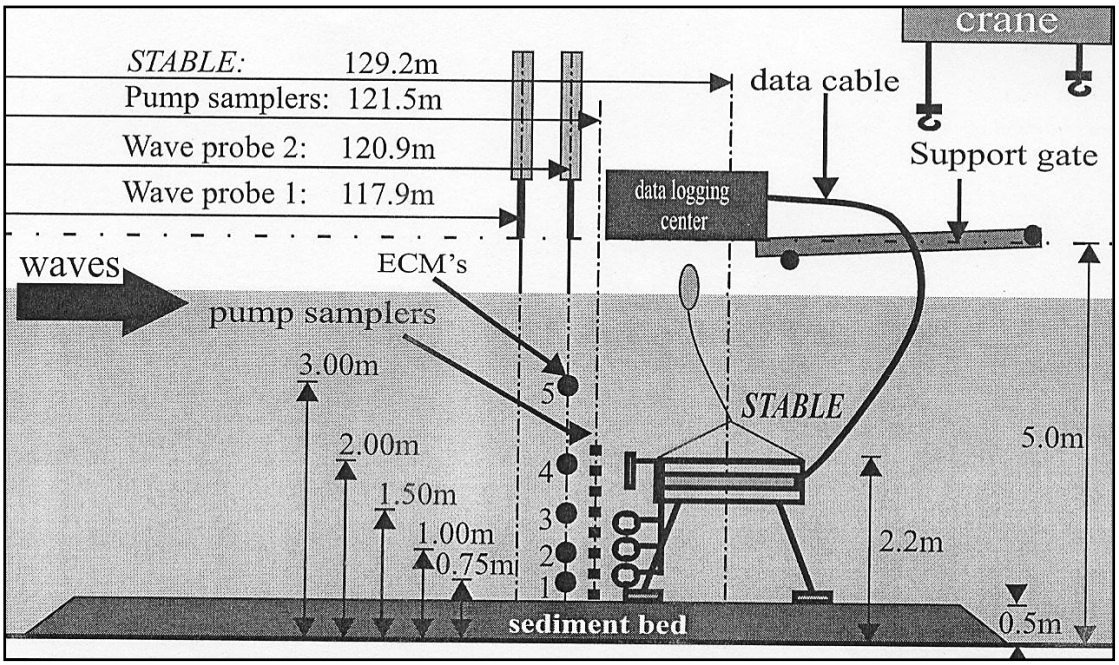

Figure 4-7 Schematic diagram showing the position of STABLE, wave probes and Delft Hydraulics ECM's in the Deltaflume

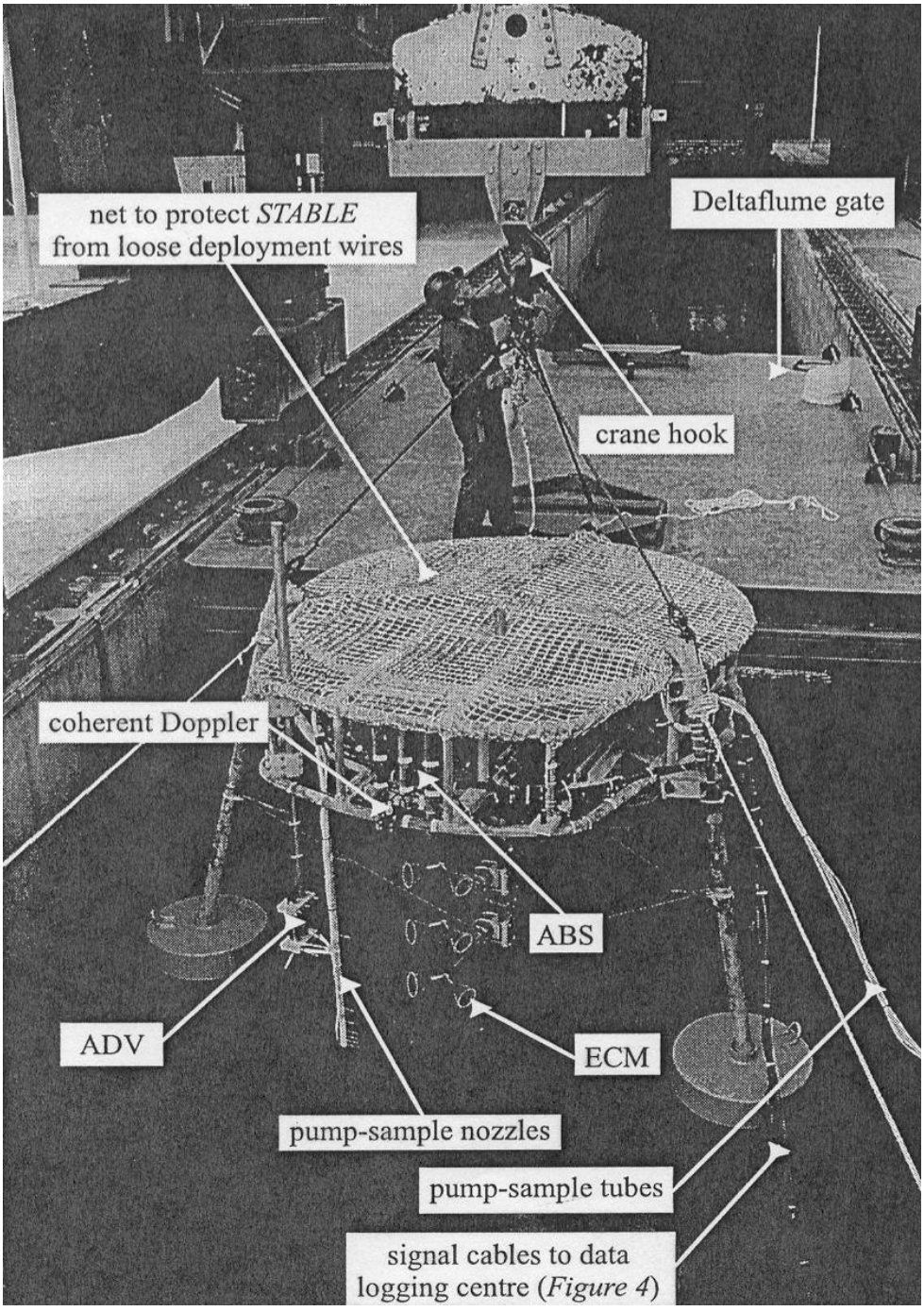

Figure 4-8 Deployment of STABLE in the Deltaflume

A *Digiquartz* pressure sensor with integral pressure housing was used to measure the water-depth at wave frequencies (deployed at z ≈ 170 cm).

Near-bed fluid motion induced by waves was measured using Valeport Series 800 **electromagnetic current meters (*ECM*'s)** with a diameter of 10 cm and a resolution of ±0.1 cm/s. ECM sensors were arranged in pairs set at 90° to each other at $z \approx 30$ cm, 60 cm, and 91 cm. Horizontal separation between each ECM sensor was 20 cm. Measurements of flow turbulence were also obtained at $z \approx 35$ cm using an acoustic Doppler velocimeter, ADV

(Sontek), Ocean Probe operating at approximately 5.0 MHz (maximum measuring at a frequency of ≈ 25 Hz). The ADV measures in three orthogonal directions.
Measurements of horizontal and vertical wave induced fluid motion were measured using POL **coherent Doppler sensors**.

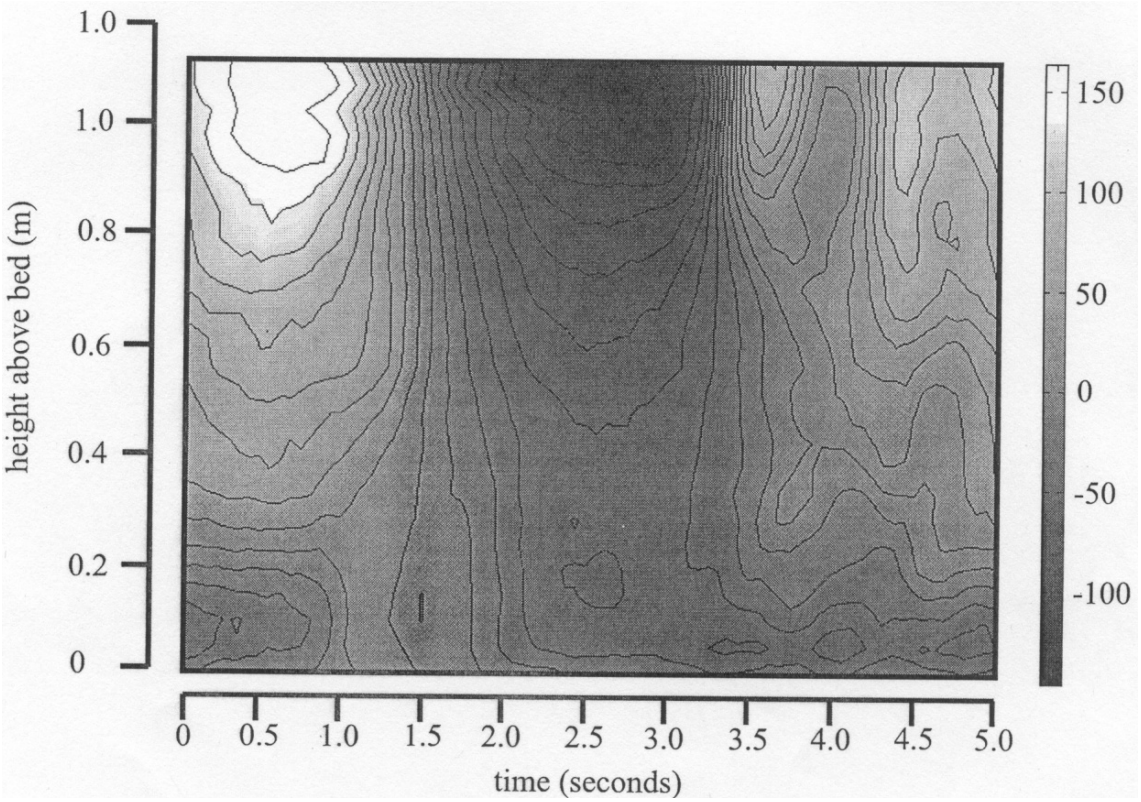

Figure 4-9 Vertical velocities measured with coherent Doppler averaged over 200 waves, test A11a, (regular waves, H=125cm, T=5s)

Ensemble averaged measurements (200 waves for regular waves with a wave height of 125cm and a wave period of 5s) of vertical wave induced velocities obtained with the coherent Doppler sensor at a height of 1295 mm are shown in Figure 4-9. The vertical velocities at the highest levels correspond with vertical velocities calculated with the linear wave theory. For 0<t<2s, the measured vertical velocity structure is relatively regular and shows no significant flow anomalies. At t=2.5s, the direction of the horizontal velocity changes, and the flow is coming from the rear of STABLE to the front, it is considered that the more disturbed vertical velocity structure is attributable to flow turbulence shed from the frame and from the sensors. However, near the bed (the most important), the influence seems to be small.
Bedforms beneath STABLE were measured using an **acoustic ripple profiler** (ABP) (2Mhz) (continuously, with a scan of 3m in the direction of the flume each half minute) and a **sector**

scanning sonar (SSS) device (Bell & Thorne, 1997) (after each test since the water had to be in rest; 2 Mhz signal, measures a full circle with a radius of 1.5 m).
Acoustic backscatter, ABS, instruments (Thorne & Hardcastle, 1997) operating at 1.0 MHz, 2.0 MHz, and 4.0 MHz, were located 15 cm in front of the ECM sensors at $z \approx 128$ cm. The instrument is developed at Proudman Oceanographic Laboratory, who did also the installation and calibration. These instruments measured the vertical suspended sediment concentration profiles from the bed to $z \approx 120$ cm at intervals of 1 cm. The ABS works in two modes: transmit and receive. In transmit mode the acoustic transceivers transmit short, high frequency acoustic pulses (1; 2 and 4 Mhz resp) down. The pencil beam of the signals is about 1cm diameter. Portions of the signals are backscattered to the ABS systems when they meet obstacles such as suspended sediments. The return echoes received by the instrument depend strongly on sediment characteristics such as grain size, shape and density, which may vary with location and height. The second ABS system mode receive, utilises time-gating in order to receive each backscattered signal over 128 measurement bins (measurement regions spaced equally from z=1.28m to 0m). 128 backscatter profiles were obtained each second at the three frequencies. These profiles were averaged over 32 records to provide measurements at 0.25 s intervals. The averaging of the data was necessary to smooth out configuration noise which arises from variations in the backscatter signal due to random phase distributions of the echoes, which arises from varying locations of the particles in each measurement volume.
A vertical array of **pump sampling nozzles (PS1)** was also fixed to the STABLE frame (see §4.3.1) . The pumped samples provided the necessary grain sizes to calibrate the ABS and concentration values to validate the ABS.

ECM and PS1 data were sampled at 8.0 Hz and ABS1, ABS2 and ABS3 data were sampled at 4.0 Hz over a period of approximately 19 minutes. ADV data were sampled at 25.76 Hz during the same period.
Rose (1997) analysed and discussed the STABLE data obtained during the measuring campaign at the Middelkerke Bank.

4.3.3 Measurement programme

A summary of all hydrodynamic and morphodynamic variables measured during Deltaflume tests, together with the instruments deployed, their accuracy and the data logging frequency selected for each sensor, is given in Table 4-1. All data sets were time and date stamped to allow easy cross-referencing and to facilitate intercomparison in subsequent analyses of the data.

Variables	Instrumentation	Accuracy	Sampling frequency
Water temperature	Thermistor	± 0.05°C	0.016Hz
Water (dynamic) pressure	Pressure sensors	± 0.15%	8Hz
Water velocity	ECM's	± 0.2cm/s	8Hz
Turbulence	ECM's	± 0.2cm/s	8Hz
Turbulence	ADV	± 0.1cm/s	25Hz
Vertical flow component	Coherent Doppler	± 0.1cm/s	8Hz
Horizontal flow cross-correlation	Coherent Doppler	± 0.1cm/s	8Hz
Horizontal flow component	Coherent Doppler	± 0.1cm/s	8Hz
Free surface elevation	Surface following gauge	± 2.5cm	10Hz
Free surface elevation	Resistance type gauge	± 1cm	10Hz
Suspended sediment	ABS (1.0; 2.0; 4.0MHz)	mg/l	4Hz
Suspended sediment	Pump sampling	± 20%	-
Bed morphology	DH ripple profiler	± 2mm	1cm grid
Bed morphology	Sector scanning sonar	± 2mm	0.016Hz
Bed morphology	Acoustic ripple profiler	± 2mm	0.032Hz
Orientation of STABLE	Compass & inclinometers	± 1°	0.016Hz

Table 4-1 Hydrodynamic and morphodynamic variables measured during Deltaflume tests

The sequence of experimental conditions is shown in Table 4-3 and Table 4-2. During the tests the mean water depth was 5 m (4.5 m above the sand bed). In between tests the sand bed (with its ripples) was not adapted, so the sand bed at the beginning of a tests corresponds with the sand bed at the end of the previous test.

STABLE was during some experiments turned in order to examine the effect of the orientation of STABLE compared to the wave direction on the results

In the series A tests medium sand was used with d_{10} =0.187 mm, d_{50} =0.329 mm and d_{90}=0.761 mm. In the series F test fine sand was used with d_{10} =0.093 mm, d_{50}=0.162mm and d_{90} =0.291 mm. (Figure 4-10)

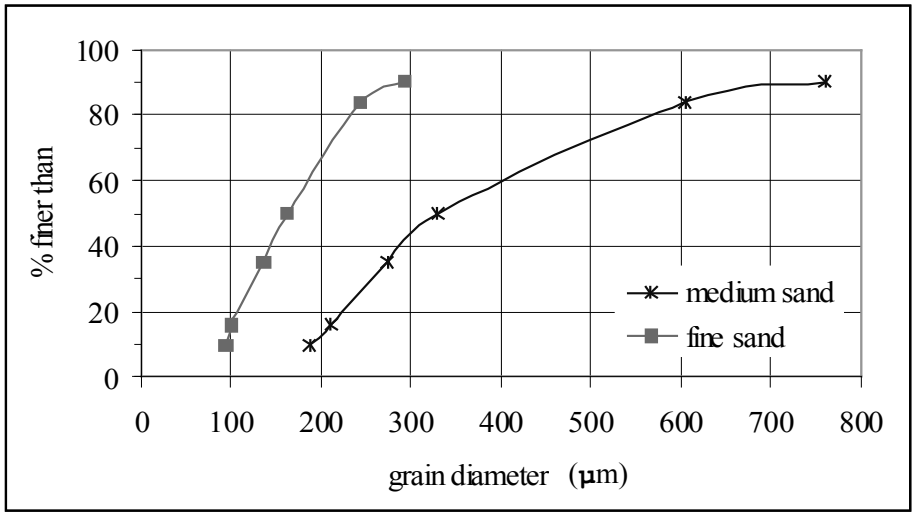

Figure 4-10 Cumulative grain size distribution for medium and fine sands

date	**experi-ment**	**wave type**	**wave height Hs (cm)**	**wave period Tp (s)**	**STABLE rotation**	**remarks**
24/07/1997	f01a	reg	75	5	out	
28/07/1997		-			out	ripple profiling
29/07/1997	f02a	reg	31	5	0°	STABLE in flume
	f02b	reg	33	5	0°	camera installed
	f02c	reg	34	5	0°	
30/07/1997	f03a	reg	52	5	0°	
	f04a	irr	50	5	0°	
	f05a	reg	75	5	0°	
31/07/1997	f06a	-			0°	zero test
	f07a	irr	75	5	0°	
	f08a	reg	100	5	0°	
	f09a	asym	50	5	0°	
01/08/1997	f10a	irr	100	5	0°	
	f11a	reg	75	6	45°	STABLE turned
04/08/1997	f13a	midd	120	4	45°	
	f14a	reg	75	4	45°	
	f15a	asym	75	5	45°	
05/08/1997	f16a	midd	100	4.5	45°	
	f17a	reg	75	5	45°	STABLE out
		-				ripple profiling

Table 4-2 Chronological summary of Deltaflume tests, fine sand bed (d_{50} =0.162mm) with reg: regular wave; irr: irregular wave; asym: asymmetrical wave; midd: wave scaled spectrum obtained during CSTAB at the Middelkerke Bank (O'Connor, 1994). Out: STABLE not in flume, STABLE rotation: angle between the front of STABLE and the wave crests

date	experi-ment	wave type	wave height Hs (cm)	wave period Tp (s)	STABLE rotation	remarks
02/07/1997	a01a	reg	50	5	out	
	a01b	reg	50	5	out	
03/07/1997	a02a	reg	75	5	out	
		-			out	ripple profiling
04/07/1997	a03a	irr	75	5	out	
07/07/1997	a03b	irr	75	5	out	
	a03c	irr	75	5	out	
	a04a	reg	100	5	0°	STABLE in flume
	a04b	reg	100	5	0°	
08/07/1997	a05a	reg	100	5	0°	
	a05b	reg	100	5	0°	
	a06a	reg	50	5	0°	bad data
	a06b	reg	50	5	0°	
09/07/1997	a07a	irr	50	5	0°	
	a08a	reg	75	5	0°	
	a09a	irr	75	5	0°	
10/07/1997	a10a	irr	100	5	0°	
	a11a	reg	125	5	0°	
	a12a	irr	125	5	0°	camera installed
11/07/1997	a13a	reg	100	5		
	a14a	reg	100	5	45°	STABLE turned
	a15a	asym	100	5	45°	
14/07/1997	a16zero	-				zero measurement
	a16a	reg	100	5	90°	STABLE turned
	a17a	irr	100	5	90°	
	a18a	asym	100	5	90°	
15/07/1997	a19a	reg	100	5	0°	
	a20a	reg	100	4	0°	
	a21a	reg	60	6	0°	
	a22a	asym	100	5	0°	
16/07/1997	a23a	reg	75	5	0°	
		-				ripple profiling

Table 4-3 Chronological summary of Deltaflume tests, medium sand bed (d_{50} =0.329mm)

The irregular waves had a JONSWAP wave spectrum with a peak factor γ of 3.3.

4.4 Bed morphology

The rate of sediment transport is very sensible to the presence and the size of ripples. Higher velocities might wash out ripple structures, causing a reduction in sediment transport. This makes the measurement of the bed profile during experiments or during calibration

measurements very important. Ripples react rather fast (order of magnitude ½ -1 hour) to changing hydrodynamic conditions. This makes continuous measurements important.
During the experiments it was possible to obtain continuous measurements of the bed profile in a line parallel with the wave flume over a distance of 3 m (it takes about 40s to scan the complete line). A sector-scanning sonar at the end of the test gives a 2 dimensional image of the structure of the bed. The mechanical ripple profiler gave a complete 2 dimensional view of the bed.
Flume experiments with glass walls indicate that the ripple near the crest is much steeper than what can be measured by instruments. The ripple is very steep (near maximal slope for sand) upstream the crest, and less steep downstream. When the water motion reverses, the other side of the crests becomes very steep. Detailed measurements after a tests with mechanical instruments cannot show these steepnesses, while acoustic measurements during tests are too much disturbed by the high concentration cloud in the vicinity of the ripple crest when this crest is steep.

4.4.1 General features of the bed

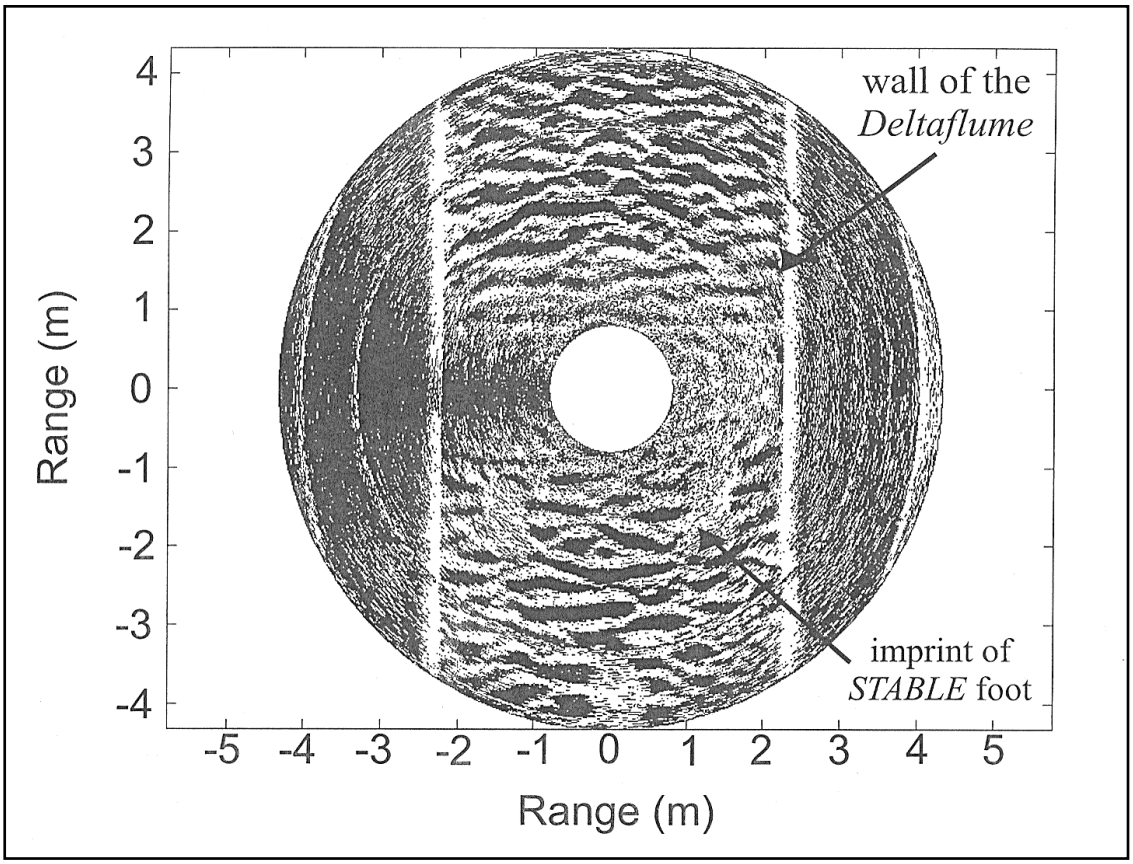

Figure 4-11 Sector-scanning sonar images of the medium sand bed showing walls of the Deltaflume and imprints left by STABLE feet

Figure 4-11 shows a typical image of vortex ripples on the medium sand bed obtained from the sector scanning sonar device while STABLE was in the flume. The image was obtained by lowering the sector scanner into the flume during still water conditions at some distance in front of STABLE. The side walls of the Deltaflume and well developed, long-crested vortex ripples are shown. Also the imprints left in the sand by STABLE are visible. No important change in ripple structure beneath STABLE can be observed.

Figure 4-12 is obtained from the data of the mechanical ripple profiler. Before STABLE was moved out of the flume after the medium sand tests were completed, regular waves with a height H of 75 cm and a wave period T of 5s were generated. STABLE was then moved out and the mechanical profiler profiled the bed on lines parallel with the flume wall, with an interval of 25 cm between the lines. An interpolation technique was used in order to obtain Figure 4-12. Also in this figure the foot imprints of STABLE are visible (since not the whole width of the flume could be profiled, the two feet near the wall are only visible at the border of the plot).

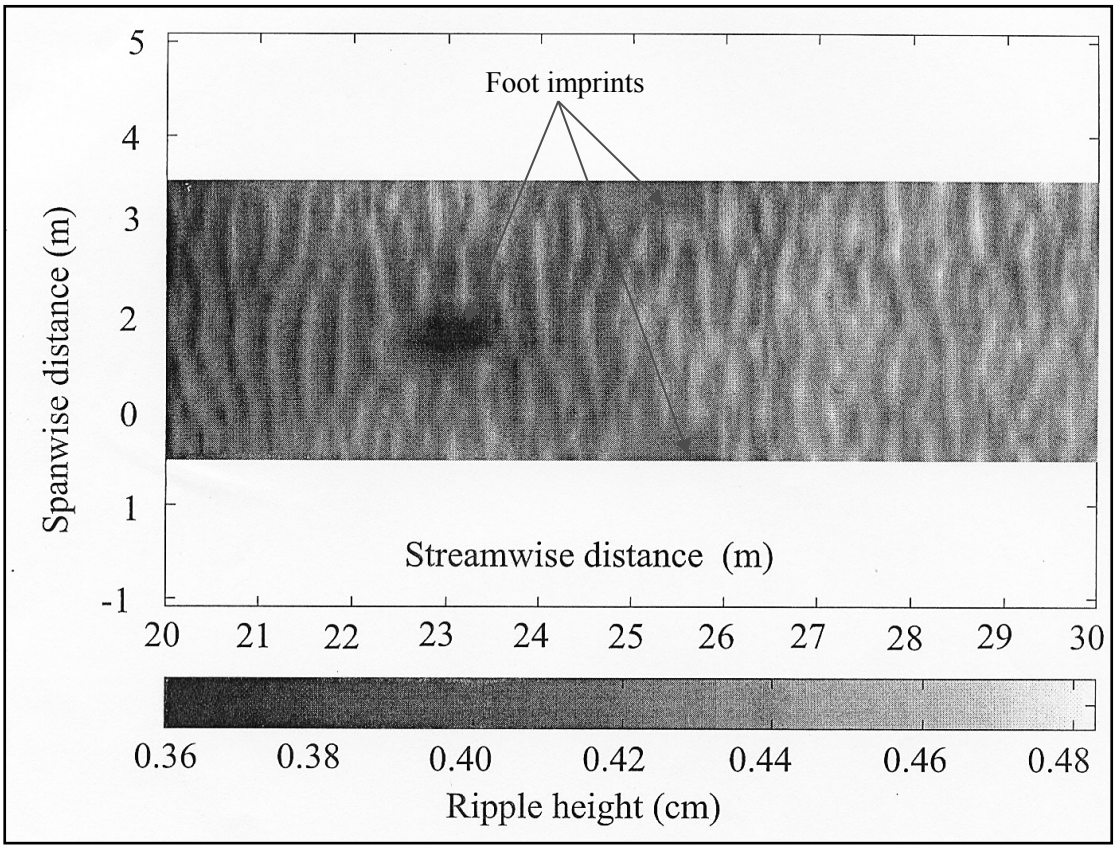

Figure 4-12 Image of vortex ripples on the medium sand bed derived from the mechanical ripple profiler data (regular waves, H=75cm, T=5s, h=4.5m)

The correlation coefficient of the different profiles (mechanical profiling) is rather low (<0.5). This suggests that the ripples are rather three-dimensional, which is also visible on

Figure 4-12. It is not obvious to state that the ripples under STABLE are different. Figure 4-12 suggests more pronounced, two-dimensional ripples at the beach-side of the leg of STABLE but no real difference in profiles are visible under the instruments (between the two side-legs). This might suggest to place STABLE with its front towards the direction from where the most important waves are expected to come.

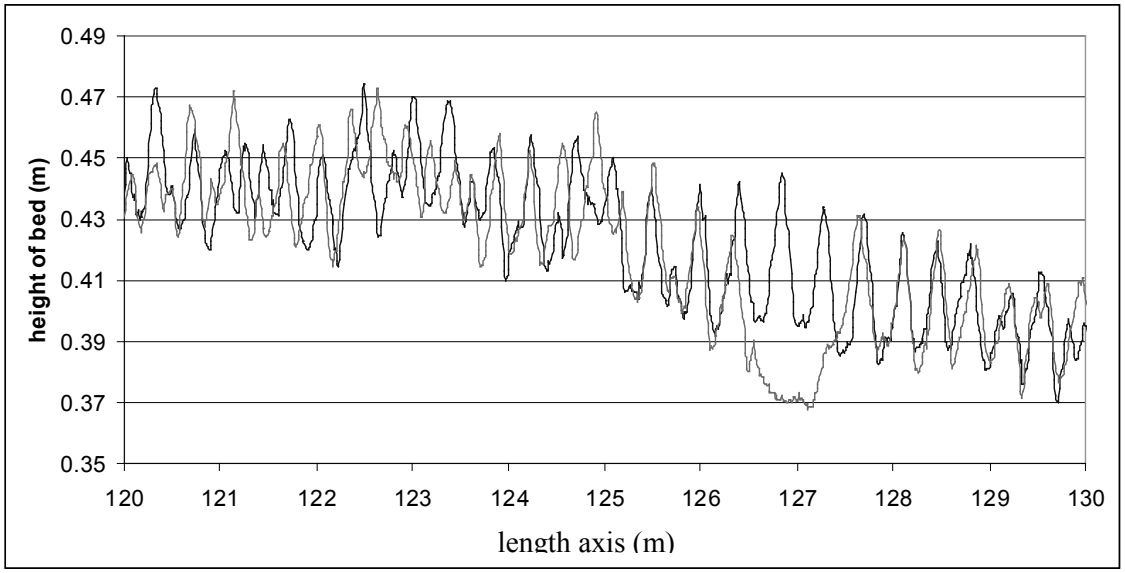

Figure 4-13 Two profiles obtained with the mechanical profiler, and separated 25 cm

Figure 4-13 shows the results of two profiles at tracks separated 25 cm. Although the correlation coefficients are low, it can be said that the ripple crests in general corresponds more or less (but far from perfect). Also the variability in ripple dimensions is clearly visible. It can be concluded that even in laboratory conditions the ripples are not perfectly regular and not 2-dimensional. This also means that the sediment concentrations will differ strongly from location to location! Possible reasons for these features are the different wave characteristics over the bed (due to second harmonics and reflected waves (partially standing waves) and possible non-uniformities in the bed material.

Evolution of the bed

Figure 4-14 and Figure 4-15 show the bed at the start of the series of tests and at the end for resp. Medium (A-tests) and fine (F-test) sand (resp. The 23 and 17 tests of about 2 hours each). It is remarkable that the medium sand bed is more eroded than the fine sand bed. It is not clear if this is only due to the smaller waves and the reduced number of runs for the fine sediments.

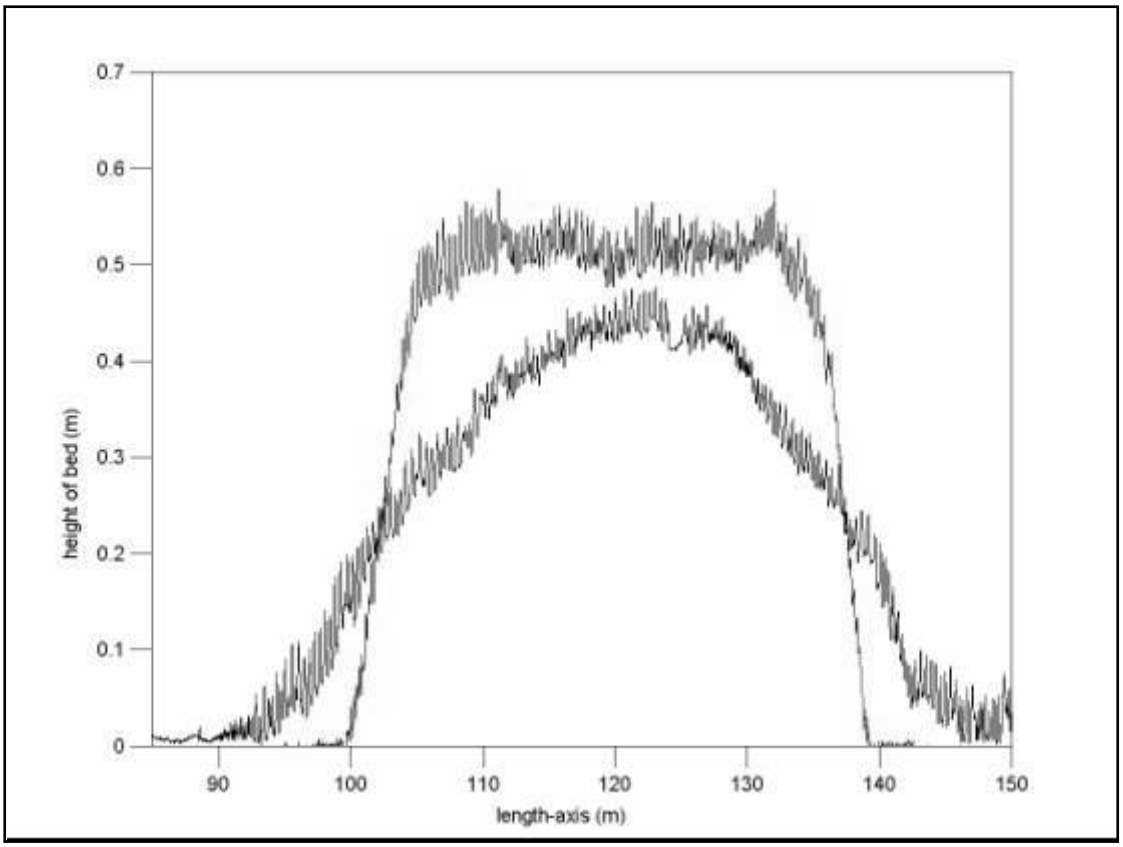

Figure 4-14 Sand bed before and after tests series with medium sand (last run: regular waves,H=75cm,T=5s)

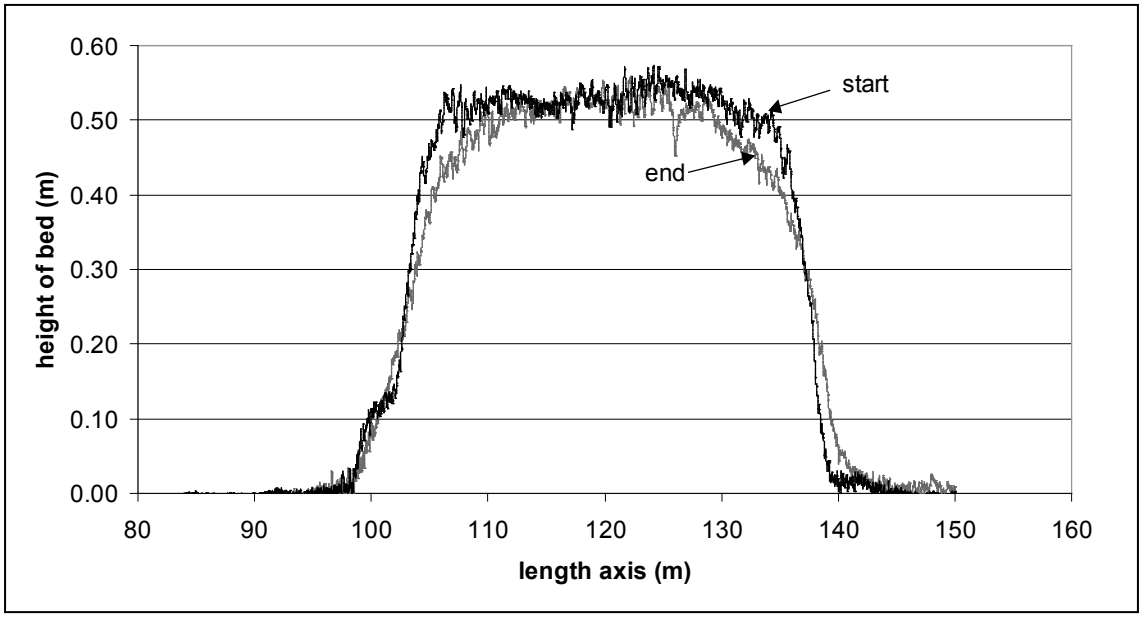

Figure 4-15 Sand bed before and after tests series with fine sand (last runs: regular waves,H=75cm,T=5s)

4.4.2 Study of the ripple dimensions

Figure 4-13 makes clear that it is not easy to identify the ripple length and the ripple height. A combination of a spectral analysis and search for minimal and maximal elevation of the bed is used. Since the short distance of the scanned bed profile (3m) relative to the ripple length (0.2 – 0.5 m), the method of searching the average length between to crests incorporates a large error due to the limit number of ripples. It was found that a spectral analysis gave better results for the ripple length (Aerts & Kinget, 1998). The frequency spectrum is analysed in order to obtain a mean ripple length. The ripple length is the inverse of the weighted average peak frequency (averaging over a limited interval around the peak frequency). The ripple height is found by comparing minimal and maximal elevations.

Table 4-4 shows the ripple height and length for the experiments where the acoustic ripple profiler was used and for which data were made available by POL. Values between brackets indicate values obtained when STABLE was turned 45 degrees. An analysis of the ripples obtained with the mechanical profiler indicated a standard deviation of 7 cm for the ripple length and 1.5 cm for the ripple height (medium bed).

Any 3-dimensional features in the ripples would cause a modification in the observed ripple length, which makes these values less reliable. For the tests with fine sand rather large dunes instead of vortex ripples are observed. In some cases no ripples at all could be observed (/), these tests correspond generally with high mobility numbers (ψ). Also Nielsen(1992) does not predict important ripples for high mobility parameters (see §4.4.3)

exp.	H (cm)	T (s)	type	height (cm)	length (cm)
a04b	100	5	reg	5.0	39
a05a	100	5	reg	5.5	40
a05b	100	5	reg	5.8	40
a06a	50	5	reg	4.0	35
a06b	50	5	reg	4.0	32
a07a	50	5	irr	4.3	30
a08a	75	5	reg	4.5	34
a09a	75	5	irr	4.5	34
a10a	100	5	irr	5.3	38
a11a	125	5	reg	6.3	43
a12a	125	5	irr	5.5	39
a14a	100	5	reg	5.0	(39)
a15a	100	5	ass	4.8	(44)
f02a	31	5	reg	1.8	18
f02b	33	5	reg	2.0	17
f02c	34	5	reg	2.0	17
f03a	52	5	reg	2.0	26
f04a	50	5	irr	1.8	27
f05a	75	5	reg	/	56
f07a	75	5	irr	/	58
f08a	100	5	reg	/	84
f09a	50	5	ass	/	22
f10a	100	5	irr	/	94
f11a	75	6	reg	1.8	(55)
f13a	120	4	mid	/	(88)
f14a	75	4	reg	1.8	(19)
f15a	75	5	ass	1.8	(19)
f16a	100	4.5	mid	/	(98)
f17a	75	5	reg	2.0	(29)

Table 4-4 Mean ripple dimensions obtained with the acoustic ripple profiler

Figure 4-16 shows all measured scanned profiles: the distance is given in the y-axis (between -1.5 and +1.5m), in the x-axis time is given (time of the moment the profile is scanned). Due to the high frequency of scanning the evolution of the ripple crests can be followed on the figure.

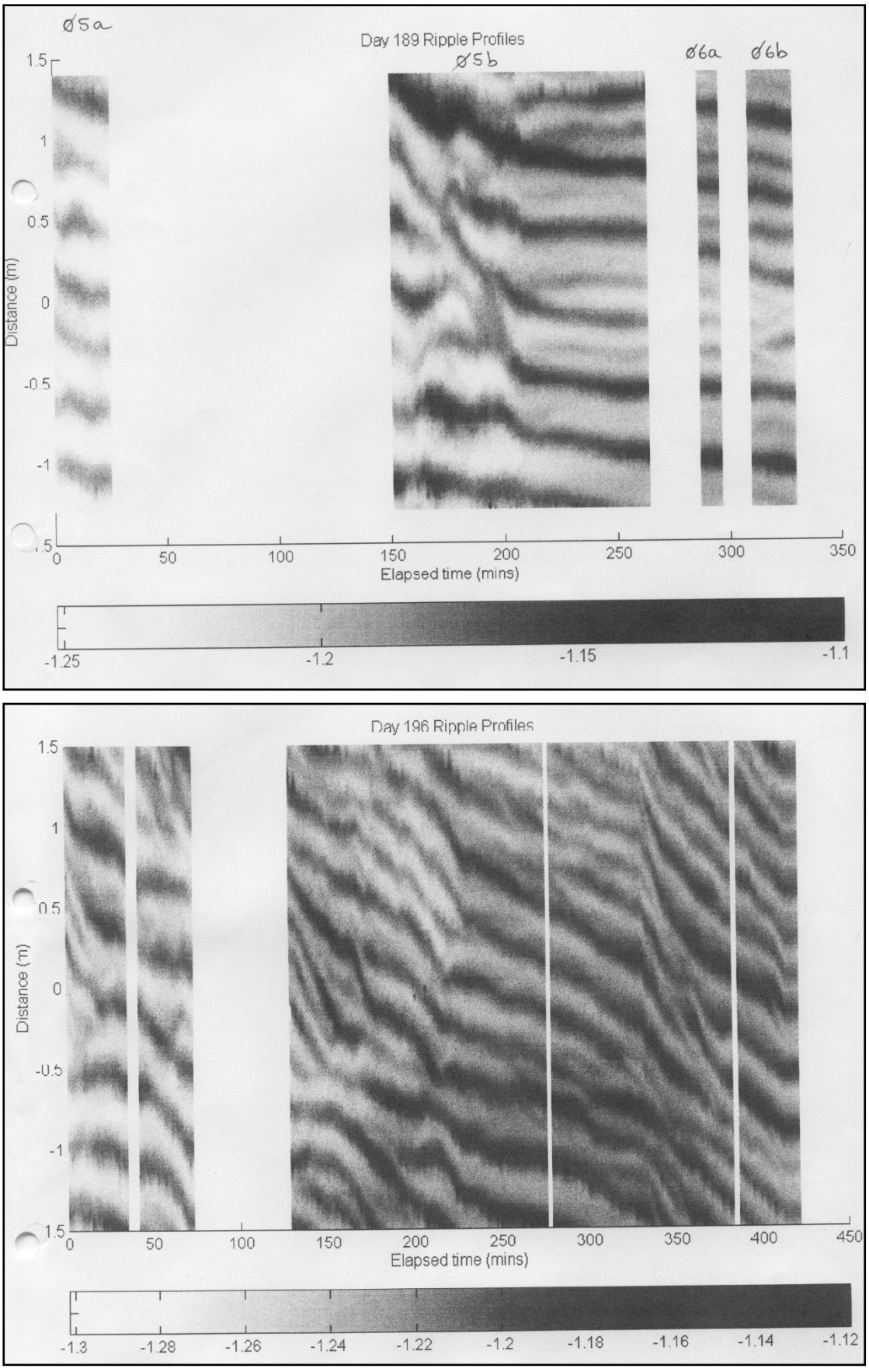

Figure 4-16 Evolution of bed during various tests (scale= depth under sensor)

Figure 4-16 indicates that the ripples are hardly changing for the irregular waves (cf test A11a and A12a). The reduced travelling rate of the ripples is clearly visible. This can partly be explained by the small amount of sediment transport during these tests. But it is remarkable that the ripples for the regular 50cm (test A6, see figure above, right site) waves adapt and move more than the irregular waves of 100cm significant wave height (test A10*).* Figure 4-17 shows the evolution of the bed during the time interval of the data logging of the ABS (=about during 20 minutes during each test). It is clear that the ripples move faster during the regular 100cm waves than during the irregular 125cm waves. A possible explanation could be that the net current near the bed is stronger, and always in the same direction than in the case of the irregular waves, where a net 'sea-ward' current near the bed exists for the higher waves (see Chapter 2).
It is presumed that the ripple dimensions of the irregular waves of 50 and 75 cm wave height with the medium sand bed depend too much on the previous runs.

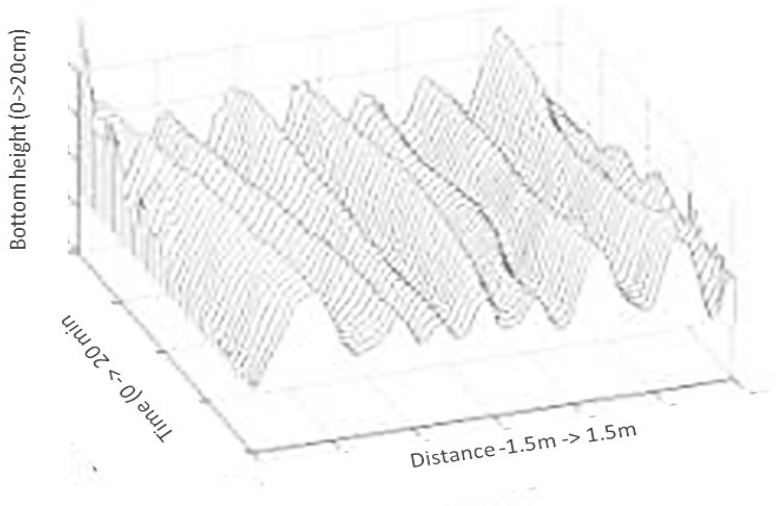

Figure 4-17a Evolution of the bed (medium grain size) for regular waves (H=100cm)

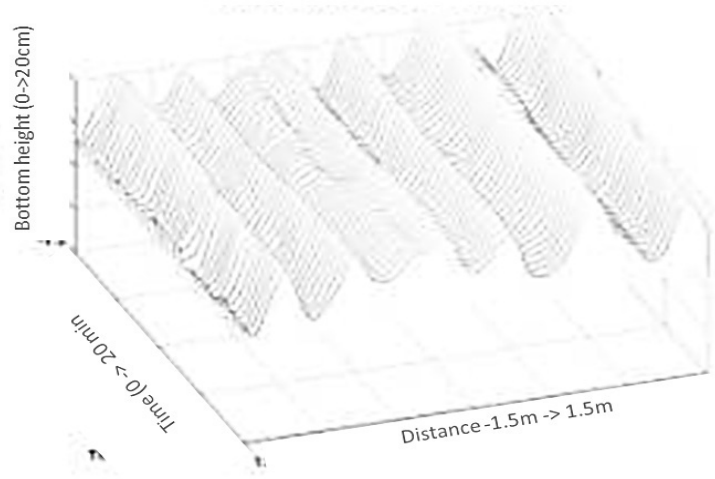

Figure 4-17b Evolution of the bed (medium grain size) for irregular waves (H_s=125cm).

4.4.3 Comparison of ripple dimensions with empirical relations

In most empirical formulae the ripple dimensions are non-dimensionalised with the orbital radius of waves: λ/A_δ en Δ/A_δ. The driving force (hydrodynamic) is divided by the stabilising force (gravity):

$$\Psi = \frac{U_\delta^{\,2}}{(s-1)gd_{50}} \qquad \text{and} \qquad A_\delta = \frac{U_\delta \; T}{2 \; \pi} \tag{4-1}$$

with U_δ = the velocity outside the boundary layer (m/s)

A_δ = the orbital amplitude outside the boundary layer (m)

s = the relative density of the sediment (= 2,65)

U_δ and A_δ are calculated with the velocity measurements at 25 cm above the bed near the wall (ECM's). These will differ slightly from these under STABLE, but the involved error is rather small (<10%).

The most used expressions to predict ripple dimensions are Nielsen (1992) and Van Rijn (1993). Nielsen based his expressions on various data sets.

For regular waves he found:

$$\frac{\lambda}{A_\delta} = 2{,}2 - 0{,}345\psi^{0{,}34} \qquad 2 < \psi < 230 \tag{4-2}$$

$$\frac{\Delta}{A_\delta} = 0{,}275 - 0{,}022\psi^{0{,}5} \qquad \psi < 156 \tag{4-3}$$

and for irregular waves:

$$\frac{\lambda}{A_\delta} = \exp\left(\frac{693 - 0{,}37\ln^8\psi}{1000 + 0{,}75\ln^7\psi}\right) \qquad \psi > 10 \tag{4-4}$$

$$\frac{\Delta}{A_\delta} = 21\psi^{-1{,}85} \qquad \psi > 10 \tag{4-5}$$

Van Rijn used partly different data sets, and found for irregular waves:

$$\frac{\lambda}{A_\delta} = 1.4 \quad 10^{-6}(250-\psi)^{2{,}5} \qquad 10 < \psi < 250 \tag{4-6}$$

$$\frac{\Delta}{A_\delta} = 2.8 \;\; 10^{-13}(250-\psi)^{5} \qquad 10 < \psi < 250 \tag{4-7}$$

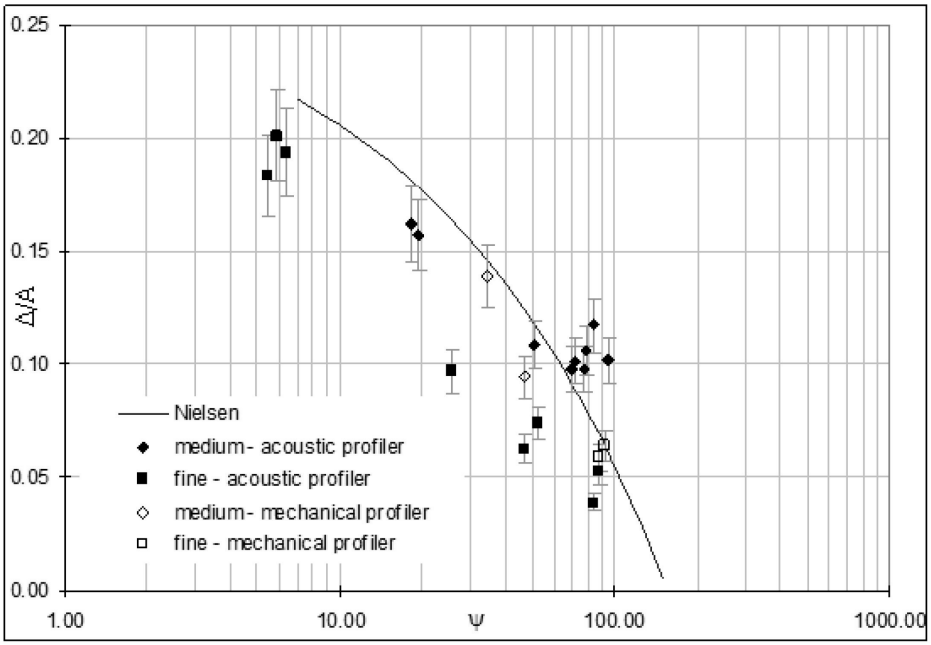

Figure 4-18 Ripple height for regular waves: comparison with Nielsen (1992)

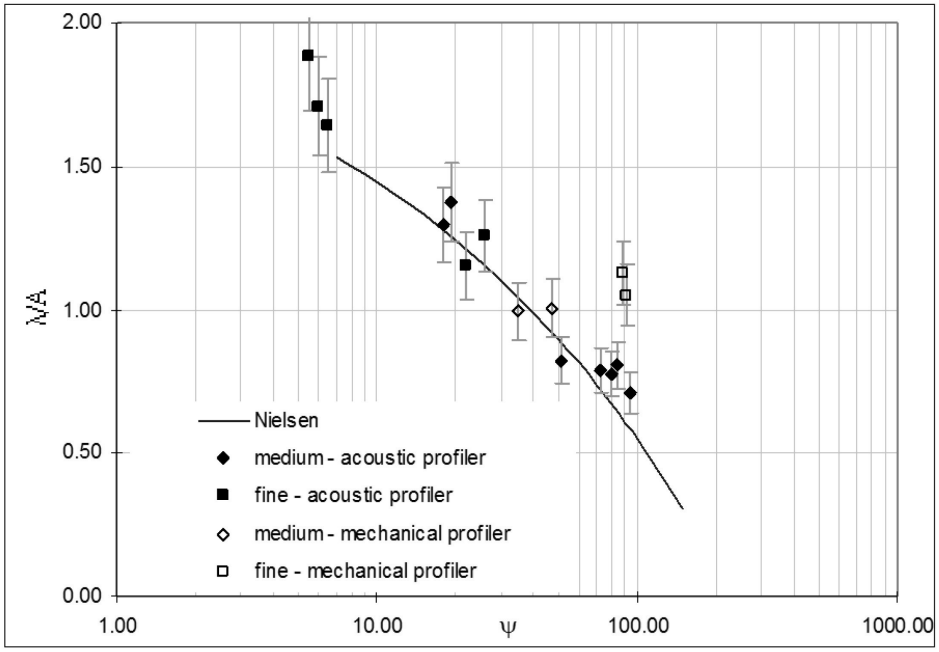

Figure 4-19 Ripple length for regular waves: comparison with Nielsen (1992)

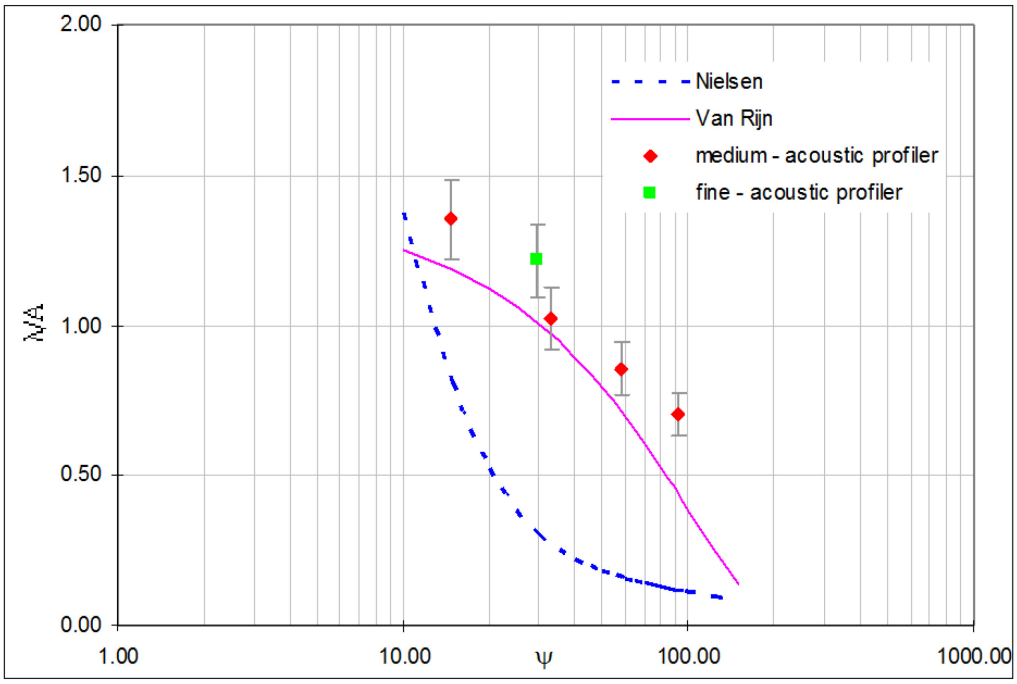

Figure 4-20 Ripple length for irregular waves: comparison with Nielsen (1992) and Van Rijn (1993)

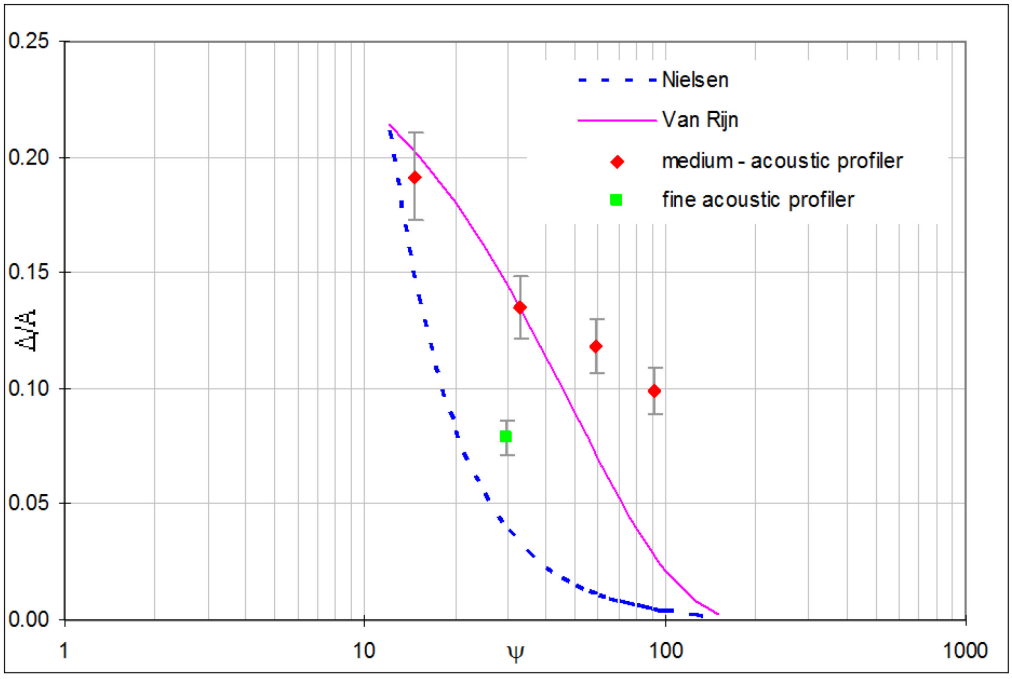

Figure 4-21 Ripple height for irregular waves: comparison with Nielsen (1992) and Van Rijn (1993)

Figure 4-18 to Figure 4-21 indicate that Nielsen's expressions predict the observed ripple dimensions well for the regular waves, but performs worse for the irregular waves. For these

cases Van Rijn‘s expressions seem to give better results. This might be because they are more based on laboratory experiments instead of field experiments.

4.5 Hydrodynamics

The study of the hydrodynamics in a wave flume is complicated by a lot of factors: second order waves and reflected waves (5% - 20% of the incoming wave) makes the hydrodynamics not uniform over the length of the flume, which is strengthened by the presence of ripples and dunes (see §4.4). It makes it also difficult to ensemble average the waves. A misalignment of the velocimeter causes leakage of the horizontal velocity in the observed vertical velocity, which is difficult to remove. The exact position of the instruments (height above bed and horizontal distance from the ripple crest) is difficult to determine since the irregularities in the bed morphology. Instruments in the Deltaflume have to be very robust and Laser-Doppler velocimetry is not possible.
But these experiments have the advantage that it was possible to have a good idea of the bed during the experiments with the acoustic scanning of the bed, and the presence of some good velocimeters (ECM and ADV) delivers interesting information for near field conditions. It is however a pity that the closest position of the velocimeter to the bed was 25 cm. This was necessary in order to test the standard set-up of STABLE.

4.5.1 General features

The reflection coefficient has been obtained by analysing the signal of the two wave followers (cf. Chapter 3). The coefficient was generally between 10 and 15 %.
Regular waves contain an important second harmonic wave component, the free part of this second harmonic travels with a different speed than the first harmonic (cf. Chapter 3).
Due to these two features, no real regular monochromatic waves can be generated and the wave characteristics will vary along the flume.
For imposed regular waves with a wave height H of 100 cm, the r.m.s. wave heights are resp. 97 and 106 cm (test #a14a) at the two wave followers, indicating important partial standing waves due to reflection. As an example, Figure 4-22 shows the water level measurements at the two probes during the same test (regular H=100cm waves).
This makes it also difficult to compare ADV velocities with velocities measured near the wall, and comparing results from the tests with the same test conditions.

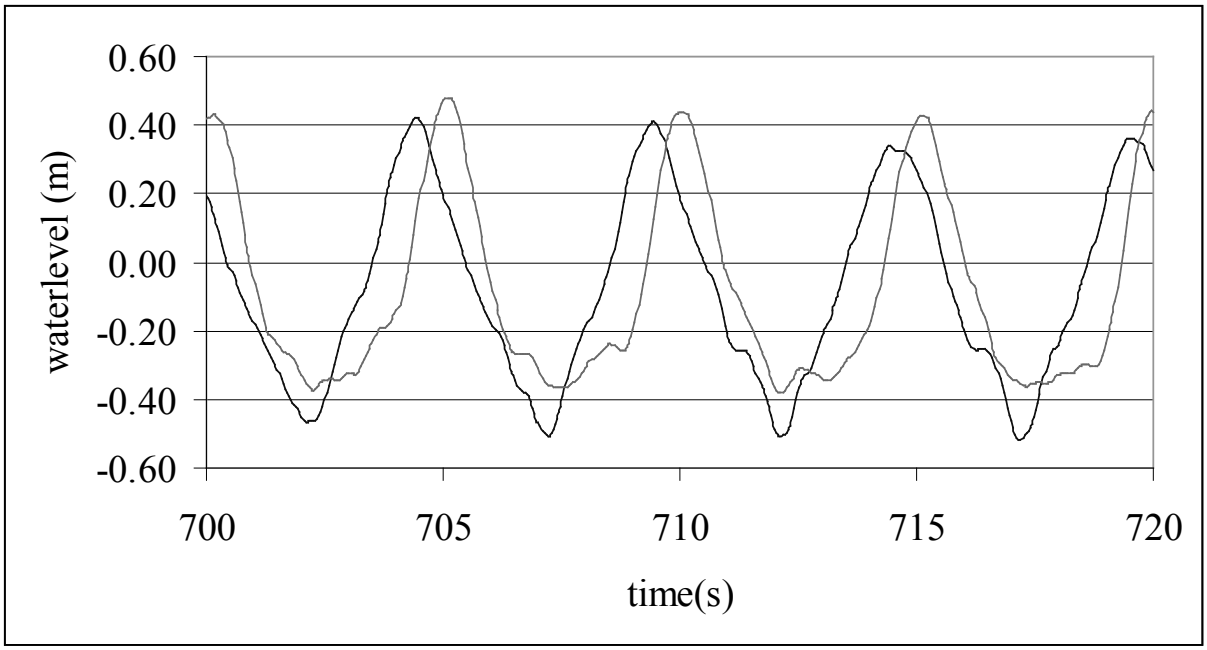

Figure 4-22 Water levels measured with two wave probes, 3 m separated

During measurements in a wave flume in 'rest', velocities of 1 to 2 cm/s were recorded. This makes it difficult to measure drift velocities. Even if the drift velocities could be obtained, they are difficult to interpret, since the wave flume is closed: the vertically averaged drift velocity should be zero, but it is difficult to estimate the height at which the return current occurs.

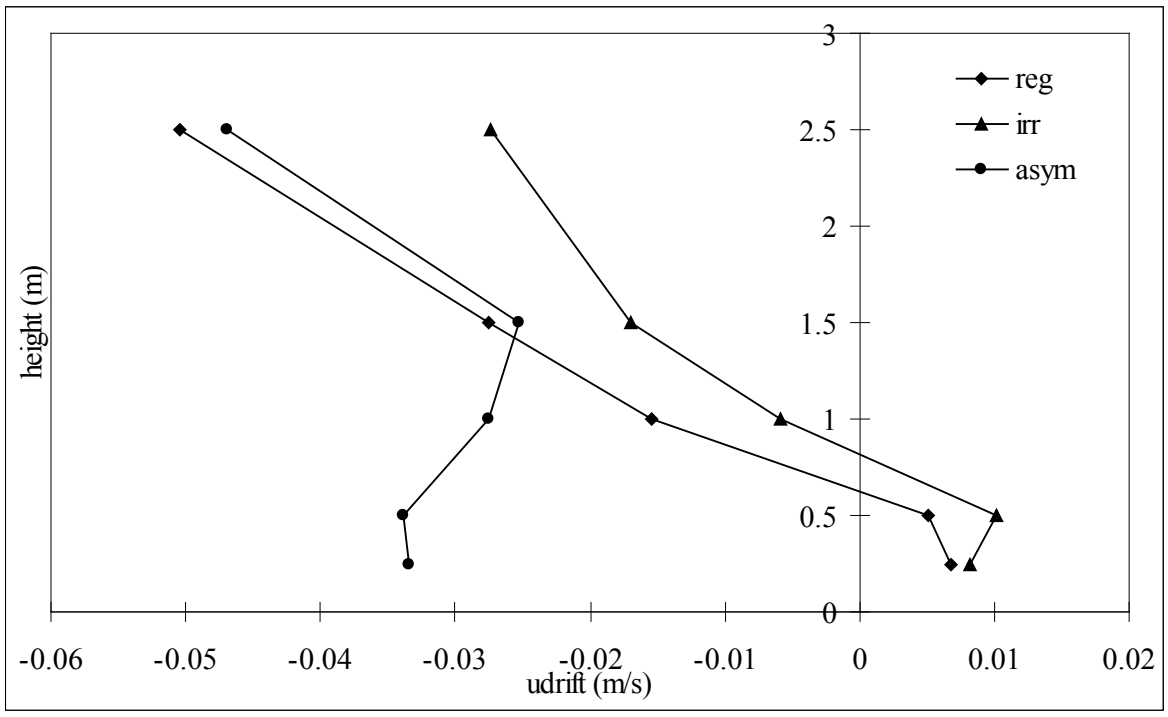

Figure 4-23 Drift velocity for regular, irregular and asymmetric waves, H=100cm

Figure 4-23 gives the drift velocity for regular, irregular and asymmetric waves. Close to the bed the velocity is positive (shear current) (except for the asymmetric waves), further from the bed the velocity is negative (return current). Due to measuring inaccuracy, it does not make sense to analyse these drift velocities in more detail.

4.5.2 Velocity profiles

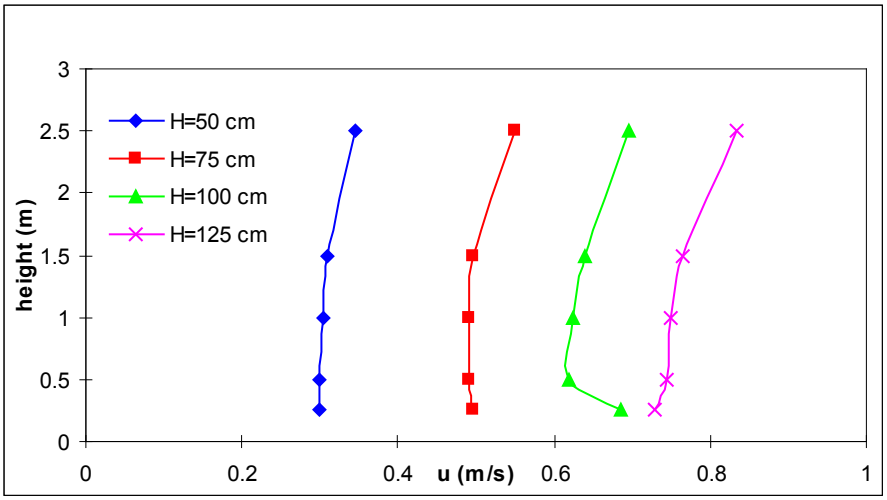

Figure 4-24 Amplitude of orbital velocity profiles for different waves

Figure 4-24 suggests the presence of a wave boundary layer for the two highest waves (H=100cm and H=125cm). For the smaller waves the boundary layer is too thin to be detectable by the lowest ECM (25 cm above the bed). This is in agreement with the theory that the thickness of the wave boundary layer is about 4 times the ripple height. In Figure 4-25 tests with the same conditions (regular waves with H=100cm, T=5s) are compared. The important difference between A05 and A14/A16 is due to the important lowering of the bed level in between these tests (10 cm) due to erosion, while the ECM sensor is fixed to the wall: the distance between bed and sensor becomes higher. The height of the ADV above the bed is rather decreasing due to the sinking of STABLE. For the fine sand bed, the ripples are much lower and the boundary layer is too low to be picked up by the ECM's.

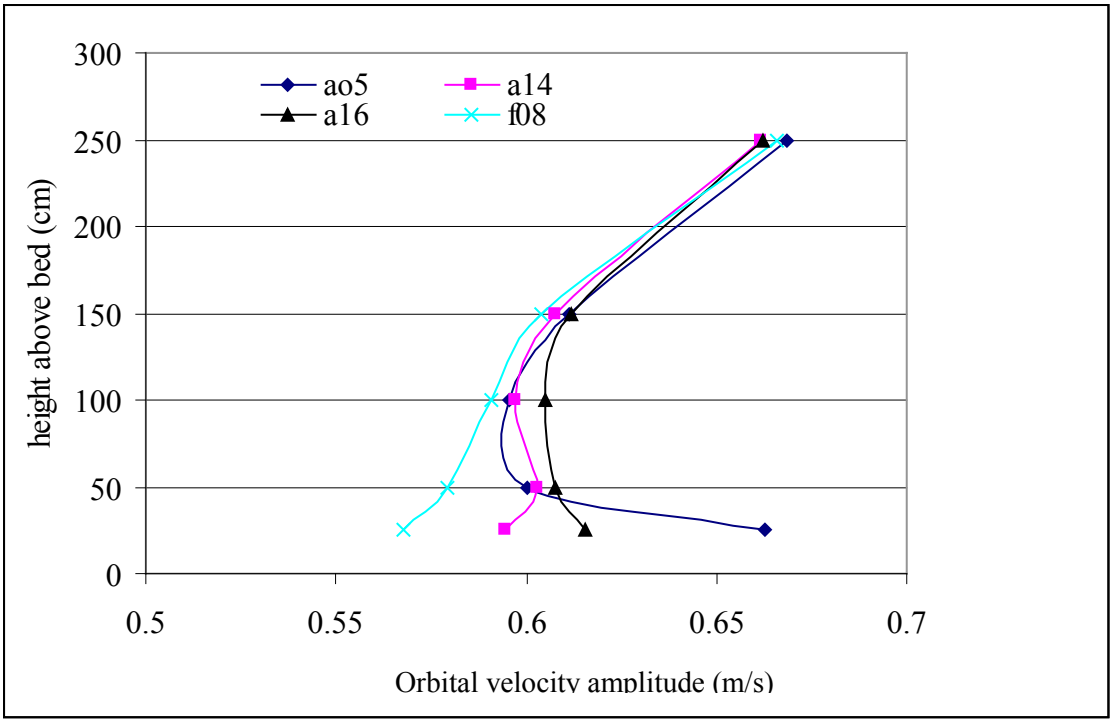

Figure 4-25 Orbital velocity profiles for different tests with the same wave conditions (regular waves with H=100cm, T=5s) (a:medium bed;f:fine)

4.5.3 Turbulence

The instruments deployed during the experiments are not optimal to detect turbulence. Their measuring volume is too large and they are too far from the bed. However, the presence of the wave boundary layer is suggested by:

a) Figure 4-24 and Figure 4-25 show velocity profiles for regular waves with H=100 and 125 cm, which are typically for a wave boundary layer (see Figure 4-27). For the waves over the rough bed (for the medium sediment) an overshoot in the velocity profile is visible. The velocity profile above the bed with fine sediments does not show any overshoot; the bed is smooth and the boundary layer is much lower.

b) The velocity phase near the bed. One could expect that this phase lag would by higher for higher boundary layers (higher ripples). This is however not really pronounced (Figure 4-26)

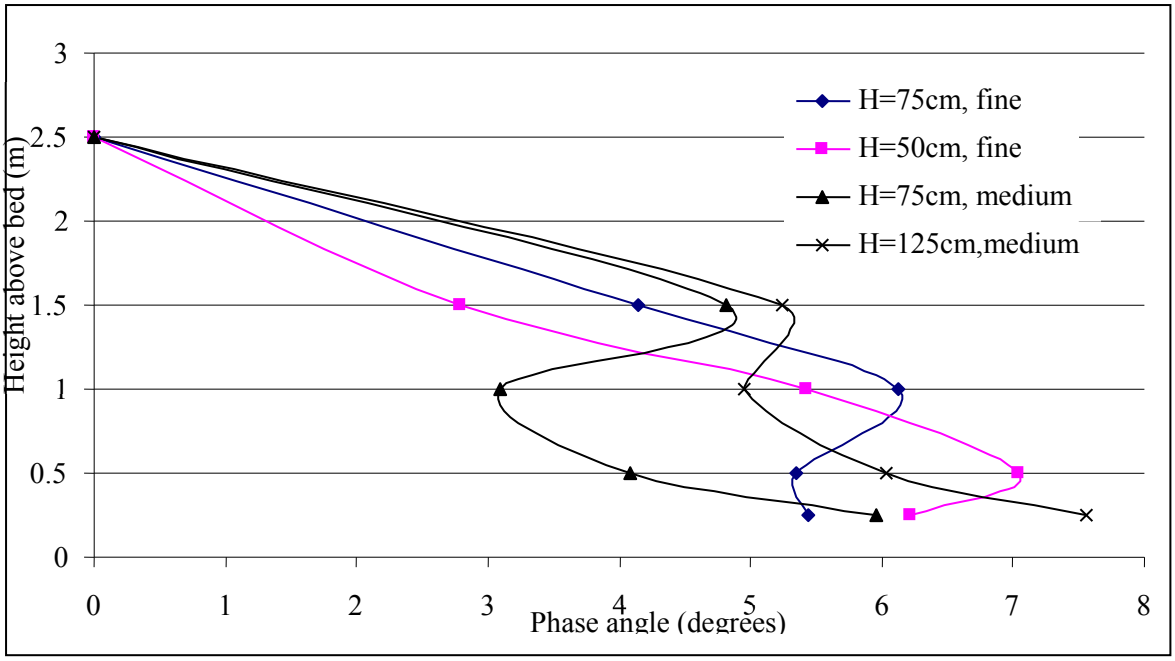

Figure 4-26 Velocity phase near bed velocity, relative to the velocity 2.5 m above the bed for different wave heights

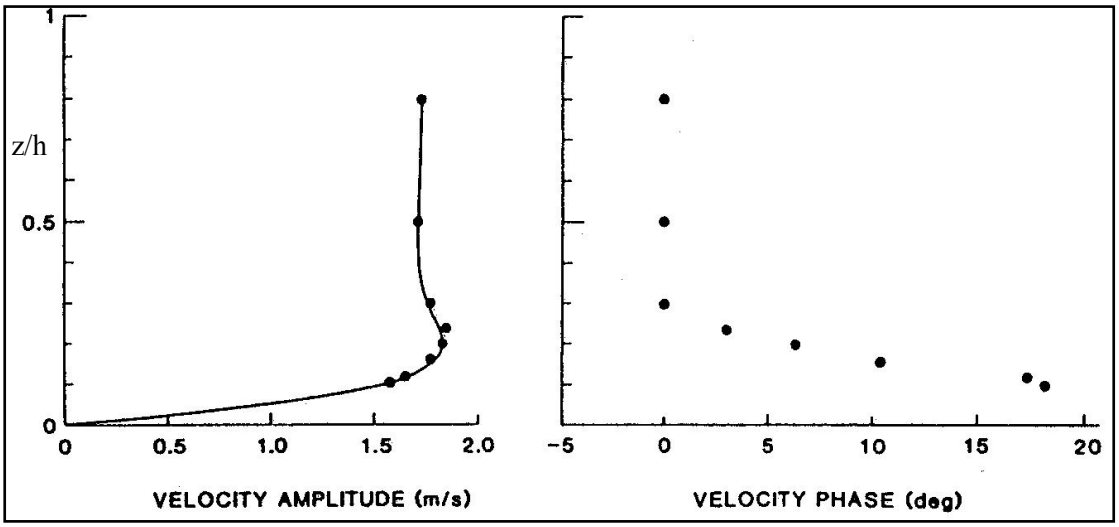

Figure 4-27 Theoretical velocity profile and velocity phase in the boundary layer = wave only conditions (Myrhaug et al., 1992)

c) Study of the powerspectra.

Figure 4-28 shows the power spectra for test A14, regular waves with a wave height of 100 cm, measured with different instruments (ADV and ECM, at the wall of the Deltaflume). Also the expected decay of turbulent energy ($S \sim f^{(-5/3)}$) (Tennekes&Lumley, 1972) is shown (the frequency associated with the energy peak at the wave component is outside the domain of the figure). Since the bed has been eroded considerably, it is estimated that the ECM's are 10 cm further from the bed than in the beginning of the tests (ECM at '25 cm' is now at 35 cm), STABLE sinks together with the ADV deeper in the bed, so that the ADV measures now at 28 cm

from the bed. The ECM's show the expected decay of turbulent energy, however, the ADV doesn't: for the higher frequencies its signal is dominated by noise. The ECM's placed 50 and 100 cm from the original bottom registered much less turbulent energy and no difference between the two is observable: the turbulence is probably not anymore influenced by the bottom. Figure 4-29 compares results from different tests with the same hydrodynamic conditions. The tests A05 and F08 are done before tests with high waves. The sand bed is not yet eroded. As expected F08 (fine sand bed, no ripples) shows much less energy since the bed is flat. A05 contains also more energy than A14 (same test conditions but the ECM's are further from the bottom in test A14). One can conclude that most energy is picked up by the ECM 'at 25 cm' from the bottom in test A05. This conclusion is consistent with Figure 4-25, where in test A05 the velocity close to the bed is much higher (boundary layer effect).

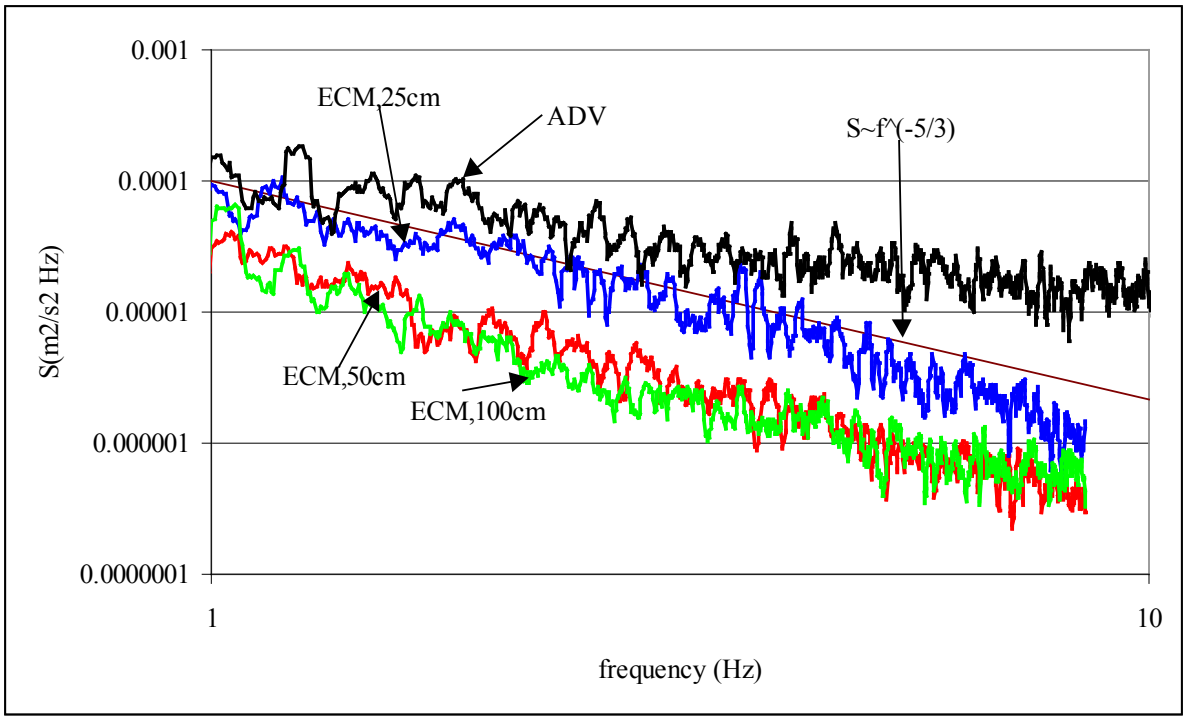

Figure 4-28 Comparison of powerspectra for the same test (A14) with different instruments/heights

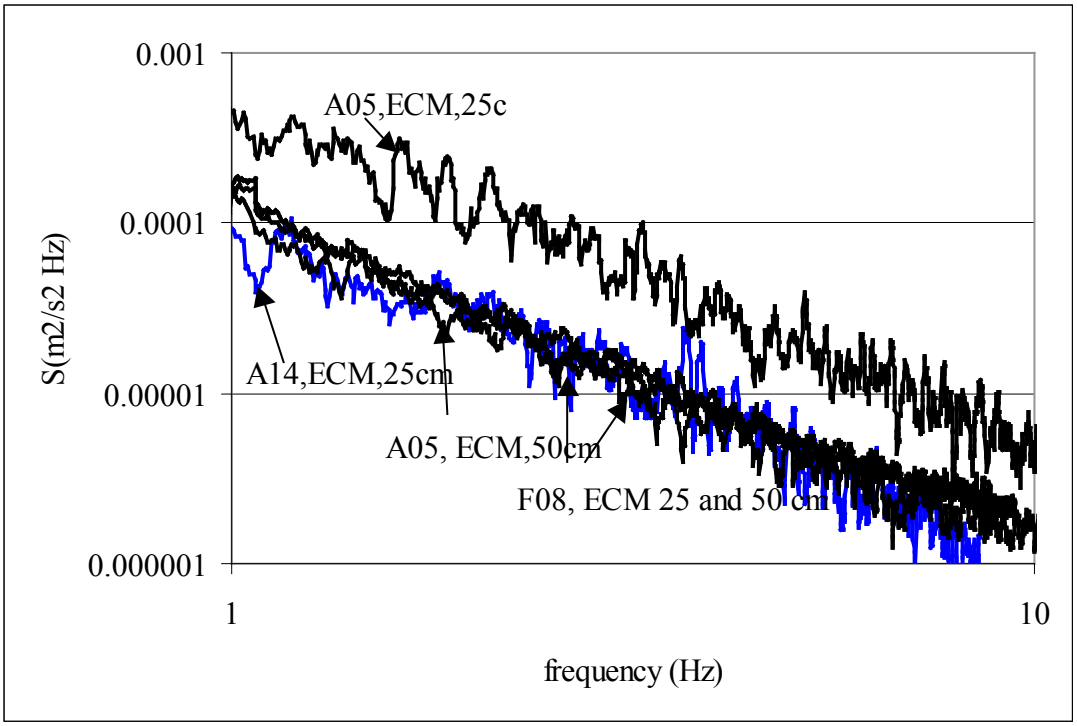

Figure 4-29 Comparison of powerspectra for the different test (A14) the same conditions (A: medium sand, F:fine sand)

It can be concluded that the ECM's can pick up a considerable part of the turbulence, although their measuring volume is relatively large (thickness of 10mm). The closer to the bed the more turbulence can be expected. However, the length scale of turbulent motion is expected to become smaller. The ECM will average out these small turbulent motions, and the performance of the ECM to measure turbulence will deteriorate.

4.5.4 Intra wave turbulence

The measured signal can be split in three parts: u= ū+ ũ+ u' with u the measured velocity, ū the mean velocity, ũ the ensemble averaged velocity and u' the (turbulent) fluctuations. The ensemble averaged velocity is here defined as the oscillating part of the velocity, which is obtained by averaging the measured velocities per phase in the wave cycle. The same can be done for the vertical velocity. If ū and ũ can be filtered out of the signal, one can obtain for each phase in the wave cycle a series of turbulent fluctuations u'. On these series a statistical analysis can be carried out in order to obtain turbulent characteristics for each phase.

For irregular waves it is not possible to determine the ensemble averaged velocity since the wave pattern repeats with a frequency of 40 minutes, it would take too long to obtain enough cycles to make a statistical analysis.

For regular waves the wave cycle is divided in a number of classes. The more classes the smaller the time step and the less the velocity is expected to vary in the class (e.g. with a time step of 1s, velocities recorded in the beginning of the class will differ substantially from the

velocities at the end of the time step, since the velocity is oscillating). But the smaller the class, the less measurements it will contain for statistical analysis.
Some methods are analysed to divide the measured signal in classes (thesis of Aerts & Kinget, 1998).

Method 1

First a reference signal is determined: this signal should correspond as much as possible with the original signal, but without the turbulent part. One option for the reference signal is the velocity far from the bottom, which should not contain turbulence anymore. However, due to phase lags and long waves (what results in different velocities near the bottom compared to higher levels) this option introduces important errors. It is decided to do an harmonic analysis of the signal, and using the lower harmonics (up to the first harmonic) and the second and third harmonic as reference signal, the other frequencies contain only turbulent energy. The reference signal is then divided in velocity classes: each point of the reference signal is put in the class with a velocity as close as possible to the characteristic velocity of the class (for each velocity two classes are identified to distinguish increasing and decreasing velocities). The characteristic velocities of a class are identified from the phases of a sinus, in order to relate velocities to phases. The amplitude of this sinus-signal is a little bit larger than the maximum velocity of the reference signal. For each point in the measured signal the value is compared with the corresponding point of the reference signal. The difference is due to turbulence (u') and is kept in the appropriate class. Classes that contain only a few velocities are skipped. After classes are skipped, the retained classes are identified with new phases (e.g. if 185 of the original 240 classes are retained, class i corresponds with phase (360/185).i.) Since the waves are asymmetric more classes are skipped for negative than for positive velocities, and downward zero crossing will be seen at a phase higher than 180 degrees. So turbulent quantities do not have to be compared with the phase, but relative to the velocity (e.g. turbulence at maximum velocity or at zero crossing).

Figure 4-30 compares the reference signal and the measured signal. Important turbulent fluctuations occur at the velocity peaks.

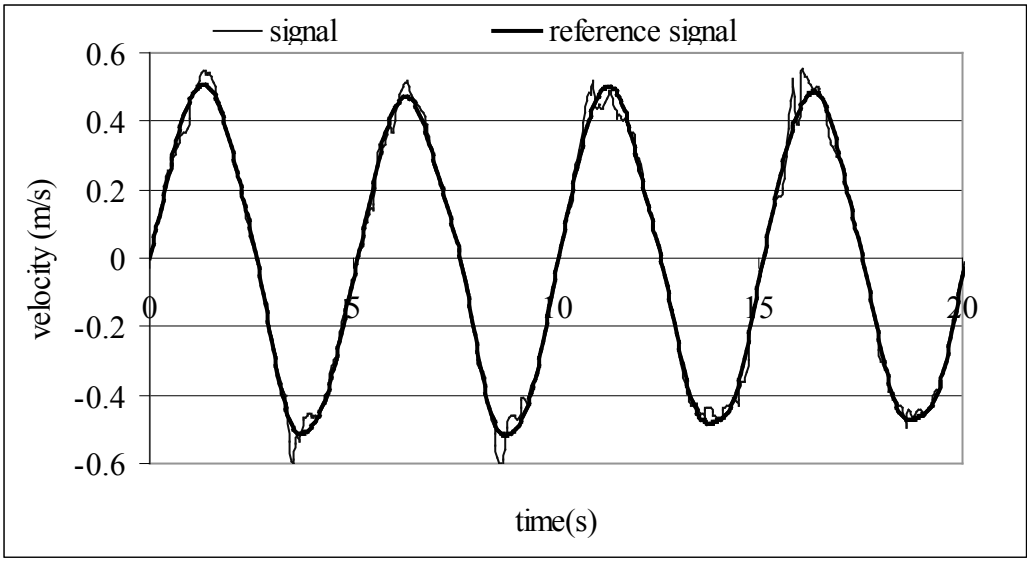

Figure 4-30 Comparison of measured and reference signal

No additional reference signal for the vertical velocity is necessary. The vertical velocity is kept in the same phase (class) as the class for the corresponding horizontal velocity. For each class the averaged vertical velocity can be determined.

Method 2

Method 2 is basically the same as method 1. The classes are not anymore determined by comparing the velocity of the reference signal with the velocities of a sinusoidal signal (method 1) but by making n classes, where class 0 corresponds with the first point after zero crossing of the reference signal, class i for the points after i time steps. (e.g. if each class has a time step of 0.04s, a point 2s after zero crossing of the reference signal is put in class 50). Classes cannot be shorter than 0.04s since the measuring frequency is 25Hz. For each class, one can again calculate the averaged velocity and turbulence characteristics.

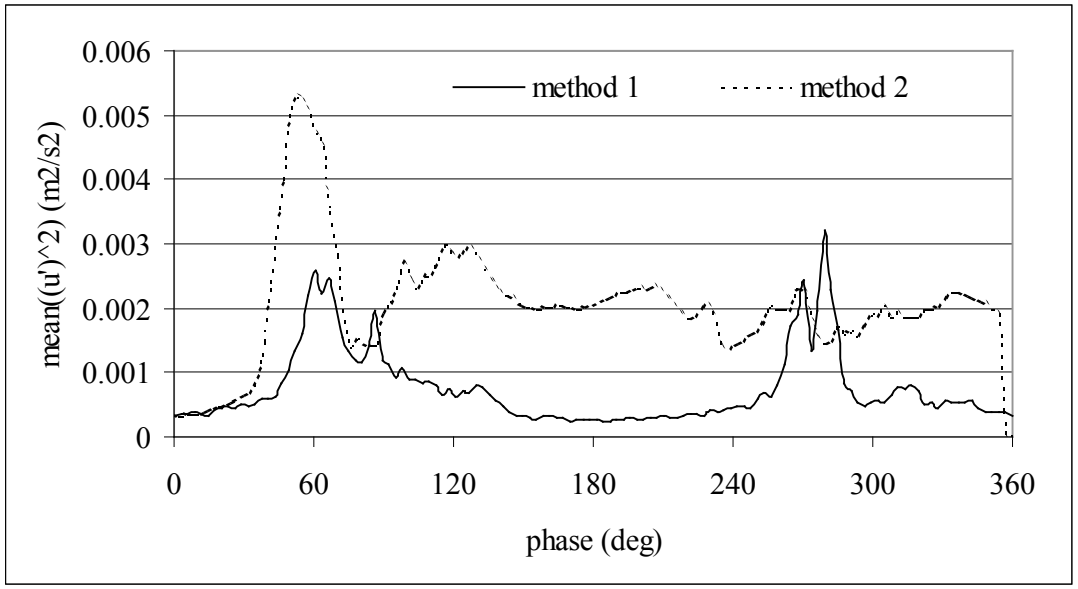

Figure 4-31 Comparison of method 1 and 2 (test A08, 25cm above bed)

Figure 4-31 compares method 1 and method 2 for the same test (A08, regular waves, H=75cm), by comparing $\overline{u'^2}$.

Method 2 seems to contain a lot of noise and the two peaks are not symmetrical. There are a number of possibilities for the worse performance of method 2. The limited number of classes can be too rough. Or because the wave period is assumed to be fixed, while maximum velocity will not for all waves be reached at the same time after zero crossing. A third possibility is that a 'wrong' zero crossing for method 2 affects all points between the zero crossing and the next zero crossing (they will all be shifted into the wrong class).

Results

Figure 4-32 to Figure 4-36 show the results of method 1 for regular waves. For test A05 (regular waves on a medium bed, H=100cm), results are shown for a height of 25 cm and 1m. At 25 cm from the bed, turbulence is mainly observed near maximal horizontal velocities, (which is about 10 degrees in advance of the maximal wave height (Figure 4-26, using H=75cm and H=125 (medium) as indication)). The calculated shear stress (multiplying the value of $-\overline{u'v'}$ in the figure with the densitiy ($\tau = -\rho\overline{u'v'}$)), is negative (-1N/m^2) for maximal positive velocity, while a positive shear stress occurs for the peak minimal velocity. A possible explanation could be the travelling of vortices (see Chapter 6). Also the vertical velocity does show unexpected characteristics: it reaches its maximum near maximal horizontal velocity, from linear wave theory a zero vertical velocity is expected. This again can be an indication of vortices. At a height of 100cm Figure 4-33 shows that the turbulence is a factor 10 smaller than at 25 cm from the bed (cf. Figure 4-29) and the vertical velocity corresponds with the expected pattern. 'Turbulence' is spread over all phases and is probably noise dominated.

For the same hydrodynamic conditions but above a fine sand bed (without ripples) Figure 4-34 shows that turbulence is also much less than above a rippled bed.(cf. Figure 4-29). The pattern of the vertical velocity is smooth, but not sinusoidal, the expected phase lag with the horizontal velocity (90˚) is smaller.

Figure 4-35 shows the results above a medium sand bed for waves with a wave height of 75 cm. Remarkable is that the peak shear stress occurs before maximum velocity. A possible explanation is that the relative horizontal position of the ECM to the ripple crest is different than for the other tests. Results of 125cm wave heights are presented in Figure 4-36. For positive velocities, three peaks in the shear stress are observed, of which only one is positive.

For the waves with a wave height of 125 cm, it is expected, due to the lowering of the bed, that the measurements 'at 25cm from the bed' are actually about 35 cm from the bed.

Closer to the bed, for a rippled bed, turbulence will not be the only important parameter for the movement of sediments: the vortex mechanism will be dominant (cf. chapter 6) . The vertical velocities (which are no-zero and about 90 degrees out of phase with the horizontal velocities) suggest the presence of the vortices.

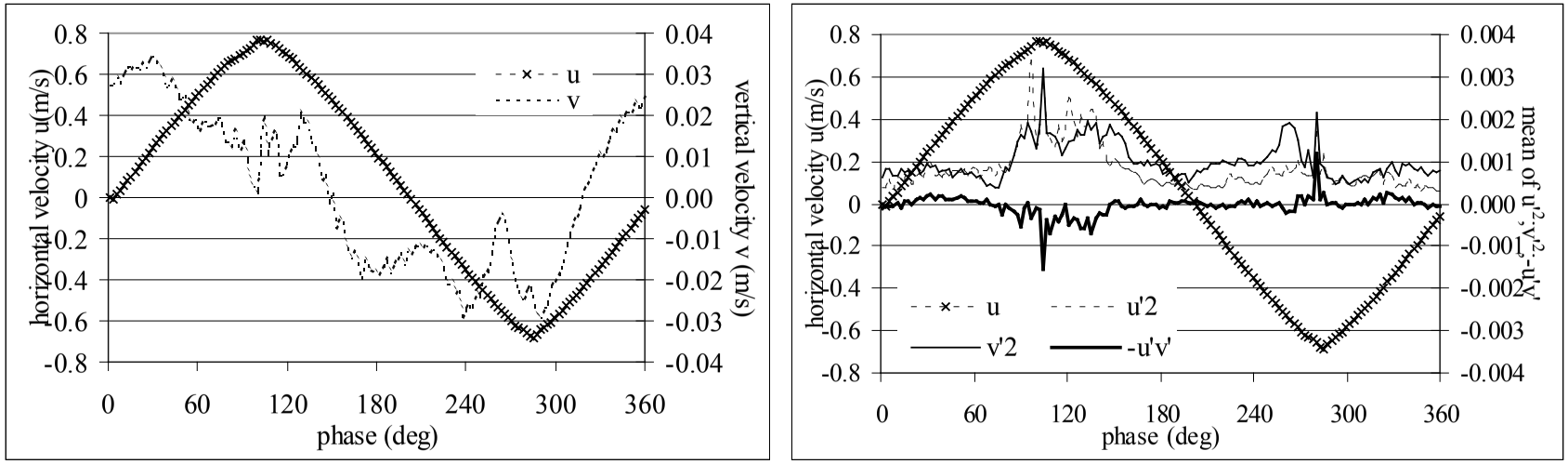

Figure 4-32 Turbulence parameters for test A05a, 25cm from the bed (medium sand, regular waves, H=100cm, T=5s)

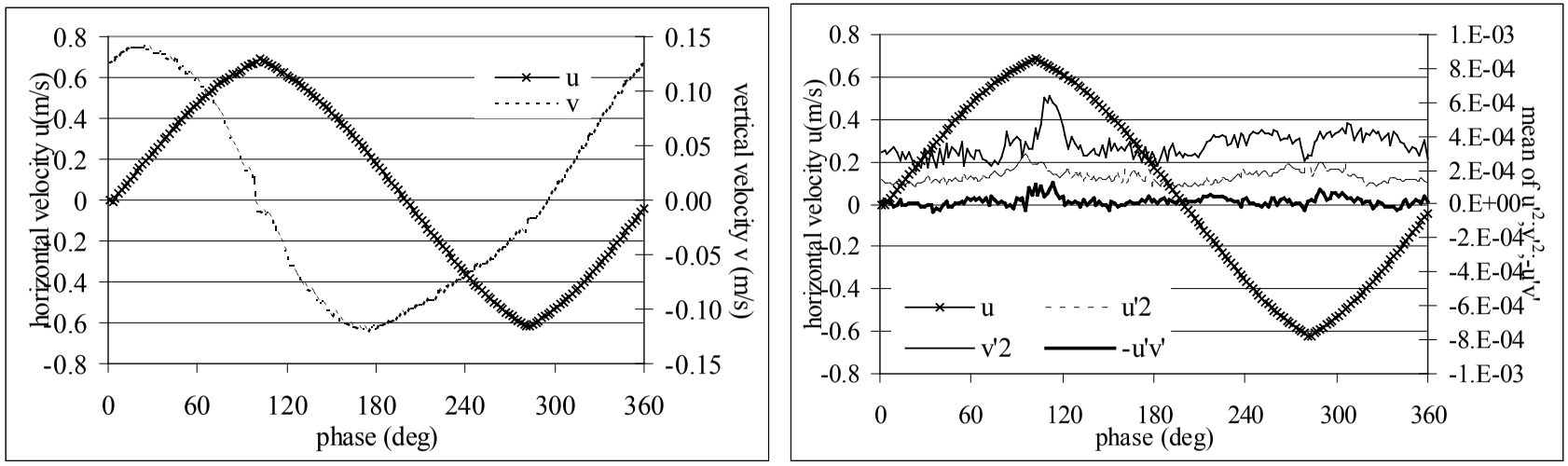

Figure 4-33 Turbulence parameters for test A05a, 100cm from the bed (medium sand, regular waves, H=100cm, T=5s)

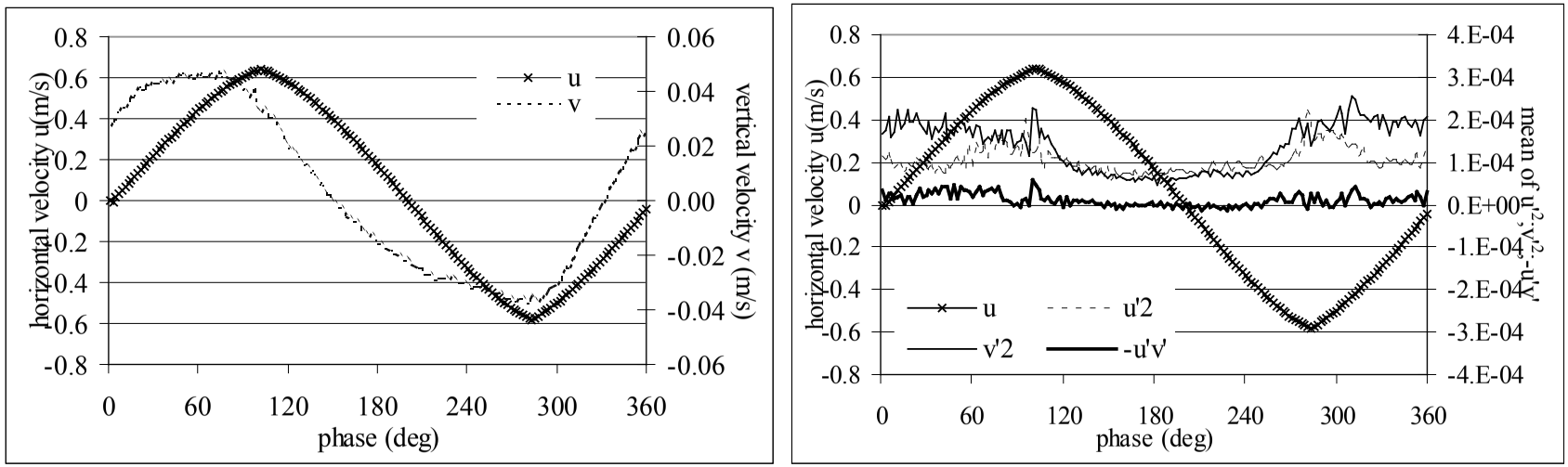

Figure 4-34 Turbulence parameters for test F08a, 25cm from the bed (fine sand, regular waves, H=100cm, T=5s)

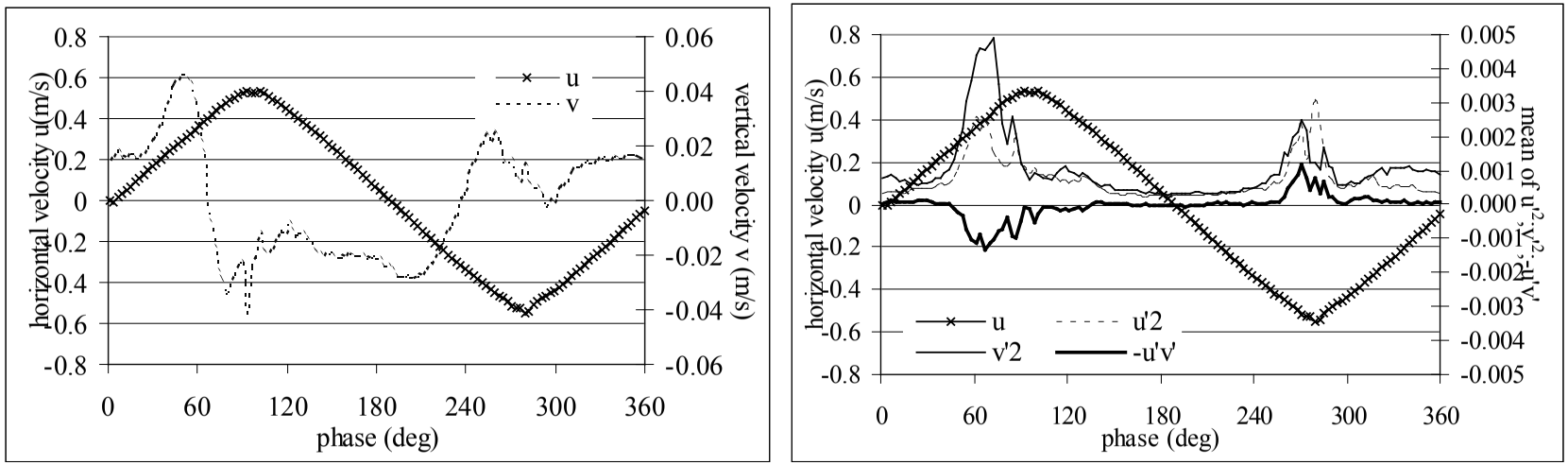

Figure 4-35 Turbulence parameters for test A08a, 25cm from the bed (medium sand, regular waves, H=75 cm, T=5s)

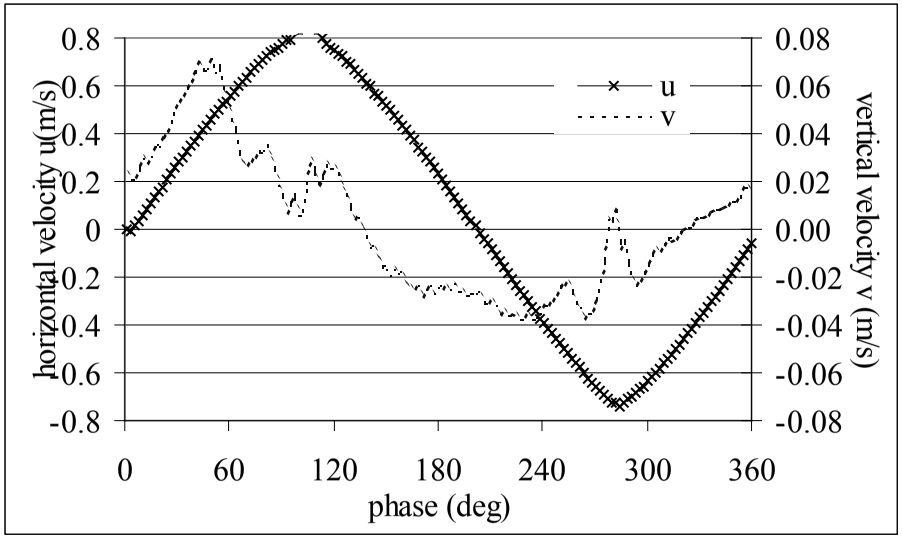

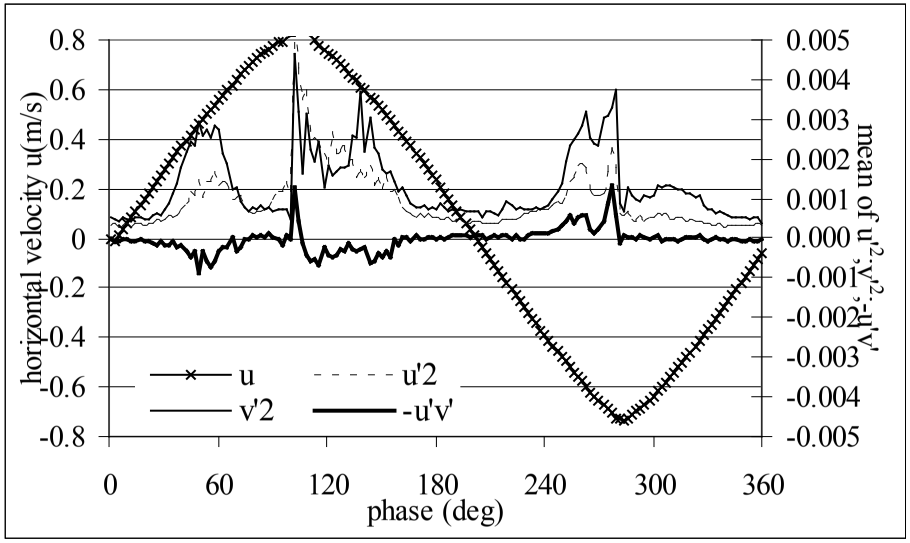

Figure 4-36 Turbulence parameters for test A11a, 25cm from the bed (medium sand, regular waves, H=125 cm, T=5s)

4.6 Suspended sediment concentration profiles

4.6.1 Time averaged concentration profiles

Two pump sampling devices were used: one 50cm from the wall of the Deltaflume, the other mounted on STABLE. The device near the wall rests only on the (sand) bed and accordingly the vertical position of the nozzles relative to the bed does not change due to erosion/sedimentation. The one mounted on STABLE is moving with the frame, after some time the lowest nozzle was sunk under the bed level due to the (small) sinking of STABLE.
The volume (and weight) of the collected sand was determined on site by emptying the sample in a tube, reading the volume and using tables to get the original concentration. These tables take the sucking efficiency factors (≈70%) into account. Afterwards, the samples were also analysed in a lab (weight and grain size distribution).
The pump sampling was the main delaying factor during experiments, since the analysis of the samples had to be finished in order to have empty buckets to start the next test. The most optimal procedure was to fill a bucket (10 liters, necessary time 10 minutes) (Figure 4-6), let the sediment settle down in the bucket, empty most of the water in the bucket, emptying the rest of the bucket in the measuring tube, let the sediment settle down, read the height of the sediment in the tube, empty the tubes in plastic bags for further analysis (grain sizes). In the meantime the same work can be done with a second set of buckets. Mostly, the first set was used for the pump sampling under STABLE, the other set for the sampling at the wall.

4.6.1.1 Measuring accuracy

The pump sampling technique is the only technique which measures directly the amount of sediment in the water, all other techniques measure the effects of sediment in the water (attenuation of light or sound) and need calibration to relate the effect to a concentration.
Although the technique seems simple, it is not faultless due to
1) Trapping efficiency

Due to the inertia of the grains in the water, the trapping efficiency depends on the water velocity, the intake velocity in the nozzle, the direction between the nozzle and the flow and the grain size.

For steady flow conditions and with large intake velocities Bosman et al. (1987) obtained trapping efficiencies (C_s/C_c with C_s the concentration of the sucked samples and C_c the concentration in the flow) varying between 0.8 (d_{50}=70μm) and 0.7 (d_{50}=450μm).

Figure 4-37 represents the influence of flow velocity and relative intake velocity (scaled with the flow velocity). The intake velocity for the experiments in the Deltaflume was 2.4m/s. For most of the tests (if STABLE was not turned) the

direction of the nozzle was perpendicular to the flow, and the velocities were seldom higher than 1 m/s, so for these tests the trapping efficiency does not depend on the velocity during the wave cycle. If STABLE is turned 45º the trapping efficiency will become time dependent. E.g. according to Figure 4-37 the trapping efficiency will change from 0.75 to 0.5/0.6 when the flow direction reverses (or on average ≈0.65, compared to 0.72 when the nozzle is perpendicular to the flow)

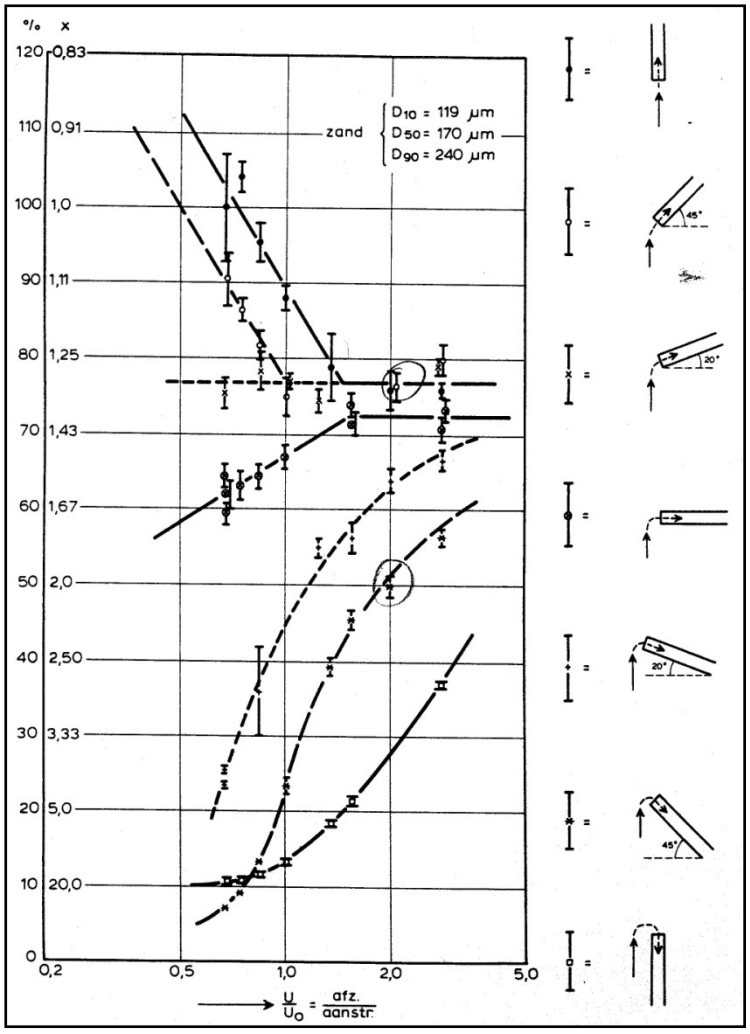

Figure 4-37 Trapping efficiency as function of flow direction and relative intake velocity (nozzle diameter = 3mm) (Bosman et al., 1987)

Figure 4-38 shows that the results of the pump sampling under STABLE 45 degrees turned (test A14) are well comparable with test A05 and A19, for which the waves were the same. In Figure 4-39 (regular waves over a fine sand bed) the concentration near the bed is even larger if STABLE is turned.
It can be concluded that other errors will be dominant.

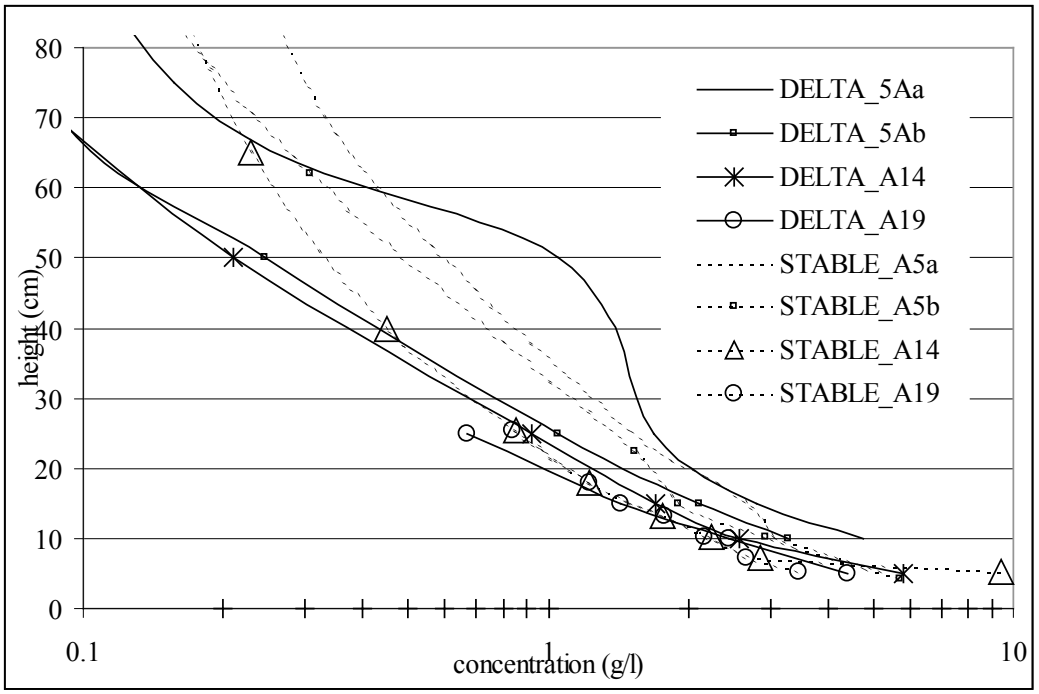

Figure 4-38 Comparison of pump sampling results for different tests with the same wave conditions (regular waves H=100cm, T=5s) on the medium bed. (ripple heights: A5a:5.5cm,A5b:5.75cm, A14:5cm, A19:?, STABLE was turned 45° for A14, log-scale for concentrations)

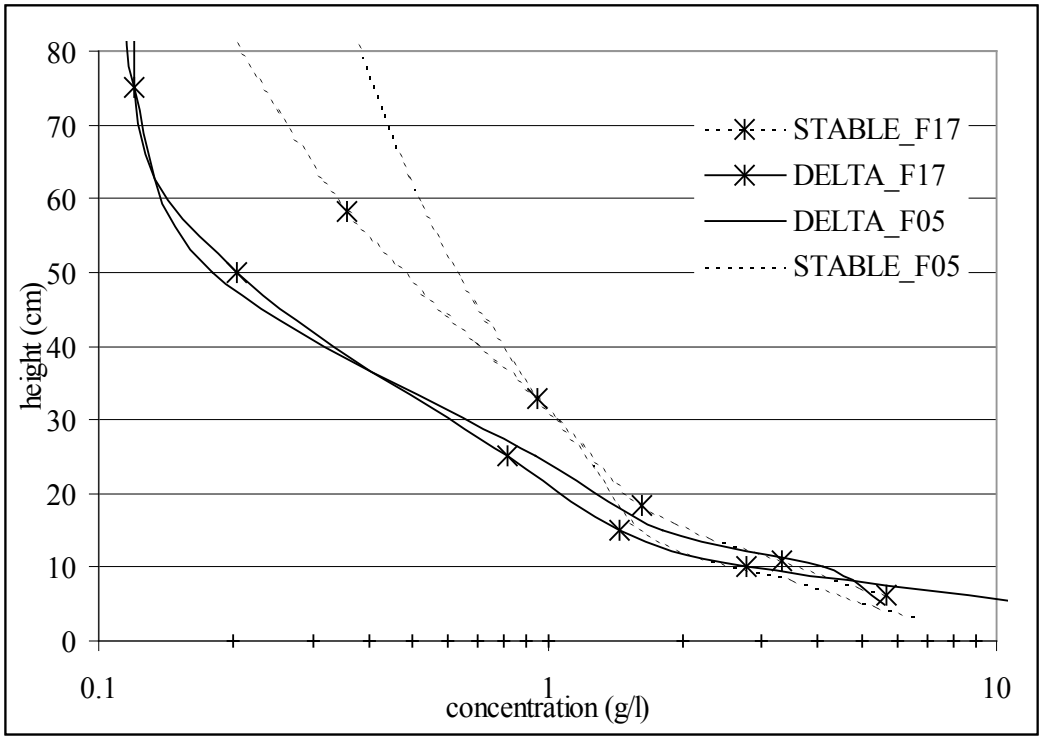

Figure 4-39 Comparison of pump sampling results for different tests with the same wave conditions (regular waves H=75cm, T=5s) on the fine bed. (ripple heights: F05a:0cm,F17:2cm, STABLE was turned 45° for F17, log scale for concentrations)

2) Measuring location

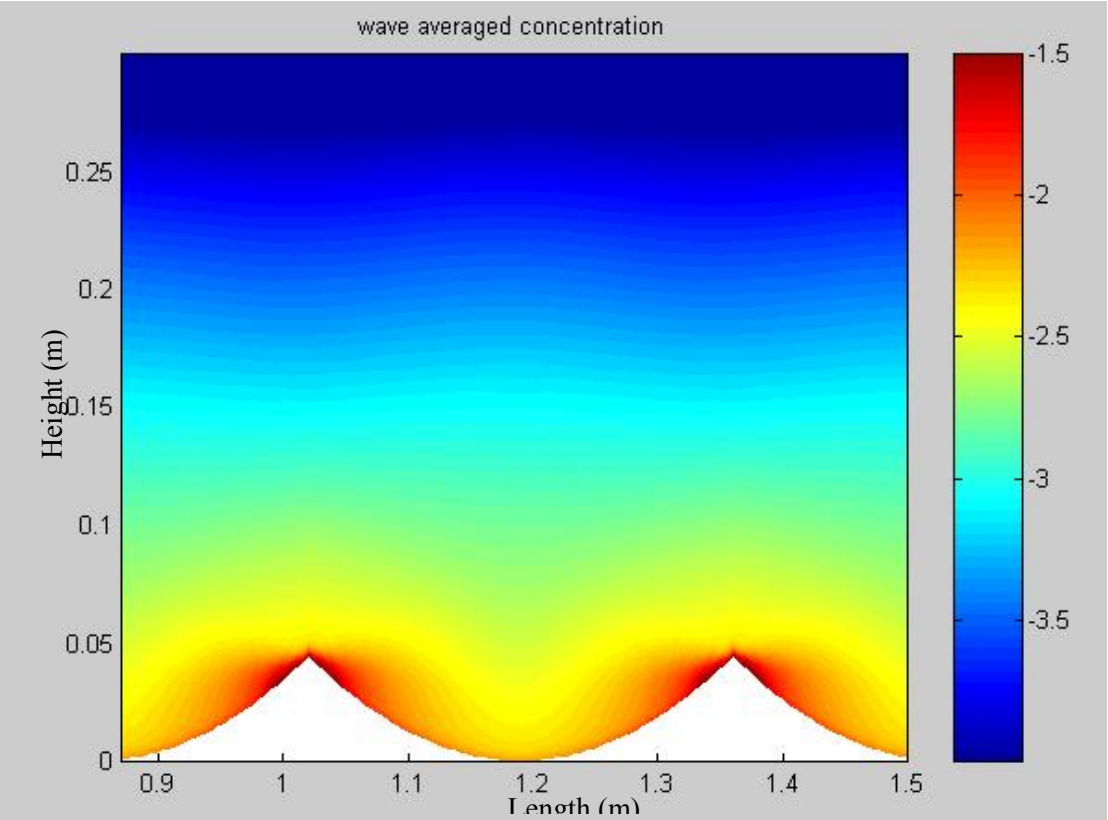

Figure 4-40 Wave averaged concentration (log-scale for concentration (m^3/m^3) (simulation of test A08, regular waves H=75 cm, medium bed) (Trouw et al., 2000)

Since the sampling takes only 10 minutes, ripples did not move fast enough (Figure 4-16 and Figure 4-17) to pass completely under the nozzle. The sampling will be averaged over only a limited part of the ripple length. The time averaged sediment concentration near the bed will depend on the relative location of the nozzle to the ripple crest as is illustrated in Figure 4-40 (from numerical model).

A second problem is the vertical position of the nozzles. The pump sampling device under STABLE is fixed to the frame, but is sinking together with the frame downward. The amount of sinking is obtained by determining the bed level registered by the ABS data. Also here, some errors occur: a) the ABS is only registering 17 minutes, which is not enough to average out ripple variations (same problem as for the pump sampling) b) the ABS is not measuring at the same horizontal location as the pump sampling device c) some variation in results exists between the 3 ABS sensors.

Also for the fine sediments, where no ripples are present, this problem exists due to the presence of dunes (large smooth structures, typically 1 m long and a few centimetres high, not steep enough to get vortices).

A rough estimation of error in vertical position is 2 cm plus half the ripple height. This error makes the error due to the height of the intake of the nozzle (=diameter=3mm) negligible.

3) Error on the mass of sand in the bucket

Some minor losses of the finest sand particles might occur when emptying the bucket after the material has settled down. These losses are estimated as unimportant.

The mass obtained on site (with the tubes) and in the lab corresponded well. The difference was less than 10%, mainly due to loss of sediment during operations and due to presence of fine material, which causes a larger packing of the sediment in the measuring tube on site than taken into account in the calibration of the tubes. During the tests on the fine sand bed, some organic material and cohesive sediment was found in the tubes. This material cannot be considered as being eroded of the bed due to wave action, and should not be taken in account. Its weight was always unimportant, but the volumes are relatively important in the measuring tubes. However, most of the time a clear separation between the sand and this material was visible.

For wave conditions Bosman et al. (1987) compared pump sampling results with a calibrated OPCON (cf. Chapter 5) in the wave tunnel. The pump sampling device and the OPCON were moved back and forth over the ripples in order to get horizontal averaged concentrations (which is hardly possible in the large Deltaflume). They estimated a 10% systematic error due to errors in vertical positioning (estimated at 1mm in the wave tunnel), 3% systematic error due to the calibration of the trapping coefficient and 5% random error due to the accuracy of the wet volume measurements.

4.6.1.2 Influence of STABLE

In Figure 4-38, Figure 4-39 and Figure 4-41 to Figure 4-43 some comparisons are shown between the measurements at STABLE and near the wall of the Deltaflume. It can be concluded that the differences near the bed are small compared with the differences between two tests at the same location (due to unknown vertical position or different ripple dimensions). At higher location the differences can become more important, probably due to the turbulence generated by the instruments mounted on STABLE (see Figure 4-8).

For the fine sediment bed, a kink is visible in the concentration profiles, which occurs at a higher level for the measurements near the wall than under STABLE.

Possible causes for differences, especially at higher levels, are the grain size distribution that might not be uniform over the whole bed (e.g. due to local washing out of fine material).

Since at higher levels only the finest bed sediments are found, the concentration depends strongly on local availability.

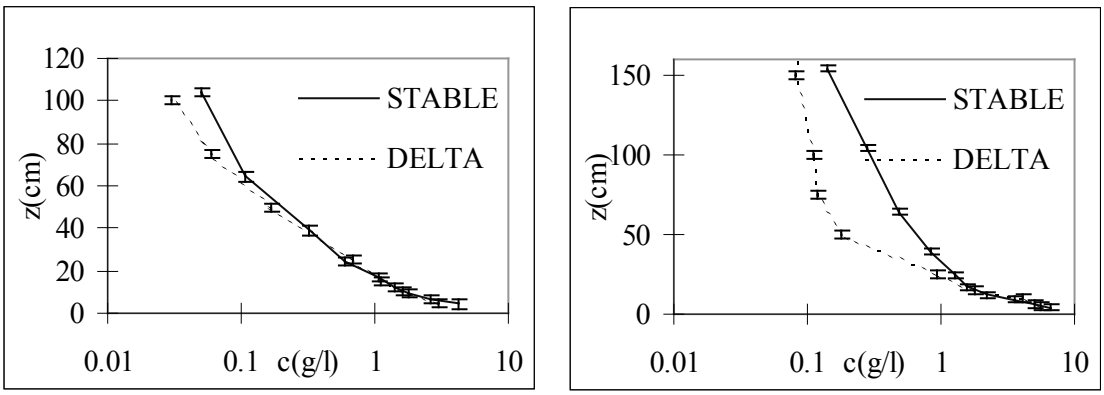

Figure 4-41 Comparison of concentration profiles measured near the wall (DELTA) and under STABLE for regular waves (H=75 cm, left: medium bed right: fine bed)

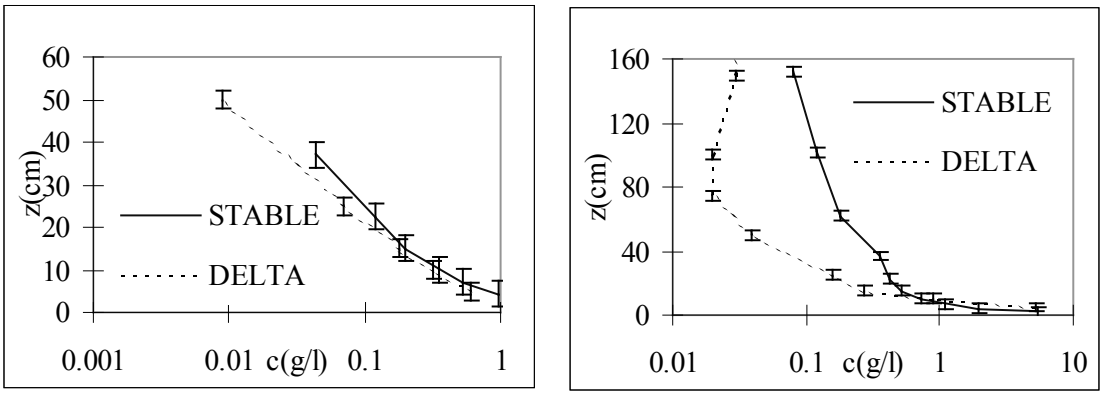

Figure 4-42 Comparison of concentration profiles measured near the wall (DELTA) and under STABLE for irregular waves (H_s=75 cm, left: medium bed right: fine bed)

4.6.1.3 Influence of the bed material

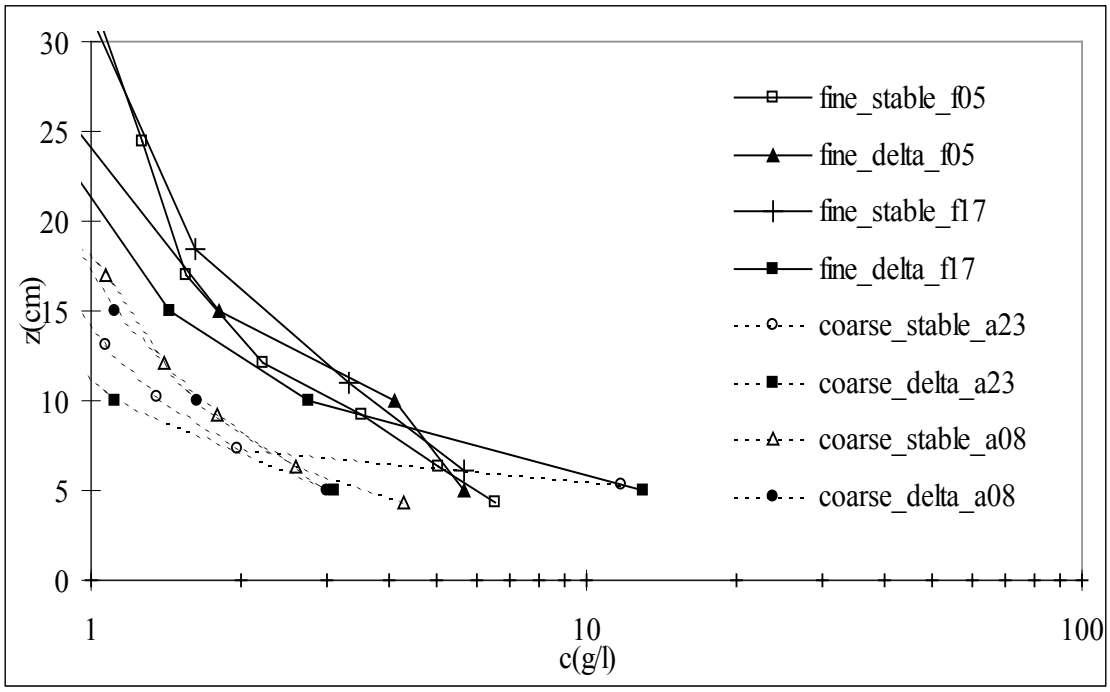

Figure 4-43 Comparison of concentrations for regular waves (H=75cm) over medium (A) and fine sand bed (F) (full lines: fine, dotted: medium;full marks:delta, empty marks:STABLE)

Figure 4-41 and Figure 4-43 make clear that the concentrations over the fine bed are higher. The difference is limited due to the absence of ripples for the fine sand bed.

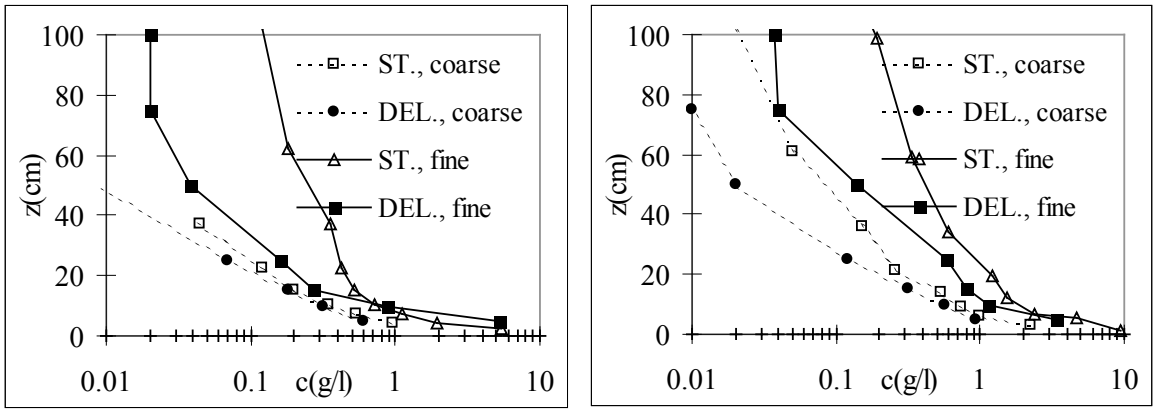

Figure 4-44 Comparison of concentrations for irregular waves over medium and fine sand bed (left: H=75cm;right:H=100cm)

Figure 4-44 suggests that for irregular waves the differences are more pronounced than for regular waves.

For regular waves with a wave height of 100 cm, no clear differences are observable (Figure 4-45). More swirling due to the presence of ripples compensates the effect of higher settling velocities for the medium sediments. For both the regular waves of 75cm and 100 cm over

the medium bed the ripples are steep, with the same dimensions, while they are absent over the fine bed. The ripple dimensions can not explain why for regular waves the concentration profiles are almost equal, while for irregular waves the concentration profiles are an order of magnitude different. A possible explanation might be that the fine sediments do not get the time to settle down when small waves pass over the bed, while the sediment settles down completely for the medium sediment. This might result in a higher influence of grain sizes for concentration profiles due to irregular waves. Since for regular waves, no small waves occur in the wave train, this effect is only observable for the irregular waves.

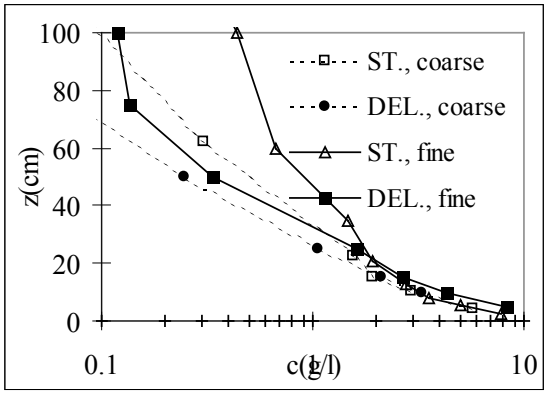

Figure 4-45 Comparison of concentrations for regular waves over medium and fine sand bed (H=100cm)

4.6.1.4 Differences between regular and irregular waves

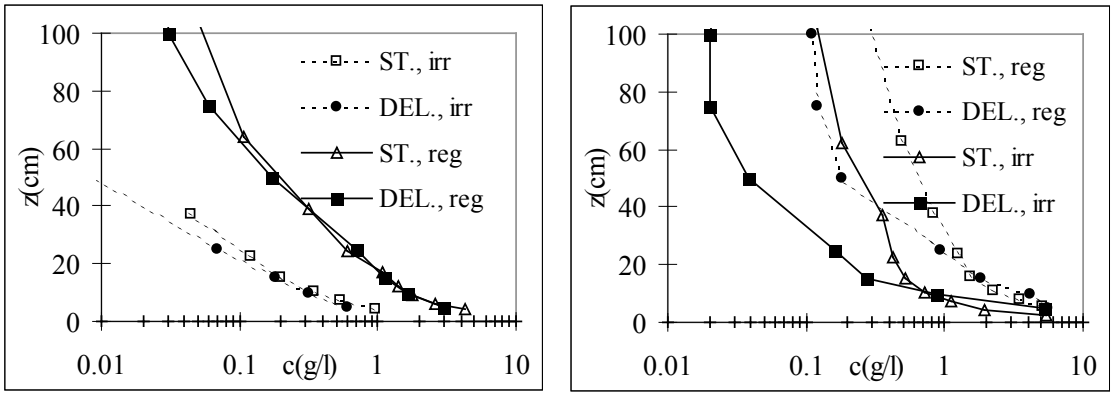

Figure 4-46 Comparison of concentrations for regular and irregular waves over left: medium and right: fine sand bed (H=75cm)

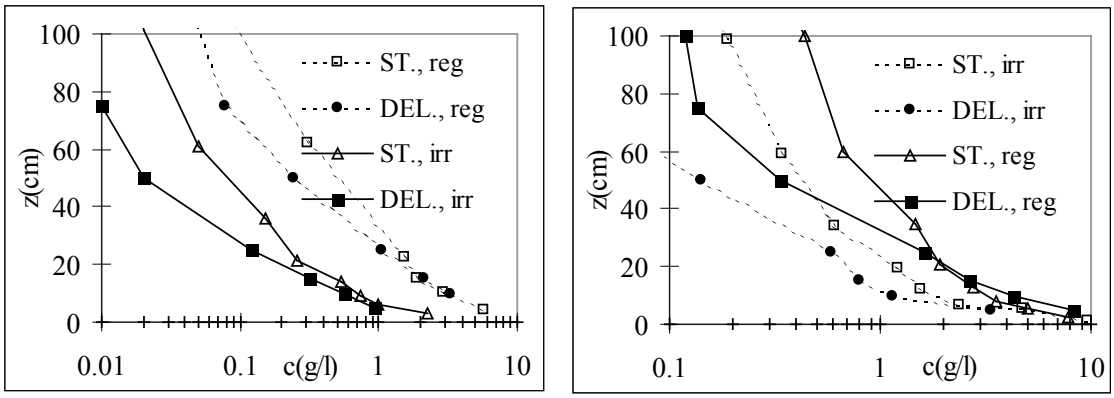

Figure 4-47 Comparison of concentrations for regular and irregular waves over left: medium and right: fine sand bed (H=100cm)

Figure 4-46 and Figure 4-47 indicate that irregular waves carry less sediment in suspension than a regular wave with a wave height equal to the significant wave height. The significant wave height is the average of only the 33% highest waves, so that a fair comparison is not possible. A better parameter to compare with is the energy of the waves (or root mean square wave height (H_{rms}). Since $H_{rms} = 1/\sqrt{2}H_s$, so it is better to compare the regular 75 cm wave with the irregular 100 cm wave, as done in Figure 4-48. For the fine bed, the concentration profiles are comparable, which is not the case for the medium bed. As is discussed for the influence of the bed material, this might be explained by the quick settlement of coarse grains when low waves pass in the irregular wave train.

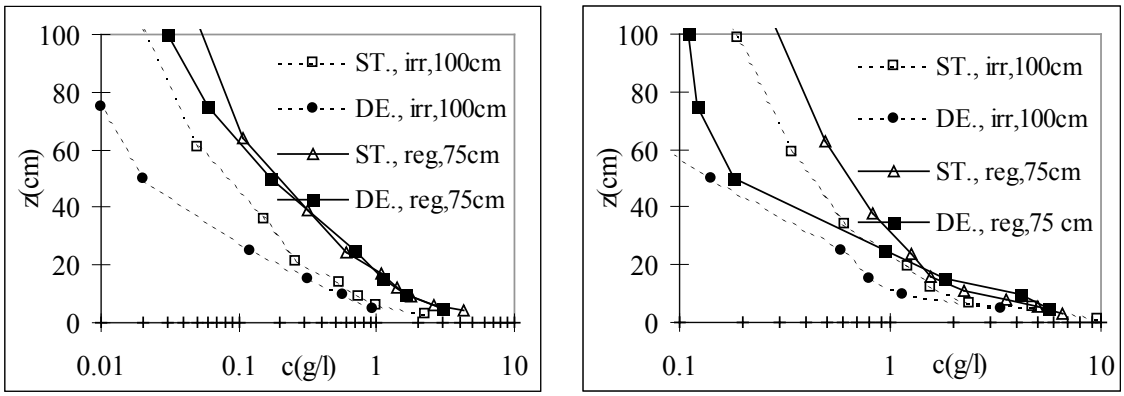

Figure 4-48 Comparison of concentrations for regular and irregular waves over left: medium and right: fine sand

4.6.1.5 Influence of wave height

Figure 4-49 and Figure 4-50 show the influence of the wave height on the concentration profiles for resp. regular and irregular waves.

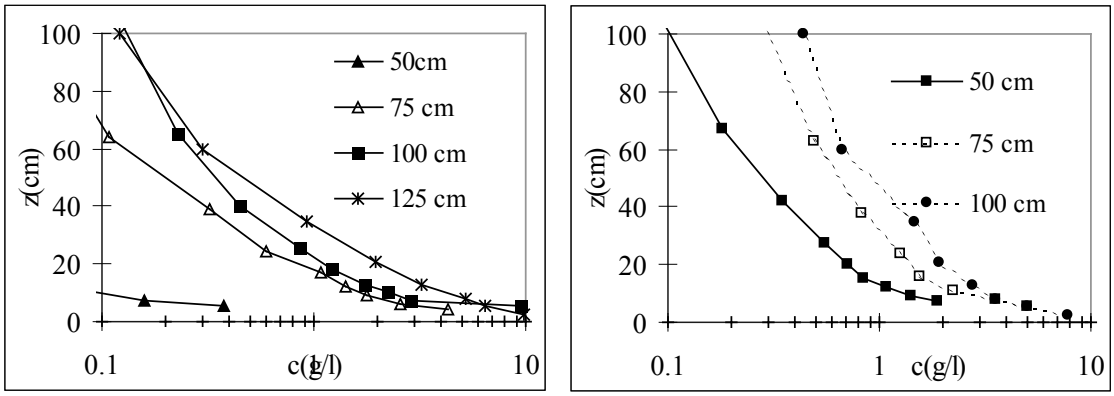

Figure 4-49 Comparison of concentrations for regular waves with different wave heights over left: medium and right: fine sand

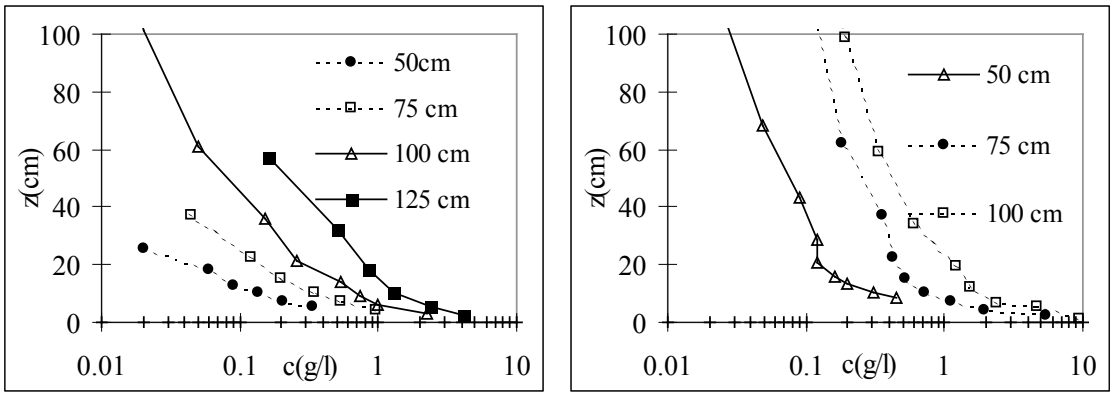

Figure 4-50 Comparison of concentrations for irregular waves with different wave heights over left: medium and right: fine sand

Higher waves cause higher concentrations. For the medium bed the ripples are not washed out when increasing the wave height (which might have caused a decrease in concentration).

4.6.1.6 Influence of wave period

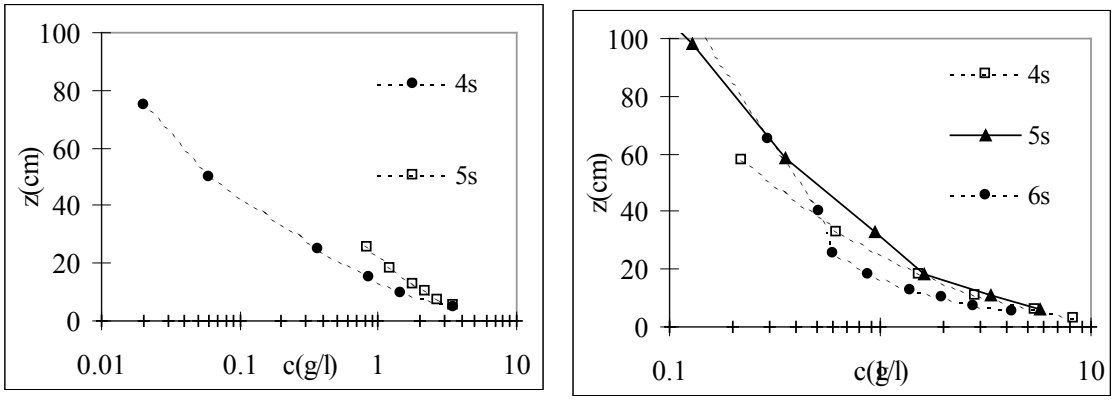

Figure 4-51 Comparison of concentrations for irregular waves with different wave periods over left: medium and right: fine sand

For the medium bed the concentration increases with increasing wave period (as expected since an increasing wave period results in an increasing wave orbital velocity). This is not the case for the fine sand bed. A possible reason is that small ripples are becoming less steep with increasing wave period.

4.6.2 Grain sizes

Figure 4-52 gives the grain size distribution of the (pumped) samples at different heights above the bed. A very clear variation in grain size distribution is visible and even close to the bed (5cm) the sediments are much finer than at the bed.

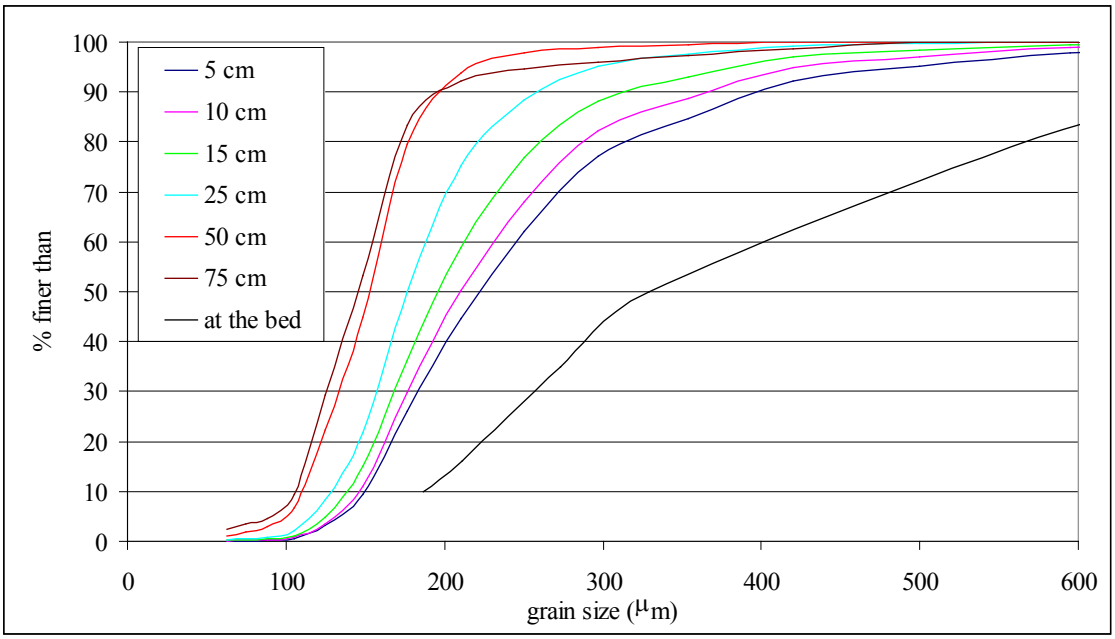

Figure 4-52 Grain size distribution for test A11A (regular waves, H=125 cm, on the medium bed), measured near the wall

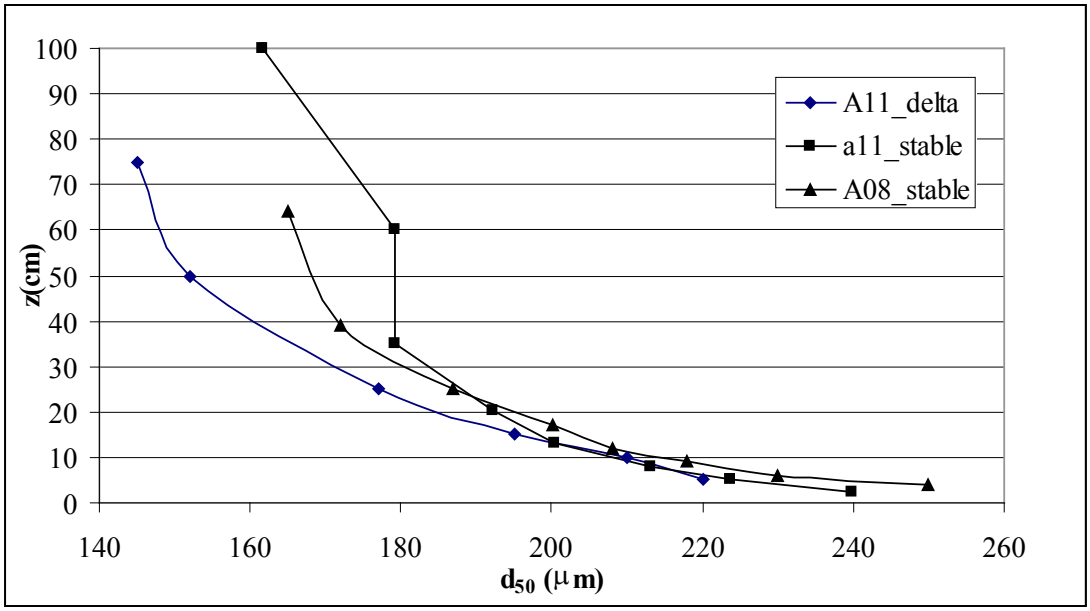

Figure 4-53 Variation of the medium grain size (medium bed, regular waves; A08:H=75 cm;A11:H=125 cm)

Figure 4-53 makes clear that close to the bed only small differences in grain sizes exist, further from the bed, the grain sizes are larger at STABLE than near the wall, which corresponds with the larger concentrations beneath STABLE.
For the fine sediments, the analysis of the dry weighted pump sampling seems unreliable, even after filtering the finest particles.

4.6.3 Intra wave concentrations

4.6.3.1 Transformation of the Acoustic backscatter signal in a concentration profile

The transformation of the Acoustic backscatter signal to concentrations is performed by Proudman Oceanographic Laboratory (POL). The technique is described by Thorne and Hardcastle (1997). It is validated for high sediment concentrations, where a lot of attenuation of the signal occurs. The technique is based on an explicit inverse modelling technique based on the assumption that the intensity of the backscattered signal depends on the grain size and the concentration. The grain size is obtained from the pumped samples. It is assumed that the grain size varies with the distance to the bed, but not with the wave conditions (which introduces an error). In order to get a concentration profile also the time the signal needs to return is registered (and linked with distance by its travelling speed). The spatial resolution was 0.01m. Each second 128 backscattered profiles are obtained, data at each range bin were averaged over 32 records to provide measurements at 0.25 s intervals. Three devices (which differ by frequency of the signal: 1;2 and 4 MHz) are used for these experiments.

The analyses of the ABS data (for test A08 to A12) took 3 years after finishing the experiments, and the differences between the 3 ABS's were sometimes large. Although this instrument will probably give nice results in the future, its handling is difficult and time consuming.

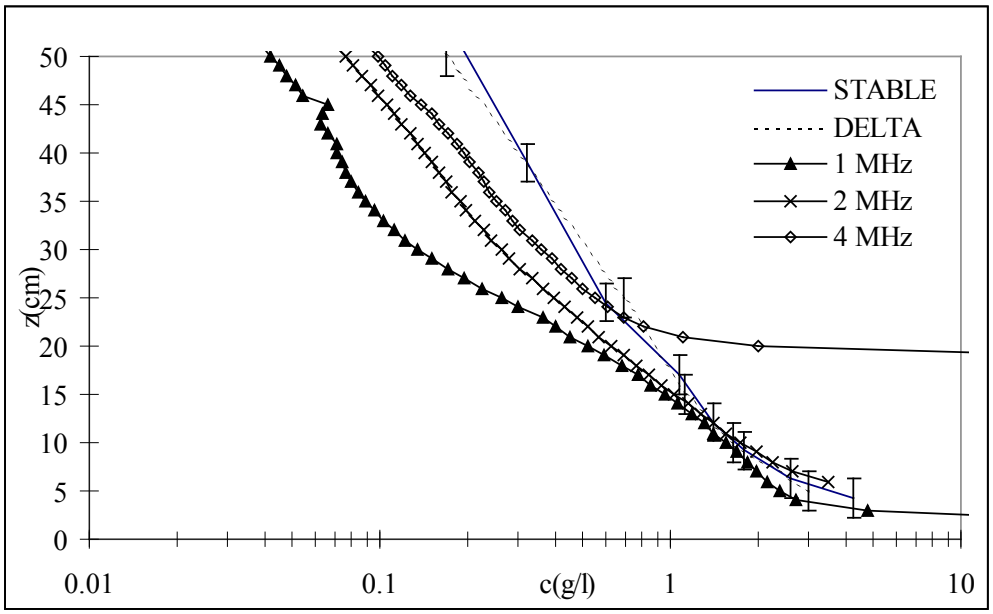

Figure 4-54 Comparison of time averaged concentration profiles obtained with the ABS and by pump sampling (test A08: regular waves with H=75 cm, medium bed)

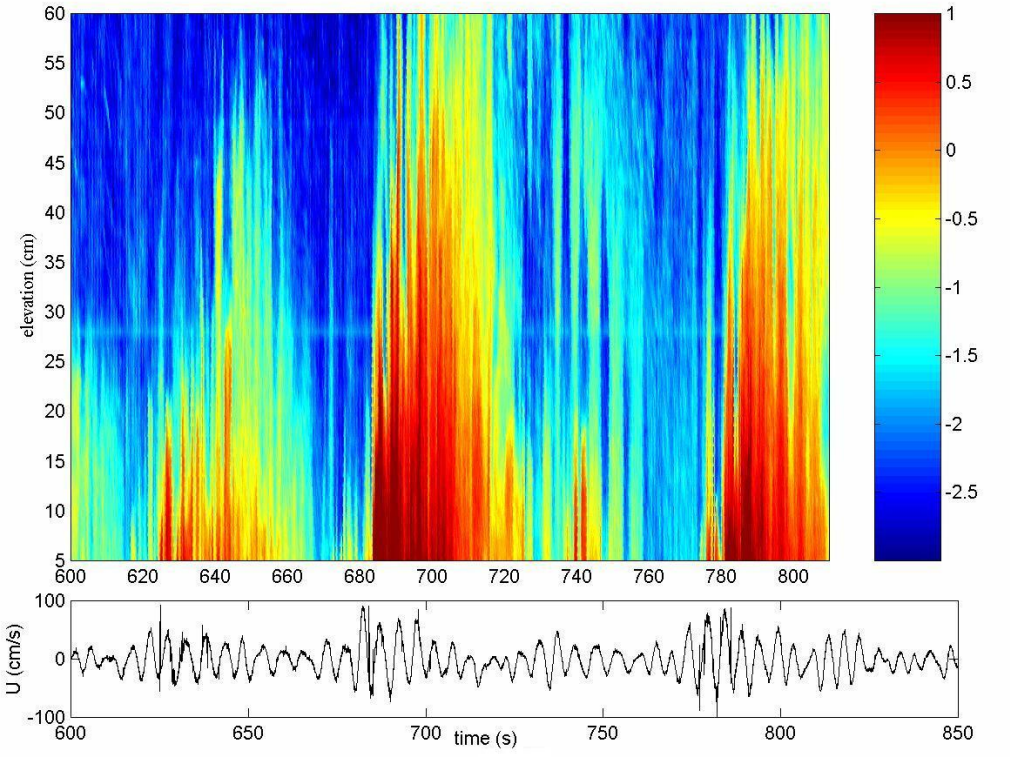

Figure 4-55 Concentration (g/l, on a log-scale) during the passing of three wave groups (test A09, irregular waves, H_s=75cm, medium bed), below the velocity recorded by the ADV

Figure 4-54 indicates that, especially near the bed, both the 1 and 2 MHz sensor give reasonable results, while the 4 MHz sensor is not able to give reasonable results. Also in the other tests, the 4 Mhz performs generally weaker. The weaker performance at higher levels is probably due to the expected bigger variation of grain sizes for different tests (e.g. Figure 4-53), while in the procedure to get concentrations from the ABS, for all test conditions the same grain size was used, only depending on the elevation from the bed.
In Figure 4-55 a clear phase lag between the highest waves and the highest concentrations is visible.
Looking in more detail to the near bed results for regular wave tests the bed elevation is important. Figure 4-56 shows that a ripple with a height of 6cm passed under the sensor.

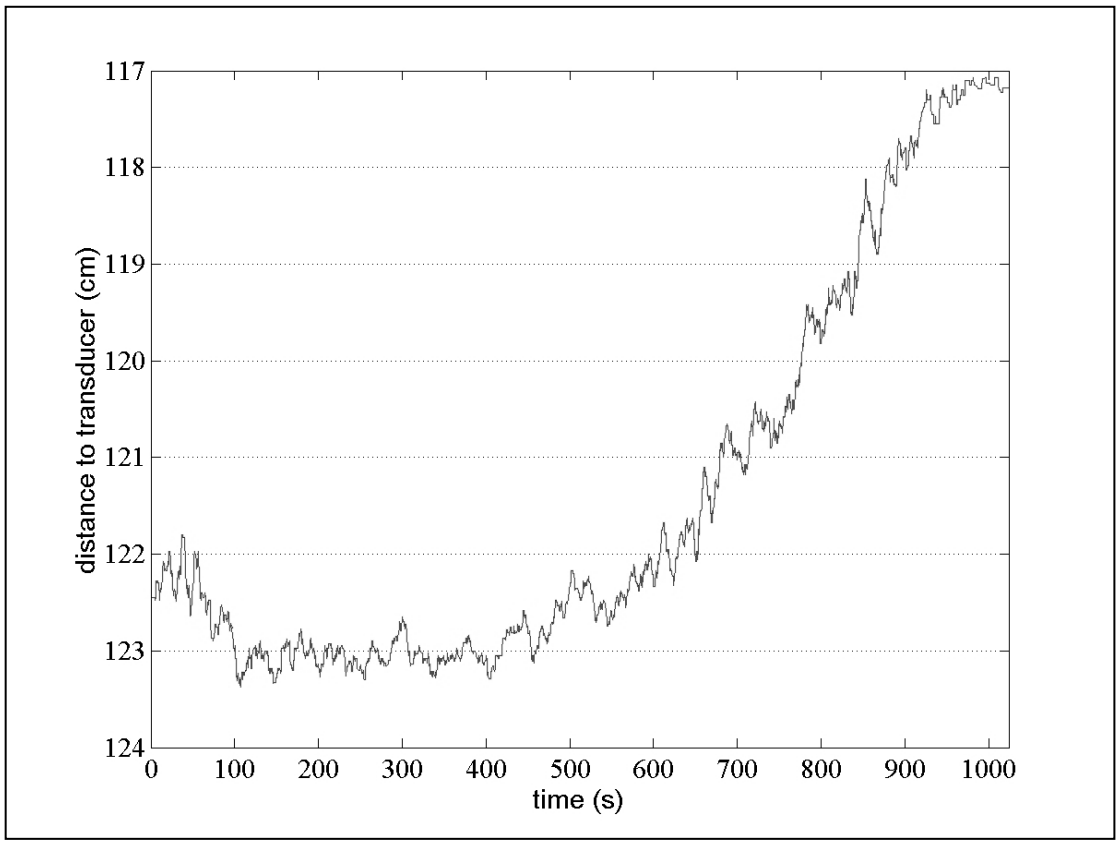

Figure 4-56 Evolution of the bed under the sensor

In Figure 4-57 the ensemble averaged concentrations are shown for resp. when the ripple trough, the ripple slope and the ripple crest passes the sensor. So results are given at 3 different moments of the 1000s recording. The ensemble averaged concentrations are defined as:

$$< F(t) >= \frac{1}{M} \sum_{m=0}^{M-1} F(t + mT) \quad for \quad 0 \le t < T \tag{4-8}$$

The averaging is carried out over different intervals (e.g. averaging over the 30 (regular) waves between 600 and 750s in the first figure).

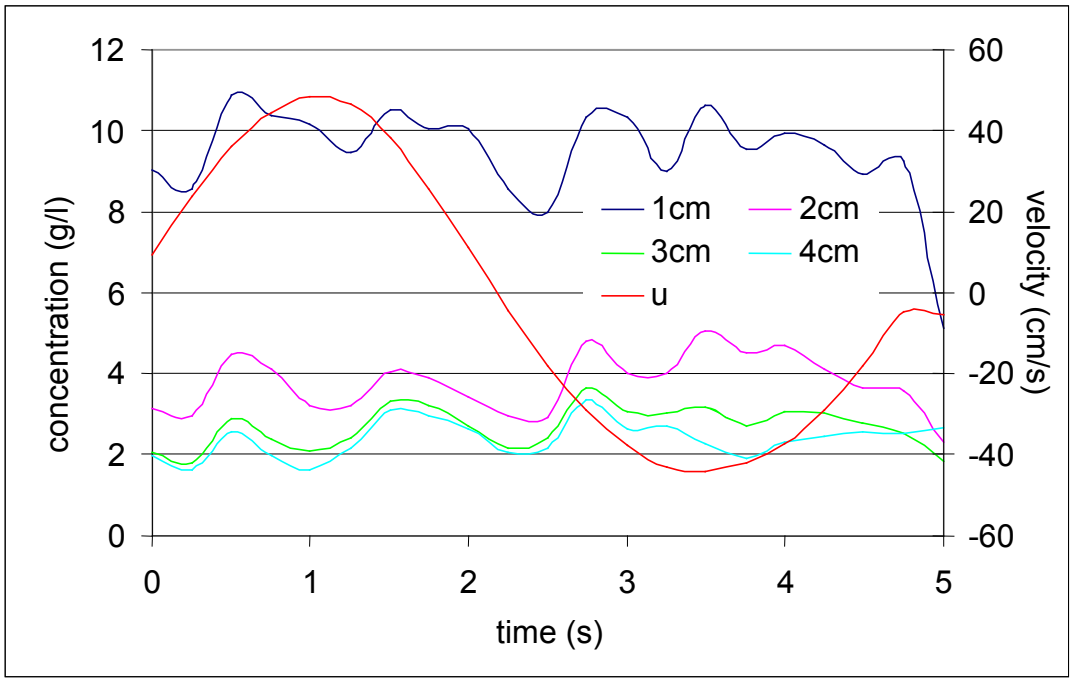

Figure 4-57a Ensemble averaged concentration at different heights above the (local) bed and velocity between 150s and 400s

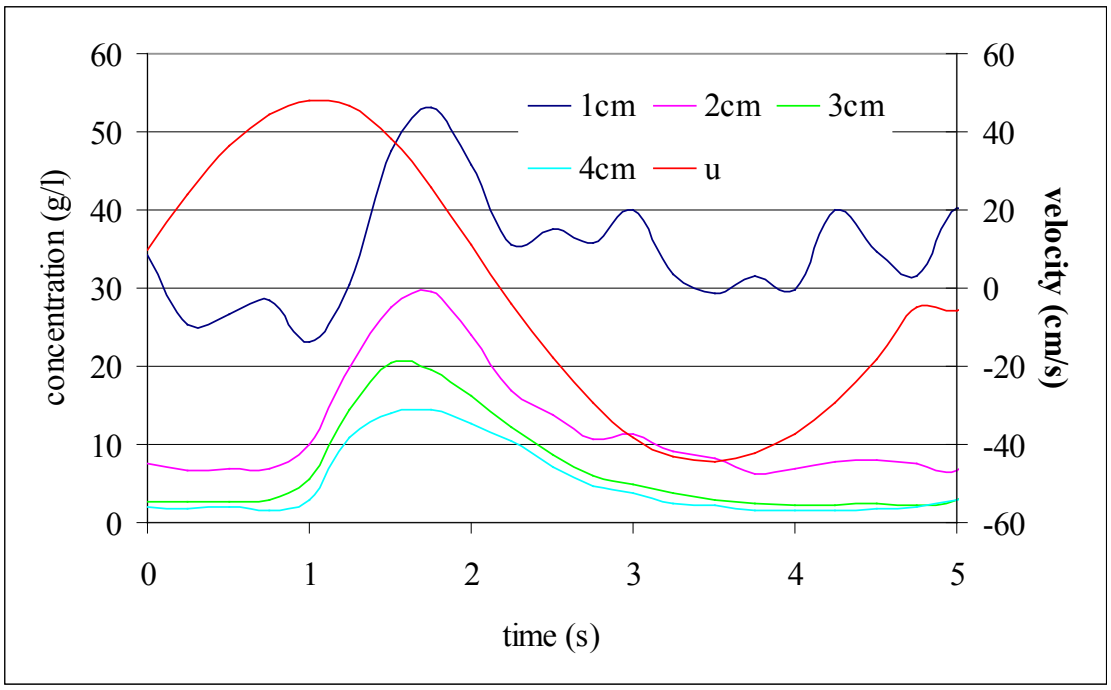

Figure 4-57b Ensemble averaged concentration at different heights above the (local) bed and velocity between 600s and 750s

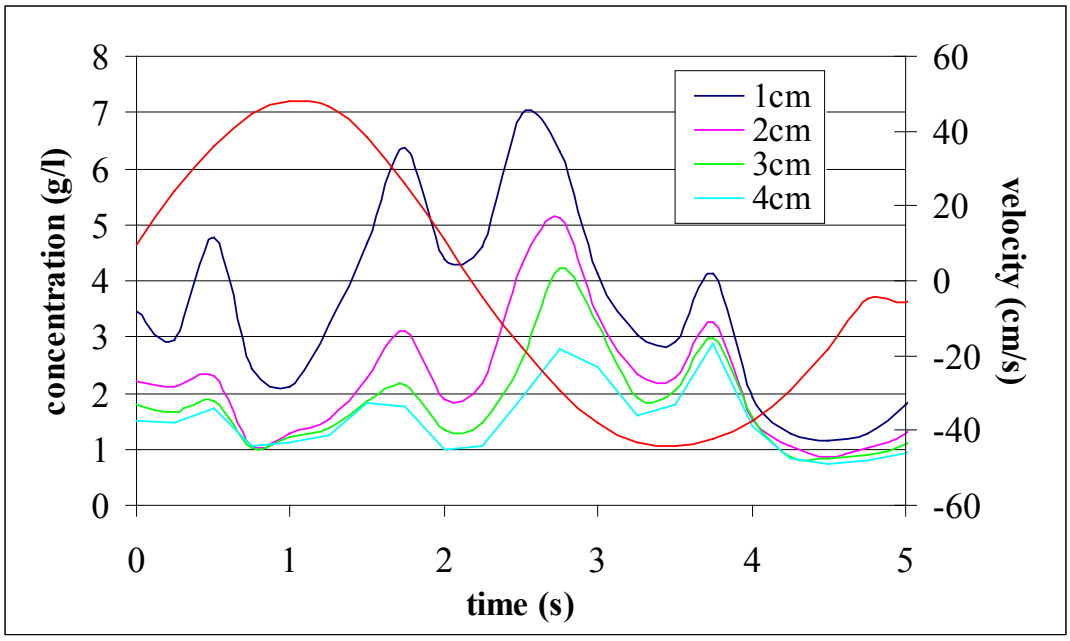

Figure 4-57c Ensemble averaged concentration at different heights above the (local) bed and velocity between 900s and 1015 s

Combining Figure 4-56 and Figure 4-57 shows that a) it does not make sense to average ABS signals over a long period since the variation in the intra wave concentrations are large b) the largest near bed concentrations do not occur at the crest but between crest and bed of the ripple, which corresponds to Figure 4-40

4.7 Recommendations

Further analysis

The influence of STABLE on the ripple dimensions can be further examined by analysing the different side scan sonars. This is important since an influence on the ripple characteristics is of direct influence on the concentration profiles.

Instead of averaging concentration profiles over the whole test, a correlation can be examined between the instantaneous ripple dimensions under the sensor and the wave averaged concentration profile. However it would be difficult to find this relation since the averaged concentration profile also depends on the relative horizontal position of the sensor to the ripple crest.

Another interesting possibility is the analysis of the presence of vortices in the ECM measurements.

Further experiments

Since the time evolution of the sediment concentration depends on the relative horizontal position to the ripple crest (see Chapter 6) it is important to know at which distance data are obtained. This makes it important to obtain bed profile data as close as possible to the ABS-profile. By lining the three ABS-sensors with the flow directions with a small separation, simultaneous concentration measurements near the crest and the trough might become possible. By using different frequencies, interference is avoided.

To resolve the discussion about the possible existence of separation vortices induced by primary vortices and associated movements of sediment clouds detailed velocity measurements close to the bed are important. Coherent Doppler velocity-meters might be less suitable since they cannot resolve high temporary changes in velocity. An acoustic Doppler profiler might be suitable (with the same remark as for the higher described ABS).

Further examination is necessary in order to know if the ADV might be used to measure turbulence close to the bed.

At the end of the medium sand bed tests, the sand bed near the instruments was not anymore horizontal (Figure 4-14), which can have influenced the concentration profiles. This indicates that for future tests, the volume of sand can certainly not be reduced (the less sand, the sooner the horizontality of the bed will disappear). It is also important to measure the shape of the sand bed regularly in order to follow the deformation of the sand bed.

The relation between hydrodynamic conditions, grain sizes and ripple dimensions is very important, but still not found. Parameters that might be of influence on the results might be the degree of present bed disturbances (which initiate the growth of the ripples) and the grain size distribution (since indications exist that ripples develop much more difficult for perfect uniform sediment).

To analyse drift currents, it is important to measure velocities during ‘still water conditions’. Due to measuring errors, non-uniform hydrodynamic conditions in the flume, and complicated bathymetry, it will be hard to analyse drift currents.

The ADV should be checked in laboratory conditions, together with a Laser Doppler velocitimeter in order to check its performance to measure turbulence. Since the length scale of turbulence decays to the bed, these tests should be done for different heights above the bed. An optimum should be found for the size of the measuring volume: the smaller, the more small scale turbulence can be detected, but also the more noise is generated.

The bathymetry of the bed should be measured regularly, especially at places where instruments are located. The sequence of waves should be optimised to prevent as much as possible bed lowering. It is worth to do less experiments and reposition instruments to the new bed levels.
Doing less experiments will also allow to take more time for the pump sampling, such that a whole ripple can pass under the nozzles, in order to get horizontally averaged data. This will remain difficult for cases where ripples hardly move.
Ideally the ripple profile should be measured under all pump sampling devices. This makes it possible to know the horizontal and vertical position of the nozzles relative to the ripple crest.

4.8 Summary

The contribution of this thesis to the experiments consisted of:

- A lot of time was spent for the planning of the experiments (together with Proudman Oceanographic Laboratory), the work 'on field' (a six week measuring campaign) and the first rough analysis of the data.
- Try to get turbulence characteristics (and the shear stress) and influences of waves on the velocity profiles, out of the velocity measurements. Better results were obtained with the ECM's in the Deltaflume than with the ADV on STABLE. The latter contained too much noise.
- Calculation of ripple dimensions and verification of existing predictions with these data.
- Relating ripple dimensions with turbulence characteristics, mainly in order to verify the quality of the turbulence measurements (if no relation was found, it could be concluded that the instruments don't have the capability to detect turbulence).
- Interpretation of concentration profiles: comparison of Delta/Stable measurements, influence of grain size, influence of wave irregularity.
- Examination of grain size distribution of material in suspension at different levels above the bed.

The ABS data came too late to be able to do a thorough analysis. The author could examine only the variation of concentration profiles due to the moving ripple for 1 test case. This shows a large variation in time depending concentration, depending on the horizontal and vertical position relative to the ripple crest.
The results could be used for:

- Verification of the numerical model of sand transport above ripples in Chapter 6.
- Recommendations for more measurements both with frames in a flume as with a frame in situ: these experiments are important to learn more about real conditions, to get longer time series and to study the relation between sand transport and

morphology. At the moment of doing the experiments these kind of experiments were still in a learning phase.

- Further examination of influence of wave groupiness on sand transport (as started in Williams et al.,2000, with own contribution).
- The importance of the grain size distribution is clearly visible: more research in this topic is necessary (cf also Chapter 6).
- Further identification of important parameters on concentration profiles.

5 Physical experiments in the wave tunnel

5.1 Introduction

For increasing hydrodynamic action, the bed will evolve from flat, without sediment transport, transport in the ripple regime to sheet flow. Sheet flow occurs when the hydrodynamic forces are too high and ripples become unstable. The bed becomes plain and most of the movement of sediments occurs close to the bed (few centimeters). During the wave cycle the bed is lifted up at the peak velocities, causing a reduction of concentration under the bed level at rest and an increase of the concentration above this level. The mixture of water and sediment will move up and down during the wave cycle.
Due to phase lag effects, earlier simple numerical models were not able to predict the direction of net transport, which depends on the wave period and the grain sizes. In the field it is not yet possible to determine directly the transport due to the limited depth in which most of the transport occurs with important vertical gradients, which makes position accuracies in the order of millimetres necessary but impossible.

Accurate measurements are possible in wave tunnels, in which high, oscillating velocities can be reached. A disadvantage of the wave tunnel is that the oscillating flow is not exactly the same as wave flow. Waves are not horizontally uniform, the boundary varies along the bed, causing streaming (e.g. Chapter 2, Davies and Villaret, 1998). The absence of this streaming will influence the net sediment transport rate and hardly the sediment concentrations. The aim of this chapter is to describe a series of experiments executed in the wave tunnel of Delft Hydraulics. These experiments are part of long series of experiments executed in this tunnel. These series aimed to get more data to examine the influence of the Reynolds-number on intra wave variation of sediment concentration. However, in this chapter the work is described to use the ADV optimally. The Acoustic Doppler Velocimeter is able to measure velocities in a small measuring volume at a distance of 15 cm from the transducers. This is a big advantage to the EMF (Electromechanic Flow meter) for which the distance is only 1 cm, causing local erosion when measuring close to the bed (the most interesting location). The advantage to a LDA (Laser-Doppler Anemometer) is that the ADV signals are not harmed by high concentrations in the fluid. The disadvantage is however the larger measuring volume and lower measuring frequency compared with the LDA.
The importance of accurate velocity and concentration measurements near the bed are the typical intra wave concentration variations, with sharp increases at flow reversals. It is not yet completely clear why these increases occur.
Earlier experiments reveal convective sediment entrainment and suspension events, occurring near the reversal of the wave-induced oscillatory flow, which cannot be explained by classical turbulent diffusion arguments. For example, Ribberink and Al-Salem (1994) and

Katopodi et al.. (1994) describe this process based upon measurements obtained in an oscillating water tunnel and point out its substantial effect on the oscillatory suspended sediment transport component. Foster et al. (1994) measured high near-bed turbulence levels and suspended concentration peaks near flow reversal and explained these by the occurrence of shear instabilities in the wave boundary layer. Jensen et al. (1989) systematically studied clear-water oscillatory boundary flows in an oscillating water tunnel. They observed bed shear-stress fluctuations and turbulence generation near flow reversal in the transition regime from laminar to turbulent flow. The results indicated the influence of the wave Reynolds number on the phasing of this type of turbulence. It is still unclear from the observations whether the increased turbulence is horizontally homogeneous, or concentrated in coherent vortices. Furthermore, the mechanisms by which grains are carried upwards from the wave boundary layer to be suspended in the mean current are especially poorly understood. For mobile sandy beds, systematic observations of this kind have not yet been made.
A detailed knowledge of velocities near the bed might resolve some of the questions. The results of the experiments are described in a data report (Trouw et al., 2001) and in (Rose et al., 1999).
It is not the aim of this chapter to describe numerical models or other experimental work. This can be found in the Ph.D. thesis of Dohmen-Janssen (1999).

5.2 Objectives and framework

The main objectives of the experiments were:

- To identify the physical mechanisms behind the vertical sediment entrainment processes occurring during the wave cycle.
- To establish the parameter range for which convective flow reversal sediment injection effects occur.
- To obtain a dataset of water particle and sand particle velocity patterns in the oscillatory sheet flow and suspension layer, which can be used for the development of mathematical (two-phase) boundary layer models.

The measurements are carried out in sheet flow conditions using fine sand (120 μm) for a series of sinusoidal and random oscillatory flow conditions with and without a superimposed current. The conditions covered a wide range of Reynolds numbers and wave periods.
The experimental investigation was part of the EC programme “Access to Large-scale Facilities and Installations” of the Commission of European Communities, Directorate General for Science, Research and Development, contract number ERBFMGE-CT95-0045.

5.3 Experimental set-up

5.3.1 The Large Oscillating Water Tunnel

The measurements were conducted in the Large Oscillating Water Tunnel (LOWT) of Delft Hydraulics. In Figure 5-1 the general outline of the tunnel is shown. The tunnel has the shape of a vertical U-tube with a long rectangular horizontal section and two cylindrical risers on either end. This configuration enables the generation of a horizontal oscillatory flow, which is a simulation of the orbital velocity underneath a wave, very close to the bed.

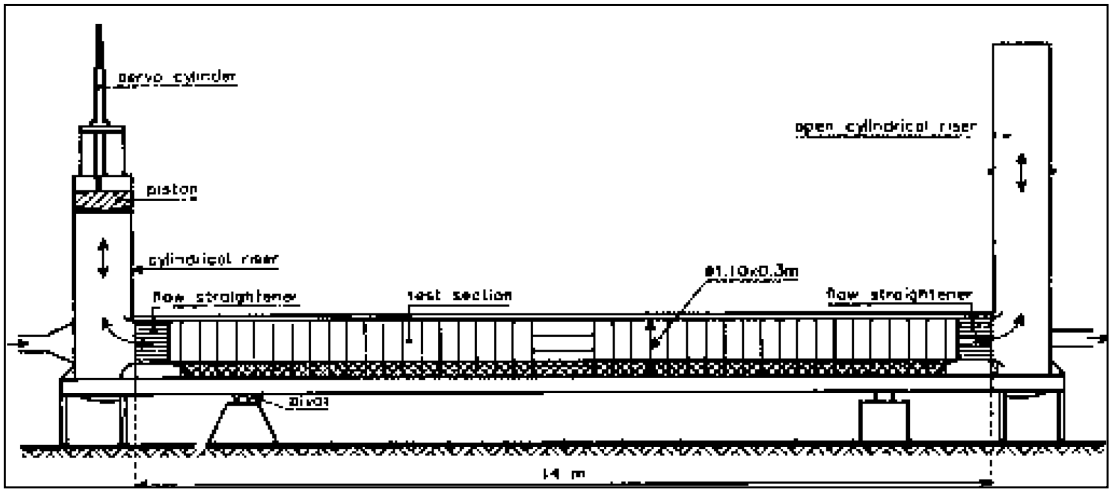

Figure 5-1 Large Oscillating Water Tunnel

The desired oscillatory water motion inside the horizontal rectangular test section of the tunnel is imposed by a steel piston in one of the risers. The other riser is open to the atmosphere. The piston is in direct contact with the water and is driven by a hydraulic servo-cylinder, mounted on top of the riser. An electro/hydraulic valve controls the piston motion on the basis of the measured difference between the (measured) actual piston position and the (desired) piston position (feedback system). The test section is 14 m long, 1.1 m high and 0.3 m wide and is provided with flow straighteners on either end. A 0.3 m thick sand bed can be brought into the test section, leaving 0.8 m height for the oscillatory flow above the bed. Two sand traps are constructed in the two cylindrical risers to collect the sand that has been removed from the test section during a test.

The maximum piston amplitude is 0.75 m, giving a maximum semi-excursion length of the water particles in the test section of 2.45 m. The working range of the tunnel is shown in Figure 5-2. It is possible to generate purely sinusoidal, regular asymmetric and irregular oscillatory motions with the piston. An extensive description of the water tunnel can be found in Ribberink (1989).

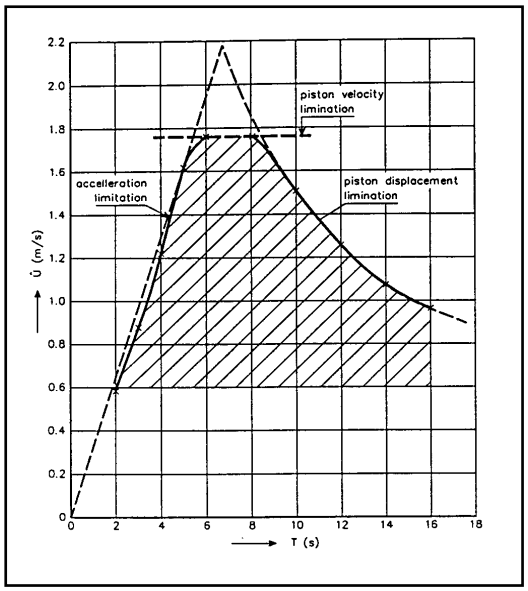

Figure 5-2 Working range of the LOWT

In 1992 the tunnel was extended with a recirculating flow system connected to the cylindrical risers, such that a steady current can be superimposed onto the oscillatory motion. The recirculating flow system is also provided with a sand trap consisting of a 12 meter long pipe with a diameter of 1.2 meter that is connected with the downstream cylindrical riser by a pipe with a diameter of 0.3 meter The trap was designed for trapping 90% of the suspended sediments (minimum grain size 100 microns) at maximum flow discharge. Downstream of the trap two pumps are installed for generating a net current. The maximum capacity of the larger pump is 100 l/s and of the smaller 20 l/s. The maximum superimposed depth averaged current velocity in the test section of the tunnel is 0.45 m/s.

5.3.2 Measured parameters and flow conditions

The following parameters were measured during the experiments:

- Bed level variation near measuring instruments
- Time-dependent flow velocities u(z,t), v(z,t) and w(z,t) at different levels above the bed in the sheet flow layer and in the suspension layer.
- Time-dependent sediment concentration c(z,t) both in the suspension layer (for z>0.01 m) and in the sheet flow layer.
- Time averaged sediment concentrations c(z) in the suspension layer (for z>0.01m)
- Sand grain velocities in the sheet flow and suspension layer

By varying the wave period (4;7.2;12s) for constant velocity amplitude (1.1m/s) and varying the velocity amplitude (0.7;0.9;1.1;1.3;1.5m/s) for constant wave period (7.2s) a wide range of Reynolds numbers are obtained. Additionally existing data of the wave tunnel can be used to complete the set. Also an irregular wave is included. The bed consists of fine quartz sand

(d_{50}=120μm, Figure 5-3). Because of the detailed measurements and the wide range of hydraulic regimes the different near-bed processes (shear instability, water-sand interactions) can be examined and quantified. For most of the tests a current is superimposed. The testing conditions are summarised in Table 5-1 on page 123.

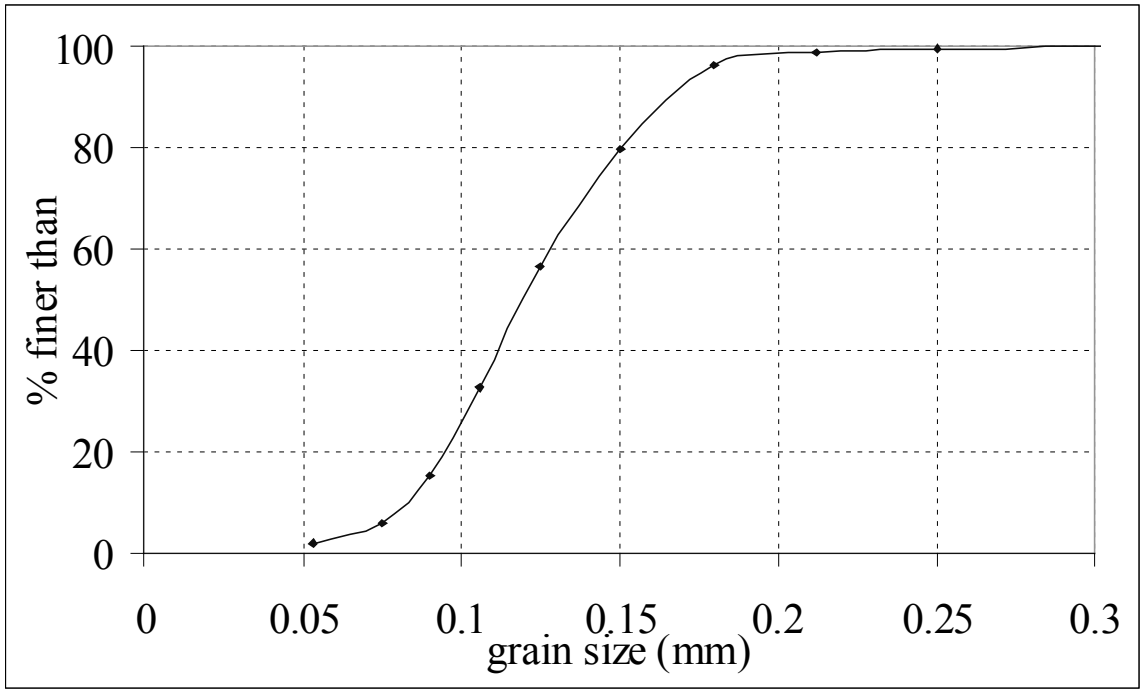

Figure 5-3 Grain size distribution of the bed material

5.3.3 Measuring facilities and measuring techniques

5.3.3.1 Laser Doppler Velocity Meter (LDA)

A forward scattering Laser Doppler Velocity meter (Anemometer) (LDA) was used for the measurement of the horizontal and vertical velocity components of the water particles between 100 and 300 mm above the bed. Below this level, it turned out to be impossible to measure velocities by LDA, because of the large amount of sediment particles below this level. The particles block the laser beams and disturb the measurement. Rather than measuring directly the horizontal (u) and vertical (w) components of the velocity, two perpendicular components v_A en v_B in the same vertical plane were measured. The reason was that the velocity range is larger in the second configuration. The components v_A and v_B were transferred to u and w afterwards. The LDA was positioned on a measurement carriage that stands over the tunnel, rather than on top of it, so that vibrations of the tunnel do not disturb the LDA.

5.3.3.2 Electromagnetic Velocity Meter (EMF)

The velocities near the bed could not be measured with the LDA due to heavy suspension that interrupted the signal. In this layer a four quadrant electromagnetic flow meter (EMF) was used for the measurement of the horizontal velocities. The EMF employs Faraday's Induction Law for the measurement of the velocity of a conductive liquid moving across a magnetic field. The diameter of the ellipsoid sensor probe were 11 and 33 mm and the height of the sensing volume 3-5 mm. The lowest point measured was about 2 cm above the bed. Measuring closer to the bed is impossible due to the scour hole that is formed under the EMF.

5.3.3.3 Optical Concentration Meter (OPCON)

The time-dependent suspended sediment (sand) concentrations were measured using an optical concentration meter (OPCON). OPCON measures volume concentrations in the range 0.005-2.0 % (= 0.1-50 g/l) and is based on the extinction of infra-red light. The height of its sensing volume is 2.6 mm. Figure 4-37 shows a schematic diagram of the OPCON probe. The distance between the optical transmitter and the receiver is 30 mm (= length of sensing volume).

The calibration of the OpCon depends on an amplification factor a_g, which can be set during the measurement at 1 or 10, and on the grain diameter. Bosman (1982, 1984) developed the OpCon probe and calibrated it extensively (in a calibration vessel), for different unsorted and sorted sand types. The relation between d_{50} (in mm) and the calibration factor K_1 (in g/l/Volt)) can be written as:

$$K_1 = 84.1\ (D_{50} - 0.05325)/a_g$$

with a_g the amplification factor of the electronic amplifier of the OpCon (=1 or 10)

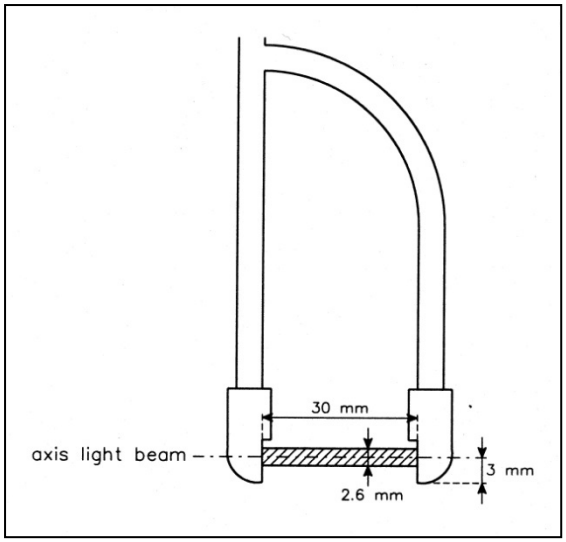

Figure 5-4 Schematic diagram of the OPCON probe

5.3.3.4 Acoustic Doppler Velocity meter (ADV)

An Acoustic-Doppler Velocity meter, developed by the U.S. Army Engineering Station (WES), implemented by NorTek, was used for velocity measurements below z = 100 mm, because it is capable of measuring velocities in high concentrations of sediment.
The ADV is based on the doppler principle to measure the three components (u, v and w) of the velocity at a single point. The system includes three modules: a measurement probe, a signal conditioning module and a signal processing module. The measurement probe consists of four ultrasonic transducers; a transmit transducer located at the bed end of the stem and three receive transducers, slanted 30^o from the axis of the transmit transducer and pointed at the sampling volume. This sampling volume is located about 0.10 m below the probe tip, which means that the flow in the sampling volume is not disturbed too much by the probe.
The receive transducers record the signal, scattered by particles in the water. Because the frequency of the received signal is shifted as a result of the velocity of the particles that scatter the signal (doppler-shift), the velocity of these particles can be determined. This implies that in practice the velocity of the particles in the water rather than the flow velocity itself is measured. However, for sediment transport measurements it is the velocity of the particles that determine the sediment transport rate. Therefore this is not a problem.
The size of the sampling volume depends on the number of pulses used for one measurement, one pulse corresponding to 3 mm, two pulses to 6 mm and three pulses to 9 mm sampling volume thickness. The horizontal dimensions of the sampling volume are determined by the diameter of the transmit transducer which is about 6 mm. The calibration coefficients of the ADV depend on the velocity range (vr).
The recorded signals can be stored and analyzed by specific ADV software (processing module). However, it is also possible to record the signals on a different data acquisition

system, via three analogue outputs. This was done in the present experiments in order to have all data in the same format. Figure 5-5 shows the configuration of the ADV system in the tunnel

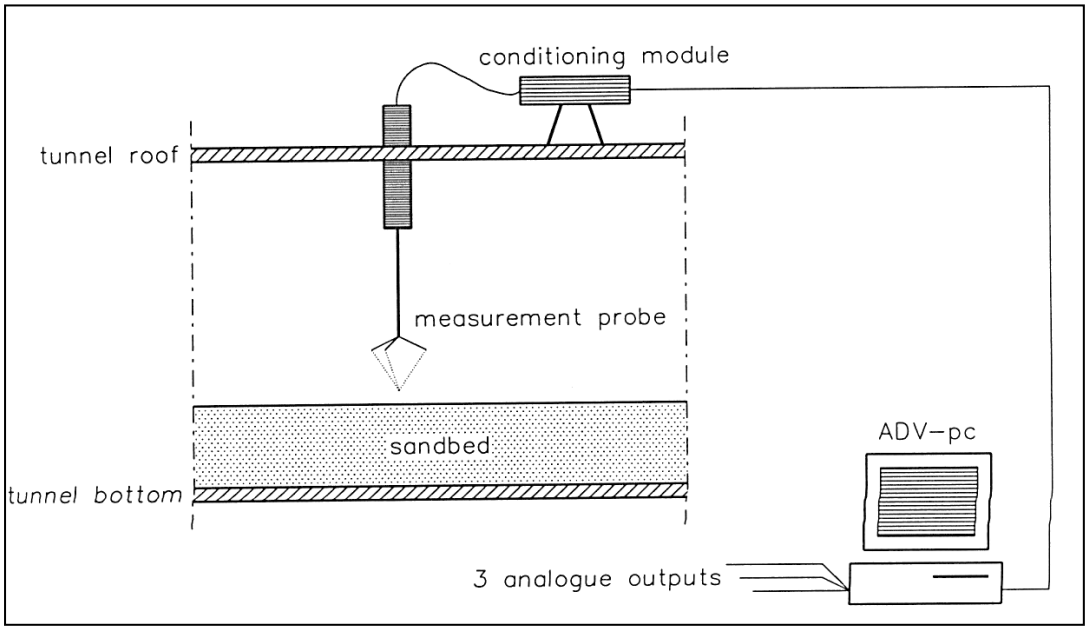

Figure 5-5 ADV configuration in the tunnel

5.3.3.5 Transverse Suction System

A transverse suction system described by Bosman et al. (1987), was used for measuring the time averaged concentration profile of the suspended sediment concentration.
The transverse suction is performed by extracting samples in a direction normal to the flow. The transvers suction system consists of 10 intake nozzles with inner diameter of 3 mm. The suction is driven by 10 peristaltic pumps. The sand samples are collected in buckets and the sand height is measured using calibrated tubes. Then the sand height is converted into sand weight using the sand density and the sand porosity of loosely packed sand.
Figure 5-6 shows an outline of the transverse suction probe. The distance of the lowest nozzle from the bed was about 1 cm. The calibration of the suction is determined by the trapping efficiency α defined as the sediment concentration in the sucked sample and the concentration in the flow. The value of the trapping efficiency depends on the nozzle dimensions, their orientation relative to the flow, the ratio of the intake velocity over the ambient flow, the sediment particle characteristics and the relative density. More details about accuracy can be found in Chapter 4.

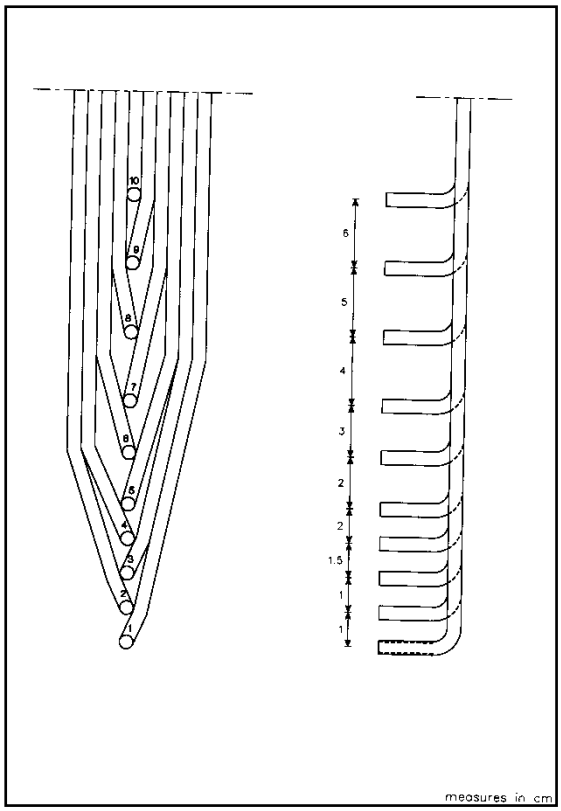

Figure 5-6 Schematic diagram of transverse suction system

5.3.3.6 Particle Image Velocimetry (PIV)

Particle Image Velocimetry is an optical technique for the non-intrusive measurement of fluid flow. The technique was deployed in the wave tunnel by the University of Edinburgh, Fluid Dynamics Unit. It relies on seeding particles in the flow being illuminated by a pulsed sheet of light, the motion of the seeding particles being recorded by camera. Here it was used to measure the velocities of sand particles stirred up by water motion in the Delft Hydraulics Wave Tunnel.

The illumination for the experiments was a 15W Argon-ion laser mounted on the roof of the wave tunnel. The beam was input to a "scanning beam" box (Figure 5-7), the beam being directed onto an octagonal, rotating mirror, which in turn scanned the beam, repeatedly and very rapidly, along a parabolic mirror. The octagonal mirror is positioned at the focus of the parabolic mirror, so that as the beam scans along the latter, it is reflected along parallel paths as in Figure 5-7. This gave the illusion of a rectangular "sheet" of light, approximately 0.5 m in width and 3 mm in thickness.

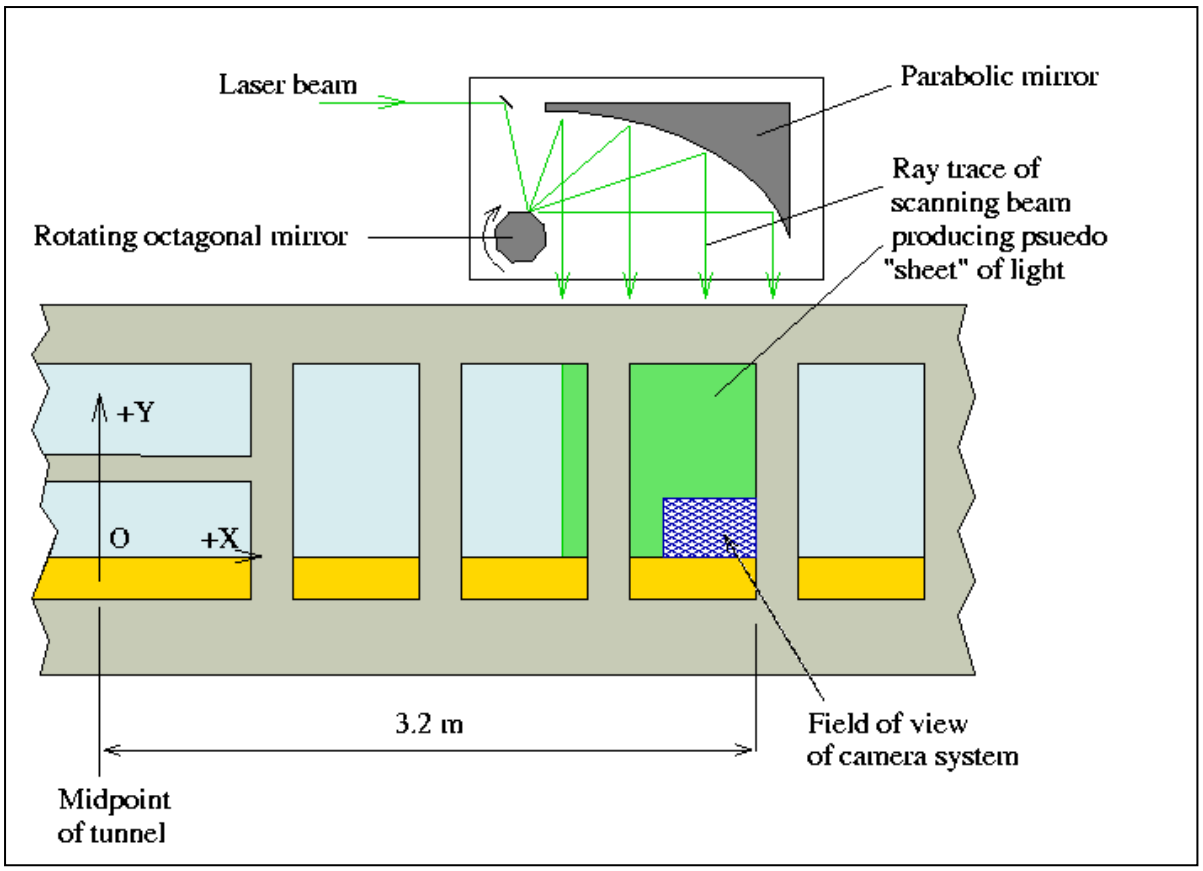

Figure 5-7 Cutaway of the scanning beam system and position of PIV measuring area

The box was positioned so as to direct this "sheet" vertically downwards into the tunnel through a glass plate in its roof.

A special, electronic camera system viewed the illuminated area through the glass sides of the tunnel. The images of the sand motion from the camera system were fed to PC's fitted with framegrabbing cards.

For the 4s wave the PC controlling the motion of the tunnel piston output pulses every 1/8 of a wave period, synchronised with the upwards zero crossing of the wave cycle. A photodiode within the scanning beam box also generated a train of pulses when the laser beam swept repeatedly over it. The pulse trains were fed into the timing control box, where on receipt of a pulse from the tunnel PC, the box would wait for the next scanning-beam pulse (this introduced a delay of upto 5 ms after the PC pulse). Immediately after this was received, the exposure pulses to the cameras are sent out. Once the cameras have exposed, their video signals are output to the 2 PCs. The images are grabbed by the computers on another pulse from the timing control box, sent out a short time after both cameras have been exposed. Once the next pulse from the tunnel steering PC was received, the process was repeated and a new pair of pictures were acquired and so on, until the PC memory was full. Using this

process 17 waves were recorded, the images saved to disk and the acquisition process repeated twice.
The wave condition was then repeated, but with the phase of the steering pulses shifted by 1/16 period. Again 51 waves were recorded in 3 batches of 17.

The images were processed to give maps of mean velocity, rms fluctuations in velocity and velocity correlation.

It was important to know exactly when through a wave the image acquisition had started. Therefore a pulse was sent from the PIV computers to the tunnel steering computer at the start of each acquisition batch and logged. This enabled the experimenters to figure out the wave sequence in the images.
Measurements and data analysis were performed by the University of Edinburgh.

5.3.4 Conductivity Concentration Meter (CCM)

The concentration in the sheet flow layer and inside the bed was measured using a Conductivity Concentration Meter (CCM). The instrument measures large sand concentrations (5-50 vol% = 100-1500 g/l) with a four point electro-resistance method.

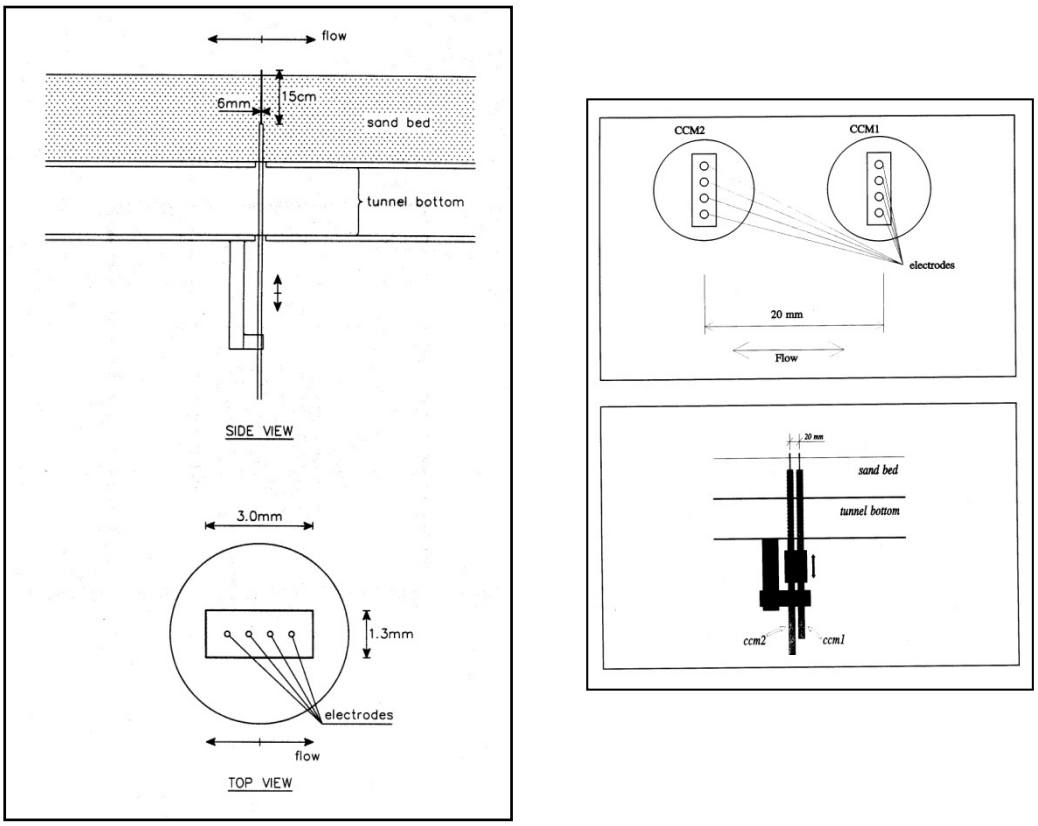

Figure 5-8 Schematic diagram of the CCM and its configuration in the tunnel

The height of the sensing volume is 1 mm. A detailed plot of the CCM probe is shown in Figure 5-8.
Two CCM probes, spaced 20 mm apart in the streamwise direction were inserted through the bed of the LOWT (2 m downstream of the middle of the tunnel working section and in the center laterally). The sensors were mounted on a positioning gage that measured the vertical position within a precision of 0.01 mm. A laser was used to assure that the levels of the two sensors was the same. To estimate the level of the sensors above the sand bed, the elevation of the bed above a datum on the side wall of the tunnel was measured during the data runs. This measurement was made near the time of the flow reversal, when much of the sand settled back to the bed. This information in conjunction with the reading of the positioning gage provided an estimate of the elevation of the CCM probes above (or below) the mean elevation of the bed. Measurements and data analysis were performed by the University of Twente (Hassan, 2001).

5.4 Experimental results

For all measured parameters the ensemble averaged signal is determined together with the time averaged value, the standard deviation, the minimum and maximum value and the root-mean-square value of the original time series and of the ensemble averaged signal.
Because not all instruments can be used at the same time, different series of experiments are done for each condition.
In the first series of experiments the EMF, the OPCON and the LDA were used. The series was given the code O (OPCON). In the second series of experiments the ADV and the LDA were used and the time averaged concentration was obtained with the transverse suction system. The series was given the code t. In the last series of experiments the CCM, PIV and LDA were used. (code c). The sand bed eroded quickly at the beginning and the end of the tunnel. After some time the scour holes influenced the results in the measuring section and the run had to be stopped. For each experimental condition in a series, typically 4 to 5 runs were necessary. During each run typically 3 to 5 measurements were done at different heights.

An overview of the experiments is summarized in Table 5-1:

Test nr	Ua (m/s)	<U> (m/s)	T (s)	EMF	OPC ON	LDA	TSS	ADV	CCM	PIV
1	1.5	0	7.2	X	X	X	X	X		
2	0.7	0.25	7.2	X	X	X	X	X		X
3	0.9	0.25	7.2	X	X	X	X	X		
4	1.1	0.25	7.2	X	X	X	X	X	X	X
5	1.3	0.25	7.2	X	X	X	X	X		
6	1.5	0.25	7.2	X	X	X	X	X		X
7	1.1	0.25	4.0	X	X	X			X	X
8	1.1	0.25	12.0			X			X	X
	urms		Tp(s)							
10	0.35	0	5.0	X	X	X	X	X		

Table 5-1 Overview of measurements

5.4.1 Velocities and turbulence

All velocities were identified with a phase in the wave cycle. For each phase the mean velocity was calculated together with the standard deviation.
The ensemble average of signal F(t) is defined by:

$$< F(t) >= \frac{1}{M}\sum_{m=0}^{M-1} F(t+mT) \quad for \quad 0 \le t < T \tag{5-1}$$

With T the wave period and M the number of waves during the test condition.
The mean value of F(t) is:

$$\overline{F} = \frac{1}{T}\sum_{t=o}^{T} < F(t) > \tag{5-2}$$

The wave part is defined as:

$$\widetilde{F}(t) = < F(t) > - \overline{F} \tag{5-3}$$

And the turbulence part as:

$$F'(t) = F(t) - < F(t) > \tag{5-4}$$

Because of the large sediment concentration and the small measuring volume, not all ADV measured velocities were reliable. An important parameter to check the reliability is the correlation between the sent and the received ADV signals. The correlation parameter can be

thought of as a quality parameter for the velocity data. Values below 0.7 indicate that the measuring regime is problematic (for example large amounts of bubbles). If this correlation was less than 0.7, that particular data point was skipped. Also spikes in the velocity signal were identified and skipped if the deviation between two consecutive velocity measurements was larger than 0.15 m/s.
For the calculation of F(t) bad points are replaced by the interpolated value, using the closest neighbouring points. For the turbulence analysis, the bad point is not used in the statistics.
The software of the ADV makes it possible to get time series of velocities and the correlation parameter.

The ADV was changed by its manufacturer just before the experiments. Improvements in the software and changes in the hardware were said to improve the measurements of turbulence characteristics. For this reason the smallest measuring volume was chosen. An experiment indicated that the phase averaged results are comparable with measurements with a bigger measuring volume. This allowed a bigger opportunity to measure small scale eddies but conversely meant more instrumentation noise. Because of lack of time a detailed test of the "new" ADV was not possible before the actual test series started. An indication for the quality of the ADV measurements is obtained by comparing velocity profiles and turbulence measurements with other instruments.

5.4.1.1 Velocity profiles

Since the erosion during a test causes changes in bed level, the section in the tunnel also changed. However, the discharge delivered by the pumping system and the volume of water moved by the oscillating pistons does not change. The velocity profiles are obtained by point measurements, for which the instrument is moved up and down during the tests, so different heights are measured at different moments and thus at different thicknesses of the sand bed. For this reason the measured velocities are adapted with the bed level in order to get comparable results.

$$U_{ad} = U_{me} \frac{(d_0 - b)}{d_{ref}} \qquad (5\text{-}5)$$

With

U_{ad}: adapted velocity (m/s)
U_{me}: measured velocity (m/s)
d_0: distance between the lowest border of the glass and the top of the flume
b: distance between the lowest border of the glass and the top of the sand layer
d_{ref}: reference distance between sand bed and top of the flume

The velocity profiles are presented in Figure 5-9 to Figure 5-12.

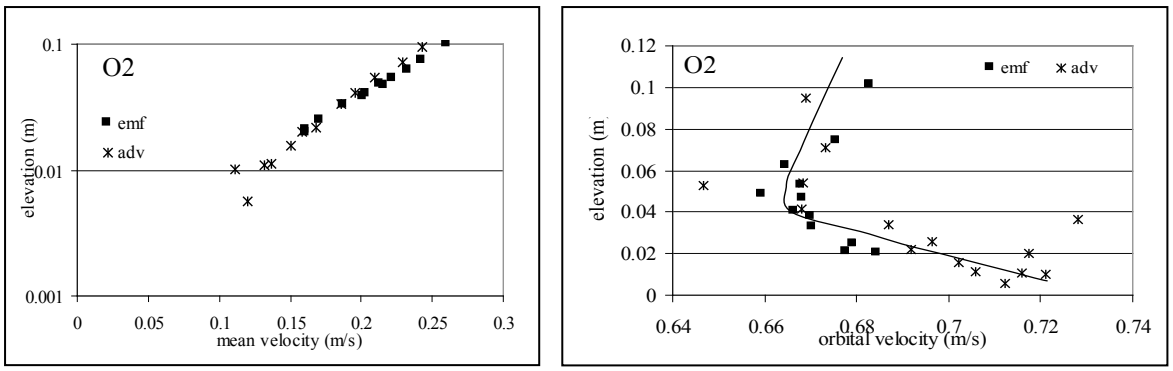

Figure 5-9 a) mean velocity profile b) orbital velocity amplitude profile test O2 (0.7m/s,T=7.2s)

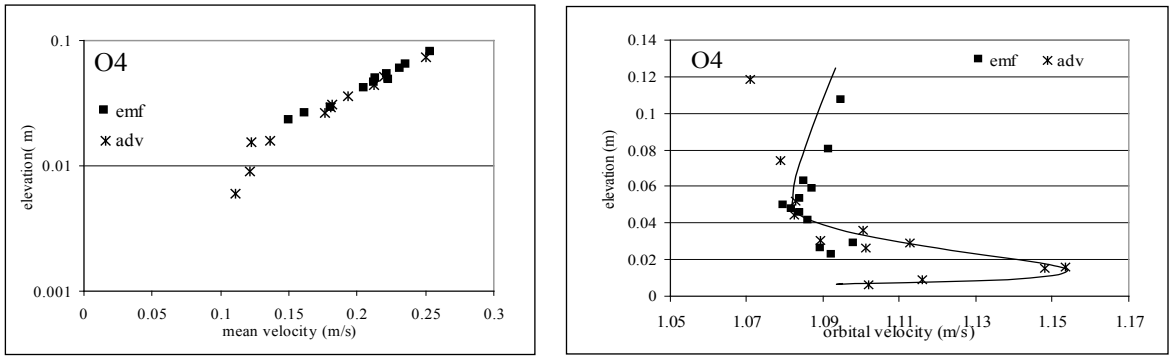

Figure 5-10a) mean velocity profile b) orbital velocity amplitude profile test O4 (1.1m/s,T=7.2s)

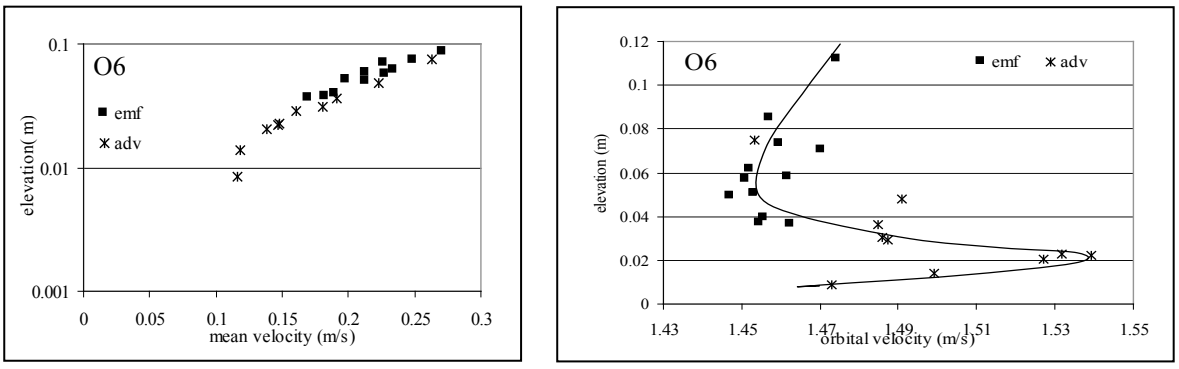

Figure 5-11a) mean velocity profile b) orbital velocity ampl. profile test O6 (1.5m/s,T=7.2s)

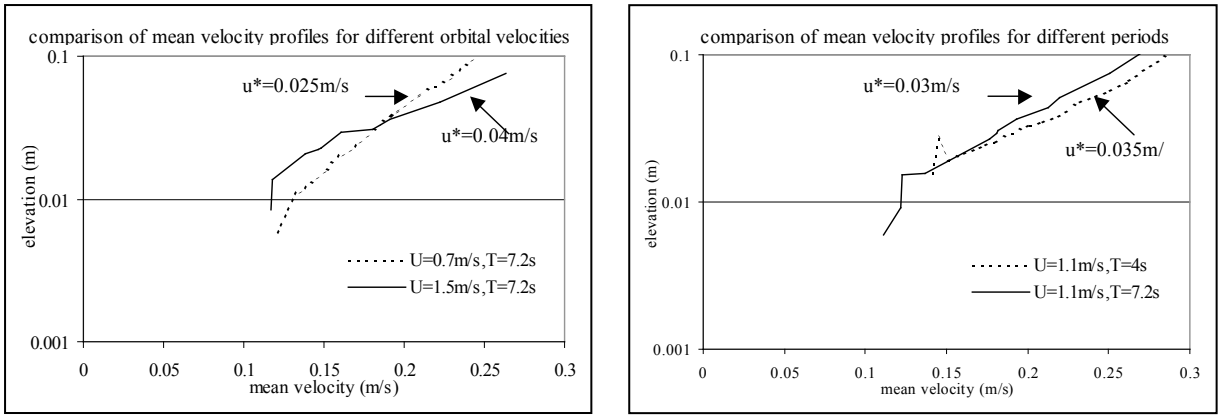

Figure 5-12 Comparison of mean velocity profiles a) variation of oscillating velocity amplitude b) variation of wave period

A curve through the measuring points is drawn "by hand". These curves are not mathematically determined but subjectively. The mean current profiles are represented on logarithmic vertical axes, in order to visualise the logarithmic velocity law.
From these figures it can be concluded that:

- nearly perfect agreement between EMF and ADV measurements
- logarithmic profile above 1cm from the bed, beneath that level a much smaller gradient
- the orbital velocity profile peaks 1-2 cm above the bed (corresponding to the theoretical orbital velocity profile).
- The shear stress corresponding with the mean current profiles increases with increasing oscillating velocity and increases slightly for a decreasing oscillating period.

5.4.1.2 Turbulence

To examine the quality of the turbulence measurements the energy density spectrum gives some useful information. The energy density S is defined as:

$$S = \frac{\sum_{\Delta f} (U/2)^2}{\Delta f} \qquad (5\text{-}6)$$

With U the amplitude of the velocity for frequencies in the considered frequency interval and determined with a Fast Fourier Transformation. The decay of the energy density at higher frequencies should be proportional to $f^{-5/3}$, with f the frequency (Tennekes & Lumley, 1972).

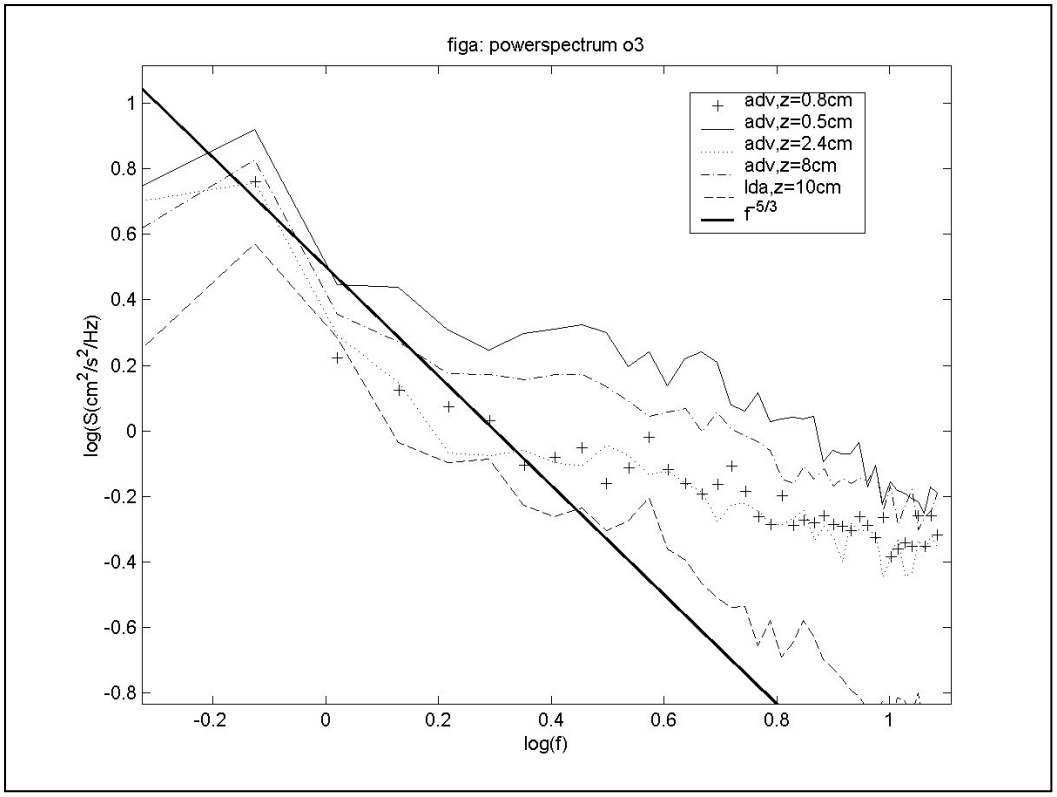

Figure 5-13 Powerspectrum of the horizontal velocity (test O3, U=0.9m/s)

In Figure 5-13 the energy density is shown for test O3. The lowest frequencies (related to the oscillating period) are not shown.

The LDA has the expected decay in energy density and does not show significant noise. For the ADV the decay of energy density is as expected for frequencies lower than 3Hz. For the higher frequencies the decay is smaller, probably because the influence of noise is becoming more and more dominant (and for the highest frequency also the limited measuring frequency of the ADV.

For the calculation of the power spectrum the corrected time signal is used: bad points are replaced by the interpolation of their neighbour points. This can partly explain the noise (since the real value is replaced by a calculated/averaged value). For the calculation of the turbulence quantities these bad points are not accounted for in the statistics.

Better turbulence quantities are obtained if the corrected signal is low pass filtered (a Chebyshev type I filter), cut off frequency 6Hz (what is comparable with measuring at a frequency of 12Hz instead of 25Hz).

Only experiments for which at least 80 wave cycles are available, are used to study turbulence. This limit is necessary to apply statistics. (Sleath, 1987)

During the two measurements for which the ADV and the LDA measured at nearly the same point during 80 wave cycles either the ADV-recording or the LDA failed.

In Figure 5-14 the standard deviation of the horizontal velocity ($\sigma_u = \sqrt{\overline{(u')^2}}$,u' calculated with Eq.5.4, with F=u)) is shown for test O3 where the result of the LDA is compared for 2

different cut off frequencies: 6 and 20 Hz. (20Hz is the maximum possible frequency for the LDA sampling frequency of 40Hz, thus the influence of using a low pass filter with cut off frequency of 6 Hz) is visible: the shape of the signal is the same but the magnitude is smaller (some turbulence is 'lost' since it occurs at higher frequencies). It is also clear that the highest turbulence occurs at the peak spectrum (orbital velocity in the same direction as the mean current).

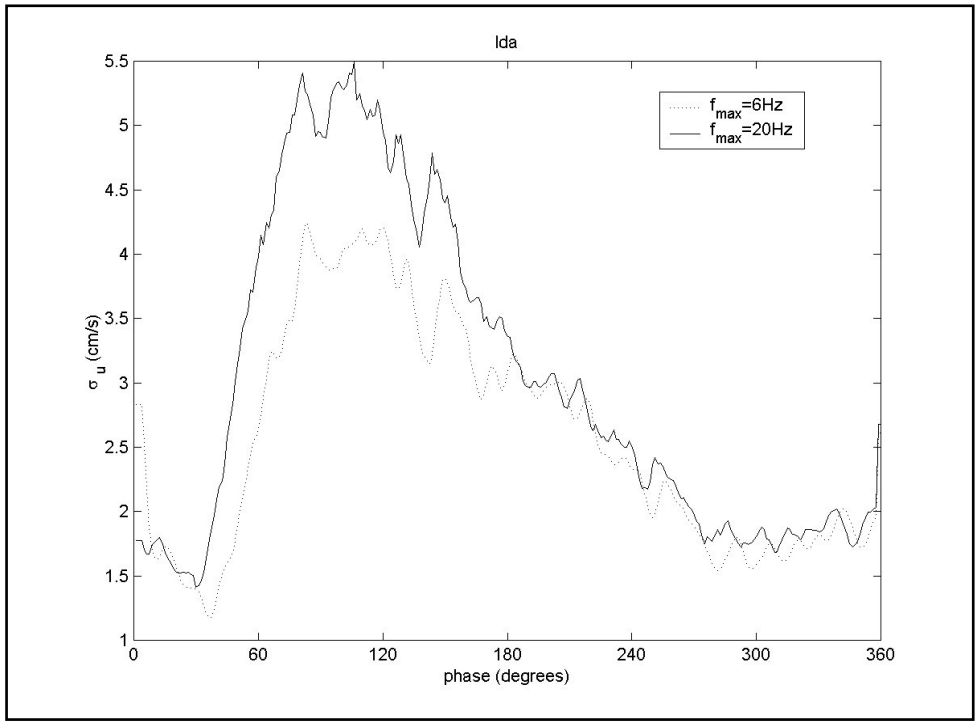

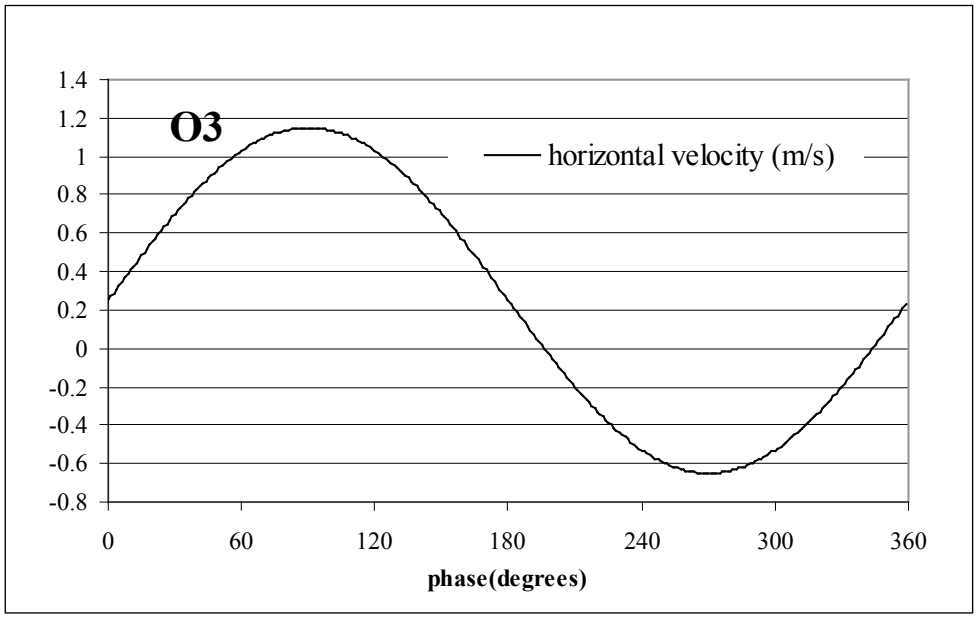

Figure 5-14 Standard deviation of the horizontal velocity as function of phase for the LDA results: influence of using a low pass filter (at a height of 10 cm)

In Figure 5-15, the results for the ADV are shown at different heights. The factor e in the legend is the percentage of data points that had to be corrected and subsequently left out of the analysis. It is clear that the signal contains a lot of noise, giving high minimum σ_u – values (3.5cm/s instead of 1.5 for the LDA). Figure 5-14 indicates that the higher frequencies are more important for the peak near maximum velocity. This might explain why the LDA and the ADV do no show a peak at the same moment.

Figure 5-15 gives best results at a height of 0.8 cm (also e is the lowest at this location). The high peak, near 170˚, corresponds with the flow reversal near the bed (e.g. Figure 5-18). At this moment an inflection point is present in the velocity profile. Foster et al. (1994) assume that the shear instabilities in the boundary layer are the result of velocity perturbations that become unstable when an inflection point (and important vertical velocity gradient) occurs. At that moment the highest shear might not anymore occur at the bed, but at a higher level.

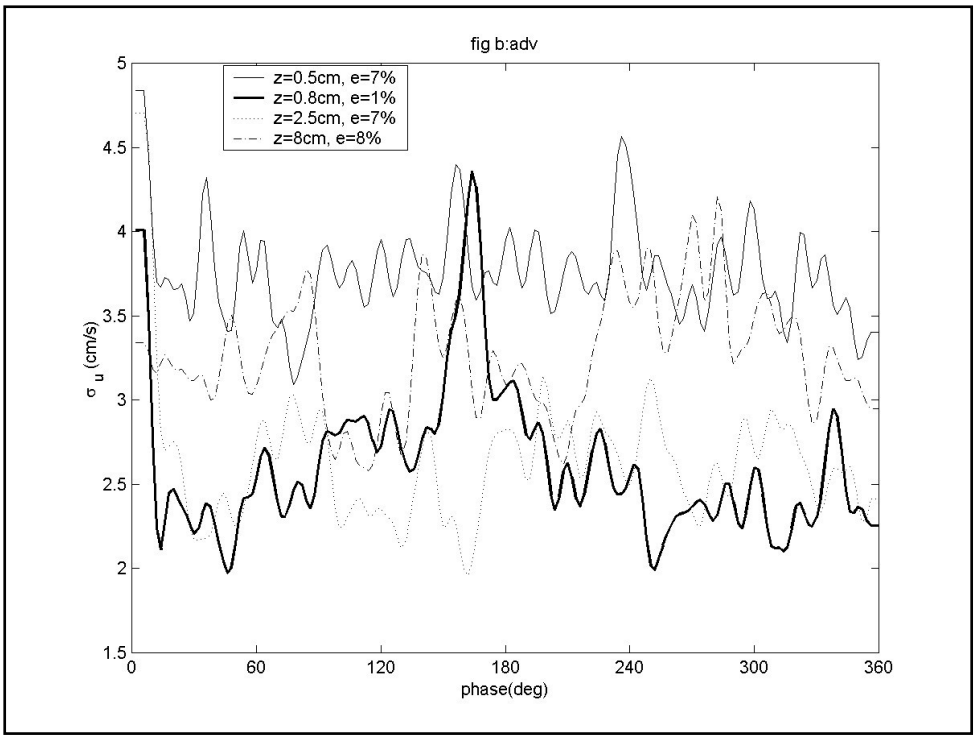

Figure 5-15 Standard deviation of the horizontal velocity as function of phase at different heights (test O3).

Assuming that part of the noise of the horizontal velocity is independent of the noise of the vertical velocity, the calculated Reynolds shear stress ($=-\rho\overline{u'v'}$) should be less influenced by the noise. Results are shown in Figure 5-16 and Figure 5-17, again with a clear peak near flow reversal at the bed (z=0.8 cm). This indicates that large turbulent eddies might be generated at flow reverse, due to shear instabilities. Due to the low frequency at which they occur the problem of the relative large measuring volume of the ADV is reduced. The LDA, which is measuring at a much higher level, does also show a peak near flow reverse. The

peak is, although its measuring volume is smaller, smaller than that of the ADV measuring at the bed. The peak at 90º for the ADV is associated with the maximum velocity.

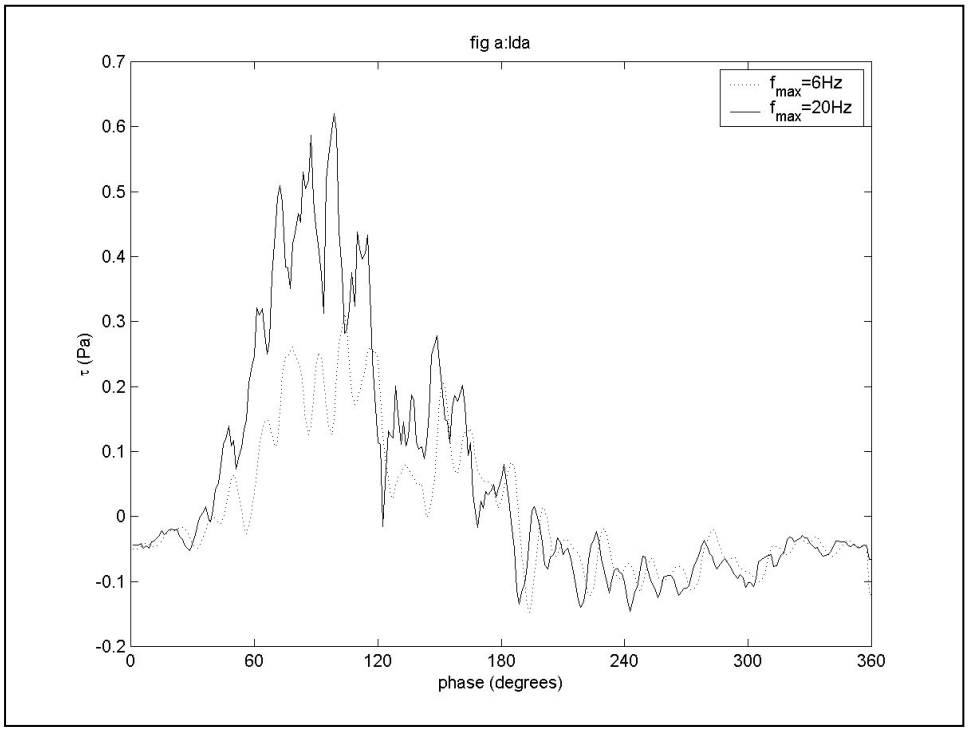

Figure 5-16 Reynolds stresses as function of phase for LDA results: influence of using a low pass filter (at z=10 cm)(test O3)

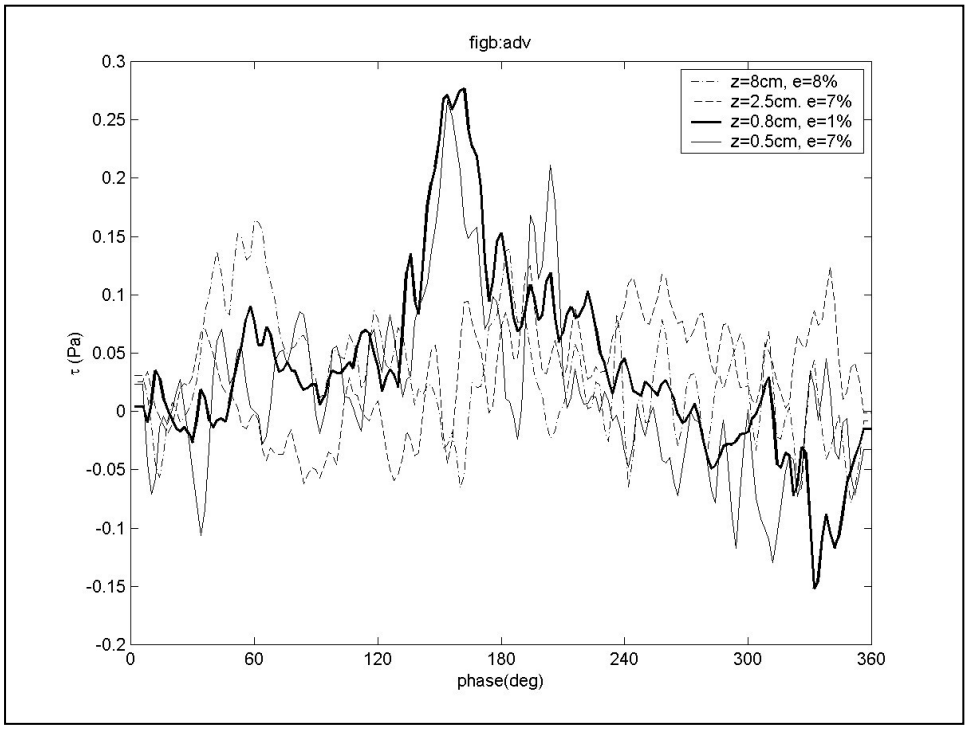

Figure 5-17 Reynolds stresses as function of phase at different heights.(test O3)

At higher levels these eddies are not visible and the signal is dominated by noise.

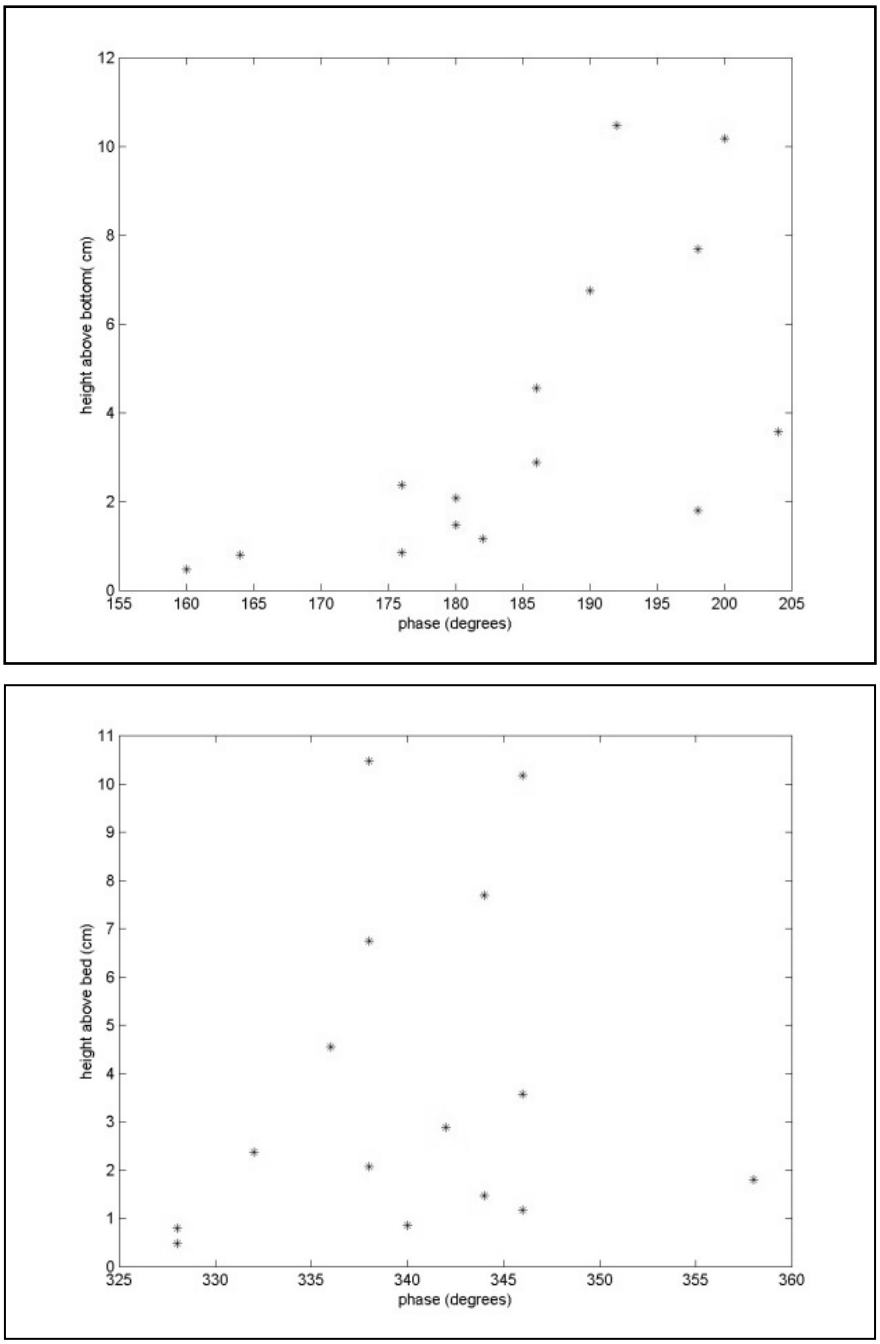

Figure 5-18 Phase at flow reversal for different heights above the bed for test 03

In Figure 5-18 the phase at flow reverse is shown for different heights (different figures for the two flow reverses, which are different because of the current). It is clear that the flow reverse associated with the maximum velocity occurs at a much larger time/phase interval than for the second phase interval. Flow reverse occurs first at the bed.
Comparable results for test O4 are shown in Trouw et al. (2001).

5.4.2 Particle Image Velocimetry (PIV)

The PIV system was used to obtain measurements of the velocity field (x,z,t) of the mobile sediment grains. The sediment concentrations in the bed 0.06 m were too large to be able to obtain reliable PIV measurements. The useable PIV results extended vertically over 0.06 m to 0.18 m from the bed level and horizontally over 0.24 m. The results were ensemble-averaged over 51 wave cycles. The data were further horizontally averaged and the horizontal velocity as a function of time at an elevation of 0.15 m is plotted in Figure 5-19 against the LDA and EMF results.

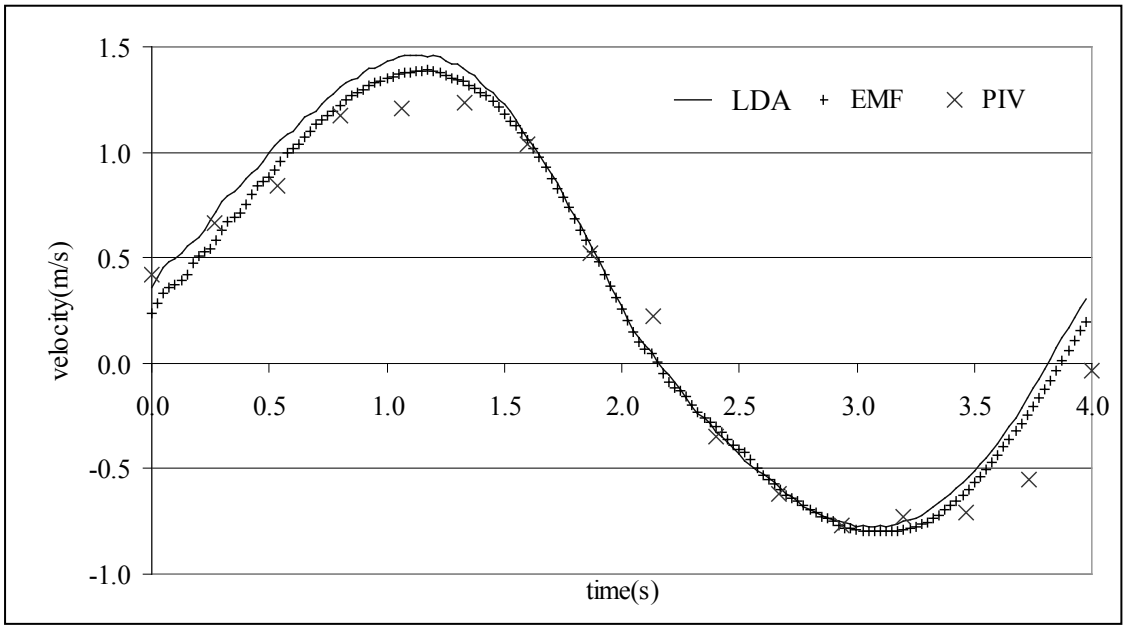

Figure 5-19 Ensemble and horizontally averaged horizontal (grain) velocities from test O7

It should be noted that the PIV measures velocities of the sediment grains rather than the fluid particles. Due to grain inertia effects and particle-particle interactions it is possible that there are small differences between the two. Generally the PIV follows the LDA measurements well over much of the wave cycle. However, the PIV measurements of the maximum and minimum oscillatory velocities were up to 25 % below the LDA, ADV and EMF results (e.g. in Figure 5-19 where the maximum velocity measured by the LDA is 1.48m/s, while only 1.24m/s for the PIV recording). These results indicate that under the particular conditions of the present test, the temporal mean PIV results were not as accurate as the velocity measurements obtained solely at a point. The test has also shown that, because of the high sediment concentration, this technique cannot be used to examine near-bed sediment particle velocities in sheet flow conditions.

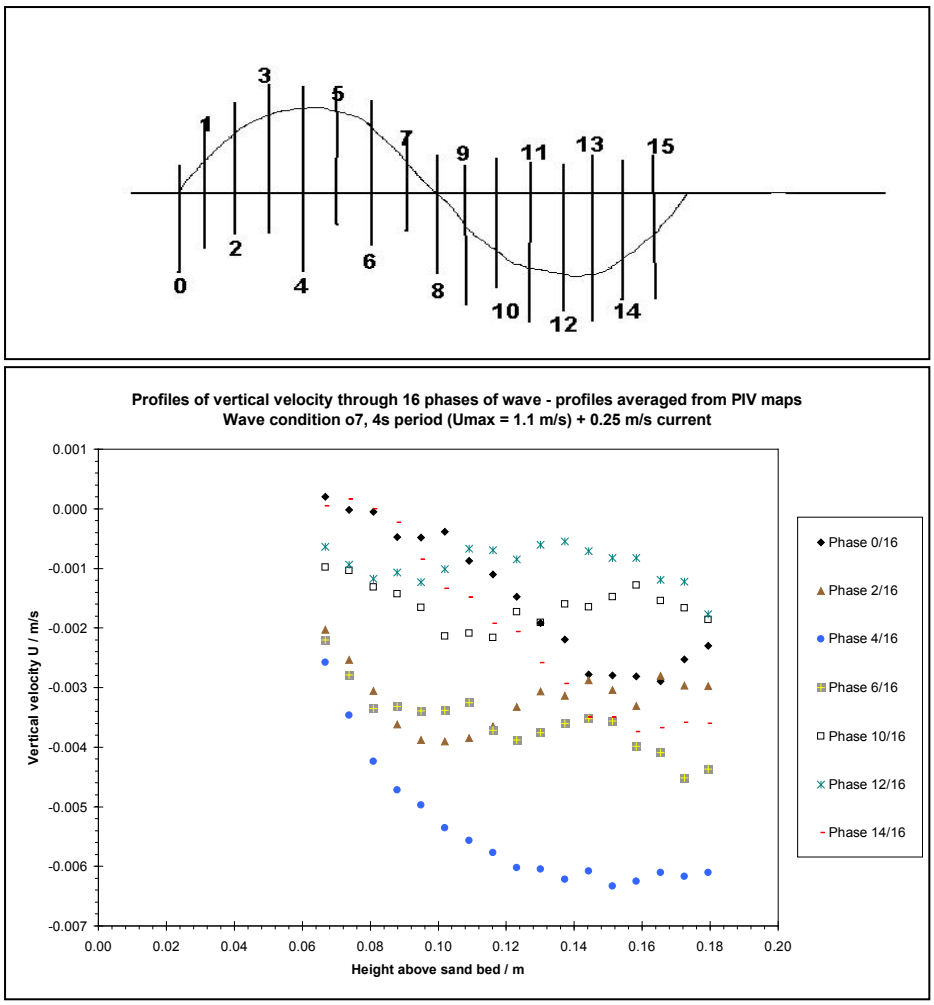

Figure 5-20 Vertical velocity at different phases

Figure 5-20 shows the vertical velocity at different phases (only even phases, since these on the odd phases are unreliable). All velocities are negative and the same order of magnitude as the settling velocity of sand particles (0.01m/s). This might be because the measured velocities are sand particle velocities. Turbulent upward moving of these particles is compensated by turbulent downward moving, without incorporating the higher concentrations for the upward movement. So the downward sand velocity is higher than the upward velocity (the difference is the settling velocity), without a net transport of sand in downward direction.

5.4.3 The transverse suction results

The results of the transverse suction are shown in Figure 5-21. Often more results at the same height for the same test condition are available, since it was required for ADV to repeat the test conditions three times in order to have information at all desired levels.

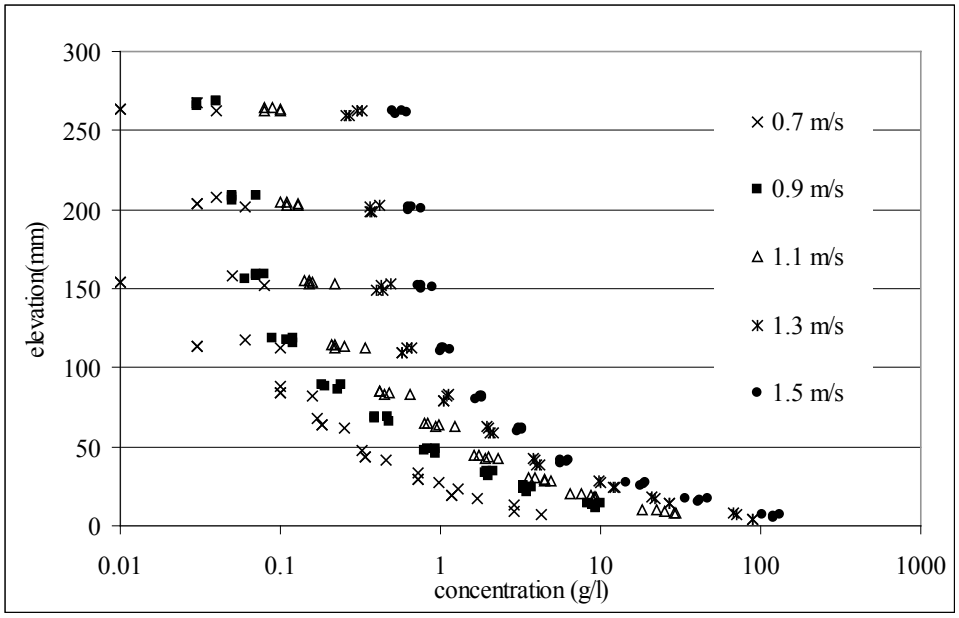

Figure 5-21 Vertical distribution of the concentration for different oscillating velocities

In every second suction test the sand samples were stored and their median diameter d_{50} was determined. The settling velocity is measured with the settling tube. From these velocities the corresponding grain size is determined using the expression of Van Rijn (1993).
In Figure 5-22 the vertical distribution of d_{50} is shown for two oscillating velocities.

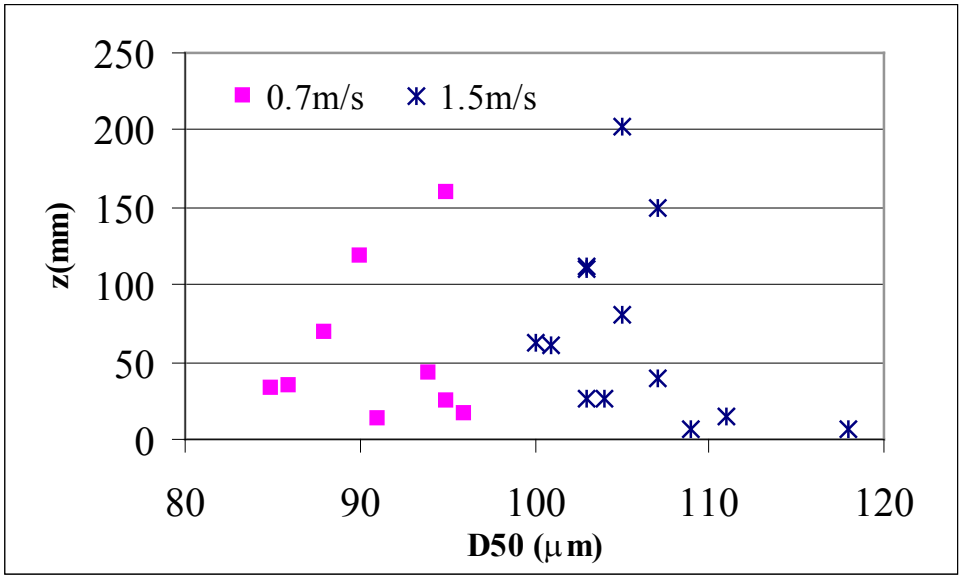

Figure 5-22 Vertical distribution of D50 for two oscillating velocities

From these figures it can be seen that the d_{50} of the suspended material (between 0.085 and 0.118 mm) is smaller than the d_{50} of the bed material (0.12 mm) (see Figure 5-3). For the lowest oscillating velocity, the mean grain size corresponds with d_{16} of the original bed material (0.09mm) and for the highest velocity the mean grain size corresponds with d_{33} of the original bed material (0.11mm).

The distribution of d_{50} over the vertical was used for the calculation of the calibration factor of the OPCON, which depends on d_{50}.

5.4.4 Optical concentration measurements

As the grain diameter changes over height, due to vertical sorting (finer grains are suspended higher), the actual calibration factor for each test was determined from the distribution of the D50 over the vertical, as measured by transverse suction. Additionally, the signal measured by OPCON should be corrected for the level of the background concentration. This could be determined as the output from the OPCON, when the pump and piston are switched off and the sand has settled back to the bed. Therefore the original measured concentration is corrected for these phenomena as follows:

$$c = \frac{(c_m - c_0)}{K_s} K_a \tag{5-7}$$

With:

c: the actual concentration (g/l)

c_m: the original concentration measured by OPCON (g/l)

c_0: background concentration (g/l)

K_s: standard value of calibration factor for D_{50} = 0.13 mm and amplification 1

K_a: actual value of calibration factor for corresponding D_{50} and amplification

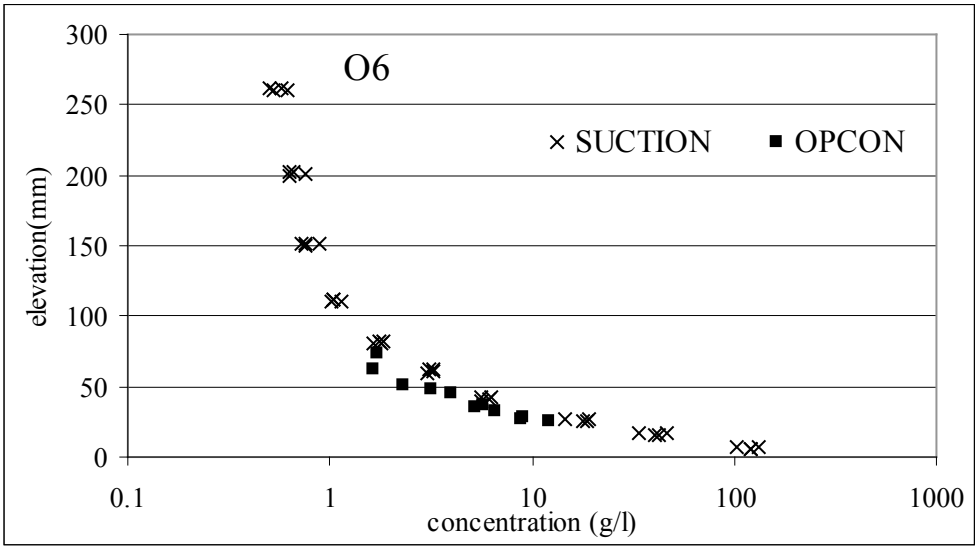

Figure 5-23 Comparison between transverse suction and OPCON

In Figure 5-23 the time-averaged concentrations obtained with the OPCON and with the transverse suction system are shown for test O6 (oscillating velocity of 1.5 m/s), which shows a very good correspondence.

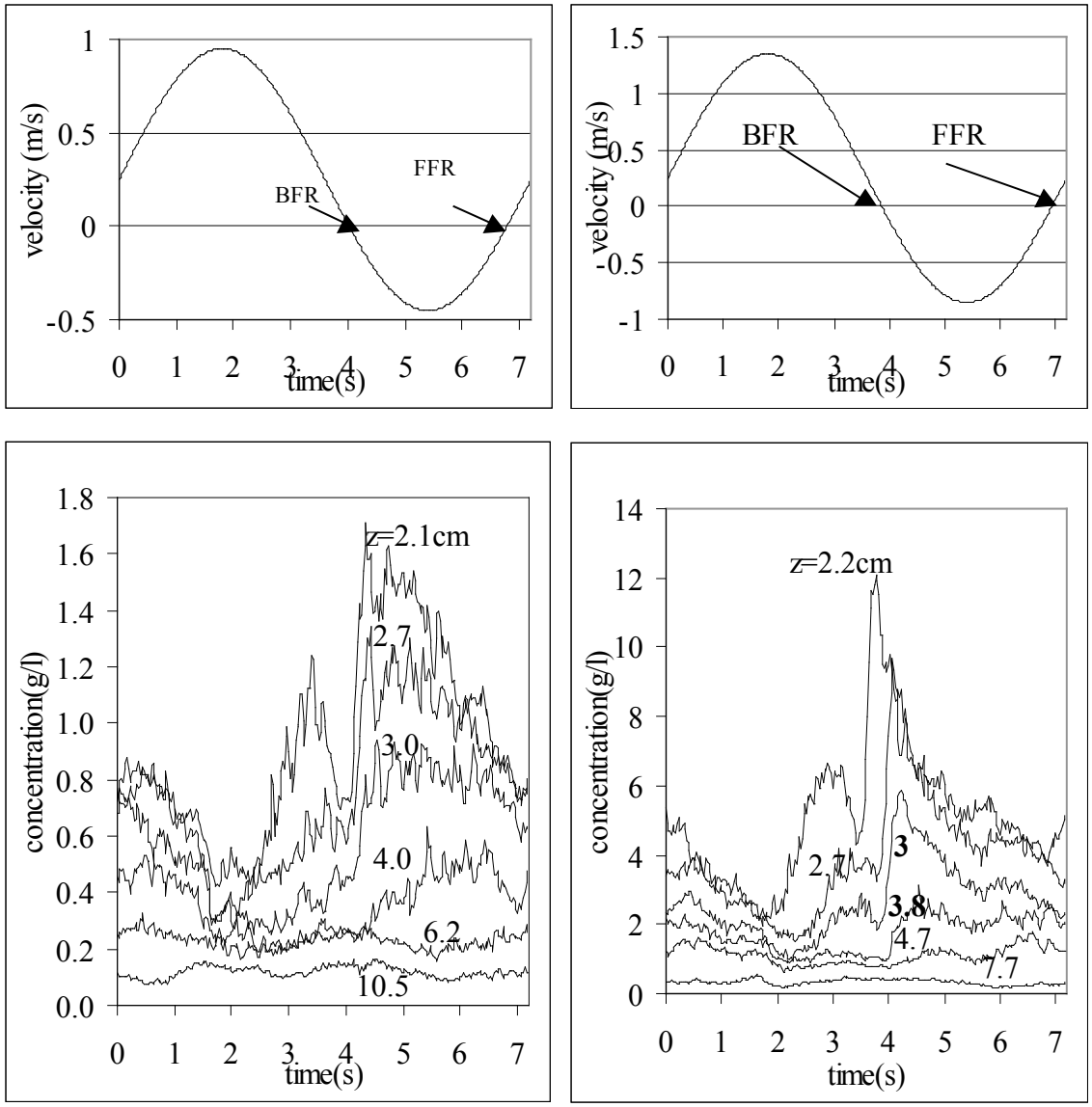

Figure 5-24 Ensemble-averaged suspended sediment concentrations at various elevations from: a) Test O2 and b) Test O4.(oscillating velocity of resp. 0.7 and 1.1 m/s, period of 7.2s)

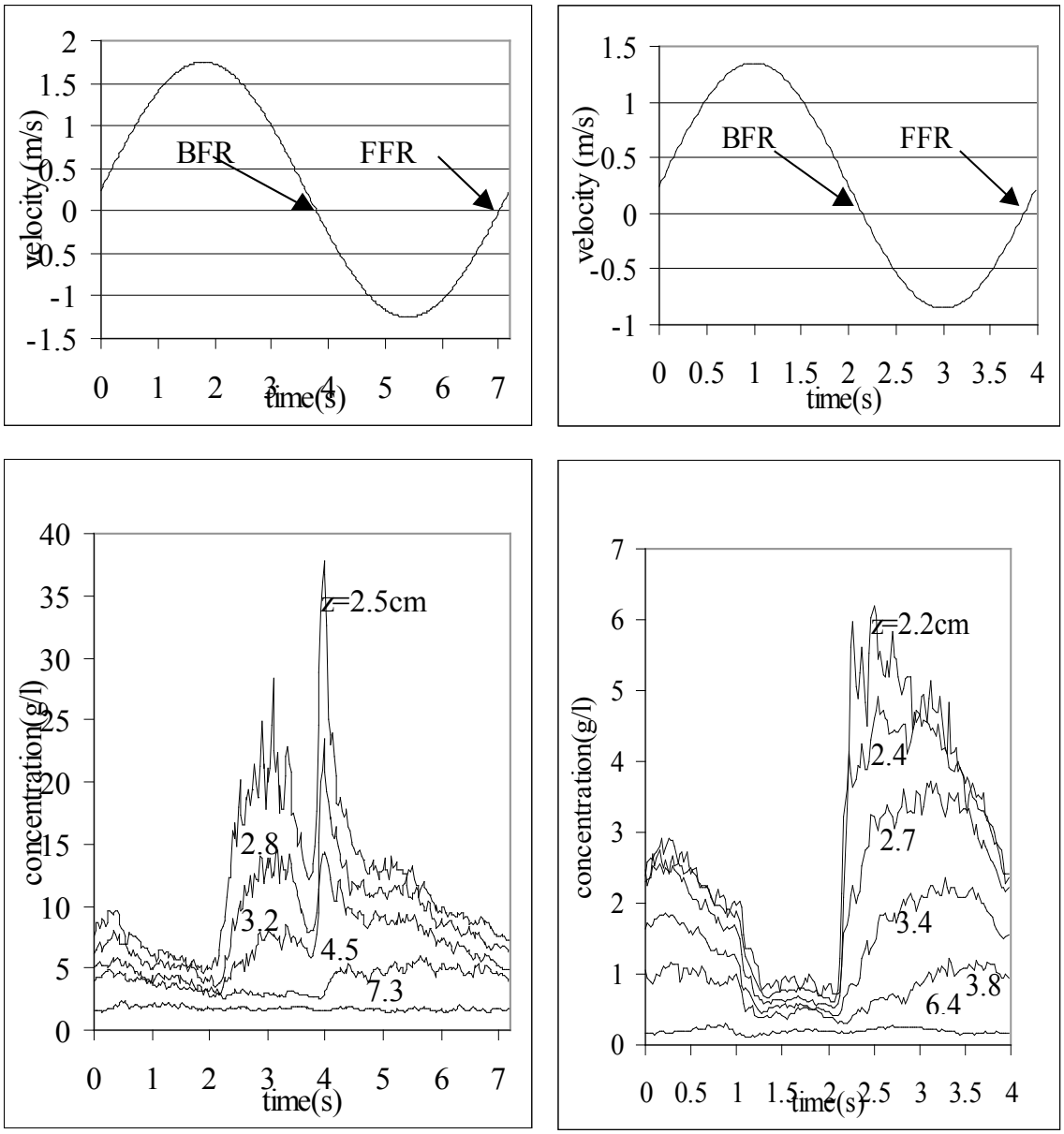

Figure 5-25 Ensemble-averaged suspended sediment concentrations at various elevations from: a) Test O6 and b) Test O7.(oscillating velocity of resp. 1.5 and 1.1 m/s, period of resp 7.2s and 4s)

The ensemble-averaged concentrations obtained with the OPCON are plotted in Figure 5-24 and Figure 5-25. The upper section of each plot shows the ensemble-averaged horizontal velocity record obtained with the LDA at an elevation of 0.20 m. The plots thus show changes in the concentration time series with increasing maximum oscillatory velocity (0.7 m/s; 1.1 m/s; 1.5 m/s) with the depth mean flow kept constant at 0.25 m/s. The plots also show the change in concentration resulting from a change in wave period in (7.2 s; 4 s). In test O7 the OPCON is "calibrated" as good as possible by using old calibration factors since

no transverse suction was done. Wrong calibration would not change the shape of the time evolution.

In the subsequent discussion, "forward" flow reversal refers to the moment immediately before the oscillatory motion moves with the mean flow direction and "backward" flow reversal refers to the moment immediately before the oscillatory motion moves against the mean flow. These phases in the wave cycle are marked as FFR and BFR respectively in the figures. The presence of the mean flow shifts the velocity time series upwards, so "forward" flow reversal would occur earlier and "backward" flow reversal later compared to the same oscillatory only conditions.

Figure 5-24(a and b) and Figure 5-25a demonstrate local concentration peaks corresponding to wave maxima and minima and flow reversals. All these peaks decrease rapidly in concentration with distance from the bed. Generally at an elevation of approximately 0.07 m above the bed the peaks are no longer easily distinguishable and the concentrations are relatively uniform with time. The general trends are comparable to those reported in Katopodi et al. (1994), who used a range of wave-current conditions and bed sediments with $D_{50} = 0.21$ mm. Data from Tests O3 and O5 demonstrate similar trends to those reported below.

The easiest peaks to identify in Figure 5-24(a and b) and Figure 5-25a are those associated with flow reversals. In all three plots there is clear asymmetry between the peaks near "forward" (at approximately 0.25 s into the cycle for the near bed measurements) and those near "backward" flow reversal (at approximately 4 s into the wave cycle for the near bed measurements). The peaks near "backward" flow reversals are clearly associated with the largest concentrations for each test condition. The effect of increasing the peak oscillatory velocity is to particularly increase the magnitude and sharpness of the peaks associated with "backward" flow reversals. These near-bed concentration peaks increase a factor of approximately 7 between Figure 5-24(a and b) and a factor of approximately 3 between Figure 5-24b and Figure 5-25a. Figure 5-24b shows the clearest evidence of an increasing time lag of the "backward" flow reversal peaks with increasing distance above the bed. The asymmetry between the flow reversal concentration peaks is more evident with the present results than those reported in Katopodi et al. (1994) with coarser sand.

Concentration peaks associated with flow maxima can also be distinguished in Figure 5-24(a and b) and Figure 5-25a, though the peaks lag the velocity maxima and occur near the bed at approximately 3 s into the wave cycle. These peaks are generally rounder than those attributed to "backward" flow reversals. Peaks at flow minima are less easy to distinguish as they appear to be masked by concentrations remaining in suspension from the "backward" flow reversals (fine sand was used in the present tests with a settling velocity of -0.01 m/s).

The increasing maximum oscillatory velocity enhanced the magnitude of the near-bed concentration peaks associated with flow maxima by a factor of approximately 5 between Figure 5-24 a and b and a factor of approximately 4 between Figure 5-24b and Figure 5-25a. The data in Figure 5-24b and Figure 5-25a suggest that the peaks corresponding to flow minima (at approximately 5.5 s into the wave cycle) are smaller in magnitude than the peaks associated with flow maxima because of the smaller wave and current combined speeds. Given the time lag between flow maxima and the associated concentration peaks the smaller peaks at t=0.25s may also be linked to the flow reverse after the flow minima.

A comparison between Figure 5-24b and Figure 5-25b demonstrates the effect of decreasing the wave period on the form of the concentration time series under the present wave-current conditions with fine sand. The concentrations at "backward" flow reversal and the smaller peak after "forward" flow reversal in Figure 5-25b show much the same general pattern as those in Figure 5-24b. However, it is clear that the decrease in the wave period has almost eliminated the peaks that occurred after flow maxima in Figure 5-24b.

Given the importance in the present tests of the concentration peaks at "backward" flow reversals, the structure of these peaks are examined in further detail Figure 5-26. Figure 5-26a demonstrates the position of the ensemble averaged "backward" flow reversal concentration peaks in the oscillatory cycle with elevation for Test O4 (x symbol) Test O5 (□ symbol) and Test O6 (+ Symbol) data (orbital velocities of resp. 1.1m/s;1.3m/s and 1.5 m/s, period of 7.2s and mean current of 0.25 m/s). Ideally the corresponding position of the peaks present in the ensemble averaged vertical velocities should also be plotted for a comparison. However, for the present tests, accurate measurement of near-bed temporal vertical velocities was found to be difficult. This is because the peak near-bed vertical velocities are typically 1 to 2 orders of magnitude less than peak horizontal velocities. Thus small bed slopes or slight sensor misalignment (of the order 1 %) result in a small but significant component of the horizontal velocity "leaking" into the vertical velocity records.

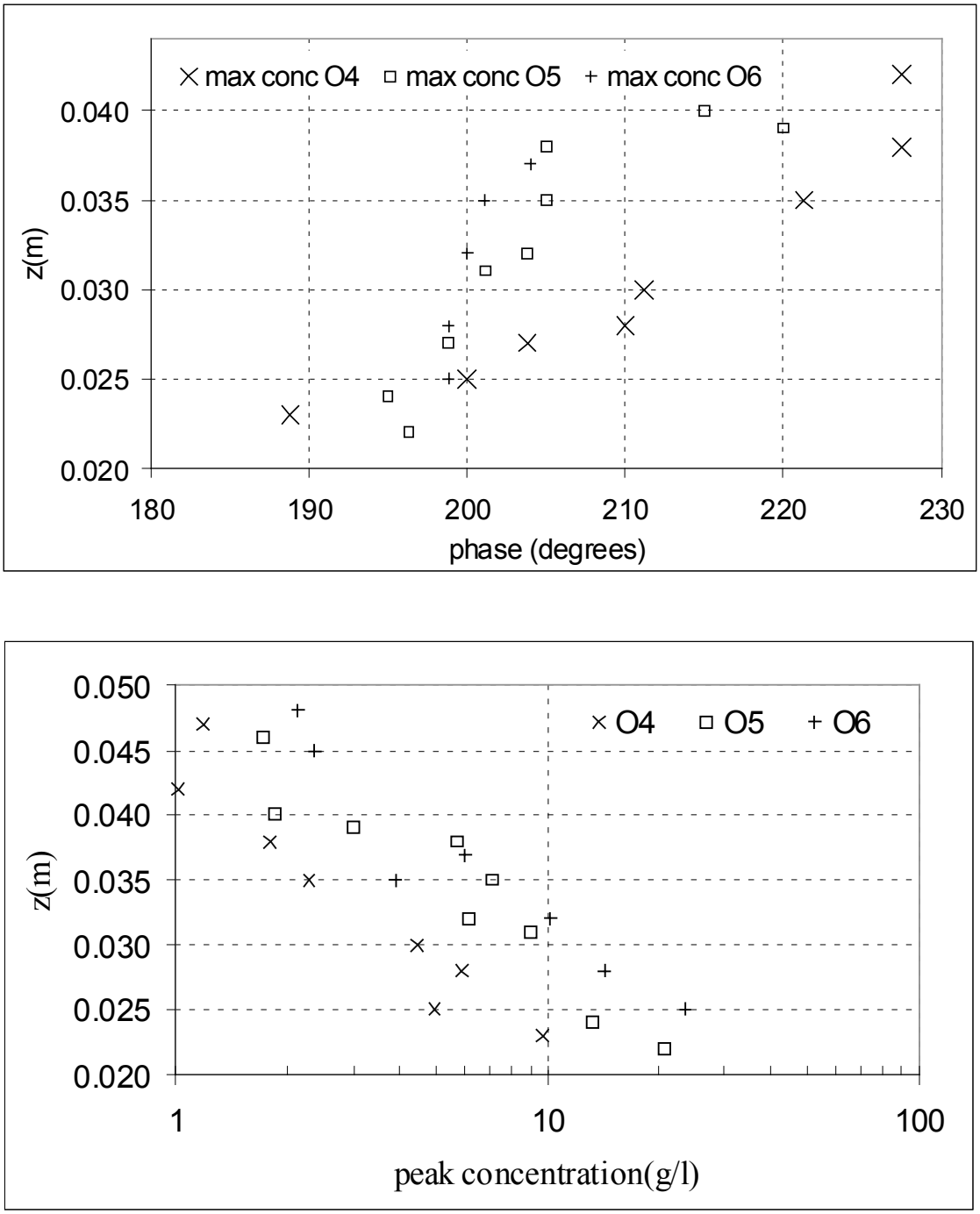

Figure 5-26 Structure of the ensemble average concentration peak at "backward" flow reversal: (a:above) position of the concentration, (b:below) peak concentration vertical profile.

The data indicate that the events near "backward" flow reversals exhibit a lag with increasing elevation above the bed. This lag decreases with increasing peak oscillatory velocity. This can be interpreted as an increasing upward convection velocity with increasing peak oscillatory velocity. The near bed gradients on this graph give estimates for the upward convection velocities of 0.02 m/s for Test O4 data, 0.06 m/s for Test O5 data and 0.15 m/s for Test O6 data. Figure 5-26b shows the peak concentrations near "backward" flow reversal as a

function of height above the bed for Test O4 (x symbol) Test O5 (□ symbol) and Test O6 (+ symbol). The data are plotted on logarithmic x-axes as the data demonstrate straight lines on this plot, though a reasonable straight line correspondence was also found on log-log axes. The fit of the data to the logarithmic x-axes suggest a decaying exponential peak concentration profile which is analogous to the form of the horizontal and temporally averaged concentration profile found for oscillatory flow over sharp crested ripples (e.g. Chapter 4). Figure 5-26 (a and b) indicate that the peak concentrations at "backward" flow reversals can be described as convective in nature (exponential concentration profile).

Tests with irregular waves (O10) are analysed by scaling the OPCON results with the TSS (Transverse suction system)-results since the limited number of analysed TSS-samples and because of the wide variation of velocities and concentrations (and D_{50}) during the test.
A sample is shown in Figure 5-27. Peak concentrations occur at flow reversal after peak velocities. At 5 cm from the bed an important time delay is visible.

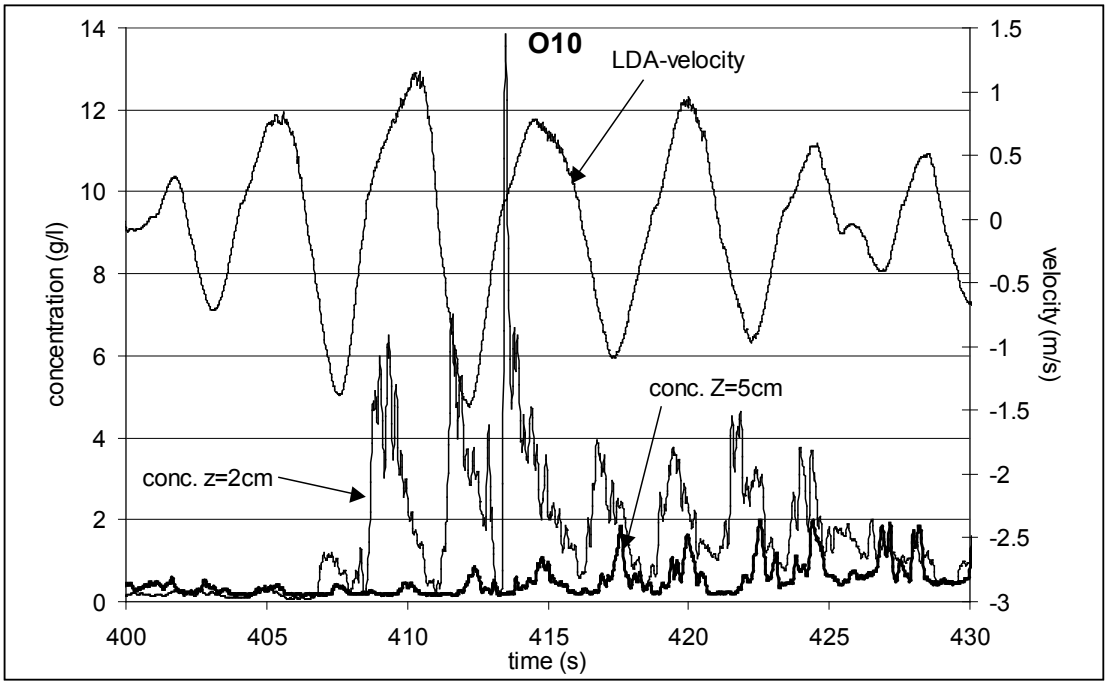

Figure 5-27 Concentrations at different heights for an irregular wave

5.4.5 Conductivity Concentration Meter (CCM)

Three different flow conditions were used during the CCM measurements (Oc4, Oc7 and Oc8). These conditions have the same current (0.25m/s) and orbital velocities (1.1m/s) with different periods 7.2 s, 4.0 s and 12.0 s respectively.

The following steps have been followed to analyze the data in order to determine both the ensemble-averaged concentrations and particle velocities (Hassan, 2001):

- The initial processing step was to locate in time the zero crossing of the piston motion;
- The next step was to create a high-pass filtered time series of the conductivity probe output to remove the mean time structure, using a simple 101 point boxcar running average;
- Next each oscillation period was divided into 36 phases;
- Using the center point of these intervals, cross-correlations between the time series for the two conductivity probes were calculated for different time shifts about the center point of the time interval. In each case 200 points from each series were used so that some overlap between adjacent phases occurred;
- The time series from each sensor were shifted in opposite directions with maximum total shift of 120 time steps, so the largest overlap with a neighboring time interval was 60 time steps;
- Correlations from several oscillations were averaged together, because the cross-correlations for a given phase from a single oscillation period were extremely noisy;
- Concentration ranges were used to group period averaged concentrations from each oscillation period;
- Cross-correlations from each wave having period-averaged concentration within a given range were also averaged together phase by phase.

The velocity of the sediment particles is given by $u = \Delta x/\Delta t$, where: Δt is the distance of the maximum correlation from the zero lag line. Rather than simply choosing the maximum value, the center of mass of all cross-correlation values between zero-crossings on either side of the maximum were calculated.

Figure 5-28 shows the ensemble averaged particles velocity and concentrations at different elevations above and inside the sand bed for the different flow conditions OC4, OC7 and OC8. (oscillating velocity of 1.1 m/s, period resp. 4;7.2 and 12s) These Figures include also the measured flow velocities at 100 mm above the sand bed, measured by LDA.

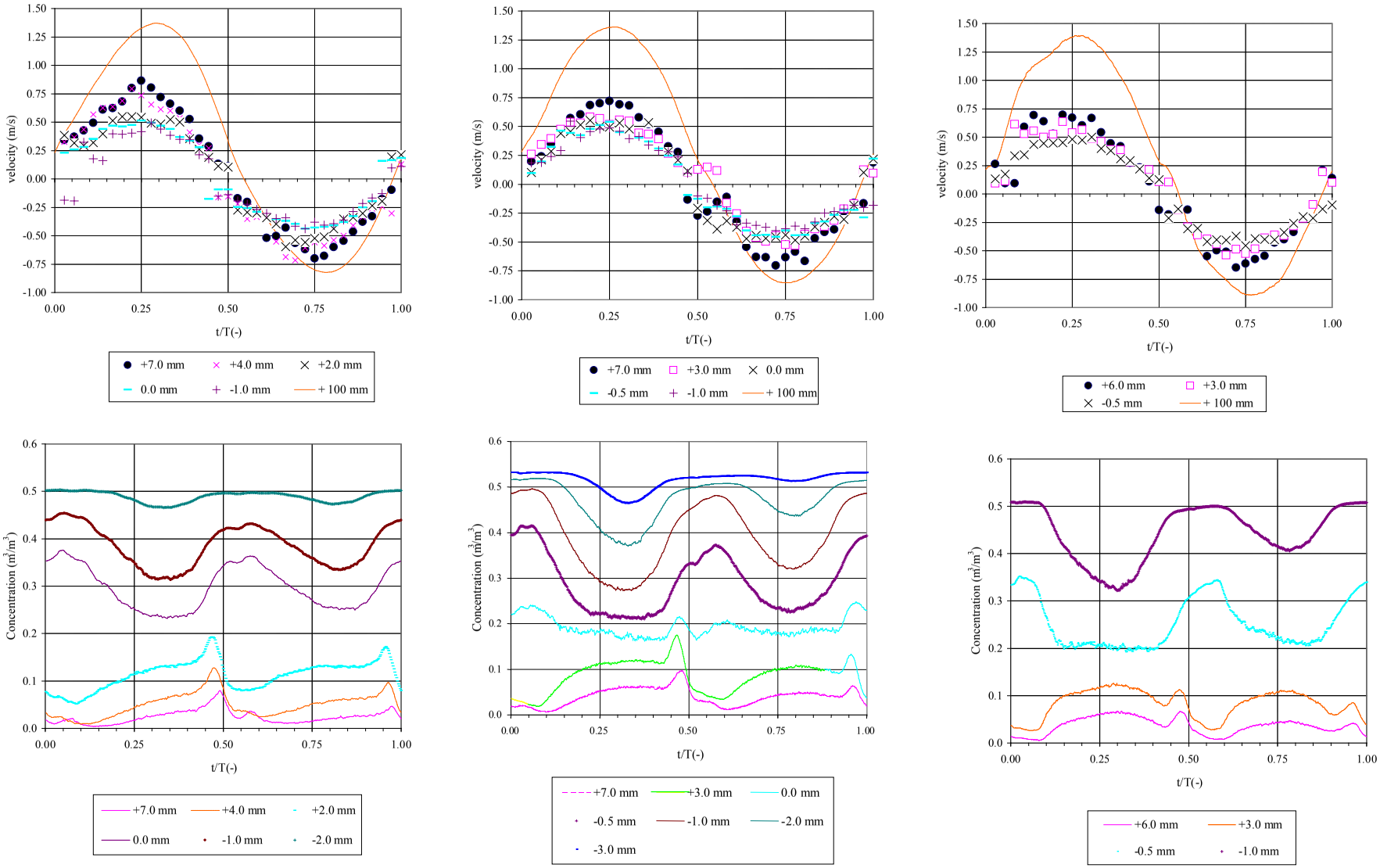

Figure 5-28 Ensemble averaged concentrations and velocities in the sheet flow layer :a) T=4s;b)T=7.2 s; c) T=12s

5.5 Conclusions

The measuring campaign was set up to have data for a variety of Reynolds numbers. This was obtained by varying the orbital velocity between 0.7 and 1.5 m/s with constant orbital period of 7.2s and a mean current of 0.25m/s. Three other tests were done with an orbital velocity of 1.1 m/s and a varying wave period (resp 4, 7.2 and 12s). Together with previous experiments, a data set is now available containing sediment concentrations and velocities in and above the sheet flow layer.

Examination of these data has led to the following conclusions:

- Mean velocity profiles demonstrated logarithmic regions in the upper flow which were deflected in the bed 0.02 m resulting in profile shapes similar to those reported previously for fixed rough bed wave-current conditions. The EMF and ADV results agreed well with each other and successfully measured in the near bed high concentration zone.
- The effect of increasing the oscillatory velocity, while keeping other hydrodynamic conditions constant, was to greatly enhance the magnitude and sharpness of the concentration peaks generated at "backward" flow reversal and to increase the magnitude of the peaks which appeared to be associated with flow maxima.
- The ADV could measure velocities close to the bed (0.5 cm above the fixed bed). With these data, velocity profiles could be extended up to the bed. The signals contain a lot of noise, however an indication of flow instabilities, with higher turbulence levels can be qualitatively shown. More testing of the ADV, together with the LDA should check the reliability of these results and the influence of the bigger measuring volume of the ADV.
- The suspension events near "backward" flow reversals exhibited a lag with increasing elevation above the bed. This lag decreased with increasing peak oscillatory velocity.
- PIV measurements were able to derive a velocity field. The vertical velocities seem to include the settling velocities of the sand particles. Close to the bed the concentrations are too high, so that no measurements were possible for the lowest 6 cm.
- A pair of CCM's made it possible to obtain velocities and concentrations inside the sheet flow layer. The lifting up of the bed is clearly visible near flow reversals, with an important increase of the concentrations above the original bed level, and a decrease of concentrations below this level. The combination of velocities and concentrations makes it possible to predict sediment transport in the sheet flow layer.

The contribution of the author consisted of:

- Coordination of the experiments and data analysis/ writing of the data report.
- First analysis of LDA, OPCON, TSS and ADV results.
- Analysis of the velocity, concentration and d50- profiles.
- Trying to get the maximum information out of the data for turbulence/shear characterisation.
- Interpretation of these results: comparison of different instruments, identification of flow reverse, influence of wave characteristics on velocity profiles and occurrence of peaks of sediment concentration.

6 Numerical modelling of the concentration field over ripples

6.1 Introduction

With a two-dimensional model sediment concentrations and velocities are calculated over ripples under wave conditions. It is shown that using a k-ε- model can give good results if the grid is constructed carefully. Using a turbulence model has the advantage that turbulent diffusion is incorporated in a natural way, without using assumptions for the turbulent viscosity.

Nielsen (1992) describes the mechanism of vortex trapping over ripple crests. For the flow direction from left to right a particle falling at the right side of the vortex (right of a ripple crest, with clockwise rotation) the particle is also moved to the left by the movement of the water; there it comes in an area with upward velocities, preventing the grain of falling to the bed. At flow reversal the vortex (and induced sediment cloud) are swept over the ripple crest to the left.

These results are compared with measured time-averaged vertical suspended sediment concentration profiles in the Deltaflume of Delft Hydraulics, using the measuring tripod STABLE of Proudman Oceanographic Laboratory and with earlier experiments in other (wave) flumes.

The numerical model makes it possible to better understand the mechanism of sediment entrainment, vortex formation and travel. It allows also visualising the effects of wave asymmetry and wave groups. A 3D visualisation (horizontal, vertical and time) gives a more complete view than measurements, which are in the best case 2D (vertical and time). Different wave conditions are studied and visualised.

Several empirical relations exist to calculate the concentration and transport of sand above rippled beds. Since these relations are based on physical experiments that only make use of a limited range of hydro-dynamical parameters and sediment characteristics, they often fail in predicting transports for other situations. E.g. the grain size distribution of sand is difficult to vary. Numerical experiments however can be an interesting additional tool to examine the concentration pattern, and hence the transport of sand. It is not only possible to easily vary wave conditions; it is also possible to ‘measure’ at each location over the ripple velocities and concentrations. This allows interpretation of real measurements, which typically measure in a few verticals only.

Oscillatory flow over wave ripples was described first by Longuet-Higgins (1981) with a discrete-vortex model. Subsequently Perrier et al. (1994) have developed further discrete-vortex models and Blondeaux and Vittori (1991) solved the vorticity transport equation with a discrete vortex model. In the past only little work is done with turbulence models (e.g. k-ε). (see Tsujimoto et al., 1991). These models perform badly if the grid is too coarse. On the other hand, discrete vortex models have the weakness that the turbulent diffusion, which is

important to bring sediments in the vortex and for the concentration at higher levels is not modelled correctly.
In this chapter it will be proved that the k-ε-model performs well if care is taken for the grid. New numerical schemes reduce numerical diffusion, which destroy otherwise the development of the vortex.

6.2 Hydrodynamical model

The basic software used for this model was the CFD packet Phoenics (Cham, 1994). Among other possibilities, Phoenics can calculate velocity fields, using different turbulence models with an implicit finite volume upwind scheme. The advantage of this software is that it is possible to incorporate own coding (which is used for the boundary conditions and to calculate the sediment concentrations). A ripple profile can be included with body fitted coordinates. The grid is orthogonalised with an algebraic Laplace solver.

6.2.1 Some characteristics of the model

The grid is optimised to get grid independent solutions, and with at least one grid point in the inner turbulent zone (turbulent inner layer of Figure 2-1) ($30 < y^+ = yu_* / \nu < 130$)
The ratio of grid cell height to grid cell width is less than 1.3.
At the wall the non-equilibrium wall functions are used. Non-equilibrium wall function uses $\sqrt{k}$ as the characteristic turbulent velocity scale, rather than the friction velocity u_*. (Launder and Spalding, 1974)
The equilibrium wall boundary law:

$$\frac{u(z)}{u_*} = \frac{1}{\kappa}\ln(\frac{z}{z_0}) = \frac{1}{\kappa}\ln(z\frac{u_* E}{\nu}) \qquad (6\text{-}1)$$

assumes that the turbulence is in local equilibrium, while for e.g. separating flows turbulent energy diffusion to the wall is significant. The non-equilibrium law becomes:

$$\frac{u}{u_*}\frac{\sqrt{k}}{u_*} = \frac{1}{\kappa(C_{D\mu})^{0.25}}\ln(z\frac{\sqrt{k}E(C_{D\mu})^{0.25}}{\nu}) \qquad (6\text{-}2)$$

in which: E a roughness parameter, $C_{D\mu}=\sqrt{C_D C_\mu}$ =0.09, a constant of the k-ε-model.
The wall is assumed to be rough, with a roughness height $k_s=3d_{50}$.

It is assumed that the turbulence is not reduced by the presence of sediment particles. The influence of particles on turbulence is discussed by Rocabado (1999).

6.2.2 Validation of the used turbulence model

To check the validity of the calculations and the turbulence models, computational results are compared with velocity measurements (at a high frequency to be able to calculate turbulence parameters) of a current over a dune in a flume (van Mierlo and de Ruiter (1988)). Behind the crest the flow separates and a vortex develops. In the sand flume of Delft Hydraulics a series of concrete bedforms with a length of 1.6m and a height of 0.08m were constructed. The downstream side of the bedform had a length of 20cm, the upstream side a length of 1.4m. The surface of the bedforms was covered with a layer of sand with a mean diameter of 1.6mm. The average water depth was 0.252m and the average velocity was 0.394 m/s.

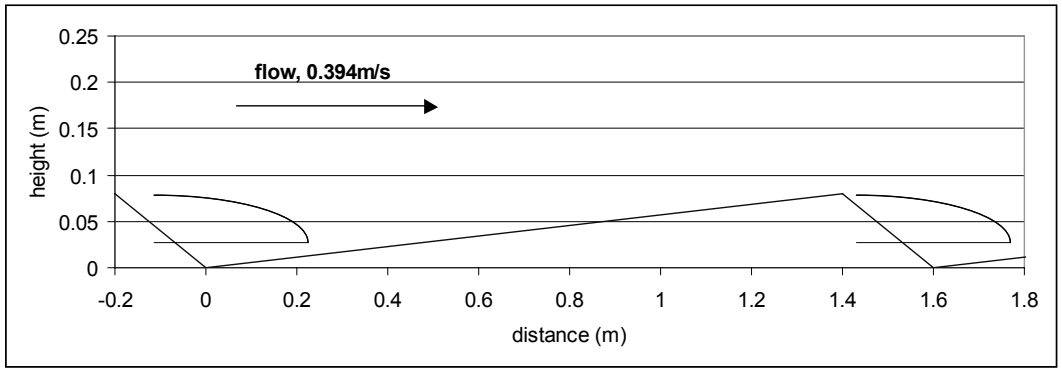

Figure 6-1 Layout of the dune

Two different turbulence models were compared: the standard k-ε model and the modified k-ε model of Chen-Kim (1987). In the latter, the dissipation of turbulent energy is augmented, because a strong mixing (due to turbulent velocity fluctuations) reduces the size of the recirculation zone. An augmentation of the dissipation thus results in a longer recirculation zone. It should be mentioned that this adaptation is not really natural because, in fact, the reduced recirculation zone is due to an underestimation of higher velocity structures in the recirculation zone and free stream zone. These structures in fact produce more turbulent kinetic energy or thus an increase of turbulent viscosity (Figure 6-4).
At the wall non-equilibrium log law wall functions are used (Launder and Spalding,1974).

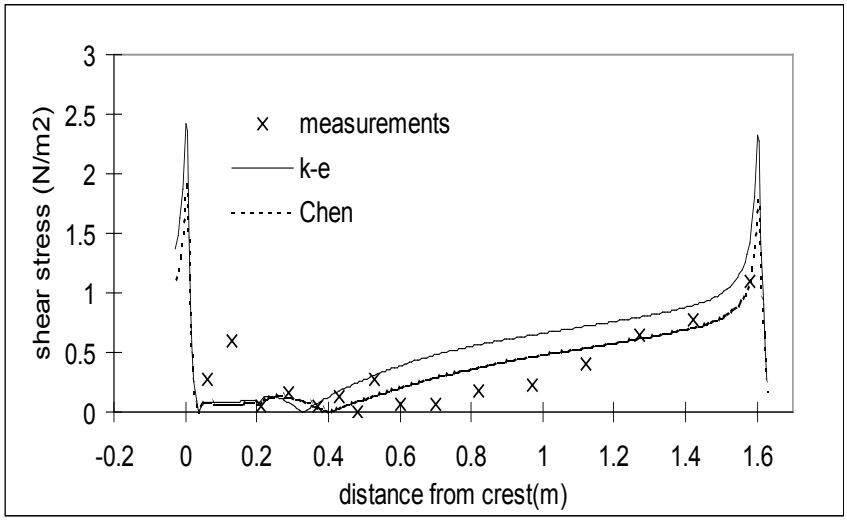

Figure 6-2 Shear stress along the dune surface

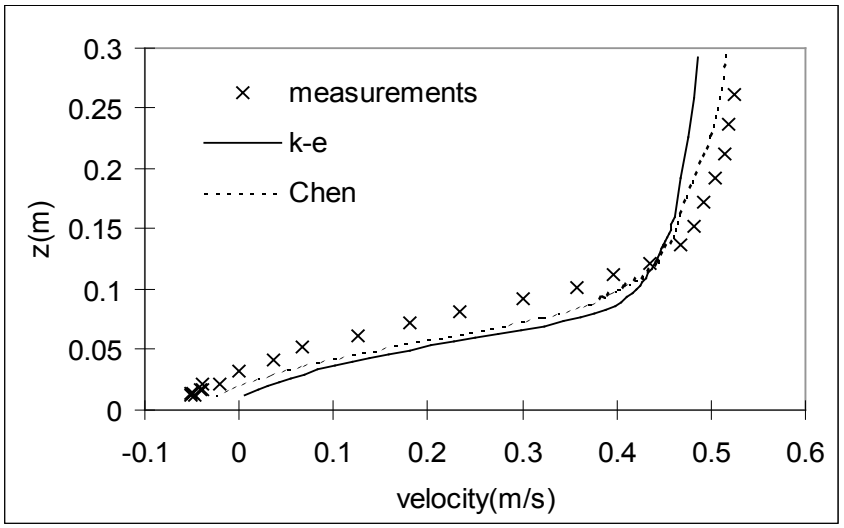

Figure 6-3 Velocity profile 40cm downstream from crest

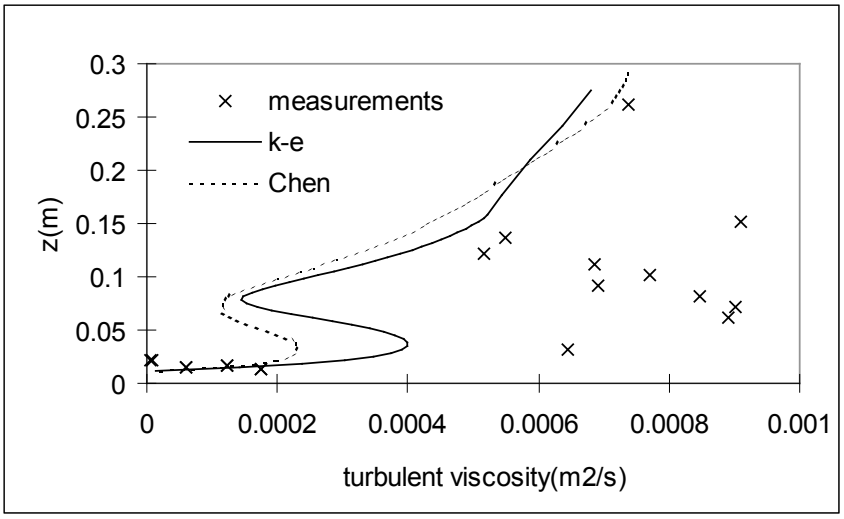

Figure 6-4 Eddy viscosity 40 cm downstream from crest

In Figure 6-2 the shear stress is shown as function of the (horizontal) distance from the dune crest (in the model also a series a (equal) bedforms is implemented in order to get equilibrium conditions, only the results of 1 dune are shown). The shear stress is maximal at the crest and zero at the reattachment point (where the free stream velocity meets the bed again at the end of the recirculation zone).
In Figure 6-3 the velocity in a vertical 40cm downstream the dune crest is shown (reference level (z-axis) is the lowest point of the dune).
In Figure 6-4 the turbulent viscosity is shown in the same vertical.
The shear stress (τ) and eddy viscosity (ν_t) can be determined from the velocity measurements: $\tau=-\rho\langle u'v'\rangle$ and $\nu_t=-\langle u'v'\rangle/(du/dz)$ (with $\langle\rangle$: time averaged value, u' and v' the instantaneous deviation of the time averaged velocity in resp. horizontal and vertical direction and du/dz the velocity gradient).
In Figure 6-2 and Figure 6-3 it can be seen that the velocity and the shear stress are predicted rather well by the Chen-model. The standard k-ε model underpredicts the recirculation zone (the backward (=negative) velocity is much smaller) and overestimates the shear stress on the upstream side of the dune. As explained previously the turbulent energy or viscosity is strongly underestimated. However, at the bed where the turbulent diffusion is important to bring the sediments to higher levels (in the vortex), the turbulent viscosity is predicted rather well. The boundary conditions at the water surface don't influence the results at lower levels as can be seen from a variation of these boundary conditions.

Discussion

It is generally believed that k-ε- models are not optimal to reproduce eddies behind backward facing steps or dunes. Computations with the presented numerical model however indicate that the length of the computed eddy depends strongly on the number of grid cells. This conclusion corresponds with the conclusion of Thangam & Speziale (1992) and Avva et al.(1988) that the main error of k-ε- models is the insufficient numerical resolution. The error on the length of the eddy (about 6 to 7 times the height of a backward facing step) is about 10 % for a classical k-ε- models and less than 3% if the model is modified to include an anistotropic eddy viscosity. Other models, specially designed for a good prediction of the reattachment can fail in predicting shear stresses.
Since this model will be used to predict sediment concentrations over ripples, the two most important factors that have to be reproduced correctly, are the size of the vortex and the shear stresses (see Figure 6-2). Turbulence is a less important factor since convective motion in the eddy is dominant for the formation of a sediment cloud and its movements. It is decided in what follows to work with the Chen-model since the better reproduction of the shear stresses and reattachment point.

6.3 Computation domain and boundary conditions

6.3.1 Domain

The flow due to waves over a rippled bed is calculated in a limited computation domain with a length of 6 ripples and a height of 3 ripple lengths. The model can be considered as a numerical wave tunnel, with oscillating velocities rather than waves. Computations are done over a time scale of a few wave periods. Since the travelling speed of the ripples is in the order of 1cm/minute, the ripples can be considered as immobile during a wave period. If runs are done for more wave periods, the computation domain can be considered as a moving domain, together with the movement of the ripples.
Since a ripple length is much smaller than the wavelength (factor 100) the flow can be considered as horizontally uniform over the ripple. Wave induced vertical velocities do not occur in a wave tunnel, in reality they will be small compared to the vertical velocities due to the vortex formation and shedding.
In reality, the non-uniformity of the waves along the bed will cause a small near bed current (streaming, e.g. Chapter 2). This current is important for the net transport of sediments, but not to calculate the concentration profile).

6.3.2 Boundary conditions

At a height of 3 times the ripple length a zero gradient is assumed for sediment concentrations, horizontal velocities and turbulent kinetic energy.
The up- and downstream boundary conditions are cyclic, which makes the bed as being horizontally infinitely long.

6.3.3 Computational grid

One wave period was divided in 360 time steps, the horizontal distance between two ripple crests was divided in 100 cells, the vertical space between the zero level (ripple trough) and a level equal to two ripple heights was divided in 40 cells (equally spaced), above this level the grid was much coarser.
The ripples in the model have a parabolic shape (Nielsen,1992):

$$y = \frac{4\Delta}{\lambda^2}x^2 - \frac{4\Delta}{\lambda}x \qquad (6\text{-}3)$$

(with Δ the ripple height, and x and y respectively the horizontal and vertical coordinates).

Although measurements of ripple shapes usually do not show sharp ripple crest, these sharp ripple crests can be seen in laboratory flumes with walls of glass. The ripple crest is not stable, but is moving with the oscillating flow, giving a sharp slope of the ripple at the side upstream the flow. This sharp slope has to be used as boundary in the model.

Ripple dimensions are obtained from measurements or are calculated with the expressions of Nielsen (1992)(for regular waves):

$$\frac{\lambda}{A_\delta} = 2.2 - 0.345\psi^{0.34} \tag{6-4}$$

$$\frac{\Delta}{A_\delta} = 0.275 - 0.022\psi^{0.5} \tag{6-5}$$

(with ψ the wave mobility number (=U^2/((s-1)gd), A_δ the orbital radius)

6.4 Sediment concentration

The sediments on the bed are divided in classes, each represented by a grain size and the relative amount available on the bed. Calculations are done for each grain class separately. The concentration of suspended sediment is calculated with the convection-diffusion equation. This equation states that the change in time of the concentration is due to convective transport of sediments (with u and w the water velocities, w_s the settling velocity of the sediments) and due to diffusion (with ν_t the turbulent viscosity)

$$\frac{\partial c}{\partial t} + u\frac{\partial c}{\partial x} + w\frac{\partial c}{\partial z} = w_s\frac{\partial c}{\partial z} + \frac{\partial}{\partial z}(\nu_t\frac{\partial c}{\partial z}) + \frac{\partial}{\partial x}(\nu_t\frac{\partial c}{\partial x}) \tag{6-6}$$

The exchange of sediments (E) per unit of time, can be estimated by considering the difference between the rate at which sediments enter suspension, defined by a pick-up function $p(t)$, and the rate at which sediments settle back to the bed. Thus

$$E=p(t)-w_s c_b \tag{6-7}$$

where c_b the concentration of suspended sediments at the defined bed level and the pick-up function is defined as (*Nielsen, 1992*) :

$$p(t) = 0.00033\left(\frac{\theta(t)-\theta_{cr}}{\theta_{cr}}\right)^{1.5}\frac{(s-1)^{0.6}\,g^{0.6}\,d_{50}^{0.8}}{\nu^{0.2}} \tag{6-8}$$

With $s = \rho_s/\rho$, ρ_s is the sediment density, ρ is the fluid density and d_{50} is the median grain diameter.

The Shields parameter, θ is defined as $\tau/(\rho_s-\rho)gd_{50}$. The critical Shields parameter, θ_{cr}, defines the threshold condition for the sediments. The bed shear stress, τ, is related to the roughness of the wall (k_s). For $d_{50} > 0.25$ mm, θ_{cr} values were calculated using the formula given by Yalin (1972). For $d_{50} < 0.25$ mm, θ_{cr} values were calculated using the formula given by Miller et al. (1977). The effects of slope on the value of θ_{cr} were also accounted for by multiplying θ_{cr} values by k_β, where $k_\beta = \sin(\varphi+\beta)/\sin(\beta)$ for up-slope flow and $k_\beta = \sin(\varphi-$

β)/sin(β) for down-slope flow. Here φ is the natural angle of grain repose and β is the bed slope.

For each sediment size-class, the critical shear stress and the settling velocity were calculated. Since the hydrodynamic forces acting on a grain not only depends on the grain size of the fraction considered, but also on the size of the neighbouring grains, a (small) correction is applied to the Shields parameter so that $\theta_{cr,c} = \zeta_{eff}\theta_{cr}$, with:

$$\xi_{eff} = \left[\frac{0.4}{(d_i/d_a)^{0.5}} + 0.6 \right] \tag{6-9}$$

and

$$\frac{d_a}{d_{50}} = 1.6\left(\frac{d_{84}}{d_{16}} \right)^{-0.28} \tag{6-10}$$

It is assumed that the bed ripples are regular and long-crested and that ripple movement is small compared with the motion of the suspended sand. The problem is solved in two dimensions (with the horizontal in the direction of the wave induced fluid motion). It is considered that the processes are uniform in the horizontal direction, and thus the values of k, ε and c_b at the upstream boundary are taken equal to the values of the downstream boundary. The grid used in the simulations was staggered and values of suspended sediment concentration were computed at the centre of each grid cell.

Numerical scheme

The values of the suspended sediment concentrations at the boundaries of the cell were calculated with the improved Quick-scheme. In this scheme a quadratic upwind interpolation is used, but the flux is limited to prevent instabilities (Ferziger et al., 1996). This scheme produces much less numerical diffusion than the traditional upwind schemes. The used solution method was implicit.

The method to calculate the in/outflux at the left boundary of cell c(i,j) is explained below (based on Figure 6-5), for the other boundaries the method is analogous.

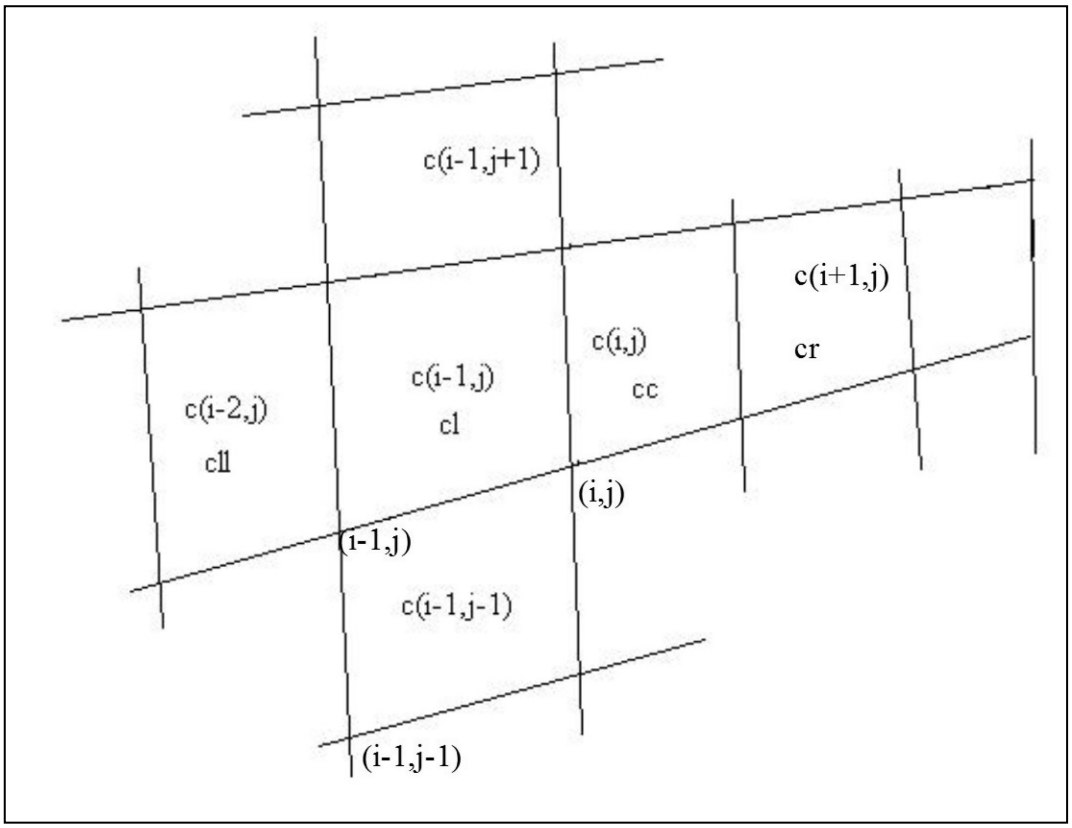

Figure 6-5 Grid with definitions of parameters

The sediment flux is the integration of concentration multiplied with the projected velocity over the left boundary. Concentrations are calculated at the middle of the resp. cells. However, to calculate fluxes, an averaged concentration over the cell height (for transport in i-direction) or cell with (for transport in j-direction) has to be known. This averaged concentration (in this case for the transport in i-direction, at the left boundary of cell (i,j)) is indicated in the figure as cc, cl, cll, … Integration is done by fitting a parabola through the upper, middle and lower cell. This results in a mean value over the height of the (left) cell equal to cl=1/24c(i-1,j+1)+1/24c(i-1,j-1)+11/12c(i-1,j).

This is done for the considered cell and for the first two cells left of it, giving resp. cc, cll (most left cell), cl and cr for the right cell

The mean velocities over the cell length are obtained at the same way (=ul).

With the improved quick-scheme the sediment flux ql is obtained by (Ferziger et al., 1996):

If the velocity is from left to right:

smr=(cc-cl)/(cl-cll)

smb=max(0,min(2smr,3/4smr+0.25,4))

smc=cl+0.5*smb*(cl-cll)

ql=ul x smc

Smb is minimal 0 (resulting in an influx equal to the upward concentration (cl) multiplied by the velocity at the boundary). This case occurs if the sign of the gradient of the concentration changes in the left cell. Since it is not know exactly where in the cell this reverse occurs, the concentration at the boundary is simply taken equal to the concentration in the left cell (upwind principle)

Smb is maximal 4, which occurs if the gradient in concentration increases a lot (high smr; cc-cl>>cl-cll). The concentration is taken as 3cl-2cll

For more smooth variations :

smb is 2smr, giving smc=cc since the horizontal concentration gradient is assumed to decrease, with a concentration approaching cc (cc-cl<0.2(cl-cll)

or smb=3/4smr+0.25, giving smc=3/8cc+6/8cl-1/8cll, as the parabolic approximation of a second order scheme.

If the velocity is from right to left:

smr=(cl-cc)/(cc-cr)

smb=max(0,min(2.0smr,3/4smr+0.25,4))

smc=cc+0.5*smb*(cc-cr)

ql=ul x smc

The vertical velocity is obtained by subtracting the settling velocity of the sand from the hydrodynamically calculated vertical velocity.

The flux due to diffusion is obtained by calculating the gradient of the concentration (e.g. (cl-cc)/Δx) and multiplying it by the diffusion coefficient.

For all cells the net influx is calculated, giving resulting concentrations (cres) for each cell. To avoid instabilities only a fraction of the resulting concentration is used to recalculate new concentrations (cnew). cnew=a cres+(1-a)cold. (cold the 'old' concentration, the concentration obtained in the previous iteration step) For each time step this procedure is iterated until cnew=cres. Since this will never exactly be achieved the stop criterium is based on maximum relative difference of 0.1% if the absolute difference is smaller than $5\ 10^{-8}$.

The time step of concentration calculations is three times smaller than the hydrodynamic time step, in order to get faster convergence.

6.5 Validation

The numerical model is validated using two independent physical experiments, one in the Deltaflume and one in the wave tunnel of Delft Hydraulics. No calibration is performed since the model is mainly used to compare test cases. Scaling could be done by scaling the pick up function, which is an empirical function with a lot of uncertainties. If the steepness of the concentration profile is wrong, one could scale with the mixing coefficients, however, in that case one should first examine carefully the physical reasons for the error.

6.5.1 Delta-flume experiment: validation and asymmetrical waves

In order to test the performance of the numerical model described above, a *Deltaflume* experiment was selected in which well-developed, long-crested vortex ripples were present on the bed. During the selected test above the medium sand bed, the wave height and period were respectively 75 cm and 5 s, and the water depth was 4.5 m. The velocity near the bed had an amplitude of 50 cm/s and ripples with a height of 4.5 cm and a length of 34 cm were developed.(test A08, see Chapter 4). The modelled concentration is averaged in time and in length (between two ripple crests, or between two points in the ripple through with the same height) varying with height above the ripple trough (which explains the peak in concentration at a height of 4.5cm (corresponding with the ripple crest)).

Since the sand was not uniform, it was important to make concentration calculations for different size fractions (i.e. d_6, d_{16}, d_{27}, d_{50} and d_{84} (= 170 μm, 211 μm, 273 μm, 329 μm, 761 μm). These fractions represent the 11% finest sediments, 11% to 22%, 22% to 33%, 33% to 66% and the 33% coarsest sediments, respectively. Since the contribution of the 33% finest sediments to the total concentration is much more important, this class was further sub-divided into 3 additional classes. For all the classes the pick-up rate is calculated independently from each other, this assumes that no armouring is occurring.

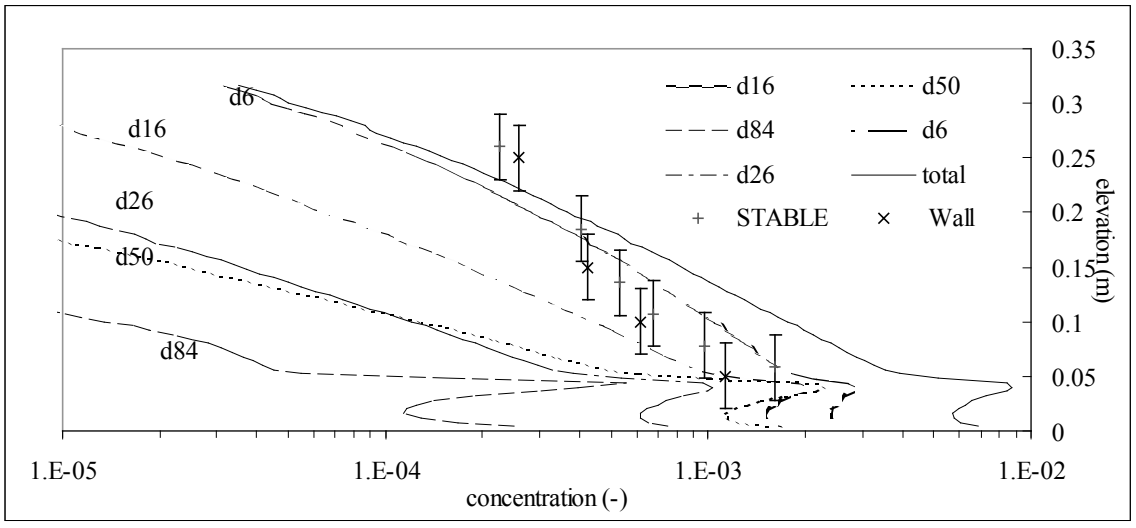

Figure 6-6 Validation with the Deltaflume experiments - contribution of the different grain classes to the total concentration (λ=35cm,Δ=4.5cm,$\hat{U}_\delta$=0.51m/s,T=5s, d_{50}=0.329mm)

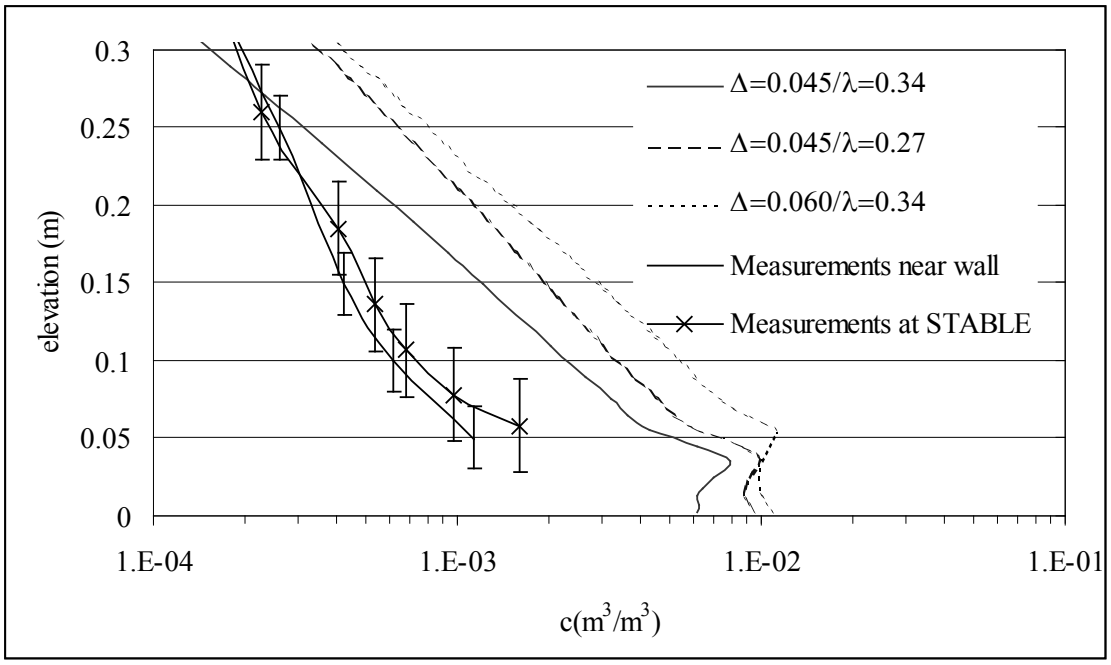

Figure 6-7 Comparison of concentration profiles for different ripple sizes and measurements in the Deltaflume

In Figure 6-6 the contribution to the total suspended sediment concentration profile of each grain size class is shown. The numerical model (and pick-up rate calculation) was run for each sand diameter separately. The total concentration is obtained by adding the contribution of the 5 classes, multiplied with their resp. occurrence at the bed (so the near bed concentration of a sand class is related to its percentage of occurance). Near the bed the contribution of the d_{50} class is larger than the contribution of the finer d_{26} since it is represented for 33% in the bed, while d_{26} only represents 11% of the bed material. At higher levels the contribution of the fine sediments becomes dominant. This was also observed during the experiment. A sample obtained during pump sampling (Chapter 4) indicated that at a level of 30 cm above the bed, the mean grain size (d_{50}) was 0.18 mm. This compares well with the observation that at this level the contribution of d_6 (0.17mm), which only represents 11% of the bed material, is dominant. A further subdivision of this class might give different results, but one may wonder if it makes much sense to make many very small classes. It is clear that a good knowledge of the grain size distribution is important, but very difficult in practice since sediments can be transported from locations where no bed samples are available. The sensitivity of the results to the grain sizes might explain partly the in literature observed large differences between different measurements and the differences between model results and observed results.

Figure 6-7 also shows the suspended sediment concentration values calculated using the numerical model and suspended sediment concentration values measured in the *Deltaflume* by pump-sampling. The error bars associated with the pump-sample values result from some

uncertainty associated with the exact position of the zero level. Here we focus attention on the gradient of the concentration profile.

The gradient of the predicted suspended sediment concentration shown in Figure 6-7, matches well the measured gradient (and the best match with ripples with a height of 4.5 cm and a length of 27 cm). The peak in concentration at approximately z =4.5/6cm is coincident with the ripple crest where maximum shear stresses are experienced. A difference in gradient can be attributed to a number of causes e.g. additional turbulence generated by the Deltaflume (walls or change in bed profile), enhance resuspension of sediments at the beginning of the sand bed, influence of grains which are still smaller than d_6 (cf the difference in concentration profile between d_6 and d_{16}), too much turbulent damping in the numerical model.

The computed suspended sediment concentrations are higher than the measured suspended sediment concentrations. This may result from a number of different causes. Firstly, the sediment pick-up function is considered to be a weak point in the numerical computations since the use of an empirical formulation is required to parameterise the resuspension process. Secondly, the results are sensitive to the roughness height, which is also derived empirically. But the main goal of these computations is to compare different cases, without paying much attention to absolute values.

Figure 6-8 shows the development and travel of sediment clouds (published as a movie on CD-rom in Trouw et al., 2000). Because the concentration range is quite large, the logarithmic of the concentration is shown. At the bottom of the figure the velocity outside the boundary layer is shown.

When the velocity becomes larger, also the shear stress becomes larger and more sediment goes in suspension. The sediment particles move along the ripple and over the crest where they are caught by the vortex that is being developed.

At 160 degrees the vortex starts moving over the bed. This occurs before flow reversal since the pressure reverse at the bed starts earlier (Fredsøe and Deigaard, 1992, Chapter 2). The sediments caught in the vortex travel together with vortex. It can be seen that the sediment cloud travels about two ripple lengths (e.g. starting at 0°, travelled almost one length at 60°, passing the next ripple crest (e.g. green cload between x=1.1 and 1.2m) and reaching the next crest at about 120°, where it is being caught by a new vortex. It is not caught by the vortex formed near 90 degrees because it is swept over the crest and the new vortex.

The resulting time averaged concentration is shown in Chapter 4 (Figure 4-40). It can be seen that time averaged concentration measurements (such as transverse suction) do not depend on the position of the measurements for levels higher than two ripple heights. Figure 6-8 indicates that this is not the case for time dependent measurements.

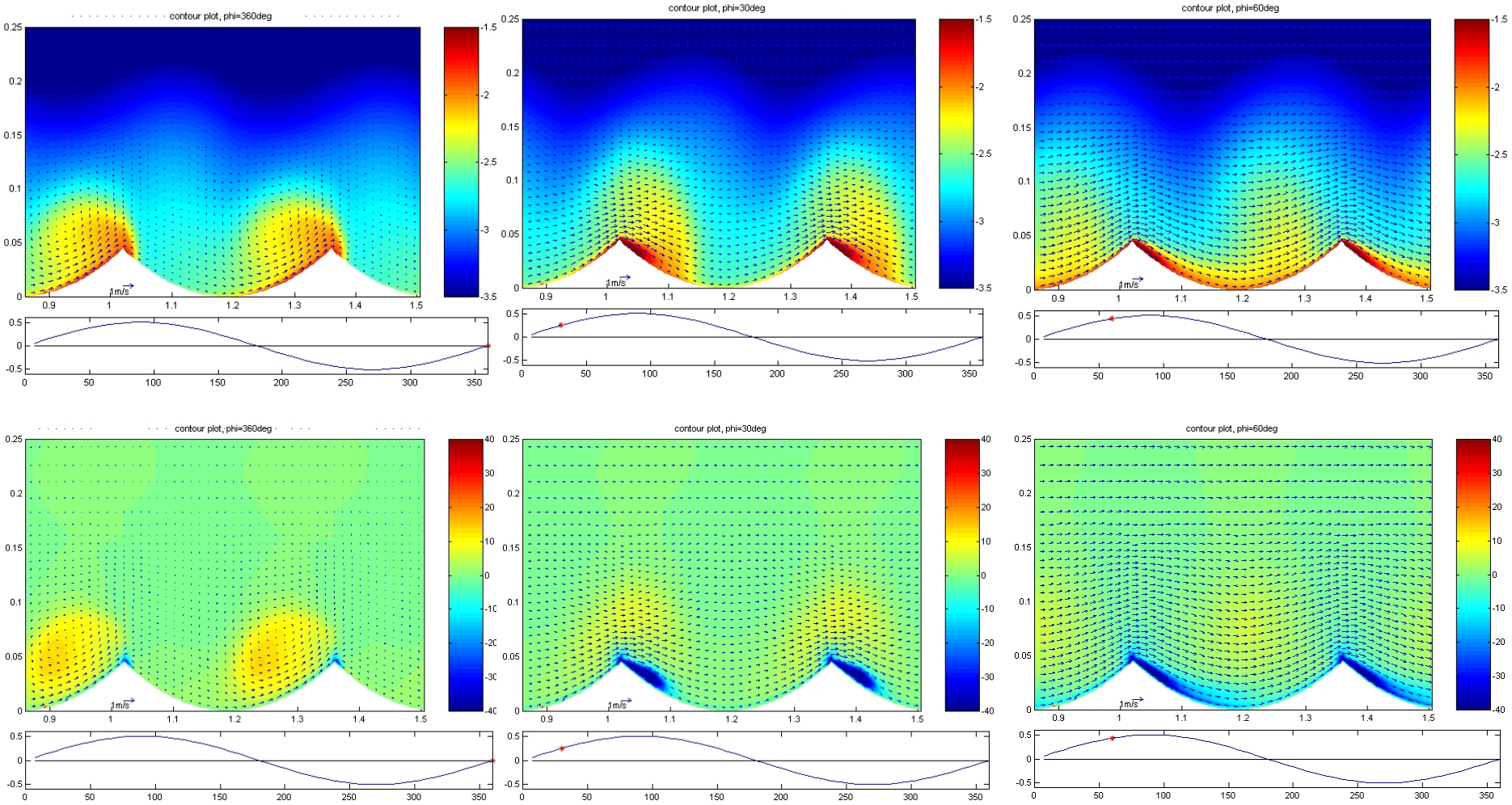

Figure 6-8a Concentration (top) (log. scale), vorticity (middle) and velocity outside boundary layer (bed) for regular wave at 0°, 30°and 60°

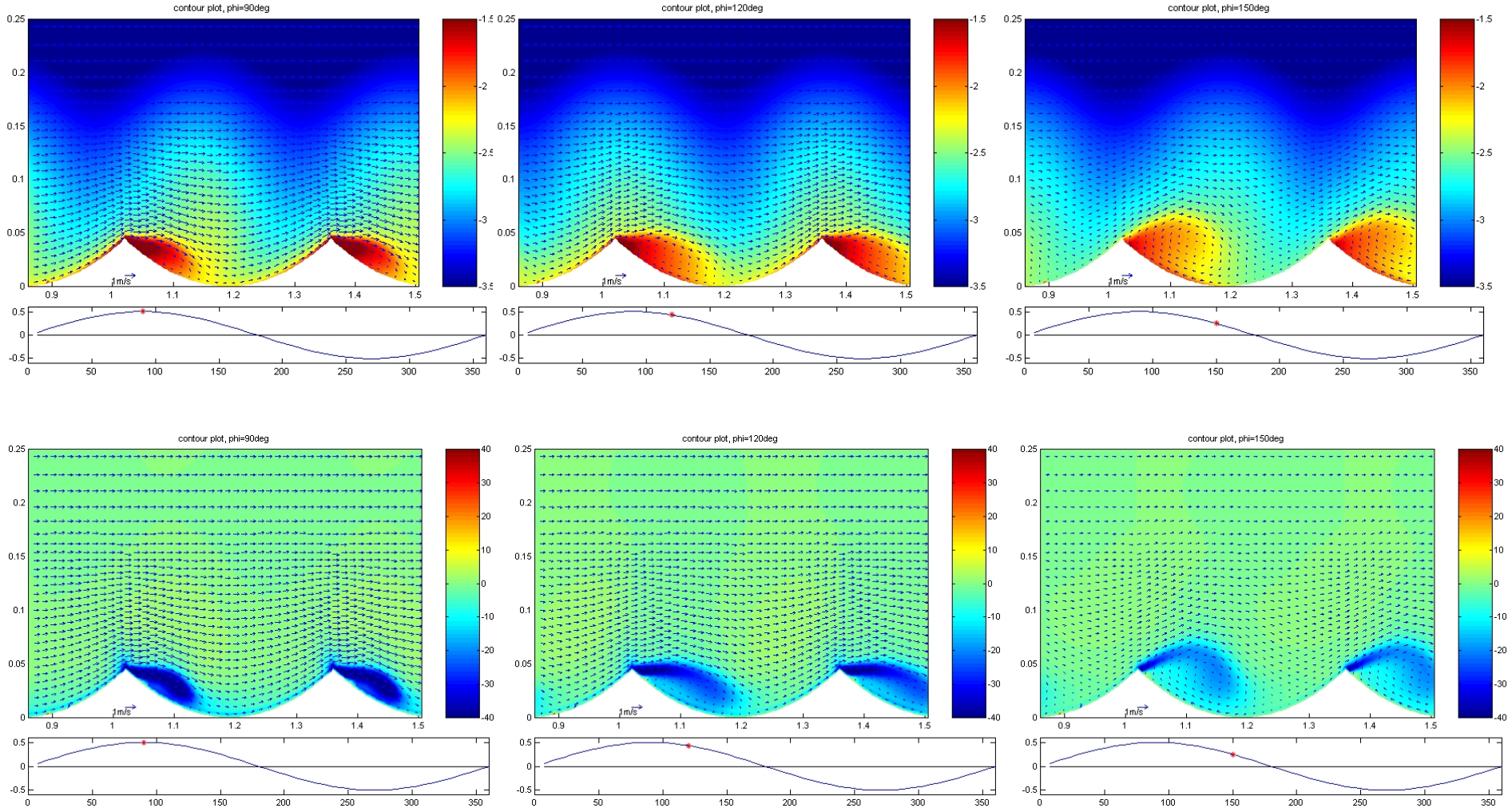

Figure 6-8bConcentration (top) (log. scale),vorticity(middle) and velocity outside boundary layer (bed) for regular wave at 90°,120° and 150°

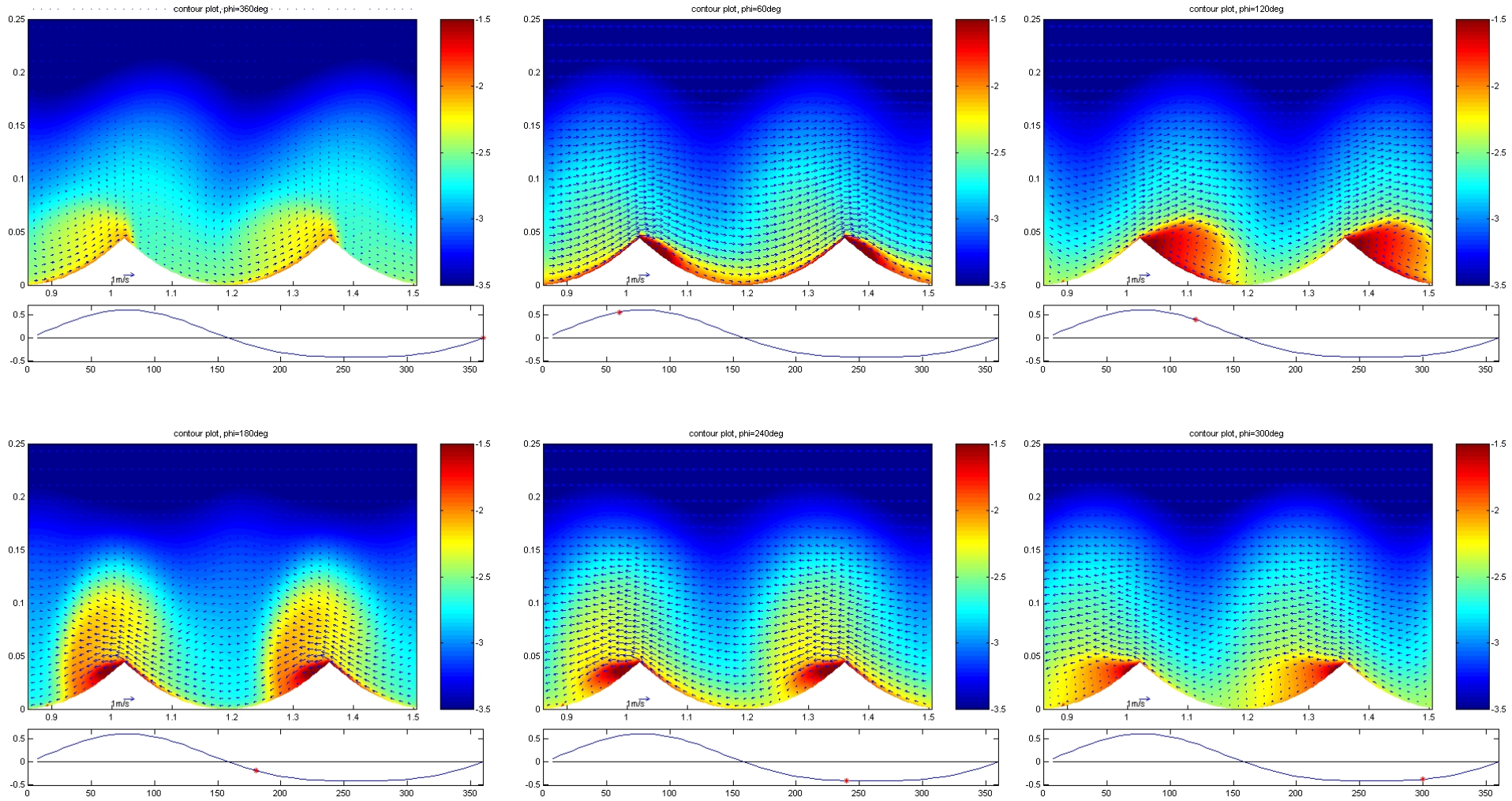

Figure 6-9 Concentration (log. scale) for asymmetric wave at (top) 0°, 60° and 120° and (bed) 180°, 240° and 300°

Figure 6-8 also shows the development and travel of vorticity (ω=dv/dx-du/dy). The vortex develops between 0 and 90 degrees since vorticity is developed at the upstream side of the ripple (high shear) and swept over the top. This explains why vorticity is not maximal at the bed at the downstream side.

When the velocity is decreasing also vorticity decreases by dissipation. Also the new developing vortex in front is hindering a little bit. The vortex curls up and travels over the crest. When the vortex is at the crest, it induces another vortex with opposite sign. They will travel some distance together.

Figure 6-9 shows the concentration for an asymmetric wave. Often it is seen in wave flumes and at sea that the crest velocity is higher than the trough velocity due to second order effects (e.g. Stokes second order wave, Dean et al., 1991). The crest velocity U_c is 0.6 m/s, the trough velocity U_t is 0.4 m/s. (wave asymmetry degree $R=U_c/(U_c+U_t)=0.6$) Much sediment is caught when the velocity is positive (crest) but it can not travel further away. After flow reversal a big sediment cloud travels in opposite direction. When the velocity is negative only a small sediment cloud is formed, which travels after flow reversal in positive direction. The effect on net sediment transport is shown in Figure 6-10 for different grain sizes (no reduction due to limited availability at the bed applied): only close to the bed the net transport is in the direction of the highest velocities, but the main transport is backward!

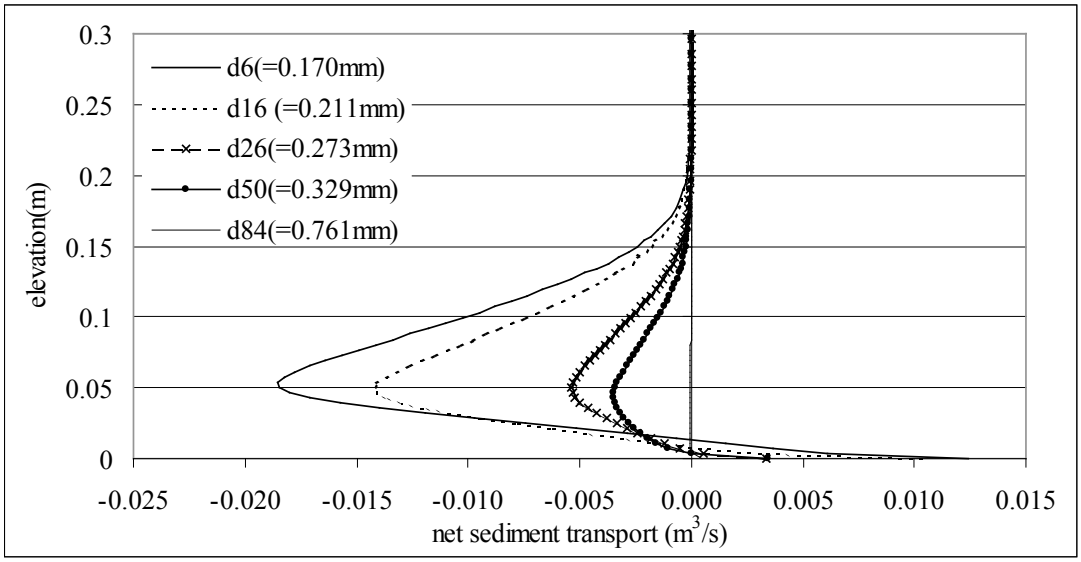

Figure 6-10 Net sediment transport rates due to asymmetric wave (the flux for d84 is almost zero)

6.5.2 Experiment in the wave tunnel

An experiment in the wave tunnel of Delft Hydraulics (Ribberink et al., 1989) is used as second validation. In the wave tunnel it is possible to simulate waves with a high orbital velocity (up to 2 m/s) and period. Test T4 was simulated. (λ=25.6cm, Δ=3cm, $\hat{U}_\delta$=0.35m/s, T=5s, d_{50}=0.21mm).

Figure 6-11 shows the calculated and measured results. The concentrations are averaged horizontally between two ripple crests. The peak at z=3cm corresponds with the ripple crest, around which the highest concentrations occur. Near the bed the measurements and model results correspond well, while further from the bed the concentration decays too fast compared to the experimental results. This can be explained by the finer sediments (d_{10} =0.15mm) which have a much steeper concentration gradient (e.g. §6.5.1).

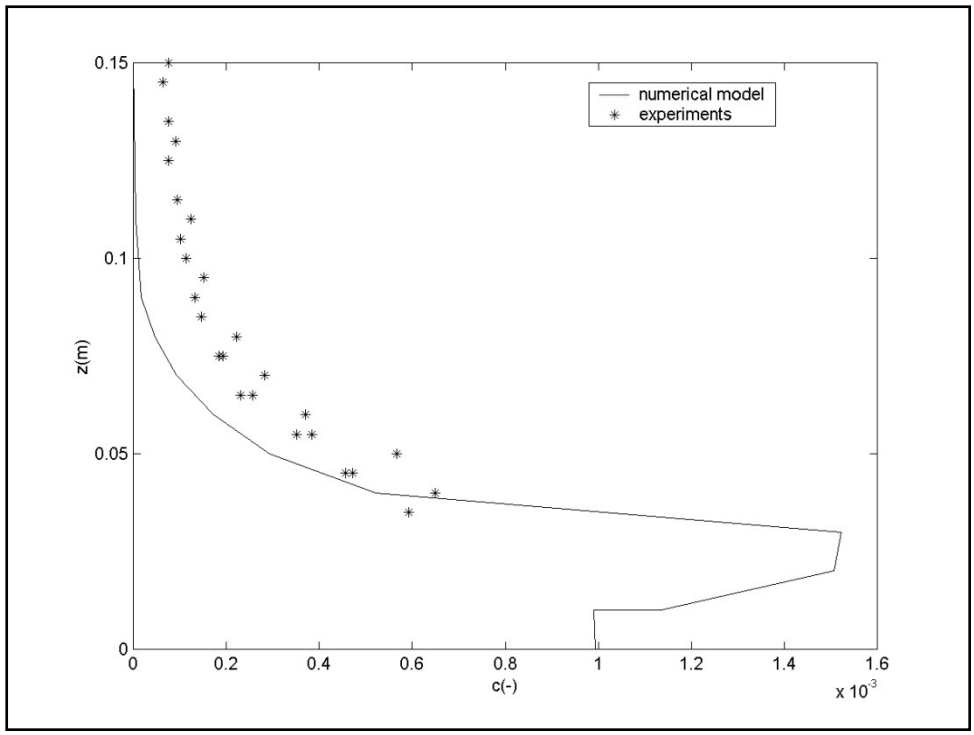

Figure 6-11 Validation with wave tunnel experiments of Delft Hydraulics (λ=25.6cm,Δ=3cm,$\hat{U}_\delta$=0.35m/s,T=5s, d_{50}=0.21mm) (concentration in m^3/m^3)

6.6 Wave groups

In nature, it can be observed that the bigger waves are clustered in a group). These groups can be represented by a fast moving component and an envelope, the boundary for the wave heights. The mean orbital bed velocity for these waves can be presented by:

$$U_\delta = 0.51\sin(\omega t)\sin(\omega t / g) \qquad (6\text{-}11)$$

The first factor (0.51, equal to observed velocities in the wave flume experiments) is the maximum amplitude of the velocity, the second part the fast oscillating component, and the third factor is the envelope wave. g is the number of half waves in the group. Figure 6-12 shows the velocity for the two cases discussed in this chapter (for g=8 and 16 and with $\omega=2\pi/T$, T=5s). The same bed material is used as during the Deltaflume experiments.

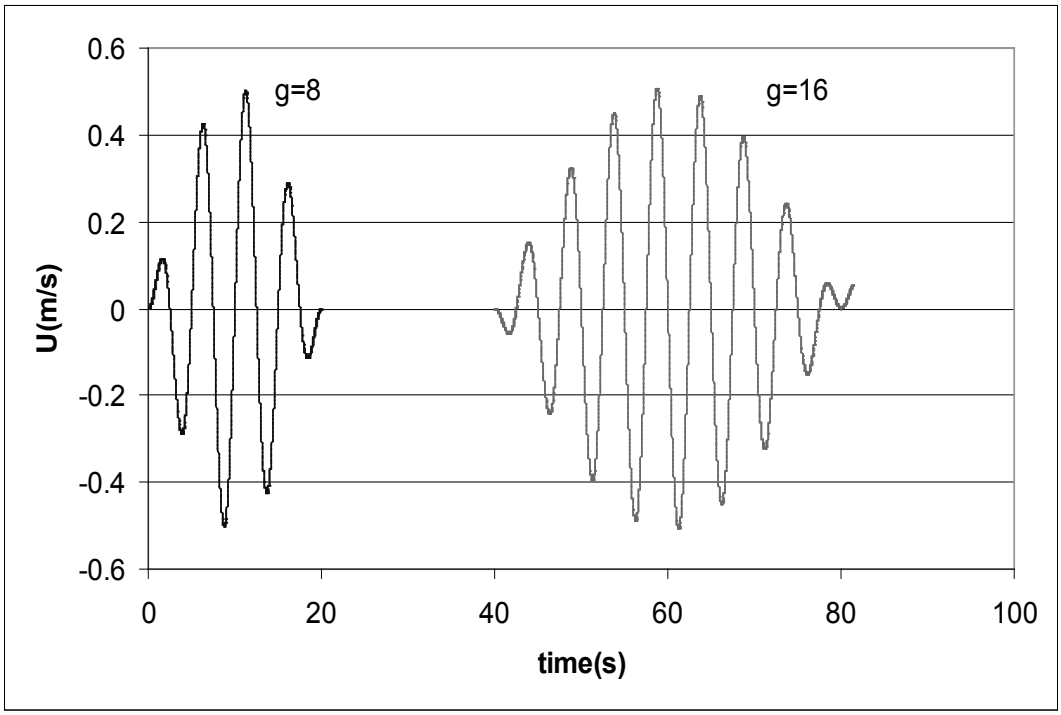

Figure 6-12 Two wave groups with resp. 8 and 16 half waves

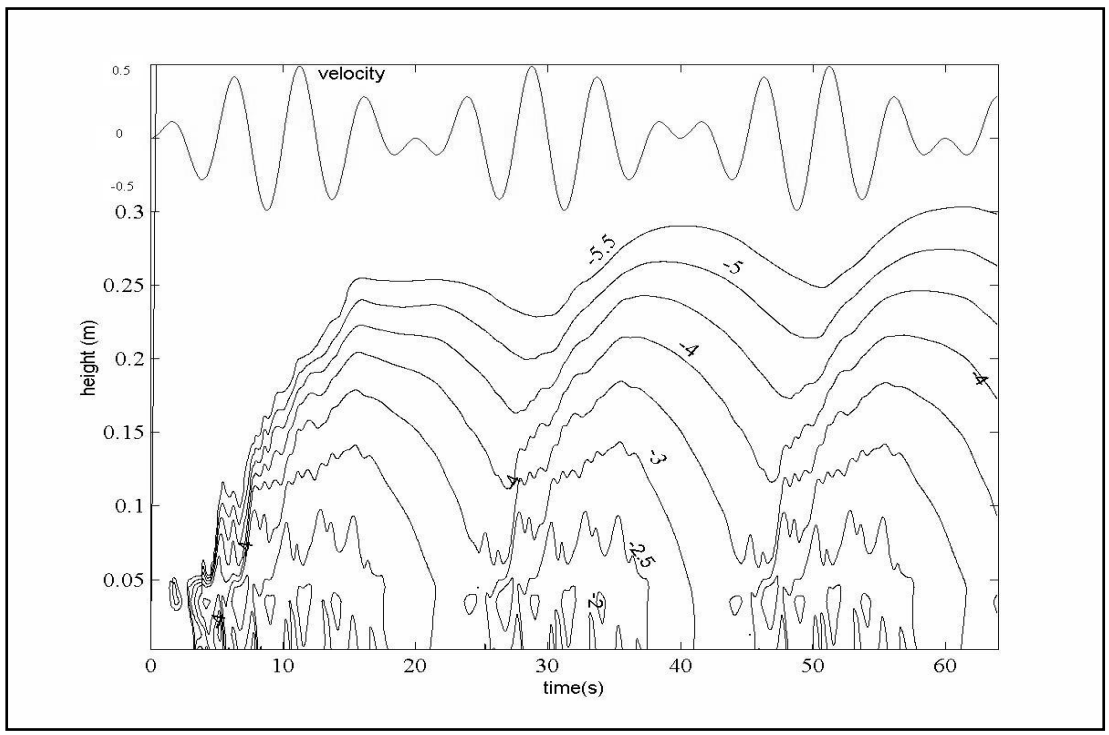

Figure 6-13 Iso-concentration lines: evolution of the concentration over time and height (the logarithm of the concentration(-) is shown)(g=8) (for grains with $d=d_{16}=0.21mm$)

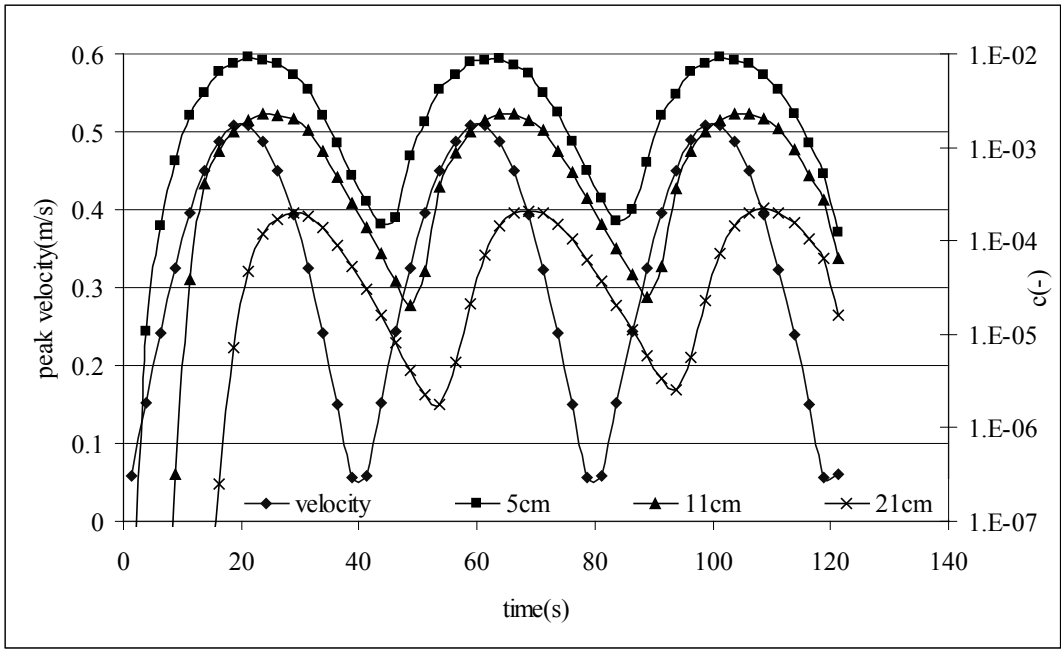

Figure 6-14 Evolution of the concentration for 3 heights.(g=16) (for grains with $d=d_{16}=0.21mm$)

Figure 6-13 shows the evolution of the concentration (concentration averaged between two ripple crests for different heights) in time. The vertical axis has the level of the ripple trough as origine. It is clear that close to the bed, the concentration adapts almost instantaneously to the hydrodynamic conditions (with intra wave variations). At higher levels, the concentration still increases after three wave groups have passed, with temporary maxima for the lowest waves and concentration minimum for the highest waves (due to time lag effects).

In Figure 6-14 the concentration is not only averaged between two ripple crests, but also time averaged between two zero-crossings of the velocity. The corresponding velocity for this period is the maximum orbital velocity during this (half wave) period. The lines in the figure do not have any physical meaning, they connect discrete points (maximal velocity (peak) and averaged concentration). Also for this longer wave group (g=16) the time lag is important at higher levels. 21 cm above the bed the maximum concentration is only reached 4 half waves after the highest wave passed.

Figure 6-15 and Figure 6-16 show the concentration at resp. 5 cm and 21 cm above the ripple trough for different wave groups. (Again averaged over half a wave period and spatially averaged between two ripple crests). C8 and C16 are the concentrations of the third wave group (for the third group, the concentration does not anymore depend of the previous group) for g=8, and g=16 respectively. C8 (in 16) are the concentrations for a group with 8 half waves, occurring after a group with g=16 (“in 16”) (and the opposite for C16 (in 8)) C16 bis denotes the results for a group with g=16, but after a series of symmetrical waves with the amplitude of the maximal wave in the group (U=51 cm/s). (V is velocity)

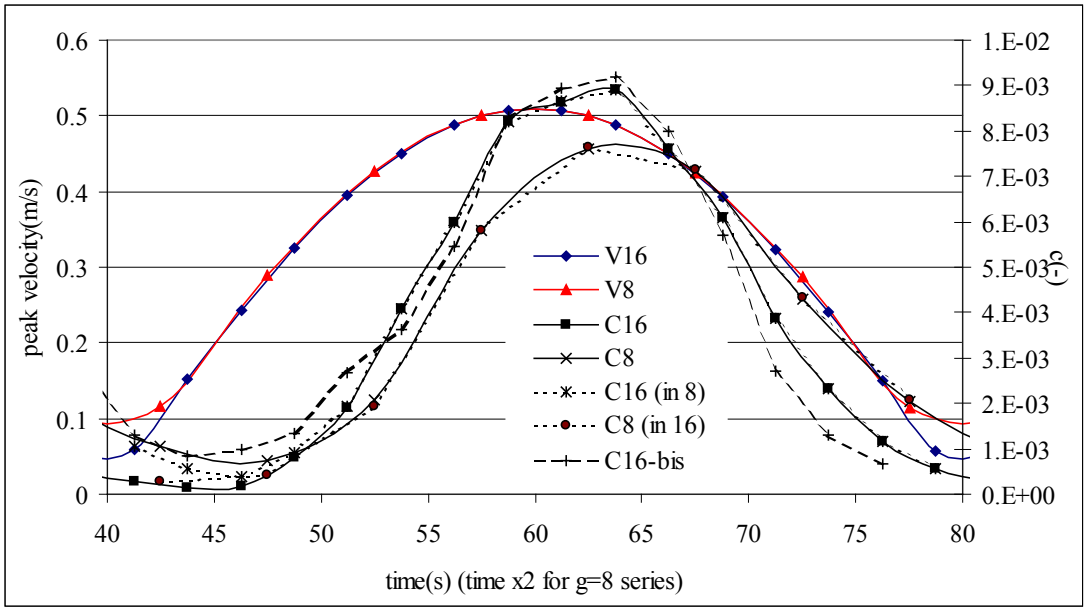

Figure 6-15 Half wave averaged concentration at a level 5 cm above the ripple trough for different wave groups (for grains with $d=d_{16}=0.21mm$)

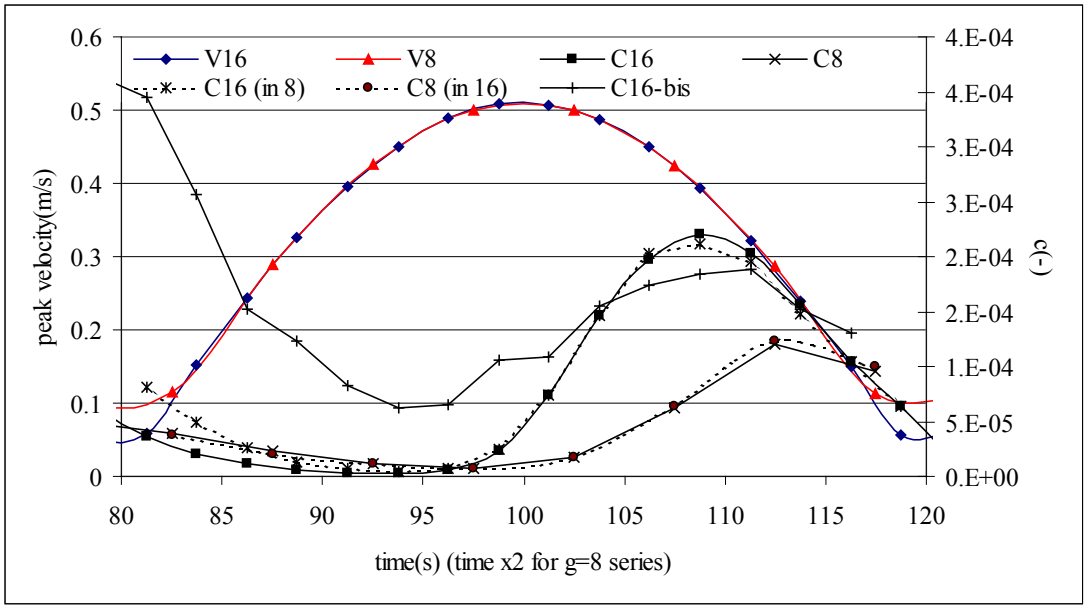

Figure 6-16 Half wave averaged concentration at a level 21 cm above the ripple trough for different wave groups (for grains with $d=d_{16}=0.21mm$)

From Figure 6-15 and Figure 6-16 it can be concluded that the maximum concentration near the bed occurs more or less at the same moment after the maximum wave has passed, while at higher levels the group of 16 half waves reacts (relatively!) faster. Also the concentration is much higher for the group of 16 half waves. Close to the bed the maximum concentration is also higher for the group of 16 half waves, but the concentrations drops faster to its minimum value.

In Figure 6-17 the half wave averaged concentration profiles during the wave group (g=8) are visible (the maximum value of the orbital velocity during the corresponding half wave period is given in the label). The profiles cannot be represented by a traditional exponential function, and the steepest profiles occur with the smallest waves

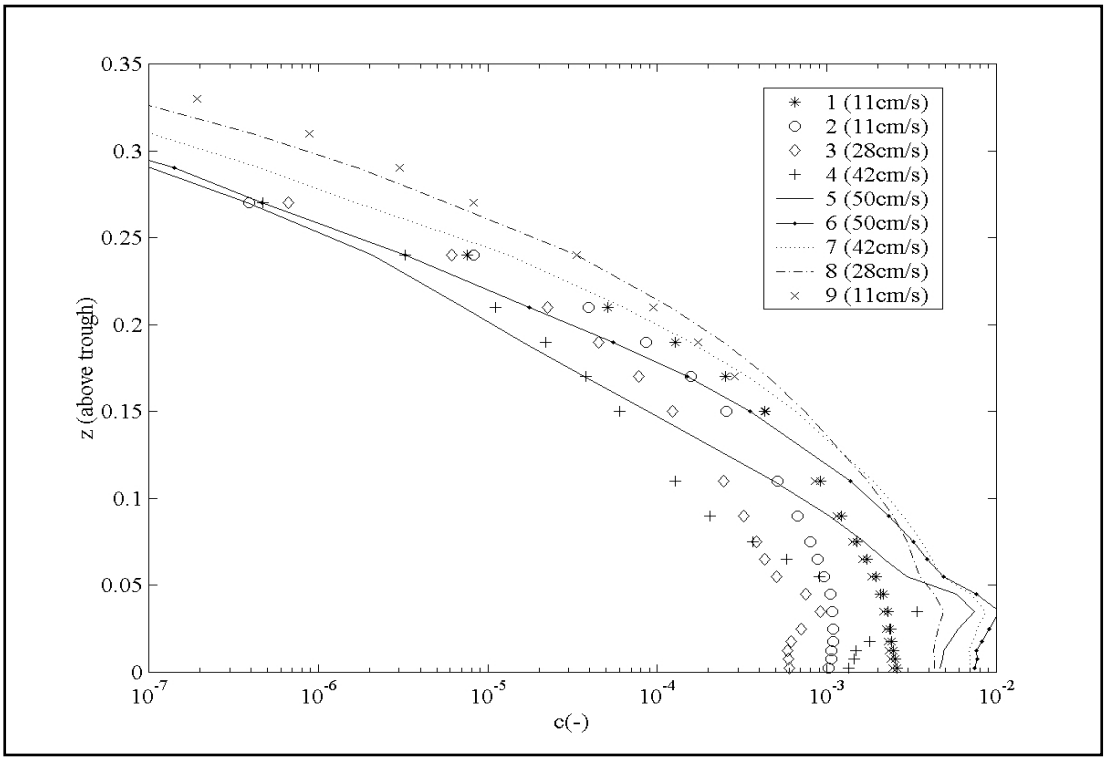

Figure 6-17 Evolution of the concentration profiles during a wave group (g=8)

Figure 6-18 compares the concentration profile averaged over the whole group for a group with resp. 8 and 16 half waves and for a regular symmetrical wave with the same amplitude as the biggest wave in the group. Close to the bed, the averaged concentration does not depend on the number of waves in the group, but at higher levels, the concentration does get less time to increase when the largest waves are passing, and the averaged concentrations remain lower for smaller wave groups. Regular waves produce of course much larger concentrations (e.g. Figure 6-17).

Although the two concentration profiles do not differ that much, the number of waves in the group can be important for the net sediment transport. Wave groups cause bound long waves, with offshore velocities under the highest waves, and onshore transport for the lowest waves. From Figure 6-15 and Figure 6-16 it is clear that smaller wave groups (e.g. g=8) have relatively higher concentrations under the lower waves and lower concentrations for the highest waves (e.g. g=16). They tend to produce more onshore transport than the larger wave groups.

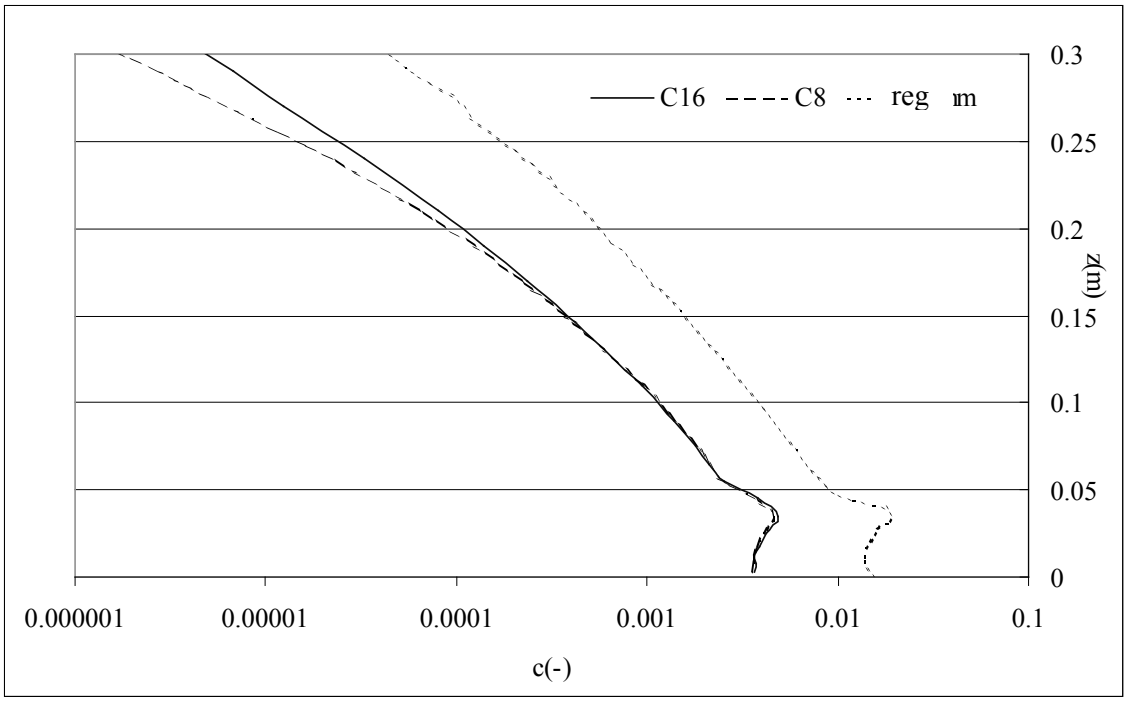

Figure 6-18 Time averaged concentration profiles for wave groups with g=8 and 16 and for regular waves

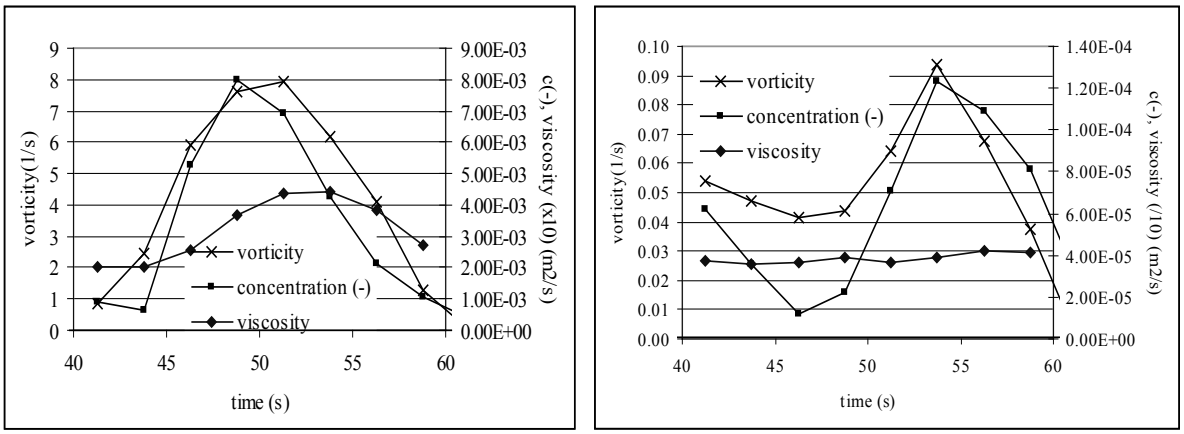

Figure 6-19 Concentration, vorticity and eddy viscosity at a height of resp. 5 and 21 cm from the ripple trough

In Figure 6-19 the concentration, eddy viscosity and vorticity are averaged over half a wave period and spatially between two ripple crests. The vorticity is here defined as:

$$\omega = \left| \frac{du}{dy} - \frac{dv}{dx} \right| \tag{6-12}$$

Both close to the bed (5cm) and at higher levels (21cm) the relation between concentration and vorticity is much clearer than the relation between the concentration and the eddy viscosity. Mostly, expressions to calculate sediment concentrations are based on the eddy viscosity. It might be better to work with the vorticity.

Figure 6-20 shows the difference in concentration if only the ripple length is changed. Originally the ripple length and height were resp. 34cm and 4.5 cm (a), while for (b) the ripple length is reduced to 24 cm. Since the orbital radius is not changed, a sediment cloud will travel relatively further away from the ripple crest where it has been produced. Figure 6-20 shows that the time lag becomes larger and the concentrations are higher (which is mainly because the ripple is steeper). More tests are needed to explain the larger time lag.

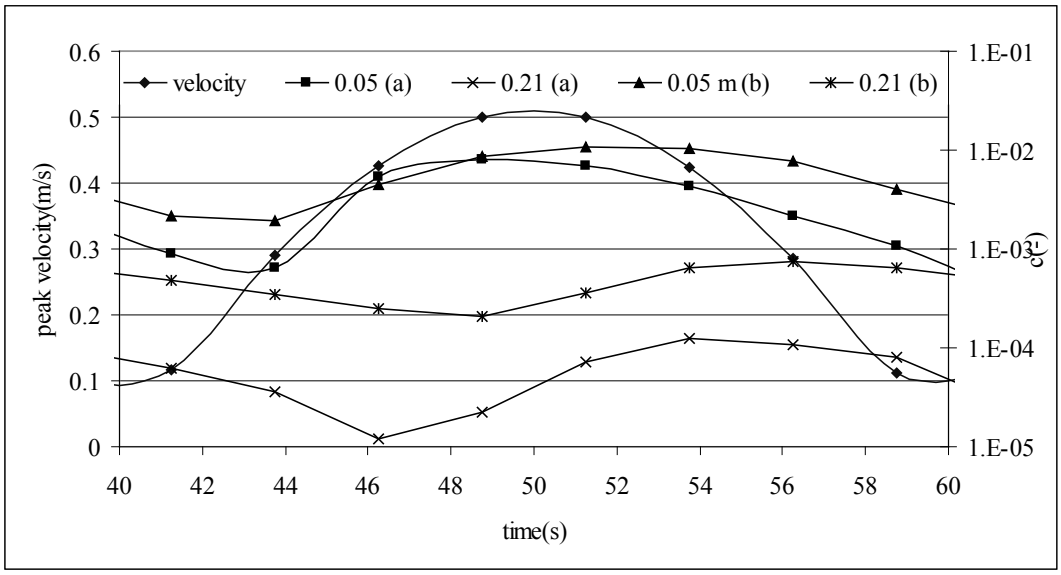

Figure 6-20 Evolution of the concentration at two heights (5 and 21 cm) for the same hydrodynamic conditions, but with different ripple lengths (ripple length a:34cm, b:24 cm)

6.7 Reproduction of physical experiments

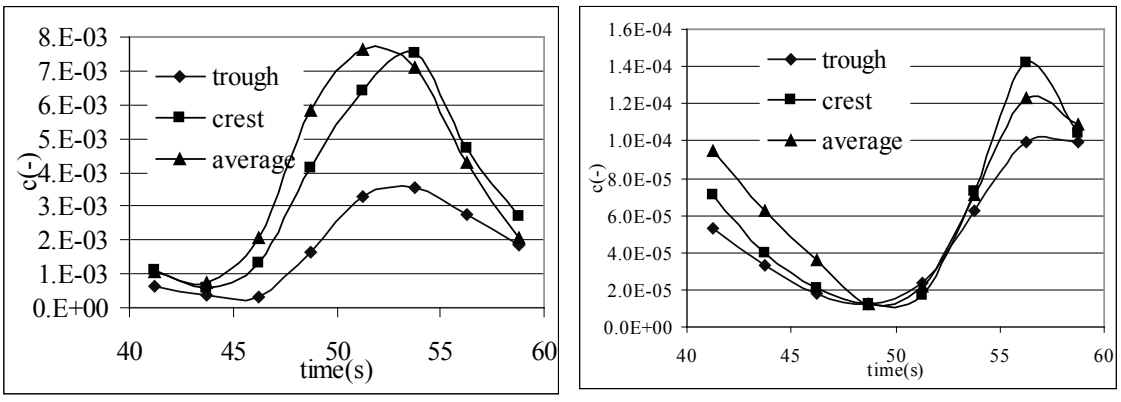

Figure 6-21 Averaged concentration and concentration above ripple crest and trough at 5cm (left) and 21 cm (right) height.

In physical experiments or during measuring campaigns at sea, one generally works with only one instrument to measure vertical concentration profiles. This means that only at one

horizontal position relatively to the ripple crest is measured. Numerical experiments can give an insight in the error involved. Figure 6-21 shows for the same tests as discussed earlier the averaged concentration between two ripple crests (as before) and what an imaginary transducer would see if it is positioned respectively above the ripple crest and trough. Concentrations are again always averaged over half a wave period (between two zero velocity crossings). It can be seen that especially close to the bed measurements above the ripple crest give significant lower concentrations, while at higher levels the difference becomes smaller.

6.8 Conclusions

In this chapter a CFD-package (Phoenics) was used to set-up an hydrodynamical model for the simulation of the flow over ripples. Once this was set up and optimised/verified (with special attention to grid dimensions and turbulence closure formulation), a code was written in order to calculate the transport of sand in the model, including boundary conditions at the bed and convection and diffusion of sand particles. This model was verified with own experiments in the Delta-flume (see Chapter 4) and other experiments in the oscillating wave tunnel. Doing a lot of simulations permitted the author to derive following conclusions :

- The averaged concentration near the bed does not depend much on the number of waves in a wave group.
- The concentration profile depends strongly on the number of waves, averaging over the whole group reduces this effect to the higher levels.
- Averaging the near bed concentration at the time interval of the highest waves gives an important difference with averaging them over the time interval of the lowest waves, which is important since wave groups induce bound long waves, with an offshore flux for the big waves and onshore for the small ones. However, it is also clear that some time lag exists !
- One must be careful with the interpretation of measurements in one vertical, since they are not representative for the whole ripple length (measuring above the trough or the crest will give different results).
- A tool is available for system identification. An expression needs to be sought, which relates the concentration to the previous ‘half wave cycle averaged’ concentration and some other parameters. Vorticity might in some cases be a more important parameter than turbulence in estimating sediment concentrations.

7 Summary, conclusions and recommendations

This thesis combines numerical modelling and physicals experiments and tries to combine these two.

After a summary of the existing theories about wave hydrodynamics, the scale effects associated with physical modelling are examined. The basic scale laws and their applications are summarised. The problems were quantified by using the developed numerical model of the transport of sediments over a rippled bed. It became clear that even for the optimal model (the 'Sand Model') important scale effects exist. The ripple length is not scaled with the hydrodynamic length scale of the orbital motion (orbital amplitude) and thus the movement of sediment clouds relative to the ripple crests is not scaled appropriately. When scaling the vertical distribution of sediment concentrations, not the hydrodynamic length scale should be used, but the length scale of the ripple height.

The wrong scaling of the movement of the sediment cloud can become severe in conditions with asymmetrical waves and/or a weak current: in that case the net sediment transport direction can reverse due to the scaling. In physical morphological models with these specific hydrodynamic conditions the erosion/sedimentation pattern can be modelled completely wrong compared to in situ observations.

However, physical models are still required since they allow examining the basic physics in detail. Compared to in situ measurements/observations, experiments in models can be repeated easily, hydrodynamic conditions can be changed as required and instruments can be positioned easier and more accurate. A wave flume of Flanders Hydraulics Research Division was prepared and tested. This task included the installation of appropriate wave absorption material, elimination of the spurious oscillations and programming software to generate irregular waves with the required wave spectrum. The residual reflection was calculated in function of the frequency and the higher harmonics were determined with wave analysis.

After the setting up of the flume, a Laser-Doppler Anemometer was used to measure turbulence above a movable bed and the erosion due to waves and currents was studied. The knowledge obtained was also integrated in further experiments in the Deltaflume.

The experiments in the Deltaflume were carried out in the framework of the EU Programme "Access to large-scale facilities". A frame with velocimeters, sand concentration recorders and a ripple profiler was deployed on two sandy beds in the Deltaflume (fine and medium sand). The frame can also be used for in situ experiments, but in the Deltaflume it was possible to generate and maintain the desired hydrodynamic conditions.

The planning of the experiments, the work 'in field' and the first rough analysis of the data required a considerable amount of time. In a second stage special attention was paid to extract out of the velocity measurements turbulence characteristics, the shear stress and

influence of waves on the velocity profiles. Better results were obtained with the ECM's mounded on the site wall of the Deltaflume than with the ADV on STABLE. The latter contained too much noise.

Ripple dimensions were determined and compared with existing predictions. It was observed that turbulence decreased when the ripples are washed out.

A thorough analysis of the ABS data was outside the scope of this thesis. Only the variation of concentration profiles due to the moving ripple was examined for 1 test case. They show a large variation of the evolution of the sediment concentration during a wave cycle in a point, depending on the horizontal and vertical position of the measuring point relative to the ripple crest.

Since this variation it is important to know at which distance data are obtained. Or in other words, it is important to obtain bed profile data at the position of the ABS-profile.

By lining the three ABS-sensors along the flow directions with a small separation, simultaneous concentration measurements near the crest and the trough might become possible.

To resolve the discussion about the possible existence of separation vortices and sediment clouds detailed velocity measurements close to the bed are important. Coherent Doppler velocity-meters might be less suitable since they cannot resolve high temporary changes in velocity. The use of a row of acoustic Doppler profiler is recommended.

In the Deltaflume-experiments the bed was almost always rippled. For higher waves, the ripples wash out and the sediment transport is dominated by sheet flow. In case of sheet flow, the sediment transport is concentrated in a very thin layer at the bed, for which in situ instruments (as in the Deltaflume) would not be suitable. Tests were done in de Oscillating Wave Tunnel (also in the framework of the EU Programme "Access to large-scale facilities").

Since Laser-velocity measurements cannot be done in water with a high concentration of sand, acoustic ADV results have to be used. Until now, it was doubtful, if ADV can be used to measure turbulence characteristics. A thorough analysis was done, and it could be concluded that the most important energy containing eddy turbulence can be measured. Measuring small-scale turbulence is not possible, since the measuring volume is too big for this aim. This item should be examined in more detail, with possible indications for in situ measurements.

Sharp concentration peaks at backward flow reversal (backward relative to the mean current) were visible. A second peak was visible at maximum flow.

With PIV a velocity field could be derived. The settling velocities of the sand particles seem to influence the measured vertical velocities. Close to the bed the concentrations are too high, so that no measurements were possible for the lowest 6 cm.

A pair of CCM's made it possible to obtain velocities and concentrations inside the sheet flow layer. The lifting up of the bed is clearly visible near flow reversals, with an important increase of the concentrations above the original bed level, and a decrease of concentrations below this level. The combination of velocities and concentrations makes it possible to predict sediment transport in the sheet flow layer.
In situ, it is not yet possible to measure these phenomena, and with classical concentration and velocimeters, it is not possible to estimate the sediment transport during storm conditions. More attention should be paid to have reliable sediment transport measurements for these conditions.

Finally, a numerical model was developed to calculate sediment concentrations and velocities over a rippled bed. Using very fine grids, it was possible to simulate the vortices reliably. The sediment pick-up function was calibrated using measurements of the Deltaflume.
In the next stage the numerical model was used to estimate the effect on the time depending sediment concentration profiles due to changes in measuring position relative the ripple crest. These effects seem to be important close to the bed, indicating that it is very important to know the relative position of the concentration meter to the ripple crest.
Tests were done with wave groups with different number of waves in the group and showed that the averaged concentration near the bed does not depend much on the number of waves for the sediment transport rates. However, the concentration profile depends strongly on the number of waves. Averaging the concentration over the whole wave group, the effect is only visible at the higher levels.
Near bed concentration averaged over the time interval of the highest waves deviate strongly from the mean concentration near the bed (averaged over a large time period). This is important for cross shore sediment transport where sediment flux direction (onshore/offshore) depends on the wave height (offshore for the high waves, onshore for the small waves).
One must be careful with the interpretation of measurements in one vertical, since they are not representative for the whole ripple length.
A tool is available for system identification. An expression needs to be sought, which relates the concentration to the previous half wave cycle. Vorticity might in some cases be a more important parameter than turbulence in estimating sediment concentrations.

This thesis showed that numerical and physical modelling has to be used together in order to examine and quantify sediment transport with irregular waves. The observations can be used to improve sediment transport formulae, e.g. by using vorticity instead of (or together with) turbulence characteristics and by using the number of waves in a wave group. More insight is available in the possible scale effects on sediment transport in wave flumes.

8 New developments

8.1 Introduction

This chapter gives an overview of publications about research which is directly connected to the research described in this thesis, but not yet available at the moment of doing the research. The three considered items are sheet flow, sediment concentrations over rippled beds and measuring techniques. Of course, also many other relevant research is published (e.g. about prediction of ripple dimensions, sand transport calculations) but these were not directly a research theme in this thesis.

8.2 Sheet flow

Ribberink (1998) developed a quasi-steady bed load model that is valid for both waves as well as for steady flow conditions. This model has the time varying Shields parameter as driving parameter. The instantaneous bed transport (in the direction of the shear stress) is given as

$$q_b = 11\sqrt{\left(\frac{\rho_s}{\rho}-1\right)gd_{50}^3}(\theta(t)-\theta_{cr})^{1.65} \qquad (8\text{-}1)$$

Ribberink specifies the method to calculated the instantaneous shear stress for wave-current conditions.
Nielsen (2006) proposed a comparable expression:

$$q_b = 12\sqrt{\left(\frac{\rho_s}{\rho}-1\right)gd_{50}^3}(\theta(t)-\theta_{cr})\,\theta(t)^{0.5} \qquad (8\text{-}2)$$

Dohmen-Janssen (1999) extended the formulation of Ribberink, by multiplying the sediment transport with a reduction factor r, which depends on the ratio $\bar{u}/\hat{U}$ (represents the importance of the net current velocity compared to the oscillatory velocity) and on the phase lag parameter p : $p = \frac{\delta_s \omega}{w_s} = \frac{5 f_w \hat{U}_\delta^2 \omega}{(s-1) g w_s}$
Experiments in the Large Wave Flume of Hannover (SISTEC99-experiments (Dohmen-Janssen and Hanes, 2005) concentrated on the effect of wave groups and are in line with the findings in this thesis for sediment concentrations above rippled beds for wave groups. They concluded that within the sheet flow layer, the concentrations are highly coherent with the instantaneous nearbed velocities due to each wave within the wave group. However, in the suspension layer concentrations respond much more slowly to changes in near-bed velocity. At several centimetres above the bed, the suspended sediment concentrations vary on the time scale of the wave group, with a time delay relative to the peak wave within the wave group.

The thickness of the sheet flow layer only depends on the instantaneous wave, not on the history of the wave group.
A numerical model POINT-SAND (Uittenbogaard (2000)) solves the relevant equations for momentum, turbulence and sediment as a function of the height above the bottom and time, for wave-current-turbulence-sediment interactions in free-surface flows as well as in wave tunnels.
Also research is carried out about the effect of graded sediments. Hassan (2003) concluded, based on experiments in a wave tunnel, that sediment transport formulae adapted for graded sediments :

- Predict the coarse fraction better than the fine fraction
- The model of Ribberink (1998) and Dibajnia & Watanabe (1996) shows the best performance for predicting the coarse fraction
- The transport of the fine fraction is still difficult to predict

Improvements for the different models were suggested. It seems that the hiding/exposure effects play an important role, and the phase-lag correction of Dohmen-Janssen (1999) should be applied. Other research on sheet flow sediment transport for graded sediments can be found in Ahmen (2002) and Wright (2002).
Hassan and Ribberink (2010) developed a 1DV – RANS model to study sand transport processes in oscillatory flat-bed/sheet flow conditions. The model is able to give a correct representation of the observed trends in the data with respect to the influence of the velocity, wave period and grain diameter. Also detailed mean sediment flux profiles in the sheet flow layer are well reproduced by the model, including the direction change from 'onshore' to 'offshore' due to a difference in grain size from 0.34 mm (medium sand) to 0.13 mm (fine sand).

8.3 Rippled beds

New experiments in the large wave flumes of Aberdeen and Deltares are carried out and reported in Van der Werf et al. (2006). From analysis of these and other full-scale data, it is concluded that the lower part of the time- and bed-averaged concentration profile (up to two times the ripple height above the ripple crest level) has an exponential profile. A new reference concentration formula is proposed. A new transport model is proposed for the wave-related net transport over full-scale ripples based on a modified half wave cycle concept of Dibajnia and Watanabe. The magnitudes of the half wave cycle transport contributions are related to the grain-related Shields parameter, the degree of wave asymmetry and a newly defined vortex suspension parameter P, which is the ratio between the ripple height and the median grain-size. This stresses once more that vorticity is an important parameter for transport of sand over ripples.

Delgado (2006) reported physical experiments done for a sand bed with ripples and with double peaked spectra (swell and sea waves superimposed). The tests indicated that the swell waves causes a significant increase in sediment concentration compared to wind sea waves only conditions, while adding wind sea waves to swell waves causes a decrease in sediment concentration. Both conclusions are in agreement with the importance of the vortices, since swell waves increase the vorticity, while sea waves decrease the vorticity. The double peaked spectra also influence the ripple geometry, which has also an influence on the sediment concentration.

Davies and Thorne (2005) developed a 1DV model for the calculation of sand transport over ripples. Close to the bottom (total height of two time the ripple height) vortex shedding is represented by a time-varying eddy viscosity with peak values at flow reversal while higher up, traditional advection-diffusion formulations are used.

8.4 Measuring techniques

McLean et al. (2001) developed a new measuring technique to measure sediment concentrations in the sheet flow layer based on electo-resistance. The technique was further improved (Hassan and Ribberink, 2005) for the improved measurement of sediment dynamics inside the sheet-flow layer. This technique enabled the measurements of particle velocities during the complete wave cycle.

Also frames with instruments are further extended. E.g. at Proudman (Betteridge et al., 2003) a frame is installed to measure simultaneous, co-located suspended sediments, near-bed velocities and bed morphology using new acoustic instruments, including a triple frequency acoustic backscatter system, (ABS); a uniaxial, and triple axis, coherent Doppler velocity profiler, (CDVP); a sand ripple imager (SRI); and a sand ripple profiler (SRP).

And more recently, a new instrument is developed: Acoustic Concentration and Velocity Profiler (ACVP) (Hurther et al., 2011). Until relatively recently, separate acoustic systems were used to measure flow and suspended sediment concentration. But with this instrument flow and sediment measurements can be integrated into a single system. This integration provides, quasi-instantaneous, non-intrusive, co-located, high temporal-spatial resolution measurements of benthic flow and sediment processes.

9 References

Aerts,G., Kinget,G., 'Meten en interpreteren van een dataset m.b.t. sedimenttransport in een grote golfgoot', master thesis, K.U.Leuven, Hydraulics Laboratory, 1998 (in dutch)

Ahmed, S.M.A. (2002): Sheet flow transport mechanism of heterogeneous sediments under nonlinear oscillatory flows. Ph.D. Thesis, Dep. of Civil Eng., Univ. of Tokyo, Japan.

Al-Salem, A.A., Sediment transport in oscillatory boundary layers under sheet-flow conditions. Ph.D. Thesis, Delft University of Technology, 1993

Avva,R.K., Kline,S.J., Ferziger,J.H., Computations of the Turbulent Flow Over a Backward Facing Step Using the Zonal Modelling Approach, Stanford University, TR TF33, Stanford, CA, 1988

Bell P. S., Thorne P. D. , Measurements of sea bed ripple evolution in an estuarine environment using a high resolution acoustic sand ripple profiling system. *Oceans '97*, Volume 1, MTS/IEEE, Washington D.C., pp 339-343.,1997

Betteridge, K., Williams, J., Thorne, P., Bell, P., Acoustic instrumentation for measuring near-bed sediment processes and hydrodynamics, Journal of Experimental Marine Biology and Ecology, Volumes 285-286, 2003

Blondeaux,P., Vittori,G., Vorticity Dynamics In An Oscillatory Flow Over A Rippled Bed, J. Of Fluid Mechanics, 226, P.257-290, 1991

Bosman, J.J., Concentration measurements under oscillatory water motion. Rep. M1695, Delft Hydraulics, The Netherlands, 1982.

Bosman, J.J., Calibration of optical systems for sediment concentration measurements. Rep. R716, Part V, Delft Hydraulics, The Netherlands, 1984.

Bosman, J. J., Velden, E. T. J. M. Van Der, Hulsbergen C. H. Sediment concentration measurements by transverse suction. *Coastal Engineering*, **11**, 353-370, 1987

Brøker,I.H., Wave generated ripples and resulting sediment transport in waves. Series Paper No.36, Inst. Of Hydrodynamics and Hydraulic Engineering, ISVA, Techn. Univ. of Denmark, 1985

Cham, Polis: Phoenics on line information system, part of PHOENICS version 2.0, 1994

Chen,Y.S., Kim,S.W., Computation of turbulent flows using an extended k-ε turbulence closure model, NASA CR-179204, 1987

Craik, A.D.D., The drift velocity of water waves, Journal of Fluid Dynamics, Vol. 116, 1982

Dally, W.R., Long wave effects in laboratory studies of cross-shore transport, Proceedings of Coastal Sediments 91, ASCE Vol.1 pp.85-99, 1991

Davies,A.G., Villaret, C., Wave induced currents above rippled beds, Proceedings of the PECS conference, Den Haag, Balkema Publ., 1998

Davies, A.G., Thorne, P., Modeling and measurement of sediment transport by waves in the vortex ripple regime, Journal of Geophysical Research, VOL. 110, C05017, 25 PP., 2005

Dean, R.G., “Physical modelling of littoral processes”, in Physical modelling in coastal engineering, R.A. Dalrymple, Ed.,, Balkema - Rotterdam/Boston, 1985

Dean, R.G., Dalrymple,R.A., Water wave mechanics for engineers and scientists, Advanced series on Ocean Engineering – vol 3, World Scientific,1991

Delgado, R., Flow and sediments under random waves: experimental study for rippled beds, Ph.D. thesis, KULeuven, 2006

Dibajnia, M.and A. Watanabe, A transport rate formula for mixed-size sands. Proc. of the 25th Int. Conf. on Coast. Eng., Orlando, pp. 3791-3803, 1996

Dohmen-Janssen, C.M., Grain size influence on sediment transport in oscillatory sheet flow; phase lags and mobile-bed effects, Ph.D. thesis, Delft University, 1999

Dohmen-Janssen, M. Hanes, D., Sheet flow and suspended sediment due to wave groups in a large wave flume, Continental Shelf Research (25), 2005

Ferziger,J.H., Peric,M, Computational methods for fluid dynamics, Springer, Berlin, 1996

Flick, R.E., Guza,R.T., Paddle generated waves in laboratory channals, Journal of Waterway, Port, Coastal and Ocean division, ASCE, 1980

Flokman,Y., Goemaere,S., Fysisch modelleren van sedimenttransport in een kustzone (in dutch), master thesis, Vakgroep Civiele Techniek, R.U.Gent, 1996

Foster, D., R. Holman and R. Beach, Correlation between sediment suspension events and shear instabilities in the bottom boundary layer of the surf zone". Proc. Coastal Dynamics '94, ASCE, Barcelona, Spain, Feb. 1994, pp. 712-726, 1994

Fredsøe,J., Deigaard,R., Mechanics of Coastal Sediment transport. Advanced series on Ocean Engineering – vol 3, World Scientific - Singapore, 1992

Goda,Y., Suzuki,Y., Estimation of incident and reflected waves in random wave experiments. Proc. of the 15th Coastal Engineering Conference, Hawai, 1976

Hannay,A., Williams,J.J., West, J.R., Coates, L.E., A field study of wave-current interactions over a rippled sandy bed. EUROMECH 310: Sediment transport Mechanics in Coastal Environments and Rivers, M. Belorgey, R.D. Rayaona & J.A.F. Sleath (editors), World Scientific, 1994

Hassan, W.N., Sand transport processes in oscillatory sheet flows with different wave periods - CCM measurements in the Large Oscillating Water Tunnel, MICS report, Dept. of Civil Engineering, University of Twente, 2001

Hassan, W., Transport of size-graded and uniform sediments under oscillatory sheet-flow conditions, Ph.D. thesis, Univ. Of Twente, 2003

Hassan, W. Ribberink, J., Transport processes of uniform and mixed sands in oscillatory sheet, Coastal Engineering, Volume 52, Issue 9, September 2005

Hasselmann, K., Barnett, T.P., Bouws,E., Carlson,H., Cartwright, D.E., Ewing, J.A., Gienapp,H., Hasselmann,D.E., Kruseman,P., Meerburg,A., Muller,P., Olbers,D.J., Richter,K., Sell, W. and Walden,H., Measurements of wind-wave growth and swell

decay during the Joint North Sea Wave Project (JONSWAP), Dtsch. Hydrogr. Z., A8, 12, 95p., 1973

Havinga, F. J.,Sediment concentrations and sediment transport in case of irregular non-breaking waves with a current, Report H840 Parts E, F & G, Delft Hydraulics, Delft University of Technology, Delft, The Netherlands,1992

Horikawa, K. Nearshore dynamics and coastal processes, University of Tokyo Press- Japan, 1988

Hughes, S.A. Physical models and laboratory techniques in coastal engineering, World Scientific - Singapore, 1993

Humphery, J. D. & Moores, S. P.,STABLE II - An improved benthic lander for the study of turbulent wave-current-bed interactions and associated sediment transport. Electronic Engineering in Oceanography, IEE Conference Publication No. 394, 170-174.,1994

Hurther,D., Thorne,P., Bricaulta,M., Lemminc,U., Barnouda,J.M., A multi-frequency Acoustic Concentration and Velocity Profiler (ACVP) for boundary layer measurements of fine-scale flow and sediment transport processes, Coastal Engineering, in press, 2011

Huthnance,J.M., Circulation, exchange and water masses at the ocean margin: the role of physical processes at the shelf edge, Ocean Margin Experiment: OMEX First Annual Report, ULBruxelles, 1994

Janssen, C.M., W.N. Hassan, R.J. Van der Wal, & J.S. Ribberink, Net sand transport rates and transport mechanisms of fine sand in combined wave-current sheet flow conditions. DELFT HYDRAULICS, Data report H2462, Part IV., 1996

Jensen, B.L., Sumer, B.M. and Fredsøe, J., Turbulent oscillatory boundary layers at high Reynolds numbers, J. Fluid Mech., 206, 265-297, 1989

Jonsson, I.G., Wave boundary layer and friction factors, Proc. 10th Conf. Coastal Eng., p. 127-148, Tokyo, Japan, 1966

Kamphuis, J.W., “On the understanding scale effect in coastal mobile bed models” in Physical modelling in coastal engineering, ed. Dalrymple,R.A., Balkama Rotterdam/ Boston, 1985

Katopodi, I., J.S. Ribberink, P. Ruol, H. Koelewijn, C. Lodahl, S. Longo, A. Crosato & H. Wallace, Intra-wave sediment transport in an oscillatory flow superimposed on a mean current. Data Report H1684, Part III, DELFT HYDRAULICS, The Netherlands. 1994.

Klopman,G., Vertical structure of the flow due to waves and currents, Progress report H840.30 Part II, Delft Hydraulics, 1994

Launder,B.E., Spalding,D.B., The numerical computation of turbulent flow, Comp. Meth. in Appl. Mech. and Eng., vol 3, 1974

Longuet-Higgins,M.S., Mass transport in water waves, Philosophical Transactions of the Royal Society of London, Series A, 1953

Longuet-Higgins,M.S., The mechanisms of the boundary layer near the bottom in a progressive wave, Proceedings of the 6th ICCE conference, ASCE, 1956

Longuet-Higgins,M.S., Stewart,R.W., Radiation in water waves: a physical discussion with applications, Deep Sea Research, Vol II, 1964

Longuet-Higgins, M.S., Oscillatory Flow Over Steep Sand Ripples, J. Of Fluid Mech., 107, 1-35, 1981

Luo, W., Wind wave modelling in shallow water, with applications to the Southern North Sea, Ph.D. thesis, Hydraulics Laboratory, KULeuven, 1995

Matthé,J. Correct modelling of a sea state in a wave flume, Bulletin PIANC, nr. 86, 1995

McLean, S.R., Ribberink, J.S., Dohmen-Janssen, C.M. and Hassan, W.N.M., Sediment transport measurements within the sheet flow layer under waves and currents. J. Waterw., Port, Coast., Ocean Eng., ISSN 0733-950X], 2001

Miche, M., Le pouvoir réfléchissant des ouvrages maritimes exposés à l'action de la houle, Annales des Ponts et Chaussées, Paris, 1951

Miller,M.C., McCave,I.N., Komar,P.D., Threshold of Sediment Motion under Unidirectional Current Sedimentology, Vol. 24, 1977

Monbaliu,J., Scientific report of a stay in London, Canada, unpublished, 1986

Monbaliu,J., Wind and waves: Investigation of an optimization approach to parameter estimation, Ph.D. thesis, Dept. Burgerlijke Bouwkunde, KULeuven, 1992

Myrhaug, D., Lambrakos,K.F., Slaattelid, O., Wave boundary layer in flow measurements near the seabed, Coastal Engineering, 18, 1992

Nielsen, P., Coastal bottom boundary layers and sediment transport, Advanced series on Ocean Engineering – vol 4, World Scientific - Singapore, 1992

Nielsen, P.. Sheet flow sediment transport under waves with acceleration skewness and boundary layer streaming. *Coastal Engineering* 53, 749-758, 2006.

Nieuwjaar,M., Van der Kaaij, Th., Sediment transport in irregular non-breaking waves. Coastal. Eng. Dep. TuDelft, 1987

O'Connor, B.A., Kim,H.S., Williams,J.J., Hydrodynamics of random wave boundary layers. Coastal Dynamics '94 Barcelona, 1994

Perrier,G., Hansen,E.A., Villaret,C. Deigaard,R. and Fredsøe,J., Sediment transport over ripples in waves and current, Proceedings ICCE'94, 1994

Ribberink, J.S. & A.A. Al-Salem, Sediment transport in oscillatory boundary layers in cases of rippled bed and sheet-flow. J. Geoph. Res., Vol. 99, No. C6, pp. 12707-12727, 1994.

Ribberink, J.S. Al-Salem, A., Bedforms, near bed concentrations and sediment transport in simulated regular wave conditions, Rep. H840, part III, Delft Hydraulics, 1989

Ribberink, J.S., The large oscillating water tunnel. Technical specifications and performances. DELFT HYDRAULICS, Rep. H840, Part I. 1989

Ribberink, J. (1998). Bed-load transport for steady flows and unsteady oscillatory flows. *Coastal Engineering* 34, 52-82.

Rivero,F.J., Arcilla,A., On the vertical distribution of <ũw>, Coastal Engineering No. 25, Elsevier, 1995

Rocabado, O.I., Modelling Highly Concentrated Turbulent Flows with Non-cohesive sediments, Ph.D. Thesis, Katholieke Universiteit Leuven, 1999

Rose,C., Suspended sediment transport in storm conditions, Ph.D. thesis Univ. of Birmingham, 1997

Rose, C.P., Trouw, K., Cloin, B., Arnott, A.D., Sistermans, P.G.J., van de Graaff, J., Dong, P., Ribberink, J. and O'Connor, B.A., Vertical Sediment Entrainment Characteristics In Oscillatory Sheet Flow Conditions, Proc. of the conf. Coastal Sediments, 1999

Sand,S.E., Long wave problems in laboratory models, Journal of Waterway, Port, Coastal and Ocean division, ASCE, 1982

Sleath, J.F.A., Turbulent oscillatory flow over rough beds, Journal of Fluid Mechanics, nr. 182, 1987

Slezak,R., Microcomputer control of spectral conditions in a wave tank, M.E.Sc thesis, U.W.O., London, Ontario, 1986

Soulsby R. L., Goldberg D. G. & Stevenson E. C., Norfolk Sand Banks. Analysis of STABLE data. HR Wallingford, Report Number EX 2345, 18 pp.,1991

Svendsen,I.A., "Physical modelling of water waves" in Physical modelling in coastal engineering, R.A. Dalrymple, Ed.,, Balkema - Rotterdam/Boston, 1985

Tenneks and Lumley, A first course in turbulence, MIT Press, Cambridge, USA, 1972

Thangam,S., Speziale,C.G., Turbulent Flow Past a Backward-Facing Step: A Critical Evaluation of Two-Equation Models, AIAA Journal, Vol.30, No. 5, 1992

Thorne, P. D. & Hardcastle, P. J., Acoustic measurements of suspended sediments in turbulent currents and comparison with in-situ samples. Journal of the Acoustic Society of America, 101(5), 2603-2614.,1997

Trouw,K., Experiments in a wave flume, Proc., Progress in Belgian Oceanographic research, 1996

Trouw,K., Williams,J.J., Rose,C.P., Modelling Sand resuspension by waves over a rippled bed, Estuarine, Coastal and Shelf Science, Vol.50 no.1, Acad. Press, 2000

Trouw,K., Cloin,B., Arnott,A., Hassan,W., Dong,P., van de Graaff,J., Rose,C., Ribberink,J., Sistermans,P.G., Vertical sediment entrainment characteristics in oscillatory sheet flow conditions, Data report Z2454, Delft Hydraulics, 2001

Tsujimoto,G., Hayakawa,N., Ichiyama,M., Fukushima,Y., Nakamura,Y., A study on suspended sediment concentration and sediment transport mechanism over rippled sand bed using a turbulence model, Coastal Engineering in Japan, Vo. 34 N.2, 1991

Uittenbogaard, R.E., 1DV Simulation of Wave Current Interaction. In Proc. 27th Int. Conf. On Coast. Eng., Sydney, Australia, pp. 255-268, 2000

Van Mierlo, M.C.L.M., De Ruiter,J.C.C., Turbulence measurements above artificial dunes, TOW A55, Q789., Delft Hydraulics, 1988

van der Werf, J., Ribberink, J., O'Donoghue,T., Doucette, J., Modelling and measurement of sand transport processes over full-scale ripples in oscillatory flow, Coastal Engineering, Volume 53, Issue 8, June 2006

Van Rijn, L.C., Sediment transport and morphology in rivers, estuaries and coastal seas, Aqua publications - Amsterdam, 1993

Van Rijn,L.C., Principles of fluid flow and surface waves for rivers, estuaries, seas and oceans, Aqua Publications - Amsterdam, 1990

Williams,J.J., Moores, S.P., Clipson,D., Analysis of STABLE data from LOIS RACS(C)-I,Holderness UK. Proudman Oceanographic Laboratory, Report No. 42, 1996

Williams, J. J., Rose, C. P., Thorne, P. D., Coates, L. E., West, J. R., Hardcastle P. J., Humphery, J. D., Moores, S. P. & Wilson, D. J. Observed suspended sediments in storm conditions. *Proceedings ICCE'96,* ASCE, Volume **3**, 3257-3269.,1997

Williams, J. J., Bell, P. S., Coates, L. E., Hardcastle, P. J., Humphery, J. D., Moores, S. P., Thorne, P. D. & Trouw, K. Evaluation of field equipment used in studies of sediment dynamics. *POL Report* **53**, 45pp.,1998

Williams, J. J., Bell, P. S., Thorne, P. D., Trouw, K., Hardcastle, P. J. & Humphery, J. D. Vertical suspended sediment concentration profiles and bedforms in oscillatory-only flow. *Coastal Engineering*. ,1998

Williams J. J., Bell P. S., Thorne P. D., Trouw K., Hardcastle P. J. & Humphery J. D. Observed and Predicted Vertical Suspended Sediment Concentration Profiles and Bedforms in Oscillatory-Only Flow. *Journal of Coastal research,* Vol. 16, nr. 3, 2000

Wright, S., Well-sorted and graded sands in oscillatory sheet-flow. *Ph.D. thesis,*Univ. of Aberdeen, Scotland, 2002

Yalin,M.S., Mechanics of Sediment Transport, Pergamon Press, 1972